

SECTION 5

Heat and Mass
Transfer

PERRY'S CHEMICAL ENGINEERS' HANDBOOK

8TH EDITION



HOYT C. HOTTEL, JAMES J. NOBLE
ADEL F. SAROFIM, GEOFFREY D. SILCOX
PHILLIP C. WANKAT, KENT S. KNAEBEL

Copyright © 2008, 1997, 1984, 1973, 1963, 1950, 1941, 1934 by The McGraw-Hill Companies, Inc. All rights reserved. Manufactured in the United States of America. Except as permitted under the United States Copyright Act of 1976, no part of this publication may be reproduced or distributed in any form or by any means, or stored in a database or retrieval system, without the prior written permission of the publisher.

0-07-154212-4

The material in this eBook also appears in the print version of this title: 0-07-151128-8.

All trademarks are trademarks of their respective owners. Rather than put a trademark symbol after every occurrence of a trademarked name, we use names in an editorial fashion only, and to the benefit of the trademark owner, with no intention of infringement of the trademark. Where such designations appear in this book, they have been printed with initial caps.

McGraw-Hill eBooks are available at special quantity discounts to use as premiums and sales promotions, or for use in corporate training programs. For more information, please contact George Hoare, Special Sales, at george_hoare@mcgraw-hill.com or (212) 904-4069.

TERMS OF USE

This is a copyrighted work and The McGraw-Hill Companies, Inc. (“McGraw-Hill”) and its licensors reserve all rights in and to the work. Use of this work is subject to these terms. Except as permitted under the Copyright Act of 1976 and the right to store and retrieve one copy of the work, you may not decompile, disassemble, reverse engineer, reproduce, modify, create derivative works based upon, transmit, distribute, disseminate, sell, publish or sublicense the work or any part of it without McGraw-Hill’s prior consent. You may use the work for your own noncommercial and personal use; any other use of the work is strictly prohibited. Your right to use the work may be terminated if you fail to comply with these terms.

THE WORK IS PROVIDED “AS IS.” McGRAW-HILL AND ITS LICENSORS MAKE NO GUARANTEES OR WARRANTIES AS TO THE ACCURACY, ADEQUACY OR COMPLETENESS OF OR RESULTS TO BE OBTAINED FROM USING THE WORK, INCLUDING ANY INFORMATION THAT CAN BE ACCESSED THROUGH THE WORK VIA HYPERLINK OR OTHERWISE, AND EXPRESSLY DISCLAIM ANY WARRANTY, EXPRESS OR IMPLIED, INCLUDING BUT NOT LIMITED TO IMPLIED WARRANTIES OF MERCHANTABILITY OR FITNESS FOR A PARTICULAR PURPOSE. McGraw-Hill and its licensors do not warrant or guarantee that the functions contained in the work will meet your requirements or that its operation will be uninterrupted or error free. Neither McGraw-Hill nor its licensors shall be liable to you or anyone else for any inaccuracy, error or omission, regardless of cause, in the work or for any damages resulting therefrom. McGraw-Hill has no responsibility for the content of any information accessed through the work. Under no circumstances shall McGraw-Hill and/or its licensors be liable for any indirect, incidental, special, punitive, consequential or similar damages that result from the use of or inability to use the work, even if any of them has been advised of the possibility of such damages. This limitation of liability shall apply to any claim or cause whatsoever whether such claim or cause arises in contract, tort or otherwise.

DOI: 10.1036/0071511288

This page intentionally left blank

Heat and Mass Transfer*

Hoyt C. Hottel, S.M. *Deceased; Professor Emeritus of Chemical Engineering, Massachusetts Institute of Technology; Member, National Academy of Sciences, National Academy of Arts and Sciences, American Academy of Arts and Sciences, American Institute of Chemical Engineers, American Chemical Society, Combustion Institute (Radiation)*¹

James J. Noble, Ph.D., P.E., CE [UK] *Research Affiliate, Department of Chemical Engineering, Massachusetts Institute of Technology; Fellow, American Institute of Chemical Engineers; Member, New York Academy of Sciences (Radiation Section Coeditor)*

Adel F. Sarofim, Sc.D. *Presidential Professor of Chemical Engineering, Combustion, and Reactors, University of Utah; Member, American Institute of Chemical Engineers, American Chemical Society, Combustion Institute (Radiation Section Coeditor)*

Geoffrey D. Silcox, Ph.D. *Professor of Chemical Engineering, Combustion, and Reactors, University of Utah; Member, American Institute of Chemical Engineers, American Chemical Society, American Society for Engineering Education (Conduction, Convection, Heat Transfer with Phase Change, Section Coeditor)*

Phillip C. Wankat, Ph.D. *Clifton L. Lovell Distinguished Professor of Chemical Engineering, Purdue University; Member, American Institute of Chemical Engineers, American Chemical Society, International Adsorption Society (Mass Transfer Section Coeditor)*

Kent S. Knaebel, Ph.D. *President, Adsorption Research, Inc.; Member, American Institute of Chemical Engineers, American Chemical Society, International Adsorption Society; Professional Engineer (Ohio) (Mass Transfer Section Coeditor)*

HEAT TRANSFER			
Modes of Heat Transfer	5-3	Unsteady-State Conduction	5-6
HEAT TRANSFER BY CONDUCTION		One-Dimensional Conduction: Lumped and Distributed Analysis	5-6
Fourier's Law	5-3	Example 2: Correlation of First Eigenvalues by Eq. (5-22)	5-6
Thermal Conductivity	5-3	Example 3: One-Dimensional, Unsteady Conduction Calculation ..	5-6
Steady-State Conduction	5-3	Example 4: Rule of Thumb for Time Required to Diffuse a Distance R	5-6
One-Dimensional Conduction	5-3	One-Dimensional Conduction: Semi-infinite Plate	5-7
Conduction with Resistances in Series	5-5	HEAT TRANSFER BY CONVECTION	
Example 1: Conduction with Resistances in Series and Parallel	5-5	Convective Heat-Transfer Coefficient	5-7
Conduction with Heat Source	5-5	Individual Heat-Transfer Coefficient	5-7
Two- and Three-Dimensional Conduction	5-5		

*The contribution of James G. Knudsen, Ph.D., coeditor of this section in the seventh edition, is acknowledged.

¹Professor H. C. Hottel was the principal author of the radiation section in this *Handbook*, from the first edition in 1934 through the seventh edition in 1997. His classic zone method remains the basis for the current revision.

5-2 HEAT AND MASS TRANSFER

Overall Heat-Transfer Coefficient and Heat Exchangers	5-7
Representation of Heat-Transfer Coefficients	5-7
Natural Convection	5-8
External Natural Flow for Various Geometries	5-8
Simultaneous Heat Transfer by Radiation and Convection	5-8
Mixed Forced and Natural Convection	5-8
Enclosed Spaces	5-8
Example 5: Comparison of the Relative Importance of Natural Convection and Radiation at Room Temperature	5-8
Forced Convection	5-9
Flow in Round Tubes	5-9
Flow in Noncircular Ducts	5-9
Example 6: Turbulent Internal Flow	5-10
Coiled Tubes	5-10
External Flows	5-10
Flow-through Tube Banks	5-10
Jackets and Coils of Agitated Vessels	5-12
Nonnewtonian Fluids	5-12

HEAT TRANSFER WITH CHANGE OF PHASE

Condensation	5-12
Condensation Mechanisms	5-12
Condensation Coefficients	5-12
Boiling (Vaporization) of Liquids	5-14
Boiling Mechanisms	5-14
Boiling Coefficients	5-15

HEAT TRANSFER BY RADIATION

Introduction	5-16
Thermal Radiation Fundamentals	5-16
Introduction to Radiation Geometry	5-16
Blackbody Radiation	5-16
Blackbody Displacement Laws	5-18
Radiative Properties of Opaque Surfaces	5-19
Emissance and Absorptance	5-19
View Factors and Direct Exchange Areas	5-20
Example 7: The Crossed-Strings Method	5-23
Example 8: Illustration of Exchange Area Algebra	5-24
Radiative Exchange in Enclosures—The Zone Method	5-24
Total Exchange Areas	5-24
General Matrix Formulation	5-24
Explicit Matrix Solution for Total Exchange Areas	5-25
Zone Methodology and Conventions	5-25
The Limiting Case of a Transparent Medium	5-26
The Two-Zone Enclosure	5-26
Multizone Enclosures	5-27
Some Examples from Furnace Design	5-28
Example 9: Radiation Pyrometry	5-28
Example 10: Furnace Simulation via Zoning	5-29
Allowance for Specular Reflection	5-30
An Exact Solution to the Integral Equations—The Hohlraum	5-30
Radiation from Gases and Suspended Particulate Matter	5-30
Introduction	5-30
Emissivities of Combustion Products	5-31
Example 11: Calculations of Gas Emissivity and Absorptivity	5-32
Flames and Particle Clouds	5-34
Radiative Exchange with Participating Media	5-35
Energy Balances for Volume Zones—The Radiation Source Term	5-35

Weighted Sum of Gray Gas (WSGG) Spectral Model	5-35
The Zone Method and Directed Exchange Areas	5-36
Algebraic Formulas for a Single Gas Zone	5-37
Engineering Approximations for Directed Exchange Areas	5-38
Example 12: WSGG Clear plus Gray Gas Emissivity Calculations	5-38
Engineering Models for Fuel-Fired Furnaces	5-39
Input/Output Performance Parameters for Furnace Operation	5-39
The Long Plug Flow Furnace (LPFF) Model	5-39
The Well-Stirred Combustion Chamber (WSCC) Model	5-40
Example 13: WSCC Furnace Model Calculations	5-41
WSCC Model Utility and More Complex Zoning Models	5-43

MASS TRANSFER

Introduction	5-45
Fick's First Law	5-45
Mutual Diffusivity, Mass Diffusivity, Interdiffusion Coefficient	5-45
Self-Diffusivity	5-45
Tracer Diffusivity	5-45
Mass-Transfer Coefficient	5-45
Problem Solving Methods	5-45
Continuity and Flux Expressions	5-49
Material Balances	5-49
Flux Expressions: Simple Integrated Forms of Fick's First Law	5-49
Stefan-Maxwell Equations	5-50
Diffusivity Estimation—Gases	5-50
Binary Mixtures—Low Pressure—Nonpolar Components	5-50
Binary Mixtures—Low Pressure—Polar Components	5-52
Binary Mixtures—High Pressure	5-52
Self-Diffusivity	5-52
Supercritical Mixtures	5-52
Low-Pressure/Multicomponent Mixtures	5-53
Diffusivity Estimation—Liquids	5-53
Stokes-Einstein and Free-Volume Theories	5-53
Dilute Binary Nonelectrolytes: General Mixtures	5-54
Binary Mixtures of Gases in Low-Viscosity, Nonelectrolyte Liquids	5-55
Dilute Binary Mixtures of a Nonelectrolyte in Water	5-55
Dilute Binary Hydrocarbon Mixtures	5-55
Dilute Binary Mixtures of Nonelectrolytes with Water as the Solute	5-55
Dilute Dispersions of Macromolecules in Nonelectrolytes	5-55
Concentrated, Binary Mixtures of Nonelectrolytes	5-55
Binary Electrolyte Mixtures	5-57
Multicomponent Mixtures	5-57
Diffusion of Fluids in Porous Solids	5-58
Interphase Mass Transfer	5-59
Mass-Transfer Principles: Dilute Systems	5-59
Mass-Transfer Principles: Concentrated Systems	5-60
HTU (Height Equivalent to One Transfer Unit)	5-61
NTU (Number of Transfer Units)	5-61
Definitions of Mass-Transfer Coefficients \hat{k}_G and \hat{k}_L	5-61
Simplified Mass-Transfer Theories	5-61
Mass-Transfer Correlations	5-62
Effects of Total Pressure on \hat{k}_G and \hat{k}_L	5-68
Effects of Temperature on \hat{k}_G and \hat{k}_L	5-68
Effects of System Physical Properties on \hat{k}_G and \hat{k}_L	5-74
Effects of High Solute Concentrations on \hat{k}_G and \hat{k}_L	5-74
Influence of Chemical Reactions on \hat{k}_G and \hat{k}_L	5-74
Effective Interfacial Mass-Transfer Area a	5-83
Volumetric Mass-Transfer Coefficients \hat{k}_{cA} and \hat{k}_{lA}	5-83
Chilton-Colburn Analogy	5-83

HEAT TRANSFER

GENERAL REFERENCES: Arpaci, *Conduction Heat Transfer*, Addison-Wesley, 1966. Arpaci, *Convection Heat Transfer*, Prentice-Hall, 1984. Arpaci, *Introduction to Heat Transfer*, Prentice-Hall, 1999. Baehr and Stephan, *Heat and Mass Transfer*, Springer, Berlin, 1998. Bejan, *Convection Heat Transfer*, Wiley, 1995. Carslaw and Jaeger, *Conduction of Heat in Solids*, Oxford University Press, 1959. Edwards, *Radiation Heat Transfer Notes*, Hemisphere Publishing, 1981. Hottel and Sarofim, *Radiative Transfer*, McGraw-Hill, 1967. Incropera and DeWitt, *Fundamentals of Heat and Mass Transfer*, 5th ed., Wiley, 2002. Kays and Crawford, *Convective Heat and Mass Transfer*, 3d ed., McGraw-Hill, 1993. Mills, *Heat Transfer*, 2d ed., Prentice-Hall, 1999. Modest, *Radiative Heat Transfer*, McGraw-Hill, 1993. Patankar, *Numerical Heat Transfer and Fluid Flow*, Taylor and Francis, London, 1980. Pletcher, Anderson, and Tannehill, *Computational Fluid Mechanics and Heat Transfer*, 2d ed., Taylor and Francis, London, 1997. Rohsenow, Hartnett, and Cho, *Handbook of Heat Transfer*, 3d ed., McGraw-Hill, 1998. Siegel and Howell, *Thermal Radiation Heat Transfer*, 4th ed., Taylor and Francis, London, 2001.

MODES OF HEAT TRANSFER

Heat is energy transferred due to a difference in temperature. There are three modes of heat transfer: conduction, convection, and radiation. All three may act at the same time. Conduction is the transfer of energy between adjacent particles of matter. It is a local phenomenon and can only occur through matter. Radiation is the transfer of energy from a point of higher temperature to a point of lower energy by electromagnetic radiation. Radiation can act at a distance through transparent media and vacuum. Convection is the transfer of energy by conduction and radiation in moving, fluid media. The motion of the fluid is an essential part of convective heat transfer.

HEAT TRANSFER BY CONDUCTION

FOURIER'S LAW

The heat flux due to conduction in the x direction is given by Fourier's law

$$\dot{Q} = -kA \frac{dT}{dx} \quad (5-1)$$

where \dot{Q} is the rate of heat transfer (W), k is the thermal conductivity [W/(m·K)], A is the area perpendicular to the x direction, and T is temperature (K). For the homogeneous, one-dimensional plane shown in Fig. 5-1a, with constant k , the integrated form of (5-1) is

$$\dot{Q} = kA \frac{T_1 - T_2}{\Delta x} \quad (5-2)$$

where Δx is the thickness of the plane. Using the thermal circuit shown in Fig. 5-1b, Eq. (5-2) can be written in the form

$$\dot{Q} = \frac{T_1 - T_2}{\Delta x/kA} = \frac{T_1 - T_2}{R} \quad (5-3)$$

where R is the thermal resistance (K/W).

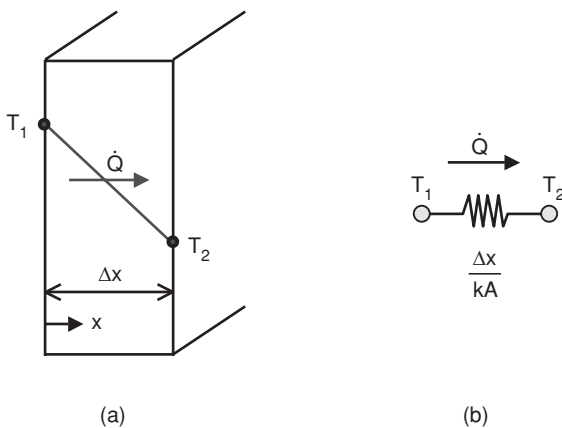


FIG. 5-1 Steady, one-dimensional conduction in a homogeneous planar wall with constant k . The thermal circuit is shown in (b) with thermal resistance $\Delta x/(kA)$.

THERMAL CONDUCTIVITY

The thermal conductivity k is a transport property whose value for a variety of gases, liquids, and solids is tabulated in Sec. 2. Section 2 also provides methods for predicting and correlating vapor and liquid thermal conductivities. The thermal conductivity is a function of temperature, but the use of constant or averaged values is frequently sufficient. Room temperature values for air, water, concrete, and copper are 0.026, 0.61, 1.4, and 400 W/(m·K). Methods for estimating contact resistances and the thermal conductivities of composites and insulation are summarized by Gebhart, *Heat Conduction and Mass Diffusion*, McGraw-Hill, 1993, p. 399.

STEADY-STATE CONDUCTION

One-Dimensional Conduction In the absence of energy source terms, \dot{Q} is constant with distance, as shown in Fig. 5-1a. For steady conduction, the integrated form of (5-1) for a planar system with constant k and A is Eq. (5-2) or (5-3). For the general case of variables k (k is a function of temperature) and A (cylindrical and spherical systems with radial coordinate r , as sketched in Fig. 5-2), the average heat-transfer area and thermal conductivity are defined such that

$$\dot{Q} = \overline{kA} \frac{T_1 - T_2}{\Delta x} = \frac{T_1 - T_2}{R} \quad (5-4)$$

For a thermal conductivity that depends linearly on T ,

$$k = k_0(1 + \gamma T) \quad (5-5)$$

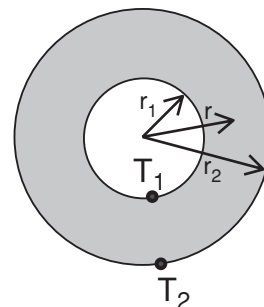


FIG. 5-2 The hollow sphere or cylinder.

5-4 HEAT AND MASS TRANSFER

Nomenclature and Units—Heat Transfer by Conduction, by Convection, and with Phase Change

Symbol	Definition	SI units	Symbol	Definition	SI units
A	Area for heat transfer	m^2	Ra_x	Rayleigh number, $\beta \Delta T g x^3 / \nu \alpha$	
A_c	Cross-sectional area	m^2	Re_D	Reynolds number, GD/μ	
A_f	Area for heat transfer for finned portion of tube	m^2	S	Volumetric source term	W/m^3
A_i	Inside area of tube		S	Cross-sectional area	m^2
A_o	External area of bare, unfinned tube	m^2	S_1	Fourier spatial function	
A_{of}	External area of tube before tubes are attached = A_o		t	Time	s
A_T	Total external area of finned tube	m^2	t_{sv}	Saturated-vapor temperature	K
A_{uf}	Area for heat transfer for unfinned portion of finned tube	m^2	t_s	Surface temperature	K
A_1	First Fourier coefficient		T	Temperature	K or °C
a_c	Cross-sectional area of fin	m^2	T_b	Bulk or mean temperature at a given cross section	K
b	Geometry; $b = 1$, plane; $b = 2$, cylinder; $b = 3$, sphere		\bar{T}_b	Bulk mean temperature, $(T_{b,in} + T_{b,out})/2$	K
b_f	Height of fin	m	T_C	Temperature of cold surface in enclosure	K
B_1	First Fourier coefficient		T_f	Film temperature, $(T_s + T_\infty)/2$	K
Bi	Biot number, hR/k		T_H	Temperature of hot surface in enclosure	K
c	Specific heat	J/(kg·K)	T_i	Initial temperature	K
c_p	Specific heat, constant pressure	J/(kg·K)	T_e	Temperature of free stream	K
D	Diameter	m	T_s	Temperature of surface	K
D_i	Inner diameter	m	T_∞	Temperature of fluid in contact with a solid surface	K
D_o	Outer diameter	m	U	Overall heat-transfer coefficient	$W/(m^2 \cdot K)$
f	Fanning friction factor		V	Volume	m^3
Fo	Dimensionless time or Fourier number, $\alpha t/R^2$		V_F	Velocity of fluid approaching a bank of finned tubes	m/s
g_c	Conversion factor	1.0 kg·m/(N·s ²)	V_∞	Velocity upstream of tube bank	m/s
g	Acceleration of gravity, 9.81 m/s ²	m^2/s	W_F	Total rate of vapor condensation on one tube	kg/s
G	Mass velocity, \dot{m}/A_c ; G_e for vapor mass velocity	kg/(m ² ·s)	x	Cartesian coordinate direction, characteristic dimension of a surface, or distance from entrance	m
G_{max}	Mass velocity through minimum free area between rows of tubes normal to the fluid stream	kg/(m ² ·s)	x	Vapor quality, x_i for inlet and x_o for outlet	
Gz	Graetz number = Re Pr		\tilde{z}_p	Distance (perimeter) traveled by fluid across fin	m
\bar{h}	Heat-transfer coefficient	$W/(m^2 \cdot K)$	Greek Symbols		
h	Average heat-transfer coefficient	$W/(m^2 \cdot K)$	α	Thermal diffusivity, $k/(\rho c)$	m^2/s
h_f	Heat-transfer coefficient for finned-tube exchangers based on total external surface	$W/(m^2 \cdot K)$	β	Volumetric coefficient of expansion	K^{-1}
$h_{f,0}$	Outside heat-transfer coefficient calculated for a bare tube for use with Eq. (5-73)	$W/(m^2 \cdot K)$	β'	Contact angle between a bubble and a surface	°
h_{fi}	Effective outside heat-transfer coefficient based on inside area of a finned tube	$W/(m^2 \cdot K)$	Γ	Mass flow rate per unit length perpendicular to flow	kg/(m·s)
h_i	Heat-transfer coefficient at inside tube surface	$W/(m^2 \cdot K)$	ΔP	Pressure drop	Pa
h_o	Heat-transfer coefficient at outside tube surface	$W/(m^2 \cdot K)$	Δt	Temperature difference	K
h_{am}	Heat-transfer coefficient for use with ΔT_{am} ; see Eq. (5-33)	$W/(m^2 \cdot K)$	ΔT	Temperature difference	K
h_{im}	Heat-transfer coefficient for use with ΔT_{im} ; see Eq. (5-32)	$W/(m^2 \cdot K)$	ΔT_{am}	Arithmetic mean temperature difference, see Eq. (5-32)	K
\bar{k}	Thermal conductivity	$W/(m \cdot K)$	ΔT_{lm}	Logarithmic mean temperature difference, see Eq. (5-33)	K
k	Average thermal conductivity	$W/(m \cdot K)$	Δx	Thickness of plane wall for conduction	m
L	Length of cylinder or length of flat plate in direction of flow or downstream distance. Length of heat-transfer surface	m	δ_1	First dimensionless eigenvalue	
m	Fin parameter defined by Eq. (5-75).		$\delta_{1,0}$	First dimensionless eigenvalue as Bi approaches 0	
\dot{m}	Mass flow rate	kg/s	$\delta_{1,\infty}$	First dimensionless eigenvalue as Bi approaches ∞	
Nu_D	Nusselt number based on diameter D , hD/k		δ_s	Correction factor, ratio of nonnewtonian to newtonian shear rates	
\bar{Nu}_D	Average Nusselt number based on diameter D , $\bar{h}D/k$		ϵ	Emissivity of a surface	
Nu_{im}	Nusselt number based on h_{im}		ζ	Dimensionless distance, r/R	
n'	Flow behavior index for nonnewtonian fluids		θ/θ_1	Dimensionless temperature, $(T - T_\infty)/(T_1 - T_\infty)$	
p	Perimeter	m	λ	Latent heat (enthalpy) of vaporization (condensation)	J/kg
p_f	Fin perimeter	m	μ	Viscosity; μ_L , viscosity of liquid; μ_g , μ_v , viscosity of gas or vapor	kg/(m·s)
p'	Center-to-center spacing of tubes in a bundle	m	ν	Kinematic viscosity, μ/ρ	m^2/s
P	Absolute pressure; P_c for critical pressure	kPa	ρ	Density; ρ_L , ρ_l for density of liquid; ρ_G , ρ_v for density of vapor	kg/m ³
Pr	Prandtl number, ν/α		σ	Stefan-Boltzmann constant, 5.67×10^{-8}	$W/(m^2 \cdot K^4)$
q	Rate of heat transfer	W	σ	Surface tension between and liquid and its vapor	N/m
Q	Amount of heat transfer	J	τ	Time constant, time scale	s
\dot{Q}	Rate of heat transfer	W	Ω	Efficiency of fin	
\dot{Q}/Q_i	Heat loss fraction, $Q/[\rho c V(T_i - T_\infty)]$				
r	Distance from center in plate, cylinder, or sphere	m			
R	Thermal resistance or radius	K/W or m			

and the average heat thermal conductivity is

$$\bar{k} = k_0(1 + \gamma\bar{T}) \quad (5-6)$$

where $\bar{T} = 0.5(T_1 + T_2)$.

For cylinders and spheres, A is a function of radial position (see Fig. 5-2): $2\pi rL$ and $4\pi r^2$, where L is the length of the cylinder. For constant k , Eq. (5-4) becomes

$$\dot{Q} = \frac{T_1 - T_2}{[\ln(r_2/r_1)]/(2\pi kL)} \quad \text{cylinder} \quad (5-7)$$

and

$$\dot{Q} = \frac{T_1 - T_2}{(r_2 - r_1)/(4\pi k r_1 r_2)} \quad \text{sphere} \quad (5-8)$$

Conduction with Resistances in Series A steady-state temperature profile in a planar composite wall, with three constant thermal conductivities and no source terms, is shown in Fig. 5-3a. The corresponding thermal circuit is given in Fig. 5-3b. The rate of heat transfer through each of the layers is the same. The total resistance is the sum of the individual resistances shown in Fig. 5-3b:

$$Q = \frac{T_1 - T_2}{\frac{\Delta X_A}{k_A A} + \frac{\Delta X_B}{k_B A} + \frac{\Delta X_C}{k_C A}} = \frac{T_1 - T_2}{R_A + R_B + R_C} \quad (5-9)$$

Additional resistances in the series may occur at the surfaces of the solid if they are in contact with a fluid. The rate of convective heat transfer, between a surface of area A and a fluid, is represented by Newton's law of cooling as

$$\dot{Q} = hA(T_{\text{surface}} - T_{\text{fluid}}) = \frac{T_{\text{surface}} - T_{\text{fluid}}}{1/(hA)} \quad (5-10)$$

where $1/(hA)$ is the resistance due to convection (K/W) and the heat-transfer coefficient is h [W/(m²·K)]. For the cylindrical geometry shown in Fig. 5-2, with convection to inner and outer fluids at temperatures T_i and T_o , with heat-transfer coefficients h_i and h_o , the steady-state rate of heat transfer is

$$\dot{Q} = \frac{T_i - T_o}{\frac{1}{2\pi r_1 L h_i} + \frac{\ln(r_2/r_1)}{2\pi k L} + \frac{1}{2\pi r_2 L h_o}} = \frac{T_i - T_o}{R_i + R_1 + R_o} \quad (5-11)$$

where resistances R_i and R_o are the convective resistances at the inner and outer surfaces. The total resistance is again the sum of the resistances in series.

Example 1: Conduction with Resistances in Series and Parallel Figure 5-4 shows the thermal circuit for a furnace wall. The outside surface has a known temperature $T_2 = 625$ K. The temperature of the surroundings

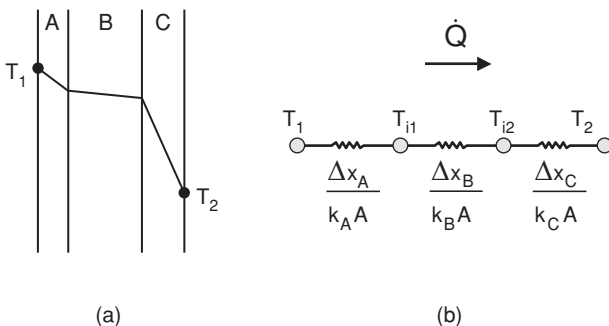


FIG. 5-3 Steady-state temperature profile in a composite wall with constant thermal conductivities k_A , k_B , and k_C and no energy sources in the wall. The thermal circuit is shown in (b). The total resistance is the sum of the three resistances shown.

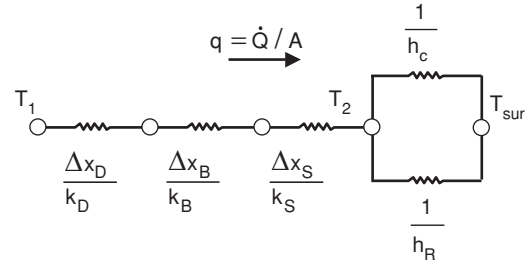


FIG. 5-4 Thermal circuit for Example 1. Steady-state conduction in a furnace wall with heat losses from the outside surface by convection (h_c) and radiation (h_r) to the surroundings at temperature T_{sur} . The thermal conductivities k_D , k_B , and k_S are constant, and there are no sources in the wall. The heat flux q has units of W/m².

T_{sur} is 290 K. We want to estimate the temperature of the inside wall T_1 . The wall consists of three layers: deposit [$k_D = 1.6$ W/(m·K), $\Delta x_D = 0.080$ m], brick [$k_B = 1.7$ W/(m·K), $\Delta x_B = 0.15$ m], and steel [$k_S = 45$ W/(m·K), $\Delta x_S = 0.00254$ m]. The outside surface loses heat by two parallel mechanisms—convection and radiation. The convective heat-transfer coefficient $h_c = 5.0$ W/(m²·K). The radiative heat-transfer coefficient $h_r = 16.3$ W/(m²·K). The latter is calculated from

$$h_r = \epsilon_2 \sigma (T_2^2 + T_{\text{sur}}^2)(T_2 + T_{\text{sur}}) \quad (5-12)$$

where the emissivity of surface 2 is $\epsilon_2 = 0.76$ and the Stefan-Boltzmann constant $\sigma = 5.67 \times 10^{-8}$ W/(m²·K⁴).

Referring to Fig. 5-4, the steady-state heat flux q (W/m²) through the wall is

$$q = \frac{\dot{Q}}{A} = \frac{T_1 - T_2}{\frac{\Delta x_D}{k_D} + \frac{\Delta x_B}{k_B} + \frac{\Delta x_S}{k_S}} = (h_c + h_r)(T_2 - T_{\text{sur}})$$

Solving for T_1 gives

$$T_1 = T_2 + \left(\frac{\Delta x_D}{k_D} + \frac{\Delta x_B}{k_B} + \frac{\Delta x_S}{k_S} \right) (h_c + h_r)(T_2 - T_{\text{sur}})$$

and

$$T_1 = 625 + \left(\frac{0.080}{1.6} + \frac{0.15}{1.7} + \frac{0.00254}{45} \right) (5.0 + 16.3)(625 - 290) = 1610 \text{ K}$$

Conduction with Heat Source Application of the law of conservation of energy to a one-dimensional solid, with the heat flux given by (5-1) and volumetric source term S (W/m³), results in the following equations for steady-state conduction in a flat plate of thickness $2R$ ($b = 1$), a cylinder of diameter $2R$ ($b = 2$), and a sphere of diameter $2R$ ($b = 3$). The parameter b is a measure of the curvature. The thermal conductivity is constant, and there is convection at the surface, with heat-transfer coefficient h and fluid temperature T_∞ .

$$\frac{d}{dr} \left(r^{b-1} \frac{dT}{dr} \right) + \frac{S}{k} r^{b-1} = 0$$

$$\frac{dT(0)}{dr} = 0 \quad (\text{symmetry condition}) \quad (5-13)$$

$$-k \frac{dT}{dr} = h[T(R) - T_\infty]$$

The solutions to (5-13), for uniform S , are

$$\frac{T(r) - T_\infty}{SR^2/k} = \frac{1}{2b} \left[1 - \left(\frac{r}{R} \right)^2 \right] + \frac{1}{b\text{Bi}} \begin{cases} b = 1, \text{ plate, thickness } 2R \\ b = 2, \text{ cylinder, diameter } 2R \\ b = 3, \text{ sphere, diameter } 2R \end{cases} \quad (5-14)$$

where $\text{Bi} = hR/k$ is the Biot number. For $\text{Bi} \ll 1$, the temperature in the solid is uniform. For $\text{Bi} \gg 1$, the surface temperature $T(R) = T_\infty$.

Two- and Three-Dimensional Conduction Application of the law of conservation of energy to a three-dimensional solid, with the

5-6 HEAT AND MASS TRANSFER

heat flux given by (5-1) and volumetric source term S (W/m^3), results in the following equation for steady-state conduction in rectangular coordinates.

$$\frac{\partial}{\partial x} \left(k \frac{\partial T}{\partial x} \right) + \frac{\partial}{\partial y} \left(k \frac{\partial T}{\partial y} \right) + \frac{\partial}{\partial z} \left(k \frac{\partial T}{\partial z} \right) + S = 0 \quad (5-15)$$

Similar equations apply to cylindrical and spherical coordinate systems. Finite difference, finite volume, or finite element methods are generally necessary to solve (5-15). Useful introductions to these numerical techniques are given in the General References and Sec. 3. Simple forms of (5-15) (constant k , uniform S) can be solved analytically. See Arpaci, *Conduction Heat Transfer*, Addison-Wesley, 1966, p. 180, and Carslaw and Jaeger, *Conduction of Heat in Solids*, Oxford University Press, 1959. For problems involving heat flow between two surfaces, each isothermal, with all other surfaces being adiabatic, the shape factor approach is useful (Mills, *Heat Transfer*, 2d ed., Prentice-Hall, 1999, p. 164).

UNSTEADY-STATE CONDUCTION

Application of the law of conservation of energy to a three-dimensional solid, with the heat flux given by (5-1) and volumetric source term S (W/m^3), results in the following equation for unsteady-state conduction in rectangular coordinates.

$$\rho c \frac{\partial T}{\partial t} = \frac{\partial}{\partial x} \left(k \frac{\partial T}{\partial x} \right) + \frac{\partial}{\partial y} \left(k \frac{\partial T}{\partial y} \right) + \frac{\partial}{\partial z} \left(k \frac{\partial T}{\partial z} \right) + S \quad (5-16)$$

The energy storage term is on the left-hand side, and ρ and c are the density (kg/m^3) and specific heat [$J/(kg \cdot K)$]. Solutions to (5-16) are generally obtained numerically (see General References and Sec. 3). The one-dimensional form of (5-16), with constant k and no source term, is

$$\frac{\partial T}{\partial t} = \alpha \frac{\partial^2 T}{\partial x^2} \quad (5-17)$$

where $\alpha = k/(\rho c)$ is the thermal diffusivity (m^2/s).

One-Dimensional Conduction: Lumped and Distributed Analysis The one-dimensional transient conduction equations in rectangular ($b = 1$), cylindrical ($b = 2$), and spherical ($b = 3$) coordinates, with constant k , initial uniform temperature T_i , $S = 0$, and convection at the surface with heat-transfer coefficient h and fluid temperature T_∞ , are

$$\frac{\partial T}{\partial t} = \frac{\alpha}{r^{b-1}} \frac{\partial}{\partial r} \left(r^{b-1} \frac{\partial T}{\partial r} \right) \quad \begin{cases} b = 1, \text{ plate, thickness } 2R \\ b = 2, \text{ cylinder, diameter } 2R \\ b = 3, \text{ sphere, diameter } 2R \end{cases}$$

$$\text{for } t < 0, \quad T = T_i \quad (\text{initial temperature}) \quad (5-18)$$

$$\text{at } r = 0, \quad \frac{\partial T}{\partial r} = 0 \quad (\text{symmetry condition})$$

$$\text{at } r = R, \quad -k \frac{\partial T}{\partial r} = h(T - T_\infty)$$

The solutions to (5-18) can be compactly expressed by using dimensionless variables: (1) temperature $\theta/\theta_i = [T(r,t) - T_\infty]/(T_i - T_\infty)$; (2) heat loss fraction $Q/Q_i = Q/[\rho c V (T_i - T_\infty)]$, where V is volume; (3) distance from center $\zeta = r/R$; (4) time $Fo = \alpha t/R^2$, and (5) Biot number $Bi = hR/k$. The temperature and heat loss are functions of ζ , Fo , and Bi .

When the Biot number is small, $Bi < 0.2$, the temperature of the solid is nearly uniform and a lumped analysis is acceptable. The solution to the lumped analysis of (5-18) is

$$\frac{\theta}{\theta_i} = \exp\left(-\frac{hA}{\rho c V} t\right) \quad \text{and} \quad \frac{Q}{Q_i} = 1 - \exp\left(-\frac{hA}{\rho c V} t\right) \quad (5-19)$$

where A is the active surface area and V is the volume. The time scale for the lumped problem is

$$\tau = \frac{\rho c V}{hA} \quad (5-20)$$

TABLE 5-1 Fourier Coefficients and Spatial Functions for Use in Eqs. (5-21)

Geometry	A_1	B_1	S_1
Plate	$\frac{2\sin\delta_1}{\delta_1 + \sin\delta_1\cos\delta_1}$	$\frac{2Bi^2}{\delta_1^2(Bi^2 + Bi + \delta_1^2)}$	$\cos(\delta_1\zeta)$
Cylinder	$\frac{2J_1(\delta_1)}{\delta_1[J_0'(\delta_1) + J_1'(\delta_1)]}$	$\frac{4Bi^2}{\delta_1^2(\delta_1^2 + Bi^2)}$	$J_0(\delta_1\zeta)$
Sphere	$\frac{2Bi[\delta_1^2 + (Bi - 1)^2]^{1/2}}{\delta_1^2 + Bi^2 - Bi}$	$\frac{6Bi^2}{\delta_1^2(\delta_1^2 + Bi^2 - Bi)}$	$\frac{\sin\delta_1\zeta}{\delta_1\zeta}$

The time scale is the time required for most of the change in θ/θ_i or Q/Q_i to occur. When $t = \tau$, $\theta/\theta_i = \exp(-1) = 0.368$ and roughly two-thirds of the possible change has occurred.

When a lumped analysis is not valid ($Bi > 0.2$), the single-term solutions to (5-18) are convenient:

$$\frac{\theta}{\theta_i} = A_1 \exp(-\delta_1^2 Fo) S_1(\delta_1\zeta) \quad \text{and} \quad \frac{Q}{Q_i} = 1 - B_1 \exp(-\delta_1^2 Fo) \quad (5-21)$$

where the first Fourier coefficients A_1 and B_1 and the spatial functions S_1 are given in Table 5-1. The first eigenvalue δ_1 is given by (5-22) in conjunction with Table 5-2. The one-term solutions are accurate to within 2 percent when $Fo > Fo_c$. The values of the critical Fourier number Fo_c are given in Table 5-2.

The first eigenvalue is accurately correlated by (Yovanovich, Chap. 3 of Rohsenow, Hartnett, and Cho, *Handbook of Heat Transfer*, 3d ed., McGraw-Hill, 1998, p. 3.25)

$$\delta_1 = \frac{\delta_{1,\infty}}{[1 + (\delta_{1,\infty}/\delta_{1,0})^n]^{1/n}} \quad (5-22)$$

Equation (5-22) gives values of δ_1 that differ from the exact values by less than 0.4 percent, and it is valid for all values of Bi . The values of $\delta_{1,\infty}$, $\delta_{1,0}$, n , and Fo_c are given in Table 5-2.

Example 2: Correlation of First Eigenvalues by Eq. (5-22) As an example of the use of Eq. (5-22), suppose that we want δ_1 for the flat plate with $Bi = 5$. From Table 5-2, $\delta_{1,\infty} = \pi/2$, $\delta_{1,0} = \sqrt{Bi} = \sqrt{5}$, and $n = 2.139$. Equation (5-22) gives

$$\delta_1 = \frac{\pi/2}{[1 + (\pi/2/\sqrt{5})^{2.139}]^{1/2.139}} = 1.312$$

The tabulated value is 1.3138.

Example 3: One-Dimensional, Unsteady Conduction Calculation As an example of the use of Eq. (5-21), Table 5-1, and Table 5-2, consider the cooking time required to raise the center of a spherical, 8-cm-diameter dumpling from 20 to 80°C. The initial temperature is uniform. The dumpling is heated with saturated steam at 95°C. The heat capacity, density, and thermal conductivity are estimated to be $c = 3500$ J/(kg·K), $\rho = 1000$ kg/m³, and $k = 0.5$ W/(m·K), respectively.

Because the heat-transfer coefficient for condensing steam is of order 10^4 , the $Bi \rightarrow \infty$ limit in Table 5-2 is a good choice and $\delta_1 = \pi$. Because we know the desired temperature at the center, we can calculate θ/θ_i and then solve (5-21) for the time.

$$\frac{\theta}{\theta_i} = \frac{T(0,t) - T_\infty}{T_i - T_\infty} = \frac{80 - 95}{20 - 95} = 0.200$$

For $Bi \rightarrow \infty$, A_1 in Table 5-1 is 2 and for $\zeta = 0$, S_1 in Table 5-1 is 1. Equation (5-21) becomes

$$\frac{\theta}{\theta_i} = 2 \exp(-\pi^2 Fo) = 2 \exp\left(-\frac{\pi^2 \alpha t}{R^2}\right)$$

TABLE 5-2 First Eigenvalues for $Bi \rightarrow 0$ and $Bi \rightarrow \infty$ and Correlation Parameter n

The single-term approximations apply only if $Fo \geq Fo_c$.

Geometry	$Bi \rightarrow 0$	$Bi \rightarrow \infty$	n	Fo_c
Plate	$\delta_1 \rightarrow \sqrt{Bi}$	$\delta_1 \rightarrow \pi/2$	2.139	0.24
Cylinder	$\delta_1 \rightarrow \sqrt{2Bi}$	$\delta_1 \rightarrow 2.4048255$	2.238	0.21
Sphere	$\delta_1 \rightarrow \sqrt{3Bi}$	$\delta_1 \rightarrow \pi$	2.314	0.18

Solving for t gives the desired cooking time.

$$t = -\frac{R^2}{\alpha\pi^2} \ln \frac{\theta}{2\theta_1} = -\frac{(0.04 \text{ m})^2}{1.43 \times 10^{-7} (\text{m}^2/\text{s})\pi^2} \ln \frac{0.2}{2} = 43.5 \text{ min}$$

Example 4: Rule of Thumb for Time Required to Diffuse a Distance R A general rule of thumb for estimating the time required to diffuse a distance R is obtained from the one-term approximations. Consider the equation for the temperature of a flat plate of thickness $2R$ in the limit as $\text{Bi} \rightarrow \infty$. From Table 5-2, the first eigenvalue is $\delta_1 = \pi/2$, and from Table 5-1,

$$\frac{\theta}{\theta_1} = A_1 \exp\left[-\left(\frac{\pi}{2}\right)^2 \frac{\alpha t}{R^2}\right] \cos \delta_1 \zeta$$

When $t = R^2/\alpha$, the temperature ratio at the center of the plate ($\zeta = 0$) has decayed to $\exp(-\pi^2/4)$, or 8 percent of its initial value. We conclude that *diffusion through a distance R takes roughly R^2/α units of time, or alternatively, the distance diffused in time t is about $(\alpha t)^{1/2}$.*

One-Dimensional Conduction: Semi-infinite Plate Consider a semi-infinite plate with an initial uniform temperature T_i . Suppose that the temperature of the surface is suddenly raised to T_∞ ; that is, the heat-transfer coefficient is infinite. The unsteady temperature of the plate is

$$\frac{T(x,t) - T_\infty}{T_i - T_\infty} = \text{erfc}\left(\frac{x}{2\sqrt{\alpha t}}\right) \quad (5-23)$$

where $\text{erf}(z)$ is the error function. The depth to which the heat penetrates in time t is approximately $(12\alpha t)^{1/2}$.

If the heat-transfer coefficient is finite,

$$\frac{T(x,t) - T_\infty}{T_i - T_\infty} = \text{erfc}\left(\frac{x}{2\sqrt{\alpha t}}\right) - \exp\left(\frac{hx}{k} + \frac{h^2\alpha t}{k^2}\right) \text{erfc}\left(\frac{x}{2\sqrt{\alpha t}} + \frac{h\sqrt{\alpha t}}{k}\right) \quad (5-24)$$

where $\text{erfc}(z)$ is the complementary error function. Equations (5-23) and (5-24) are both applicable to finite plates provided that their half-thickness is greater than $(12\alpha t)^{1/2}$.

Two- and Three-Dimensional Conduction The one-dimensional solutions discussed above can be used to construct solutions to multidimensional problems. The unsteady temperature of a rectangular, solid box of height, length, and width $2H$, $2L$, and $2W$, respectively, with governing equations in each direction as in (5-18), is

$$\left(\frac{\theta}{\theta_1}\right)_{2H \times 2L \times 2W} = \left(\frac{\theta}{\theta_1}\right)_{2H} \left(\frac{\theta}{\theta_1}\right)_{2L} \left(\frac{\theta}{\theta_1}\right)_{2W} \quad (5-25)$$

Similar products apply for solids with other geometries, e.g., semi-infinite, cylindrical rods.

HEAT TRANSFER BY CONVECTION

CONVECTIVE HEAT-TRANSFER COEFFICIENT

Convection is the transfer of energy by conduction and radiation in moving, fluid media. The motion of the fluid is an essential part of convective heat transfer. A key step in calculating the rate of heat transfer by convection is the calculation of the heat-transfer coefficient. This section focuses on the estimation of heat-transfer coefficients for natural and forced convection. The conservation equations for mass, momentum, and energy, as presented in Sec. 6, can be used to calculate the rate of convective heat transfer. Our approach in this section is to rely on correlations.

In many cases of industrial importance, heat is transferred from one fluid, through a solid wall, to another fluid. The transfer occurs in a heat exchanger. Section 11 introduces several types of heat exchangers, design procedures, overall heat-transfer coefficients, and mean temperature differences. Section 3 introduces dimensional analysis and the dimensionless groups associated with the heat-transfer coefficient.

Individual Heat-Transfer Coefficient The local rate of convective heat transfer between a surface and a fluid is given by Newton's law of cooling

$$q = h(T_{\text{surface}} - T_{\text{fluid}}) \quad (5-26)$$

where h [$\text{W}/(\text{m}^2 \cdot \text{K})$] is the local heat-transfer coefficient and q is the energy flux (W/m^2). The definition of h is arbitrary, depending on whether the bulk fluid, centerline, free stream, or some other temperature is used for T_{fluid} . The heat-transfer coefficient may be defined on an average basis as noted below.

Consider a fluid with bulk temperature T_f flowing in a cylindrical tube of diameter D , with constant wall temperature T_s . An energy balance on a short section of the tube yields

$$c_p \dot{m} \frac{dT}{dx} = \pi D h (T_s - T) \quad (5-27)$$

where c_p is the specific heat at constant pressure [$\text{J}/(\text{kg} \cdot \text{K})$], \dot{m} is the mass flow rate (kg/s), and x is the distance from the inlet. If the temperature of the fluid at the inlet is T_{in} , the temperature of the fluid at a downstream distance L is

$$\frac{T(L) - T_s}{T_{\text{in}} - T_s} = \exp\left(-\frac{\bar{h}\pi DL}{\dot{m}c_p}\right) \quad (5-28)$$

The average heat-transfer coefficient \bar{h} is defined by

$$\bar{h} = \frac{1}{L} \int_0^L h \, dx \quad (5-29)$$

Overall Heat-Transfer Coefficient and Heat Exchangers A local, overall heat-transfer coefficient U for the cylindrical geometry shown in Fig. 5-2 is defined by using Eq. (5-11) as

$$\frac{\dot{Q}}{\Delta x} = \frac{T_i - T_o}{\frac{1}{2\pi r_1 h_i} + \frac{\ln(r_2/r_1)}{2\pi k} + \frac{1}{2\pi r_2 h_o}} = 2\pi r_1 U (T_i - T_o) \quad (5-30)$$

where Δx is a short length of tube in the axial direction. Equation (5-30) defines U by using the inside perimeter $2\pi r_1$. The outer perimeter can also be used. Equation (5-30) applies to clean tubes. Additional resistances are present in the denominator for dirty tubes (see Sec. 11).

For counterflow and parallel flow heat exchanges, with high- and low-temperature fluids (T_H and T_C) and flow directions as defined in Fig. 5-5, the total heat transfer for the exchanger is given by

$$\dot{Q} = UA \Delta T_{\text{lm}} \quad (5-31)$$

where A is the area for heat exchange and the log mean temperature difference ΔT_{lm} is defined as

$$\Delta T_{\text{lm}} = \frac{(T_H - T_C)_L - (T_H - T_C)_0}{\ln[(T_H - T_C)_L / (T_H - T_C)_0]} \quad (5-32)$$

Equation (5-32) applies to both counterflow and parallel flow exchangers with the nomenclature defined in Fig. 5-5. Correction factors to ΔT_{lm} for various heat exchanger configurations are given in Sec. 11.

In certain applications, the log mean temperature difference is replaced with an arithmetic mean difference:

$$\Delta T_{\text{am}} = \frac{(T_H - T_C)_L + (T_H - T_C)_0}{2} \quad (5-33)$$

Average heat-transfer coefficients are occasionally reported based on Eqs. (5-32) and (5-33) and are written as h_{lm} and h_{am} .

Representation of Heat-Transfer Coefficients Heat-transfer coefficients are usually expressed in two ways: (1) dimensionless relations and (2) dimensional equations. Both approaches are used below. The dimensionless form of the heat-transfer coefficient is the Nusselt

5-8 HEAT AND MASS TRANSFER

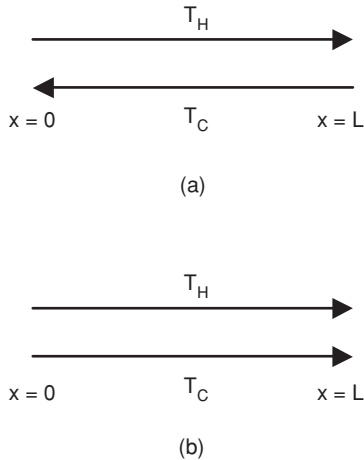


FIG. 5-5 Nomenclature for (a) counterflow and (b) parallel flow heat exchangers for use with Eq. (5-32).

number. For example, with a cylinder of diameter D in cross flow, the local Nusselt number is defined as $Nu_D = hD/k$, where k is the thermal conductivity of the fluid. The subscript D is important because different characteristic lengths can be used to define Nu . The average Nusselt number is written $\overline{Nu}_D = \overline{h}D/k$.

NATURAL CONVECTION

Natural convection occurs when a fluid is in contact with a solid surface of different temperature. Temperature differences create the density gradients that drive natural or free convection. In addition to the Nusselt number mentioned above, the key dimensionless parameters for natural convection include the Rayleigh number $Ra_x = \beta \Delta T g x^3 / \nu \alpha$ and the Prandtl number $Pr = \nu / \alpha$. The properties appearing in Ra and Pr include the volumetric coefficient of expansion β (K^{-1}); the difference ΔT between the surface (T_s) and free stream (T_∞) temperatures (K or $^\circ C$); the acceleration of gravity g (m/s^2); a characteristic dimension x of the surface (m); the kinematic viscosity ν (m^2/s); and the thermal diffusivity α (m^2/s). The volumetric coefficient of expansion for an ideal gas is $\beta = 1/T$, where T is absolute temperature. For a given geometry,

$$\overline{Nu}_x = f(Ra_x, Pr) \quad (5-34)$$

External Natural Flow for Various Geometries For vertical walls, Churchill and Chu [*Int. J. Heat Mass Transfer*, **18**, 1323 (1975)] recommend, for laminar and turbulent flow on isothermal, vertical walls with height L ,

$$\overline{Nu}_L = \left\{ 0.825 + \frac{0.387 Ra_L^{1/6}}{[1 + (0.492/Pr)^{9/16}]^{8/27}} \right\}^2 \quad (5-35)$$

where the fluid properties for Eq. (5-35) and $\overline{Nu}_L = \overline{h}L/k$ are evaluated at the film temperature $T_f = (T_s + T_\infty)/2$. This correlation is valid for all Pr and Ra_L . For vertical cylinders with boundary layer thickness much less than their diameter, Eq. (5-35) is applicable. An expression for uniform heating is available from the same reference.

For laminar and turbulent flow on isothermal, horizontal cylinders of diameter D , Churchill and Chu [*Int. J. Heat Mass Transfer*, **18**, 1049 (1975)] recommend

$$\overline{Nu}_L = \left\{ 0.60 + \frac{0.387 Ra_D^{1/6}}{[1 + (0.559/Pr)^{9/16}]^{8/27}} \right\}^2 \quad (5-36)$$

Fluid properties for (5-36) should be evaluated at the film temperature $T_f = (T_s + T_\infty)/2$. This correlation is valid for all Pr and Ra_D .

For horizontal flat surfaces, the characteristic dimension for the correlations is [Goldstein, Sparrow, and Jones, *Int. J. Heat Mass Transfer*, **16**, 1025–1035 (1973)]

$$L = \frac{A}{p} \quad (5-37)$$

where A is the area of the surface and p is the perimeter. With hot surfaces facing upward, or cold surfaces facing downward [Lloyd and Moran, ASME Paper 74-WA/HT-66 (1974)],

$$\overline{Nu}_L = \begin{cases} 0.54 Ra_L^{1/4} & 10^4 < Ra_L < 10^7 \\ 0.15 Ra_L^{1/3} & 10^7 < Ra_L < 10^{10} \end{cases} \quad (5-38)$$

and for hot surfaces facing downward, or cold surfaces facing upward,

$$\overline{Nu}_L = 0.27 Ra_L^{1/4} \quad 10^5 < Ra_L < 10^{10} \quad (5-40)$$

Fluid properties for Eqs. (5-38) to (5-40) should be evaluated at the film temperature $T_f = (T_s + T_\infty)/2$.

Simultaneous Heat Transfer by Radiation and Convection Simultaneous heat transfer by radiation and convection is treated per the procedure outlined in Examples 1 and 5. A radiative heat-transfer coefficient h_R is defined by (5-12).

Mixed Forced and Natural Convection Natural convection is commonly assisted or opposed by forced flow. These situations are discussed, e.g., by Mills (*Heat Transfer*, 2d ed., Prentice-Hall, 1999, p. 340) and Raithby and Hollands (Chap. 4 of Rohsenow, Hartnett, and Cho, *Handbook of Heat Transfer*, 3d ed., McGraw-Hill, 1998, p. 4.73).

Enclosed Spaces The rate of heat transfer across an enclosed space is described in terms of a heat-transfer coefficient based on the temperature difference between two surfaces:

$$\overline{h} = \frac{\dot{Q}/A}{T_H - T_C} \quad (5-41)$$

For rectangular cavities, the plate spacing between the two surfaces L is the characteristic dimension that defines the Nusselt and Rayleigh numbers. The temperature difference in the Rayleigh number, $Ra_L = \beta \Delta T g L^3 / \nu \alpha$ is $\Delta T = T_H - T_C$.

For a horizontal rectangular cavity heated from below, the onset of advection requires $Ra_L > 1708$. Globe and Dropkin [*J. Heat Transfer*, **81**, 24–28 (1959)] propose the correlation

$$\overline{Nu}_L = 0.069 Ra_L^{1/3} Pr^{0.074} \quad 3 \times 10^5 < Ra_L < 7 \times 10^9 \quad (5-42)$$

All properties in (5-42) are calculated at the average temperature $(T_H + T_C)/2$.

For vertical rectangular cavities of height H and spacing L , with $Pr \approx 0.7$ (gases) and $40 < H/L < 110$, the equation of Shewen et al. [*J. Heat Transfer*, **118**, 993–995 (1996)] is recommended:

$$\overline{Nu}_L = \left\{ 1 + \left[\frac{0.0665 Ra_L^{1/3}}{1 + (9000/Ra_L)^{1.4}} \right]^2 \right\}^{1/2} \quad Ra_L < 10^6 \quad (5-43)$$

All properties in (5-43) are calculated at the average temperature $(T_H + T_C)/2$.

Example 5: Comparison of the Relative Importance of Natural Convection and Radiation at Room Temperature

Estimate the heat losses by natural convection and radiation for an undraped person standing in still air. The temperatures of the air, surrounding surfaces, and skin are 19, 15, and 35 $^\circ C$, respectively. The height and surface area of the person are 1.8 m and 1.8 m 2 . The emissivity of the skin is 0.95.

We can estimate the Nusselt number by using (5-35) for a vertical, flat plate of height $L = 1.8$ m. The film temperature is $(19 + 35)/2 = 27^\circ C$. The Rayleigh number, evaluated at the film temperature, is

$$Ra_L = \frac{\beta \Delta T g L^3}{\nu \alpha} = \frac{(1/300)(35 - 19)9.81(1.8)^3}{1.589 \times 10^{-5}(2.25 \times 10^{-5})} = 8.53 \times 10^9$$

From (5-35) with $Pr = 0.707$, the Nusselt number is 240 and the average heat-transfer coefficient due to natural convection is

$$\overline{h} = \frac{k}{L} \overline{Nu}_L = \frac{0.0263}{1.8} (240) = 3.50 \frac{W}{m^2 \cdot K}$$

The radiative heat-transfer coefficient is given by (5-12):

$$h_R = \epsilon_{\text{skin}} \sigma (T_{\text{skin}}^2 + T_{\text{sur}}^2)(T_{\text{skin}} + T_{\text{sur}}) \\ = 0.95(5.67 \times 10^{-8})(308^2 + 288^2)(308 + 288) = 5.71 \frac{\text{W}}{\text{m}^2 \cdot \text{K}}$$

The total rate of heat loss is

$$\dot{Q} = \bar{h}A(T_{\text{skin}} - T_{\text{sur}}) + \bar{h}_R A(T_{\text{skin}} - T_{\text{sur}}) \\ = 3.50(1.8)(35 - 19) + 5.71(1.8)(35 - 15) = 306 \text{ W}$$

At these conditions, radiation is nearly twice as important as natural convection.

FORCED CONVECTION

Forced convection heat transfer is probably the most common mode in the process industries. Forced flows may be internal or external. This subsection briefly introduces correlations for estimating heat-transfer coefficients for flows in tubes and ducts; flows across plates, cylinders, and spheres; flows through tube banks and packed beds; heat transfer to nonevaporating falling films; and rotating surfaces. Section 11 introduces several types of heat exchangers, design procedures, overall heat-transfer coefficients, and mean temperature differences.

Flow in Round Tubes In addition to the Nusselt ($\text{Nu}_D = hD/k$) and Prandtl ($\text{Pr} = \nu/\alpha$) numbers introduced above, the key dimensionless parameter for forced convection in round tubes of diameter D is the Reynolds number $\text{Re} = GD/\mu$, where G is the mass velocity $G = \dot{m}/A_c$ and A_c is the cross-sectional area $A_c = \pi D^2/4$. For internal flow in a tube or duct, the heat-transfer coefficient is defined as

$$q = h(T_s - T_b) \quad (5-44)$$

where T_b is the bulk or mean temperature at a given cross section and T_s is the corresponding surface temperature.

For laminar flow ($\text{Re}_D < 2100$) that is fully developed, both hydrodynamically and thermally, the Nusselt number has a constant value. For a uniform wall temperature, $\text{Nu}_D = 3.66$. For a uniform heat flux through the tube wall, $\text{Nu}_D = 4.36$. In both cases, the thermal conductivity of the fluid in Nu_D is evaluated at T_b . The distance x required for a fully developed laminar velocity profile is given by $[(x/D)/\text{Re}_D] \approx 0.05$. The distance x required for fully developed velocity and thermal profiles is obtained from $[(x/D)/(\text{Re}_D \text{Pr})] \approx 0.05$.

For a constant wall temperature, a fully developed laminar velocity profile, and a developing thermal profile, the average Nusselt number is estimated by [Hausen, *Allg. Waermetech.*, **9**, 75 (1959)]

$$\bar{\text{Nu}}_D = 3.66 + \frac{0.0668(D/L) \text{Re}_D \text{Pr}}{1 + 0.04[(D/L) \text{Re}_D \text{Pr}]^{2/3}} \quad (5-45)$$

For large values of L , Eq. (5-45) approaches $\text{Nu}_D = 3.66$. Equation (5-45) also applies to developing velocity and thermal profiles conditions if $\text{Pr} \gg 1$. The properties in (5-45) are evaluated at the bulk mean temperature

$$\bar{T}_b = (T_{b,\text{in}} + T_{b,\text{out}})/2 \quad (5-46)$$

For a constant wall temperature with developing laminar velocity and thermal profiles, the average Nusselt number is approximated by [Sieder and Tate, *Ind. Eng. Chem.*, **28**, 1429 (1936)]

$$\bar{\text{Nu}}_D = 1.86 \left(\frac{D}{L} \text{Re}_D \text{Pr} \right)^{1/3} \left(\frac{\mu_b}{\mu_s} \right)^{0.14} \quad (5-47)$$

The properties, except for μ_s , are evaluated at the bulk mean temperature per (5-46) and $0.48 < \text{Pr} < 16,700$ and $0.0044 < \mu_b/\mu_s < 9.75$.

For fully developed flow in the transition region between laminar and turbulent flow, and for fully developed turbulent flow, Gnielinski's [Int. Chem. Eng., **16**, 359 (1976)] equation is recommended:

$$\text{Nu}_D = \frac{(f/2)(\text{Re}_D - 1000)(\text{Pr})}{1 + 12.7(f/2)^{1/2}(\text{Pr}^{2/3} - 1)} K \quad (5-48)$$

where $0.5 < \text{Pr} < 10^5$, $2300 < \text{Re}_D < 10^6$, $K = (\text{Pr}_b/\text{Pr}_s)^{0.11}$ for liquids ($0.05 < \text{Pr}_b/\text{Pr}_s < 20$), and $K = (T_b/T_s)^{0.45}$ for gases ($0.5 < T_b/T_s < 1.5$). The factor K corrects for variable property effects. For smooth tubes, the Fanning friction factor f is given by

$$f = 0.25(0.790 \ln \text{Re}_D - 1.64)^{-2} \quad 2300 < \text{Re}_D < 10^6 \quad (5-49)$$

TABLE 5-3 Effect of Entrance Configuration on Values of C and n in Eq. (5-53) for $\text{Pr} \approx 1$ (Gases and Other Fluids with Pr about 1)

Entrance configuration	C	n
Long calming section	0.9756	0.760
Open end, 90° edge	2.4254	0.676
180° return bend	0.9759	0.700
90° round bend	1.0517	0.629
90° elbow	2.0152	0.614

For rough pipes, approximate values of Nu_D are obtained if f is estimated by the Moody diagram of Sec. 6. Equation (5-48) is corrected for entrance effects per (5-53) and Table 5-3. Sieder and Tate [Ind. Eng. Chem., **28**, 1429 (1936)] recommend a simpler but less accurate equation for fully developed turbulent flow

$$\text{Nu}_D = 0.027 \text{Re}_D^{4/5} \text{Pr}^{1/3} \left(\frac{\mu_b}{\mu_s} \right)^{0.14} \quad (5-50)$$

where $0.7 < \text{Pr} < 16,700$, $\text{Re}_D < 10,000$, and $L/D > 10$. Equations (5-48) and (5-50) apply to both constant temperature and uniform heat flux along the tube. The properties are evaluated at the bulk temperature T_b , except for μ_s , which is at the temperature of the tube. For L/D greater than about 10, Eqs. (5-48) and (5-50) provide an estimate of Nu_D . In this case, the properties are evaluated at the bulk mean temperature per (5-46). More complicated and comprehensive predictions of fully developed turbulent convection are available in Churchill and Žajic [AIChE J., **48**, 927 (2002)] and Yu, Ozoe, and Churchill [Chem. Eng. Science, **56**, 1781 (2001)].

For fully developed turbulent flow of liquid metals, the Nusselt number depends on the wall boundary condition. For a constant wall temperature [Notter and Sleicher, Chem. Eng. Science, **27**, 2073 (1972)],

$$\text{Nu}_D = 4.8 + 0.0156 \text{Re}_D^{0.85} \text{Pr}^{0.93} \quad (5-51)$$

while for a uniform wall heat flux,

$$\text{Nu}_D = 6.3 + 0.0167 \text{Re}_D^{0.85} \text{Pr}^{0.93} \quad (5-52)$$

In both cases the properties are evaluated at T_b and $0.004 < \text{Pr} < 0.01$ and $10^4 < \text{Re}_D < 10^6$.

Entrance effects for turbulent flow with simultaneously developing velocity and thermal profiles can be significant when $L/D < 10$. Shah and Bhatti correlated entrance effects for gases ($\text{Pr} \approx 1$) to give an equation for the average Nusselt number in the entrance region (in Kaka, Shah, and Aung, eds., *Handbook of Single-Phase Convective Heat Transfer*, Chap. 3, Wiley-Interscience, 1987).

$$\frac{\bar{\text{Nu}}_D}{\text{Nu}_D} = 1 + \frac{C}{(x/D)^n} \quad (5-53)$$

where Nu_D is the fully developed Nusselt number and the constants C and n are given in Table 5-3 (Ebadian and Dong, Chap. 5 of Rohsenow, Hartnett, and Cho, *Handbook of Heat Transfer*, 3d ed., McGraw-Hill, 1998, p. 5.31). The tube entrance configuration determines the values of C and n as shown in Table 5-3.

Flow in Noncircular Ducts The length scale in the Nusselt and Reynolds numbers for noncircular ducts is the hydraulic diameter, $D_h = 4A_c/p$, where A_c is the cross-sectional area for flow and p is the wetted perimeter. Nusselt numbers for fully developed laminar flow in a variety of noncircular ducts are given by Mills (*Heat Transfer*, 2d ed., Prentice-Hall, 1999, p. 307). For turbulent flows, correlations for round tubes can be used with D replaced by D_h .

For annular ducts, the accuracy of the Nusselt number given by (5-48) is improved by the following multiplicative factors [Petukhov and Roizen, *High Temp.*, **2**, 65 (1964)].

$$\text{Inner tube heated} \quad 0.86 \left(\frac{D_i}{D_o} \right)^{-0.16}$$

$$\text{Outer tube heated} \quad 1 - 0.14 \left(\frac{D_i}{D_o} \right)^{0.6}$$

where D_i and D_o are the inner and outer diameters, respectively.

Example 6: Turbulent Internal Flow Air at 300 K, 1 bar, and 0.05 kg/s enters a channel of a plate-type heat exchanger (Mills, *Heat Transfer*, 2d ed., Prentice-Hall, 1999) that measures 1 cm wide, 0.5 m high, and 0.8 m long. The walls are at 600 K, and the mass flow rate is 0.05 kg/s. The entrance has a 90° edge. We want to estimate the exit temperature of the air.

Our approach will use (5-48) to estimate the average heat-transfer coefficient, followed by application of (5-28) to calculate the exit temperature. We assume ideal gas behavior and an exit temperature of 500 K. The estimated bulk mean temperature of the air is, by (5-46), 400 K. At this temperature, the properties of the air are $Pr = 0.690$, $\mu = 2.301 \times 10^{-5}$ kg/(m·s), $k = 0.0338$ W/(m·K), and $c_p = 1014$ J/(kg·K).

We start by calculating the hydraulic diameter $D_h = 4A_c/p$. The cross-sectional area for flow A_c is 0.005 m², and the wetted perimeter p is 1.02 m. The hydraulic diameter $D_h = 0.01961$ m. The Reynolds number is

$$Re_D = \frac{\dot{m}D_h}{A_c\mu} = \frac{0.05(0.01961)}{0.005(2.301 \times 10^{-5})} = 8521$$

The flow is in the transition region, and Eqs. (5-49) and (5-48) apply:

$$f = 0.25(0.790 \ln Re_D - 1.64)^{-2} = 0.25(0.790 \ln 8521 - 1.64)^{-2} = 0.008235$$

$$Nu_D = \frac{(f/2)(Re_D - 1000)(Pr)}{1 + 12.7(f/2)^{1/2}(Pr^{2/3} - 1)} K$$

$$= \frac{(0.008235/2)(8521 - 1000)(0.690)}{1 + 12.7(0.008235/2)^{1/2}(0.690^{2/3} - 1)} \left(\frac{400}{600}\right)^{0.45} = 21.68$$

Entrance effects are included by using (5-53) for an open end, 90° edge:

$$\overline{Nu}_D = \left[1 + \frac{C}{(x/D)^n}\right] Nu_D = \left[1 + \frac{2.4254}{(0.8/0.01961)^{0.676}}\right] (21.68) = 25.96$$

The average heat-transfer coefficient becomes

$$\bar{h} = \frac{k}{D_h} \overline{Nu}_D = \frac{0.0338}{0.01961} (25.96) = 44.75 \frac{W}{m^2 \cdot K}$$

The exit temperature is calculated from (5-28):

$$T(L) = T_s - (T_s - T_m) \exp\left(-\frac{\bar{h}pL}{\dot{m}c_p}\right)$$

$$= 600 - (600 - 300) \exp\left[-\frac{44.75(1.02)(0.8)}{0.05(1014)}\right] = 450 \text{ K}$$

We conclude that our estimated exit temperature of 500 K is too high. We could repeat the calculations, using fluid properties evaluated at a revised bulk mean temperature of 375 K.

Coiled Tubes For turbulent flow inside helical coils, with tube inside radius a and coil radius R , the Nusselt number for a straight tube Nu_s is related to that for a coiled tube Nu_c , by (Rohsenow, Hartnett, and Cho, *Handbook of Heat Transfer*, 3d ed., McGraw-Hill, 1998, p. 5.90)

$$\frac{Nu_c}{Nu_s} = 1.0 + 3.6 \left(1 - \frac{a}{R}\right) \left(\frac{a}{R}\right)^{0.5} \quad (5-54)$$

where $2 \times 10^4 < Re_D < 1.5 \times 10^5$ and $5 < R/a < 84$. For lower Reynolds numbers ($1.5 \times 10^3 < Re_D < 2 \times 10^4$), the same source recommends

$$\frac{Nu_c}{Nu_s} = 1.0 + 3.4 \frac{a}{R} \quad (5-55)$$

External Flows For a single cylinder in cross flow, Churchill and Bernstein recommend [*J. Heat Transfer*, **99**, 300 (1977)]

$$\overline{Nu}_D = 0.3 + \frac{0.62 Re_D^{1/2} Pr^{1/3}}{[1 + (0.4/Pr)^{2/3}]^{1/4}} \left[1 + \left(\frac{Re_D}{282,000}\right)^{5/8}\right]^{4/5} \quad (5-56)$$

where $\overline{Nu}_D = \bar{h}D/k$. Equation (5-56) is for all values of Re_D and Pr , provided that $Re_D Pr > 0.4$. The fluid properties are evaluated at the film temperature $(T_e + T_s)/2$, where T_e is the free-stream temperature and T_s is the surface temperature. Equation (5-56) also applies to the uniform heat flux boundary condition provided \bar{h} is based on the perimeter-averaged temperature difference between T_s and T_e .

For an isothermal spherical surface, Whitaker recommends [*AIChE*, **18**, 361 (1972)]

$$\overline{Nu}_D = 2 + (0.4 Re_D^{1/2} + 0.06 Re_D^{2/3}) Pr^{0.4} \left(\frac{\mu_e}{\mu_s}\right)^{1/4} \quad (5-57)$$

This equation is based on data for $0.7 < Pr < 380$, $3.5 < Re_D < 8 \times 10^4$, and $1 < (\mu_e/\mu_s) < 3.2$. The properties are evaluated at the free-stream temperature T_e , with the exception of μ_s , which is evaluated at the surface temperature T_s .

The average Nusselt number for laminar flow over an isothermal flat plate of length x is estimated from [Churchill and Ozoe, *J. Heat Transfer*, **95**, 416 (1973)]

$$\overline{Nu}_x = \frac{1.128 Pr^{1/2} Re_x^{1/2}}{[1 + (0.0468/Pr)^{2/3}]^{1/4}} \quad (5-58)$$

This equation is valid for all values of Pr as long as $Re_x Pr > 100$ and $Re_x < 5 \times 10^5$. The fluid properties are evaluated at the film temperature $(T_e + T_s)/2$, where T_e is the free-stream temperature and T_s is the surface temperature. For a uniformly heated flat plate, the local Nusselt number is given by [Churchill and Ozoe, *J. Heat Transfer*, **95**, 78 (1973)]

$$Nu_x = \frac{0.886 Pr^{1/2} Re_x^{1/2}}{[1 + (0.0207/Pr)^{2/3}]^{1/4}} \quad (5-59)$$

where again the properties are evaluated at the film temperature.

The average Nusselt number for turbulent flow over a smooth, isothermal flat plate of length x is given by (Mills, *Heat Transfer*, 2d ed., Prentice-Hall, 1999, p. 315)

$$\overline{Nu}_x = 0.664 Re_{cr}^{1/2} Pr^{1/3} + 0.036 Re_x^{0.8} Pr^{0.43} \left[1 - \left(\frac{Re_{cr}}{Re_x}\right)^{0.5}\right] \quad (5-60)$$

The critical Reynolds number Re_{cr} is typically taken as 5×10^5 , $Re_{cr} < Re_x < 3 \times 10^7$, and $0.7 < Pr < 400$. The fluid properties are evaluated at the film temperature $(T_e + T_s)/2$, where T_e is the free-stream temperature and T_s is the surface temperature. Equation (5-60) also applies to the uniform heat flux boundary condition provided \bar{h} is based on the average temperature difference between T_s and T_e .

Flow-through Tube Banks Aligned and staggered tube banks are sketched in Fig. 5-6. The tube diameter is D , and the transverse and longitudinal pitches are S_T and S_L , respectively. The fluid velocity upstream of the tubes is V_∞ .

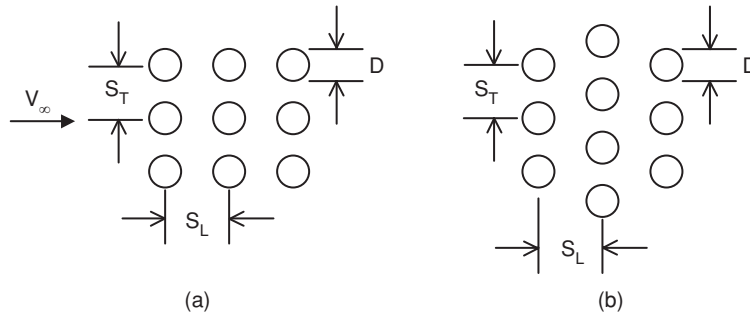


FIG. 5-6 (a) Aligned and (b) staggered tube bank configurations. The fluid velocity upstream of the tubes is V_∞ .

of the tubes is V_∞ . To estimate the overall heat-transfer coefficient for the tube bank, Mills proceeds as follows (*Heat Transfer*, 2d ed., Prentice-Hall, 1999, p. 348). The Reynolds number for use in (5-56) is recalculated with an effective average velocity in the space between adjacent tubes:

$$\frac{\bar{V}}{V_\infty} = \frac{S_T}{S_T - (\pi/4)D} \quad (5-61)$$

The heat-transfer coefficient increases from row 1 to about row 5 of the tube bank. The average Nusselt number for a tube bank with 10 or more rows is

$$\overline{Nu}_D^{10+} = \Phi \overline{Nu}_D \quad (5-62)$$

where Φ is an arrangement factor and \overline{Nu}_D is the Nusselt number for the first row, calculated by using the velocity in (5-61). The arrangement factor is calculated as follows. Define dimensionless pitches as $P_T = S_T/D$ and P_L/D and calculate a factor ψ as follows.

$$\psi = \begin{cases} 1 - \frac{\pi}{4P_T} & \text{if } P_L \geq 1 \\ 1 - \frac{\pi}{4P_T P_L} & \text{if } P_L < 1 \end{cases} \quad (5-63)$$

The arrangement factors are

$$\Phi_{\text{aligned}} = 1 + \frac{0.7}{\psi^{1.5}} \frac{S_T/S_T - 0.3}{(S_T/S_T + 0.7)^2} \quad (5-64)$$

$$\Phi_{\text{staggered}} = 1 + \frac{2}{3P_L} \quad (5-65)$$

If there are fewer than 10 rows,

$$\overline{Nu}_D = \frac{1 + (N-1)\Phi}{N} \overline{Nu}_D \quad (5-66)$$

where N is the number of rows.

The fluid properties for gases are evaluated at the average mean film temperature $[(T_{in} + T_{out})/2 + T_s]/2$. For liquids, properties are evaluated at the bulk mean temperature $(T_{in} + T_{out})/2$, with a Prandtl number correction $(Pr_b/Pr_s)^{0.11}$ for cooling and $(Pr_b/Pr_s)^{0.25}$ for heating.

Falling Films When a liquid is distributed uniformly around the periphery at the top of a vertical tube (either inside or outside) and allowed to fall down the tube wall by the influence of gravity, the fluid does not fill the tube but rather flows as a thin layer. Similarly, when a liquid is applied uniformly to the outside and top of a horizontal tube, it flows in layer form around the periphery and falls off the bottom. In both these cases the mechanism is called gravity flow of liquid layers or falling films.

For the turbulent flow of **water** in layer form down the walls of **vertical tubes** the dimensional equation of McAdams, Drew, and Bays [*Trans. Am. Soc. Mech. Eng.*, **62**, 627 (1940)] is recommended:

$$h_{lm} = b\Gamma^{1/3} \quad (5-67)$$

where $b = 9150$ (SI) or 120 (U.S. Customary) and is based on values of $\Gamma = W_F = \dot{M}/\pi D$ ranging from 0.25 to 6.2 kg/(m·s) [600 to 15,000 lb/(h·ft)] of wetted perimeter. This type of water flow is used in vertical vapor-in-shell ammonia condensers, acid coolers, cycle water coolers, and other process-fluid coolers.

The following dimensional equations may be used for **any liquid** flowing in layer form down **vertical surfaces**:

$$\text{For } \frac{4\Gamma}{\mu} > 2100 \quad h_{lm} = 0.01 \left(\frac{k^3 \rho^2 g}{\mu^2} \right)^{1/3} \left(\frac{c\mu}{k} \right)^{1/3} \left(\frac{4\Gamma}{\mu} \right)^{1/3} \quad (5-68a)$$

$$\text{For } \frac{4\Gamma}{\mu} < 2100 \quad h_{am} = 0.50 \left(\frac{k^3 \rho^{4/3} c g^{2/3}}{L\mu^{1/3}} \right)^{1/3} \left(\frac{\mu}{\mu_w} \right)^{1/4} \left(\frac{4\Gamma}{\mu} \right)^{1/9} \quad (5-68b)$$

Equation (5-68b) is based on the work of Bays and McAdams [*Ind. Eng. Chem.*, **29**, 1240 (1937)]. The significance of the term L is not clear. When $L = 0$, the coefficient is definitely not infinite. When L is large and the fluid temperature has not yet closely approached the wall temperature, it does not appear that the coefficient should

necessarily decrease. Within the finite limits of 0.12 to 1.8 m (0.4 to 6 ft), this equation should give results of the proper order of magnitude.

For falling films applied to the **outside of horizontal tubes**, the Reynolds number rarely exceeds 2100. Equations may be used for falling films on the outside of the tubes by substituting $\pi D/2$ for L .

For **water** flowing over a **horizontal tube**, data for several sizes of pipe are roughly correlated by the dimensional equation of McAdams, Drew, and Bays [*Trans. Am. Soc. Mech. Eng.*, **62**, 627 (1940)].

$$h_{am} = b(\Gamma/D_0)^{1/3} \quad (5-69)$$

where $b = 3360$ (SI) or 65.6 (U.S. Customary) and Γ ranges from 0.94 to 4 kg/(m·s) [100 to 1000 lb/(h·ft)].

Falling films are also used for evaporation in which the film is both entirely or partially evaporated (juice concentration). This principle is also used in crystallization (freezing).

The advantage of high coefficient in falling-film exchangers is partially offset by the difficulties involved in distribution of the film, maintaining complete wettability of the tube, and pumping costs required to lift the liquid to the top of the exchanger.

Finned Tubes (Extended Surface) When the heat-transfer coefficient on the outside of a metal tube is much lower than that on the inside, as when steam condensing in a pipe is being used to heat air, externally finned (or extended) heating surfaces are of value in increasing substantially the rate of heat transfer per unit length of tube. The data on extended heating surfaces, for the case of air flowing outside and at right angles to the axes of a bank of finned pipes, can be represented approximately by the dimensional equation derived from

$$h_f = b \frac{V_F^{0.6}}{D_0^{0.4}} \left(\frac{p'}{p' - D_0} \right)^{0.6} \quad (5-70)$$

where $b = 5.29$ (SI) or (5.39)(10⁻³) (U.S. Customary); h_f is the coefficient of heat transfer on the air side; V_F is the face velocity of the air; p' is the center-to-center spacing, m, of the tubes in a row; and D_0 is the outside diameter, m, of the bare tube (diameter at the root of the fins).

In atmospheric air-cooled finned tube exchangers, the air-film coefficient from Eq. (5-70) is sometimes converted to a value based on outside bare surface as follows:

$$h_{fo} = h_f \frac{A_f + A_{uf}}{A_{of}} = h_f \frac{A_T}{A_o} \quad (5-71)$$

in which h_{fo} is the air-film coefficient based on external bare surface; h_f is the air-film coefficient based on total external surface; A_T is total external surface, and A_o is external bare surface of the unfinned tube; A_f is the area of the fins; A_{uf} is the external area of the unfinned portion of the tube; and A_{of} is area of tube before fins are attached.

Fin efficiency is defined as the ratio of the mean temperature difference from surface to fluid divided by the temperature difference from fin to fluid at the base or root of the fin. Graphs of fin efficiency for extended surfaces of various types are given by Gardner [*Trans. Am. Soc. Mech. Eng.*, **67**, 621 (1945)].

Heat-transfer coefficients for finned tubes of various types are given in a series of papers [*Trans. Am. Soc. Mech. Eng.*, **67**, 601 (1945)].

For flow of air normal to fins in the form of **short strips or pins**, Norris and Spofford [*Trans. Am. Soc. Mech. Eng.*, **64**, 489 (1942)] correlate their results for air by the dimensionless equation of Pohlhausen:

$$\frac{h_m}{c_p G_{\max}} \left(\frac{c_p \mu}{k} \right)^{2/3} = 1.0 \left(\frac{z_p G_{\max}}{\mu} \right)^{-0.5} \quad (5-72)$$

for values of $z_p G_{\max}/\mu$ ranging from 2700 to 10,000.

For the general case, the treatment suggested by Kern (*Process Heat Transfer*, McGraw-Hill, New York, 1950, p. 512) is recommended. Because of the wide variations in fin-tube construction, it is convenient to convert all coefficients to values based on the inside bare surface of the tube. Thus to convert the coefficient based on outside area (finned side) to a value based on inside area Kern gives the following relationship:

$$h_{fi} = (\Omega A_f + A_o)(h_f/A_o) \quad (5-73)$$

5-12 HEAT AND MASS TRANSFER

in which h_f is the effective outside coefficient based on the inside area, h_f is the outside coefficient calculated from the applicable equation for bare tubes, A_f is the surface area of the fins, A_o is the surface area on the outside of the tube which is not finned, A_i is the inside area of the tube, and Ω is the fin efficiency defined as

$$\Omega = (\tanh mb_f)/mb_f \quad (5-74)$$

in which

$$m = (h_f p_f / ka_f)^{1/2} \quad \text{m}^{-1} \text{ (ft}^{-1}\text{)} \quad (5-75)$$

and b_f = height of fin. The other symbols are defined as follows: p_f is the perimeter of the fin, a_f is the cross-sectional area of the fin, and k is the thermal conductivity of the material from which the fin is made.

Fin efficiencies and fin dimensions are available from manufacturers. Ratios of finned to inside surface are usually available so that the terms A_f , A_o , and A_i may be obtained from these ratios rather than from the total surface areas of the heat exchangers.

JACKETS AND COILS OF AGITATED VESSELS

See Secs. 11 and 18.

NONNEWTONIAN FLUIDS

A wide variety of nonnewtonian fluids are encountered industrially. They may exhibit Bingham-plastic, pseudoplastic, or dilatant behavior

and may or may not be thixotropic. For design of equipment to handle or process nonnewtonian fluids, the properties must usually be measured experimentally, since no generalized relationships exist to predict the properties or behavior of the fluids. Details of handling nonnewtonian fluids are described completely by Skelland (*Non-Newtonian Flow and Heat Transfer*, Wiley, New York, 1967). The generalized shear-stress rate-of-strain relationship for nonnewtonian fluids is given as

$$n' = \frac{d \ln (D \Delta P / 4L)}{d \ln (8V/D)} \quad (5-76)$$

as determined from a plot of shear stress versus velocity gradient.

For **circular tubes**, $Gz > 100$, $n' > 0.1$, and laminar flow

$$Nu_m = 1.75 \delta_s^{1/3} Gz^{1/3} \quad (5-77)$$

where $\delta_s = (3n' + 1)/4n'$. When natural convection effects are considered, Metzner and Gluck [*Chem. Eng. Sci.*, **12**, 185 (1960)] obtained the following for **horizontal tubes**:

$$Nu_m = 1.75 \delta_s^{1/3} \left[Gz + 12.6 \left(\frac{\text{Pr Gr} D}{L} \right)^{0.4} \right]^{1/3} \left(\frac{\gamma_b}{\gamma_w} \right)^{0.14} \quad (5-78)$$

where properties are evaluated at the wall temperature, i.e., $\gamma = g_r K' 8^{n'-3}$ and $\tau_w = K' (8V/D)^{n'}$.

Metzner and Friend [*Ind. Eng. Chem.*, **51**, 879 (1959)] present relationships for turbulent heat transfer with nonnewtonian fluids. Relationships for heat transfer by natural convection and through laminar boundary layers are available in Skelland's book (op. cit.).

HEAT TRANSFER WITH CHANGE OF PHASE

In any operation in which a material undergoes a change of phase, provision must be made for the addition or removal of heat to provide for the latent heat of the change of phase plus any other sensible heating or cooling that occurs in the process. Heat may be transferred by any one or a combination of the three modes—conduction, convection, and radiation. The process involving change of phase involves mass transfer simultaneous with heat transfer.

CONDENSATION

Condensation Mechanisms Condensation occurs when a saturated vapor comes in contact with a surface whose temperature is below the saturation temperature. Normally a film of condensate is formed on the surface, and the thickness of this film, per unit of breadth, increases with increase in extent of the surface. This is called **film-type condensation**.

Another type of condensation, called **dropwise**, occurs when the wall is not uniformly wetted by the condensate, with the result that the condensate appears in many small droplets at various points on the surface. There is a growth of individual droplets, a coalescence of adjacent droplets, and finally a formation of a rivulet. Adhesive force is overcome by gravitational force, and the rivulet flows quickly to the bottom of the surface, capturing and absorbing all droplets in its path and leaving dry surface in its wake.

Film-type condensation is more common and more dependable. Dropwise condensation normally needs to be promoted by introducing an impurity into the vapor stream. Substantially higher (6 to 18 times) coefficients are obtained for dropwise condensation of steam, but design methods are not available. Therefore, the development of equations for condensation will be for the film type only.

The physical properties of the liquid, rather than those of the vapor, are used for determining the coefficient for condensation. Nusselt [*Z. Ver. Dtsch. Ing.*, **60**, 541, 569 (1916)] derived theoretical relationships for predicting the coefficient of heat transfer for condensation of a pure saturated vapor. A number of simplifying assumptions were used in the derivation.

The **Reynolds number** of the condensate film (falling film) is $4\Gamma/\mu$, where Γ is the weight rate of flow (loading rate) of condensate per unit perimeter $\text{kg}/(\text{s}\cdot\text{m})$ [$\text{lb}/(\text{h}\cdot\text{ft})$]. The thickness of the condensate film for Reynolds number less than 2100 is $(3\mu\Gamma/\rho^2g)^{1/3}$.

Condensation Coefficients

Vertical Tubes For the following cases Reynolds number < 2100 and is calculated by using $\Gamma = W_F/\pi D$. The **Nusselt equation** for the heat-transfer coefficient for condensate films may be written in the following ways (using liquid physical properties and where L is the cooled length and Δt is $t_{sv} - t_s$):

Nusselt type:

$$\frac{hL}{k} = 0.943 \left(\frac{L^3 \rho^2 g \lambda}{k \mu \Delta t} \right)^{1/4} = 0.925 \left(\frac{L^3 \rho^2 g}{\mu \Gamma} \right)^{1/3} \quad (5-79)^{\circ}$$

Dimensional:

$$h = b(k^3 \rho^2 D / \mu_b W_F)^{1/3} \quad (5-80)^{\circ}$$

where $b = 127$ (SI) or 756 (U.S. Customary). For steam at atmospheric pressure, $k = 0.682 \text{ J}/(\text{m}\cdot\text{s}\cdot\text{K})$ [$0.394 \text{ Btu}/(\text{h}\cdot\text{ft}\cdot^{\circ}\text{F})$], $\rho = 960 \text{ kg}/\text{m}^3$ ($60 \text{ lb}/\text{ft}^3$), $\mu_b = (0.28)(10^{-3}) \text{ Pa}\cdot\text{s}$ (0.28 cP),

$$h = b(D/W_F)^{1/3} \quad (5-81)$$

where $b = 2954$ (SI) or 6978 (U.S. Customary). For organic vapors at normal boiling point, $k = 0.138 \text{ J}/(\text{m}\cdot\text{s}\cdot\text{K})$ [$0.08 \text{ Btu}/(\text{h}\cdot\text{ft}\cdot^{\circ}\text{F})$], $\rho = 720 \text{ kg}/\text{m}^3$ ($45 \text{ lb}/\text{ft}^3$), $\mu_b = (0.35)(10^{-3}) \text{ Pa}\cdot\text{s}$ (0.35 cP),

$$h = b(D/W_F)^{1/3} \quad (5-82)$$

where $b = 457$ (SI) or 1080 (U.S. Customary).

Horizontal Tubes For the following cases Reynolds number < 2100 and is calculated by using $\Gamma = W_F/2L$.

^o If the vapor density is significant, replace ρ^2 with $\rho(\rho_l - \rho_v)$.

No.	Substance
10	Acetic Acid
6	Acetone
1	Ammonia
5	Aniline
12	Benzene
8	Carbon Disulfide
14	Carbon Tetrachloride
9	Ethyl Acetate
4	Ethyl Alcohol
13	Ethyl Ether
3	Methyl Alcohol
11	Nitrobenzene
7	n-Propyl Alcohol
2	Water

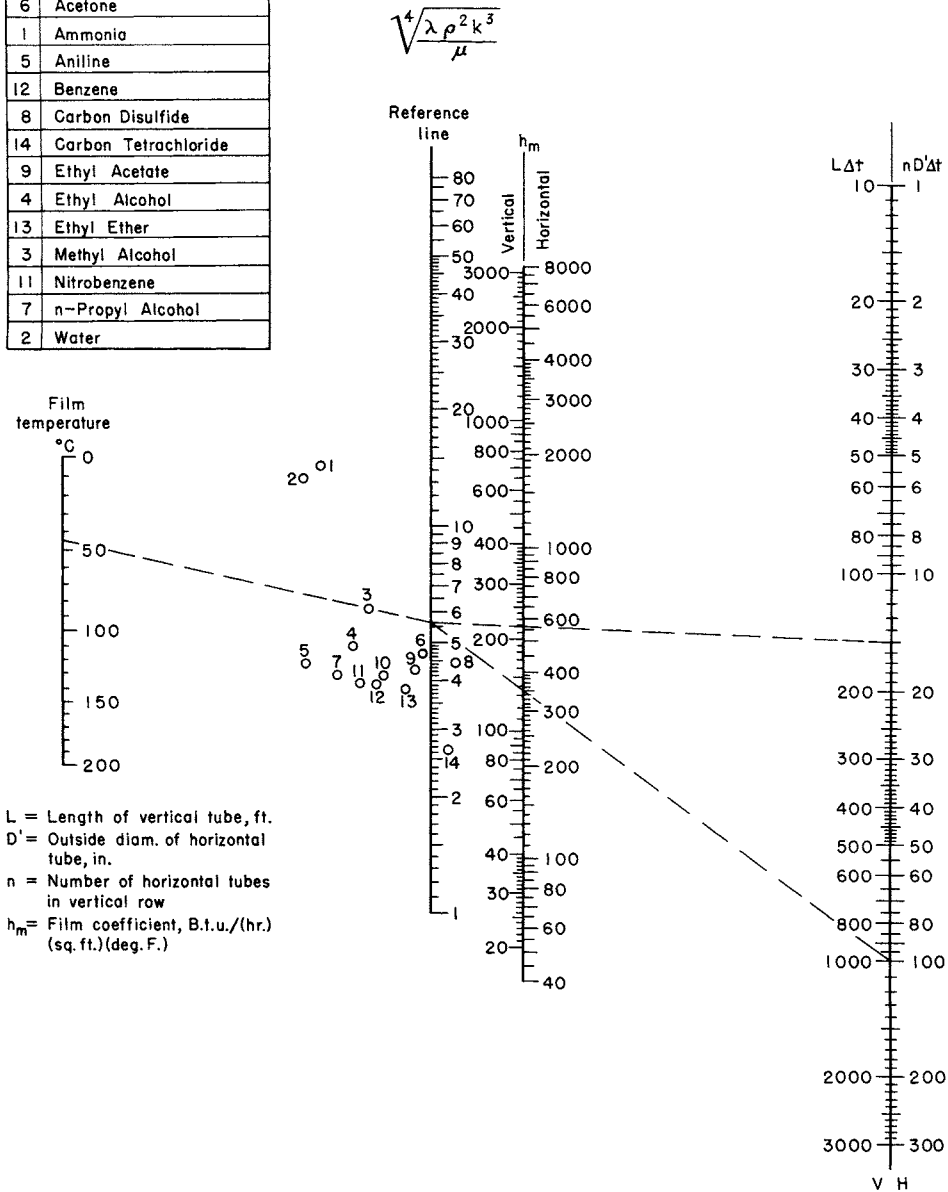


FIG. 5-7 Chart for determining heat-transfer coefficient h_m for film-type condensation of pure vapor, based on Eqs. (5-79) and (5-83). For vertical tubes multiply h_m by 1.2. If $4\Gamma/\mu$ exceeds 2100, use Fig. 5-8. $\sqrt[4]{\lambda \rho^2 k^3 / \mu}$ is in U.S. Customary units; to convert feet to meters, multiply by 0.3048; to convert inches to centimeters, multiply by 2.54; and to convert British thermal units per hour-square foot-degrees Fahrenheit to watts per square meter-kelvins, multiply by 5.6780.

Nusselt type:

$$\frac{hD}{k} = 0.73 \left(\frac{D^3 \rho^2 g \lambda}{k \mu \Delta t} \right)^{1/4} = 0.76 \left(\frac{D^3 \rho^2 g}{\mu \Gamma} \right)^{1/3} \quad (5-83)^\circ$$

Dimensional:

$$h = b(k^3 \rho^2 L / \mu_b W_F)^{1/3} \quad (5-84)^\circ$$

where $b = 205.4$ (SI) or 534 (U.S. Customary). For steam at atmospheric pressure

[°] If the vapor density is significant, replace ρ^2 with $\rho_1(\rho_1 - \rho_c)$.

$$h = b(L/W_F)^{1/3} \quad (5-85)$$

where $b = 2080$ (SI) or 4920 (U.S. Customary). For organic vapors at normal boiling point

$$h = b(L/W_F)^{1/3} \quad (5-86)$$

where $b = 324$ (SI) or 766 (U.S. Customary).

Figure 5-7 is a nomograph for determining coefficients of heat transfer for condensation of pure vapors.

Banks of Horizontal Tubes ($Re < 2100$) In the idealized case of N tubes in a vertical row where the total condensate flows smoothly from one tube to the one beneath it, without splashing, and still in laminar flow on the tube, the mean condensing coefficient h_N for the entire row of N tubes is related to the condensing coefficient for the top tube h_1 by

$$h_N = h_1 N^{-1/4} \tag{5-87}$$

Dukler Theory The preceding expressions for condensation are based on the classical Nusselt theory. It is generally known and conceded that the film coefficients for steam and organic vapors calculated by the Nusselt theory are conservatively low. Dukler [*Chem. Eng. Prog.*, **55**, 62 (1959)] developed equations for velocity and temperature distribution in thin films on vertical walls based on expressions of Deissler (NACA Tech. Notes 2129, 1950; 2138, 1952; 3145, 1959) for the eddy viscosity and thermal conductivity near the solid boundary. According to the Dukler theory, three fixed factors must be known to establish the value of the average film coefficient: the terminal Reynolds number, the Prandtl number of the condensed phase, and a dimensionless group N_d defined as follows:

$$N_d = (0.250\mu_L^{1.173} \mu_G^{0.16}) / (g^{2/3} D^2 \rho_L^{0.553} \rho_G^{0.78}) \tag{5-88}$$

Graphical relationships of these variables are available in Document 6058, ADI Auxiliary Publications Project, Library of Congress, Washington. If rigorous values for condensing-film coefficients are desired, especially if the value of N_d in Eq. (5-88) exceeds $(1)(10^{-5})$, it is suggested that these graphs be used. For the case in which interfacial shear is zero, Fig. 5-8 may be used. It is interesting to note that, according to the Dukler development, there is no definite transition Reynolds number; deviation from Nusselt theory is less at low Reynolds numbers; and when the Prandtl number of a fluid is less than 0.4 (at Reynolds number above 1000), the predicted values for film coefficient are lower than those predicted by the Nusselt theory.

The Dukler theory is applicable for condensate films on horizontal tubes and also for falling films, in general, i.e., those not associated with condensation or vaporization processes.

Vapor Shear Controlling For vertical in-tube condensation with vapor and liquid flowing concurrently downward, if gravity controls, Figs. 5-7 and 5-8 may be used. If vapor shear controls, the Carpenter-Colburn correlation (*General Discussion on Heat Transfer*, London, 1951, ASME, New York, p. 20) is applicable:

$$h\mu_i/k_i\rho_i^{1/2} = 0.065(Pr)^{1/2} F_{vc}^{1/2} \tag{5-89a}$$

$$\text{where } F_{vc} = fG_{vm}^2/2\rho_v \tag{5-89b}$$

$$G_{vm} = \left(\frac{G_{vi}^2 + G_{vi}G_{vo} + G_{vo}^2}{3} \right)^{1/2} \tag{5-89c}$$

and f is the Fanning friction factor evaluated at

$$(Re)_{vm} = D_i G_{vm} / \mu_v \tag{5-89d}$$

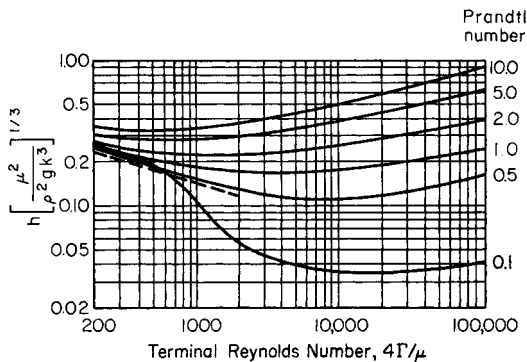


FIG. 5-8 Dukler plot showing average condensing-film coefficient as a function of physical properties of the condensate film and the terminal Reynolds number. (Dotted line indicates Nusselt theory for Reynolds number < 2100.) [Reproduced by permission from *Chem. Eng. Prog.*, **55**, 64 (1959).]

and the subscripts vi and vo refer to the vapor inlet and outlet, respectively. An alternative formulation, directly in terms of the friction factor, is

$$h = 0.065 (c\rho k_f/2\mu_v)^{1/2} G_{vm} \tag{5-89e}$$

expressed in consistent units.

Another correlation for vapor-shear-controlled condensation is the Boyko-Kruzhilin correlation [*Int. J. Heat Mass Transfer*, **10**, 361 (1967)], which gives the mean condensing coefficient for a stream between inlet quality x_i and outlet quality x_o :

$$\frac{hD_i}{k_l} = 0.024 \left(\frac{D_i G_T}{\mu_l} \right)^{0.8} (Pr)_l^{0.43} \frac{\sqrt{(\rho/\rho_m)_i} + \sqrt{(\rho/\rho_m)_o}}{2} \tag{5-90a}$$

where G_T = total mass velocity in consistent units

$$\left(\frac{\rho}{\rho_m} \right)_i = 1 + \frac{\rho_l - \rho_v}{\rho_v} x_i \tag{5-90b}$$

$$\left(\frac{\rho}{\rho_m} \right)_o = 1 + \frac{\rho_l - \rho_v}{\rho_v} x_o \tag{5-90c}$$

For horizontal in-tube condensation at low flow rates Kern's modification (*Process Heat Transfer*, McGraw-Hill, New York, 1950) of the Nusselt equation is valid:

$$h_m = 0.761 \left[\frac{Lk_i^3 \rho_l (\rho_l - \rho_v) g}{W_F \mu_l} \right]^{1/3} = 0.815 \left[\frac{k_i^3 \rho_l (\rho_l - \rho_v) g \lambda}{\pi \mu_l D_i \Delta t} \right]^{1/4} \tag{5-91}$$

where W_F is the total vapor condensed in one tube and Δt is $t_{sc} - t_s$. A more rigorous correlation has been proposed by Chaddock [*Refrig. Eng.*, **65**(4), 36 (1957)]. Use consistent units.

At high condensing loads, with vapor shear dominating, tube orientation has no effect, and Eq. (5-90a) may also be used for horizontal tubes.

Condensation of pure vapors under laminar conditions in the presence of noncondensable gases, interfacial resistance, superheating, variable properties, and diffusion has been analyzed by Minkowycz and Sparrow [*Int. J. Heat Mass Transfer*, **9**, 1125 (1966)].

BOILING (VAPORIZATION) OF LIQUIDS

Boiling Mechanisms Vaporization of liquids may result from various mechanisms of heat transfer, singly or combinations thereof. For example, vaporization may occur as a result of heat absorbed, by radiation and convection, at the surface of a pool of liquid; or as a result of heat absorbed by natural convection from a hot wall beneath the disengaging surface, in which case the vaporization takes place when the superheated liquid reaches the pool surface. Vaporization also occurs from falling films (the reverse of condensation) or from the flashing of liquids superheated by forced convection under pressure.

Pool boiling refers to the type of boiling experienced when the heating surface is surrounded by a relatively large body of fluid which is not flowing at any appreciable velocity and is agitated only by the motion of the bubbles and by natural-convection currents. Two types of pool boiling are possible: subcooled pool boiling, in which the bulk fluid temperature is below the saturation temperature, resulting in collapse of the bubbles before they reach the surface, and saturated pool boiling, with bulk temperature equal to saturation temperature, resulting in net vapor generation.

The general shape of the curve relating the heat-transfer coefficient to Δt_b , the temperature driving force (difference between the wall temperature and the bulk fluid temperature) is one of the few parametric relations that are reasonably well understood. The familiar boiling curve was originally demonstrated experimentally by Nukiyama [*J. Soc. Mech. Eng. (Japan)*, **37**, 367 (1934)]. This curve points out one of the great dilemmas for boiling-equipment designers. They are faced with at least six heat-transfer regimes in pool boiling: natural convection (+), incipient nucleate boiling (+), nucleate boiling (+), transition to film boiling (-), stable film boiling (+), and film boiling with increasing radiation (+). The signs indicate the sign of the derivative $d(q/A)/d \Delta t_b$. In the transition to film boiling, heat-transfer rate decreases with driving force. The regimes of greatest commercial interest are the nucleate-boiling and stable-film-boiling regimes.

Heat transfer by nucleate boiling is an important mechanism in the vaporization of liquids. It occurs in the vaporization of liquids in

kettle-type and natural-circulation reboilers commonly used in the process industries. High rates of heat transfer per unit of area (heat flux) are obtained as a result of bubble formation at the liquid-solid interface rather than from mechanical devices external to the heat exchanger. There are available several expressions from which reasonable values of the film coefficients may be obtained.

The boiling curve, particularly in the nucleate-boiling region, is significantly affected by the temperature driving force, the total system pressure, the nature of the boiling surface, the geometry of the system, and the properties of the boiling material. In the nucleate-boiling regime, heat flux is approximately proportional to the cube of the temperature driving force. Designers in addition must know the minimum Δt (the point at which nucleate boiling begins), the critical Δt (the Δt above which transition boiling begins), and the maximum heat flux (the heat flux corresponding to the critical Δt). For designers who do not have experimental data available, the following equations may be used.

Boiling Coefficients For the nucleate-boiling coefficient the Mostinski equation [*Teplenergetika*, **4**, 66 (1963)] may be used:

$$h = b P_c^{0.69} \left(\frac{q}{A}\right)^{0.7} \left[1.8 \left(\frac{P}{P_c}\right)^{0.17} + 4 \left(\frac{P}{P_c}\right)^{1.2} + 10 \left(\frac{P}{P_c}\right)^{10} \right] \quad (5-92)$$

where $b = (3.75)(10^{-5})$ (SI) or $(2.13)(10^{-4})$ (U.S. Customary), P_c is the critical pressure and P the system pressure, q/A is the heat flux, and h is the nucleate-boiling coefficient. The McNelly equation [*J. Imp. Coll. Chem. Eng. Soc.*, **7**(18), (1953)] may also be used:

$$h = 0.225 \left(\frac{q c_l}{A \lambda}\right)^{0.69} \left(\frac{P k_l}{\sigma}\right)^{0.31} \left(\frac{p_l}{p_c} - 1\right)^{0.33} \quad (5-93)$$

where c_l is the liquid heat capacity, λ is the latent heat, P is the system pressure, k_l is the thermal conductivity of the liquid, and σ is the surface tension.

An equation of the Nusselt type has been suggested by Rohsenow [*Trans. Am. Soc. Mech. Eng.*, **74**, 969 (1952)].

$$h D/k = C_r (D G/\mu)^{2/3} (c\mu/k)^{-0.7} \quad (5-94a)$$

in which the variables assume the following form:

$$\frac{h \beta'}{k} \left[\frac{g_c \sigma}{g(\rho_L - \rho_v)} \right]^{1/2} = C_r \left[\frac{\beta'}{\mu} \left(\frac{g_c \sigma}{g(\rho_L - \rho_v)} \right)^{1/2} \frac{W}{A} \right]^{2/3} \left(\frac{c\mu}{k} \right)^{-0.7} \quad (5-94b)$$

The coefficient C_r is not truly constant but varies from 0.006 to 0.015.* It is possible that the nature of the surface is partly responsible for the variation in the constant. The only factor in Eq. (5-94b) not readily available is the value of the contact angle β' .

Another Nusselt-type equation has been proposed by Forster and Zuber:†

$$Nu = 0.0015 Re^{0.62} Pr^{1/3} \quad (5-95)$$

which takes the following form:

$$\frac{c \rho_L \sqrt{\pi \alpha}}{k \rho_v} \frac{W}{A} \left(\frac{2\sigma}{\Delta p} \right)^{1/2} \left(\frac{\rho_L}{\Delta p g_c} \right)^{1/4} = 0.0015 \left[\frac{\rho_L}{\mu} \left(\frac{c \rho_L \Delta T \sqrt{\pi \alpha}}{\lambda \rho_v} \right)^2 \right]^{0.62} \left(\frac{c\mu}{k} \right)^{1/2} \quad (5-96)$$

where $\alpha = k/\rho c$ (all liquid properties)

Δp = pressure of the vapor in a bubble minus saturation pressure of a flat liquid surface

Equations (5-94b) and (5-96) have been arranged in dimensional form by Westwater.

The numerical constant may be adjusted to suit any particular set of data if one desires to use a certain criterion. However, surface conditions vary so greatly that deviations may be as large as ± 25 percent from results obtained.

The **maximum heat flux** may be predicted by the Kutateladse-Zuber [*Trans. Am. Soc. Mech. Eng.*, **80**, 711 (1958)] relationship, using consistent units:

$$\left(\frac{q}{A}\right)_{\max} = 0.18 g_c^{1/4} \rho_v \lambda \left[\frac{(\rho_l - \rho_v) \sigma g_c}{\rho_v^2} \right]^{1/4} \quad (5-97)$$

Alternatively, Mostinski presented an equation which approximately represents the Cichelli-Bonilla [*Trans. Am. Inst. Chem. Eng.*, **41**, 755 (1945)] correlation:

$$\frac{(q/A)_{\max}}{P_c} = b \left(\frac{P}{P_c}\right)^{0.35} \left(1 - \frac{P}{P_c}\right)^{0.9} \quad (5-98)$$

where $b = 0.368$ (SI) or 5.58 (U.S. Customary); P_c is the critical pressure, P absolute; P is the system pressure; and $(q/A)_{\max}$ is the maximum heat flux.

The lower limit of applicability of the nucleate-boiling equations is from 0.1 to 0.2 of the maximum limit and depends upon the magnitude of natural-convection heat transfer for the liquid. The best method of determining the lower limit is to plot two curves: one of h versus Δt for natural convection, the other of h versus Δt for nucleate boiling. The intersection of these two curves may be considered the lower limit of applicability of the equations.

These equations apply to single tubes or to flat surfaces in a large pool. In tube bundles the equations are only approximate, and designers must rely upon experiment. Palen and Small [*Hydrocarbon Process.*, **43**(11), 199 (1964)] have shown the effect of tube-bundle size on maximum heat flux.

$$\left(\frac{q}{A}\right)_{\max} = b \frac{P}{D_o \sqrt{N_T}} \rho_v \lambda \left[\frac{g \sigma (\rho_l - \rho_v)}{\rho_v^2} \right]^{1/4} \quad (5-99)$$

where $b = 0.43$ (SI) or 61.6 (U.S. Customary), p is the tube pitch, D_o is the tube outside diameter, and N_T is the number of tubes (twice the number of complete tubes for U-tube bundles).

For **film boiling**, Bromley's [*Chem. Eng. Prog.*, **46**, 221 (1950)] correlation may be used:

$$h = b \left[\frac{k_v^3 (\rho_l - \rho_v) \rho_v g}{\mu_v D_o \Delta t_b} \right]^{1/4} \quad (5-100)$$

where $b = 4.306$ (SI) or 0.620 (U.S. Customary). Katz, Myers, and Balekjian [*Pet. Refiner*, **34**(2), 113 (1955)] report boiling heat-transfer coefficients on finned tubes.

HEAT TRANSFER BY RADIATION

GENERAL REFERENCES: Baukal, C. E., ed., *The John Zink Combustion Handbook*, CRC Press, Boca Raton, Fla., 2001. Blokh, A. G., *Heat Transfer in Steam Boiler Furnaces*, 3d ed., Taylor & Francis, New York, 1987. Brewster, M. Quinn, *Thermal Radiation Heat Transfer and Properties*, Wiley, New York, 1992. Goody, R. M., and Y. L. Yung, *Atmospheric Radiation—Theoretical Basis*, 2d ed., Oxford University Press, 1995. Hottel, H. C., and A. F. Sarofim, *Radiative Transfer*, McGraw-Hill, New York, 1967. Modest, Michael F., *Radiative Heat Transfer*, 2d ed., Academic Press, New York, 2003. Noble, James J., "The Zone

Method: Explicit Matrix Relations for Total Exchange Areas," *Int. J. Heat Mass Transfer*, **18**, 261–269 (1975). Rhine, J. M., and R. J. Tucker, *Modeling of Gas-Fired Furnaces and Boilers*, British Gas Association with McGraw-Hill, 1991. Siegel, Robert, and John R. Howell, *Thermal Radiative Heat Transfer*, 4th ed., Taylor & Francis, New York, 2001. Sparrow, E. M., and R. D. Cess, *Radiation Heat Transfer*, 3d ed., Taylor & Francis, New York, 1988. Stultz, S. C., and J. B. Kitto, *Steam: Its Generation and Use*, 40th ed., Babcock and Wilcox, Barksonton, Ohio, 1992.

* Reported by Westwater in Drew and Hoopes, *Advances in Chemical Engineering*, vol. I, Academic, New York, 1956, p. 15.

† Forster, *J. Appl. Phys.*, **25**, 1067 (1954); Forster and Zuber, *J. Appl. Phys.*, **25**, 474 (1954); Forster and Zuber, Conference on Nuclear Engineering, University of California, Los Angeles, 1955; excellent treatise on boiling of liquids by Westwater in Drew and Hoopes, *Advances in Chemical Engineering*, vol. I, Academic, New York, 1956.

INTRODUCTION

Heat transfer by thermal radiation involves the transport of electromagnetic (EM) energy from a source to a sink. In contrast to other modes of heat transfer, radiation does not require the presence of an intervening medium, e.g., as in the irradiation of the earth by the sun. Most industrially important applications of radiative heat transfer occur in the *near infrared* portion of the EM spectrum (0.7 through 25 μm) and may extend into the *far infrared* region (25 to 1000 μm). For very high temperature sources, such as solar radiation, relevant wavelengths encompass the entire *visible region* (0.4 to 0.7 μm) and may extend down to 0.2 μm in the *ultraviolet* (0.01- to 0.4-μm) portion of the EM spectrum. Radiative transfer can also exhibit unique *action-at-a-distance* phenomena which do not occur in other modes of heat transfer. Radiation differs from conduction and convection not only with regard to mathematical characterization but also with regard to its fourth power dependence on temperature. Thus it is usually dominant in high-temperature combustion applications. The temperature at which radiative transfer accounts for roughly one-half of the total heat loss from a surface in air depends on such factors as surface **emissivity** and the convection coefficient. For pipes in free convection, radiation is important at ambient temperatures. For fine wires of low emissivity it becomes important at temperatures associated with bright red heat (1300 K). Combustion gases at furnace temperatures typically lose more than 90 percent of their energy by radiative emission from constituent carbon dioxide, water vapor, and particulate matter. Radiative transfer methodologies are important in myriad engineering applications. These include semiconductor processing, illumination theory, and gas turbines and rocket nozzles, as well as furnace design.

THERMAL RADIATION FUNDAMENTALS

In a vacuum, the wavelength λ, frequency, ν and wavenumber η for electromagnetic radiation are interrelated by λ = c/ν = 1/η, where c is the speed of light. Frequency is independent of the index of refraction of a medium n, but both the speed of light and the wavelength in the medium vary according to c_m = c/n and λ_m = λ/n. When a radiation beam passes into a medium of different refractive index, not only does its wavelength change but so does its direction (Snell's law) as well as the magnitude of its intensity. In most engineering heat-transfer calculations, wavelength is usually employed to characterize radiation while wave number is often used in gas spectroscopy. For a vacuum, air at ambient conditions, and most gases, n ≈ 1.0. For this reason this presentation sometimes does not distinguish between λ and λ_m. *Dielectric materials* exhibit 1.4 < n < 4, and the speed of light decreases considerably in such media.

In radiation heat transfer, the **monochromatic intensity** I_λ ≡ I_λ(\vec{r} , $\vec{\Omega}$, λ), is a *fundamental* (scalar) *field variable* which characterizes EM energy transport. Intensity defines the radiant energy flux passing through an infinitesimal area dA, oriented *normal* to a radiation beam of arbitrary direction $\vec{\Omega}$. At steady state, the monochromatic intensity is a function of position \vec{r} , direction $\vec{\Omega}$, and wavelength and has units of W/(m²·sr·μm). In the general case of an *absorbing-emitting* and *scattering* medium, characterized by some absorption coefficient K(m⁻¹), intensity in the direction $\vec{\Omega}$ will be modified by attenuation and by *scattering* of radiation into and out of the beam. For the special case of a nonabsorbing (transparent), nonscattering, medium of constant refractive index, the radiation intensity is *constant and independent of position in a given direction* $\vec{\Omega}$. This circumstance arises in *illumination theory* where the light intensity in a room is constant in a *given direction* but may vary with respect to *all other directions*. The basic conservation law for radiation intensity is termed the *equation of transfer* or *radiative transfer equation*. The equation of transfer is a *directional* energy balance and mathematically is an *integrodifferential equation*. The relevance of the transport equation to radiation heat transfer is discussed in many sources; see, e.g., Modest, M. F., *Radiative Heat Transfer*, 2d ed., Academic Press, 2003, or Siegel, R., and J. R. Howell, *Thermal Radiative Heat Transfer*, 4th ed., Taylor & Francis, New York, 2001.

Introduction to Radiation Geometry Consider a homogeneous medium of constant refractive index n. A pencil of radiation

originates at differential area element dA_i and is incident on differential area element dA_j. Designate \vec{n}_i and \vec{n}_j as the unit vectors normal to dA_i and dA_j, and let r_{ij} with unit direction vector $\vec{\Omega}$, define the distance of separation between the area elements. Moreover, φ_i and φ_j denote the *confined angles* between $\vec{\Omega}$ and \vec{n}_i and \vec{n}_j , respectively [i.e., cosφ_i ≡ cos($\vec{\Omega}$, \vec{r}_{ij}) and cosφ_j ≡ cos($\vec{\Omega}$, \vec{r}_{ji})]. As the beam travels toward dA_j, it will *diverge* and subtend a solid angle

$$d\Omega_j = \frac{\cos\phi_j}{r^2} dA_j \text{ sr}$$

at dA_j. Moreover, the projected area of dA_i in the direction of $\vec{\Omega}$ is given by cos($\vec{\Omega}$, \vec{r}_i) dA_i = cosφ_i dA_i. Multiplication of the intensity I_λ ≡ I_λ(\vec{r} , $\vec{\Omega}$, λ) by dΩ_j and the apparent area of dA_i then yields an expression for the (*differential*) *net monochromatic radiant energy flux* dQ_{ij} originating at dA_i and intercepted by dA_j.

$$dQ_{ij} \equiv I_{\lambda}(\vec{\Omega}, \lambda) \cos\phi_i \cos\phi_j dA_i dA_j / r^2 \quad (5-101)$$

The **hemispherical emissive power**^{*} E is defined as the radiant flux density (W/m²) associated with emission from an element of surface area dA into a surrounding unit hemisphere whose base is coplanar with dA. If the monochromatic intensity I_λ($\vec{\Omega}$, λ) of emission from the surface is *isotropic* (independent of the angle of emission, $\vec{\Omega}$), Eq. (5-101) may be integrated over the 2π sr of the surrounding unit hemisphere to yield the simple relation E_λ = πI_λ, where E_λ ≡ E_λ(λ) is defined as the monochromatic or *spectral* hemispherical emissive power.

Blackbody Radiation Engineering calculations involving thermal radiation normally employ the **hemispherical blackbody emissive power** as the thermal driving force analogous to temperature in the cases of conduction and convection. A **blackbody** is a theoretical idealization for a *perfect theoretical radiator*; i.e., it absorbs all incident radiation without reflection and emits isotropically. In practice, soot-covered surfaces sometimes approximate blackbody behavior. Let E_{b,λ} = E_{b,λ}(T, λ) denote the monochromatic blackbody hemispherical emissive power *frequency function* defined such that E_{b,λ}(T, λ)dλ represents the fraction of blackbody energy lying in the wavelength region from λ to λ + dλ. The function E_{b,λ} = E_{b,λ}(T, λ) is given by **Planck's law**

$$\frac{E_{b,\lambda}(T, \lambda)}{n^2 T^5} = \frac{c_1 (\lambda T)^{-5}}{e^{c_2/\lambda T} - 1} \quad (5-102)$$

where c₁ = 2πhc² and c₂ = hc/k are defined as Planck's first and second constants, respectively.

Integration of Eq. (5-102) over all wavelengths yields the **Stefan-Boltzman law** for the hemispherical blackbody emissive power

$$E_b(T) = \int_{\lambda=0}^{\infty} E_{b,\lambda}(T, \lambda) d\lambda = n^2 \sigma T^4 \quad (5-103)$$

where σ = c₁(π/c₂)⁴/15 is the Stephan-Boltzman constant. Since a blackbody is an *isotropic emitter*, it follows that the intensity of blackbody emission is given by the simple formula I_b = E_b/π = n²σT⁴/π. The intensity of radiation emitted over all wavelengths by a blackbody is thus uniquely determined by its temperature. In this presentation, all references to hemispherical emissive power shall be to the *blackbody* emissive power, and the subscript b may be suppressed for expediency.

For short wavelengths λT → 0, the asymptotic form of Eq. (5-102) is known as the **Wien equation**

$$\frac{E_{b,\lambda}(T, \lambda)}{n^2 T^5} \equiv c_1 (\lambda T)^{-5} e^{-c_2/\lambda T} \quad (5-104)$$

The error introduced by use of the Wien equation is less than 1 percent when λT < 3000 μm·K. The Wien equation has significant practical value in optical pyrometry for T < 4600 K when a red filter (λ = 0.65 μm) is employed. The long-wavelength asymptotic approximation for Eq. (5-102) is known as the **Rayleigh-Jeans formula**, which is accurate to within 1 percent for λT > 778,000 μm·K. The Rayleigh-Jeans formula is of limited engineering utility since a blackbody emits over 99.9 percent of its total energy below the value of λT = 53,000 μm·K.

^{*} In the literature the emissive power is variously called the emittance, total hemispherical intensity, or radiant flux density.

Nomenclature and Units—Radiative Transfer

$a, a_g, a_{g,1}$	WSGG spectral model clear plus gray weighting constants
$\bar{C}_p, \bar{C}_{p,prod}$	Heat capacity per unit mass, $J \cdot kg^{-1} \cdot K^{-1}$
$ij = s_i s_j$	Shorthand notation for direct exchange area
A, A_i	Area of enclosure or zone i , m^2
c	Speed of light in vacuum, m/s
c_1, c_2	Planck's first and second constants, $W \cdot m^2$ and $m \cdot K$
d_p, r_p	Particle diameter and radius, μm
$E_{b,\lambda} = E_{b,\lambda}(T, \lambda)$	Monochromatic, blackbody emissive power, $W/(m^2 \cdot \mu m)$
$E_n(x)$	Exponential integral of order n , where $n = 1, 2, 3, \dots$
E	Hemispherical emissive power, W/m^2
$E_b = n^2 \sigma T^4$	Hemispherical blackbody emissive power, W/m^2
f_v	Volumetric fraction of soot
$F_b(\lambda T)$	Blackbody fractional energy distribution
F_{ij}	Direct view factor from surface zone i to surface zone j
\bar{F}_{ij}	Refractory augmented black view factor; F -bar
$F_{i,j}$	Total view factor from surface zone i to surface zone j
h	Planck's constant, $J \cdot s$
h_i	Heat-transfer coefficient, $W/(m^2 \cdot K)$
H_i	Incident flux density for surface zone i , W/m^2
H	Enthalpy rate, W
\dot{H}_f	Enthalpy feed rate, W
$\dot{I}_\lambda \equiv I_\lambda(\vec{r}, \vec{\Omega}, \lambda)$	Monochromatic radiation intensity, $W/(m^2 \cdot \mu m \cdot sr)$
k	Boltzmann's constant, J/K
$k_{\lambda,p}$	Monochromatic line absorption coefficient, $(atm \cdot m)^{-1}$
K	Gas absorption coefficient, m^{-1}
L_M, L_{M0}	Average and optically thin mean beam lengths, m
\dot{m}	Mass flow rate, kg/h^{-1}
n	Index of refraction
M, N	Number of surface and volume zones in enclosure
p_k	Partial pressure of species k , atm
P	Number of WSGG gray gas spectral windows
Q_i	Total radiative flux originating at surface zone i , W
Q_{ij}	Net radiative flux between zone i and zone j , W
T	Temperature, K
U	Overall heat-transfer coefficient in WSCC model
V	Enclosure volume, m^3
W	Leaving flux density (radiosity), W/m^2

Greek Characters

$\alpha, \alpha_{1,2}$	Surface absorptivity or absorptance; subscript 1 refers to the surface temperature while subscript 2 refers to the radiation source
$\alpha_{g,1}, \epsilon_g, \tau_{g,1}$	Gas absorptivity, emissivity, and transmissivity
β	Dimensionless constant in mean beam length equation, $L_M = \beta L_{M0}$
$\Delta T_{fit} \equiv T_g - T_e$	Adjustable temperature fitting parameter for WSCC model, K
ϵ	Gray diffuse surface emissivity
$\epsilon_g(T, r)$	Gas emissivity with path length r
$\epsilon'_g(T, \Omega, \lambda)$	Monochromatic, unidirectional, surface emissivity
$\eta = 1/\lambda$	Wave number in vacuum, cm^{-1}
$\lambda = c/\nu$	Wavelength in vacuum, μm
ν	Frequency, Hz
$\rho = 1 - \epsilon$	Diffuse reflectivity
σ	Stefan-Boltzmann constant, $W/(m^2 \cdot K^4)$
Σ	Number of unique direct surface-to-surface direct exchange areas
$\tau_g = 1 - \epsilon_g$	Gas transmissivity
Ω	Solid angle, sr (steradians)
Φ	Equivalence ratio of fuel and oxidant
$\Psi^{(3)}(x)$	Pentagramma function of x
ω	Albedo for single scatter

Dimensionless Quantities

$D_{eff} = \frac{N_{FD}}{(S_i G_R/A_1) + N_{CR}}$	Effective firing density
$N_{CR} = \frac{h}{4\sigma T_{g,1}^3}$	Convection-radiation number
$N_{FD} = \dot{H}_f / \sigma T_{ref}^4 A_1$	Dimensionless firing density
η_g	Gas-side furnace efficiency
$\eta'_g = \eta_g(1 - \Theta_0)$	Reduced furnace efficiency
$\Theta_1 = T/T_{ref}$	Dimensionless temperature

Vector Notation

\vec{n}_1 and \vec{n}_2	Unit vectors normal to differential area elements dA_1 and dA_2
\vec{r}	Position vector
$\vec{\Omega}$	Arbitrary unit direction vector

Matrix Notation

$\mathbf{1}_M$	Column vector; all of whose elements are unity, $[M \times 1]$
$\mathbf{I} = [\delta_{ij}]$	Identity matrix, where δ_{ij} is the Kronecker delta; i.e., $\delta_{ij} = 1$ for $i = j$ and $\delta_{ij} = 0$ for $i \neq j$.
\mathbf{aI}	Diagonal matrix of WSGG gray gas surface zone a -weighting factors $[M \times M]$
$\mathbf{a}_g \mathbf{I}$	Diagonal matrix of gray gas WSGG volume zone a -weighting factors $[N \times N]$
$\mathbf{A} = [A_{ij}]$	Arbitrary nonsingular square matrix
$\mathbf{A}^T = [A_{ji}]$	Transpose of \mathbf{A}
$\mathbf{A}^{-1} = [A_{ij}]^{-1}$	Inverse of \mathbf{A}
$\mathbf{DI} = [D_i \delta_{ij}]$	Arbitrary diagonal matrix
$\mathbf{DI}^{-1} = [\delta_{ij}/D_i]$	Inverse of diagonal matrix
\mathbf{CDI}	$\mathbf{CI} \cdot \mathbf{DI} = [C_i D_i \delta_{ij}]$, product of two diagonal matrices
$\mathbf{AI} = [A_i \delta_{ij}]$	Diagonal matrix of surface zone areas, $m^2 [M \times M]$
$\epsilon \mathbf{I} = [\epsilon_i \delta_{ij}]$	Diagonal matrix of diffuse zone emissivities $[M \times M]$
$\rho \mathbf{I} = [\rho_i \delta_{ij}]$	Diagonal matrix of diffuse zone reflectivities $[M \times M]$
$\mathbf{E} = [E_i] = [\sigma T_i^4]$	Column vector of surface blackbody hemispherical emissive powers, $W/m^2 [M \times 1]$
$\mathbf{EI} = [E_i \delta_{ij}] = [\sigma T_i^4 \delta_{ij}]$	Diagonal matrix of surface blackbody emissive powers, $W/m^2 [M \times M]$
$\mathbf{E}_g = [E_{g,i}] = [\sigma T_{g,i}^4]$	Column vector of gas blackbody hemispherical emissive powers, $W/m^2 [N \times 1]$
$\mathbf{E}_g \mathbf{I} = [E_{g,i} \delta_{ij}] = [\sigma T_{g,i}^4 \delta_{ij}]$	Diagonal matrix of gas blackbody emissive powers, $W/m^2 [N \times N]$
$\mathbf{H} = [H_i]$	Column vector of surface zone incident flux densities, $W/m^2 [M \times 1]$
$\mathbf{W} = [W_i]$	Column vector of surface zone leaving flux densities, $W/m^2 [M \times 1]$
$\mathbf{Q} = [Q_i]$	Column vector of surface zone fluxes, $W [M \times 1]$
$\mathbf{R} = [\mathbf{AI} - \mathbf{ss} \cdot \rho \mathbf{I}]^{-1}$	Inverse multiple-reflection matrix, $m^{-2} [M \times M]$
$\mathbf{KI}_p = [\delta_{ij} K_{p,i}]$	Diagonal matrix of WSGG $K_{p,i}$ values for the i th zone and p th gray gas component, $m^{-1} [N \times N]$
$\bar{\mathbf{K}} \mathbf{I}$	Diagonal matrix of WSGG-weighted gray gas absorption coefficients, $m^{-1} [N \times N]$
\mathbf{S}'	Column vector for net volume absorption, $W [N \times 1]$
$\bar{\mathbf{ss}} = [\bar{s}_i \bar{s}_j]$	Array of direct surface-to-surface exchange areas, $m^2 [M \times M]$
$\bar{\mathbf{sg}} = [\bar{s}_i \bar{g}_j] = \bar{\mathbf{gs}}^T$	Array of direct gas-to-surface exchange areas, $m^2 [M \times N]$
$\bar{\mathbf{gg}} = [\bar{g}_i \bar{g}_j]$	Array of direct gas-to-gas exchange areas, $m^2 [N \times N]$
$\bar{\mathbf{SS}} = [\bar{S}_i \bar{S}_j]$	Array of total surface-to-surface exchange areas, $m^2 [M \times M]$
$\bar{\mathbf{SG}} = [\bar{S}_i \bar{G}_j]$	Array of total gas-to-surface exchange areas, $m^2 [M \times N]$
$\bar{\mathbf{GS}} = \bar{\mathbf{GS}}^T$	Array of total surface-to-gas exchange areas, $m^2 [N \times M]$
$\bar{\mathbf{GG}} = [\bar{G}_i \bar{G}_j]$	Array of total gas-to-gas exchange areas, $m^2 [N \times N]$
$\bar{\mathbf{SS}} = [\bar{S}_i \bar{S}_i]$	Array of directed surface-to-surface exchange areas, $m^2 [M \times M]$
$\bar{\mathbf{SG}} = [\bar{S}_i \bar{G}_i]$	Array of directed gas-to-surface exchange areas, $m^2 [M \times N]$
$\bar{\mathbf{GS}} \neq \bar{\mathbf{SG}}^T$	Array of directed surface-to-gas exchange areas, $m^2 [N \times M]$
$\bar{\mathbf{GG}} = [\bar{G}_i \bar{G}_i]$	Array of directed gas-to-gas exchange areas, $m^2 [N \times N]$
$\mathbf{VI} = [V_i \delta_{ij}]$	Diagonal matrix of zone volumes, $m^3 [N \times N]$

Subscripts

b	Blackbody or denotes a black surface zone
f	Denotes flux surface zone
h	Denotes hemispherical surface emissivity
i, j	Zone number indices
n	Denotes normal component of surface emissivity
p	Index for p th gray gas window
r	Denotes refractory surface zone
s	Denotes source-sink surface zone
λ	Denotes monochromatic variable
Ref	Denotes reference quantity

Abbreviations

CFD	Computational fluid dynamics
DO, FV	Discrete ordinate and finite volume methods
EM	Electromagnetic
RTE	Radiative transfer equation; equation of transfer
LPFF	Long plug flow furnace model
SSR	Source-sink refractory model
WSCC	Well-stirred combustion chamber model
WSGG	Weighted sum of gray gases spectral model

The blackbody fractional energy distribution function is defined by

$$F_b(\lambda T) = \frac{\int_0^\lambda E_{b,\lambda}(T, \lambda) d\lambda}{\int_0^\infty E_{b,\lambda}(T, \lambda) d\lambda} \quad (5-105)$$

The function $F_b(\lambda T)$ defines the fraction of total energy in the blackbody spectrum which lies below λT and is a unique function of λT . For purposes of digital computation, the following series expansion for $F_b(\lambda T)$ proves especially useful.

$$F_b(\lambda T) = \frac{15}{\pi^4} \sum_{k=1}^{\infty} \frac{e^{-k\xi}}{k} \left(\xi^3 + \frac{3\xi^2}{k} + \frac{6\xi}{k^2} + \frac{6}{k^3} \right) \text{ where } \xi = \frac{c_2}{\lambda T} \quad (5-106)$$

Equation (5-106) converges rapidly and is due to Lowan [1941] as referenced in Chang and Rhee [Int. Comm. Heat Mass Transfer, 11, 451-455 (1984)].

Numerically, in the preceding, $h = 6.6260693 \times 10^{-34}$ J·s is the Planck constant; $c = 2.99792458 \times 10^8$ m/s is the velocity of light in vacuum; and $k = 1.3806505 \times 10^{-23}$ J/K is the Boltzmann constant. These data lead to the following values of Planck's first and second constants: $c_1 = 3.741771 \times 10^{-16}$ W·m² and $c_2 = 1.438775 \times 10^{-2}$ m·K, respectively. Numerical values of the Stephan-Boltzmann constant σ in several systems of units are as follows: 5.67040×10^{-8} W/(m²·K⁴); 1.3544×10^{-12} cal/(cm²·s·K⁴); 4.8757×10^{-8} kcal/(m²·h·K⁴); 9.9862×10^{-9} CHU/(ft²·h·K⁴); and 0.17123×10^{-5} Btu/(ft²·h·°R⁴) (CHU = centigrade heat unit; 1.0 CHU = 1.8 Btu.)

Blackbody Displacement Laws The blackbody energy spectrum

is plotted logarithmically in Fig. 5-9 as $\frac{E_{b,\lambda}(\lambda T)}{n^2 T^5} \times 10^{13} \frac{\text{W}}{\text{m}^2 \cdot \mu\text{m} \cdot \text{K}^5}$

versus λT $\mu\text{m} \cdot \text{K}$. For comparison a companion inset is provided in Cartesian coordinates. The upper abscissa of Fig. 5-9 also shows the blackbody energy distribution function $F_b(\lambda T)$. Figure 5-9 indicates that the wavelength-temperature product for which the maximum intensity occurs is $\lambda_{\text{max}} T = 2898 \mu\text{m} \cdot \text{K}$. This relationship is known as **Wien's displacement law**, which indicates that the wavelength for maximum intensity is *inversely* proportional to the absolute temperature. Blackbody displacement laws are useful in engineering practice to estimate wavelength intervals appropriate to relevant system temperatures. The Wien displacement law can be misleading, however, because the wavelength for maximum intensity depends on whether the intensity is defined in terms of frequency or wavelength interval. Two additional useful displacement laws are defined in terms of either the value of λT corresponding to the maximum energy per unit *fractional change* in wavelength or frequency, that is, $\lambda T = 3670 \mu\text{m} \cdot \text{K}$, or to the value of λT corresponding to one-half the blackbody energy, that is, $\lambda T = 4107 \mu\text{m} \cdot \text{K}$. Approximately one-half of the blackbody energy lies within the twofold λT range *geometrically centered* on $\lambda T = 3670 \mu\text{m} \cdot \text{K}$, that is, $3670/\sqrt{2} < \lambda T < 3670\sqrt{2} \mu\text{m} \cdot \text{K}$. Some 95 percent of the blackbody energy lies in the interval $1662.6 < \lambda T < 16,295 \mu\text{m} \cdot \text{K}$. It thus follows that for the temperature range between ambient (300 K) and flame temperatures (2000 K or

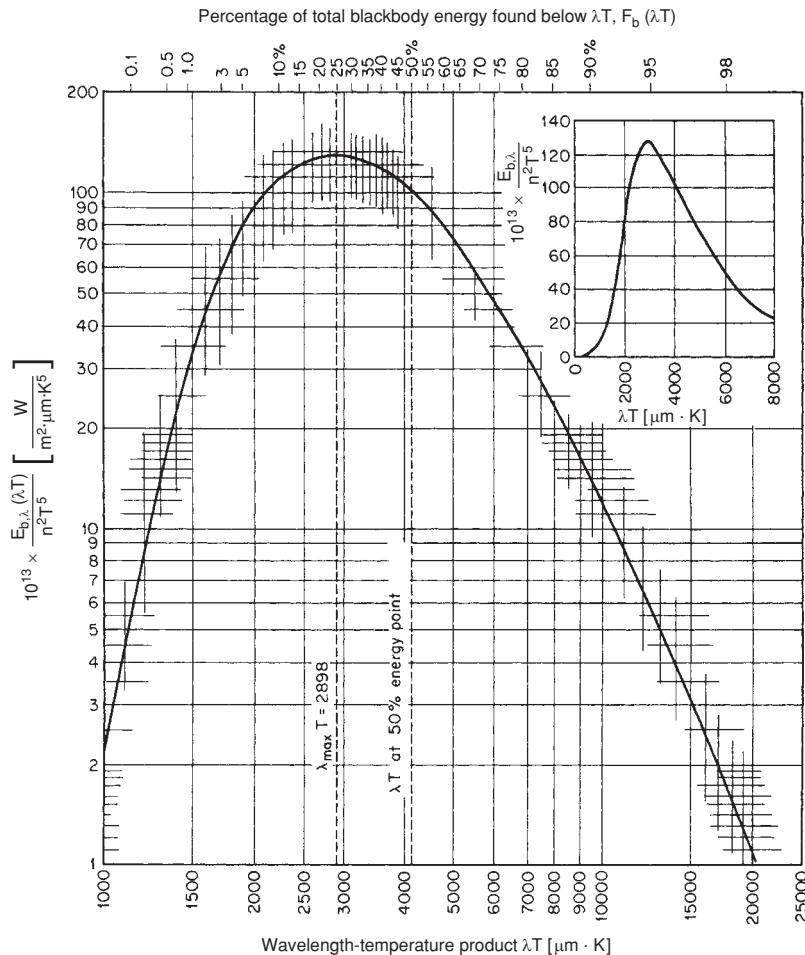


FIG. 5-9 Spectral dependence of monochromatic blackbody hemispherical emissive power.

3140°F), wavelengths of engineering heat-transfer importance are bounded between 0.83 and 54.3 μm .

RADIATIVE PROPERTIES OF OPAQUE SURFACES

Emittance and Absorptance The ratio of the total radiating power of any surface to that of a black surface at the same temperature is called the **emittance** or **emissivity**, ϵ of the surface.^o In general, the monochromatic emissivity is a function of temperature, direction, and wavelength, that is, $\epsilon_\lambda = \epsilon_\lambda(T, \Omega, \lambda)$. The subscripts n and h are sometimes used to denote the normal and hemispherical values, respectively, of the emittance or emissivity. If radiation is incident on a surface, the fraction absorbed is called the **absorptance** (**absorptivity**). Two subscripts are usually appended to the absorptance $\alpha_{1,2}$ to distinguish between the temperature of the absorbing surface T_1 and the spectral energy distribution of the emitting surface T_2 . According to **Kirchhoff's law**, the emissivity and absorptivity of a surface exposed to surroundings at its own temperature are the same for both monochromatic and total radiation. When the temperatures of the surface and its surroundings differ, the total emissivity and absorptivity of the surface are often found to be unequal; but because the absorptivity is substantially independent of irradiation density, the monochromatic emissivity and absorptivity of surfaces are equal for all practical purposes. The difference between *total* emissivity and absorptivity depends on the variation of ϵ_λ with wavelength and on the difference between the temperature of the surface and the effective temperature of the surroundings.

Consider radiative exchange between a real surface of area A_1 at temperature T_1 with black surroundings at temperature T_2 . The *net* radiant interchange is given by

$$Q_{1,2} = A_1 \int_{\lambda=0}^{\infty} [\epsilon_\lambda(T_1, \lambda) \cdot E_{b,\lambda}(T_1, \lambda) - \alpha_\lambda(T_1, \lambda) \cdot E_{b,\lambda}(T_2, \lambda)] d\lambda \quad (5-107a)$$

$$\text{or} \quad Q_{1,2} = A_1 (\epsilon_1 \sigma T_1^4 - \alpha_{1,2} \sigma T_2^4) \quad (5-107b)$$

$$\text{where} \quad \epsilon_1(T_1) = \int_{\lambda=0}^{\infty} \epsilon_\lambda(T_1, \lambda) \cdot \frac{E_{b,\lambda}(T_1, \lambda)}{E_b(T_1)} d\lambda \quad (5-108)$$

$$\text{and since} \quad \alpha_\lambda(T, \lambda) = \epsilon_\lambda(T, \lambda),$$

$$\alpha_{1,2}(T_1, T_2) = \int_{\lambda=0}^{\infty} \epsilon_\lambda(T_1, \lambda) \cdot \frac{E_{b,\lambda}(T_2, \lambda)}{E_b(T_2)} d\lambda \quad (5-109)$$

For a *gray surface* $\epsilon_1 = \alpha_{1,2} = \epsilon_\lambda$. A *selective surface* is one for which $\epsilon_\lambda(T, \lambda)$ exhibits a strong dependence on wavelength. If the wavelength dependence is *monotonic*, it follows from Eqs. (5-107) to (5-109) that ϵ_1 and $\alpha_{1,2}$ can differ markedly when T_1 and T_2 are widely separated. For example, in solar energy applications, the nominal temperature of the earth is $T_1 = 294$ K, and the sun may be represented as a blackbody with radiation temperature $T_2 = 5800$ K. For these temperature conditions, a *white paint* can exhibit $\epsilon_1 = 0.9$ and $\alpha_{1,2} = 0.1$ to 0.2. In contrast, a *thin layer of copper oxide on bright aluminum* can exhibit ϵ_1 as low as 0.12 and $\alpha_{1,2}$ greater than 0.9.

The effect of radiation source temperature on low-temperature absorptivity for a number of representative materials is shown in Fig. 5-10. Polished aluminum (curve 15) and anodized (surface-oxidized) aluminum (curve 13) are representative of metals and nonmetals, respectively. Figure 5-10 thus demonstrates the generalization that metals and nonmetals respond in *opposite directions* with regard to changes in the radiation source temperature. Since the effective solar temperature is 5800 K (10,440°R), the extreme right-hand side of Fig. 5-10 provides surface absorptivity data relevant to solar energy applications. The dependence of emittance and absorptance on the real and imaginary components of the refractive index and on the geometric

structure of the surface layer is quite complex. However, a number of generalizations concerning the radiative properties of opaque surfaces are possible. These are summarized in the following discussion.

Polished Metals

1. In the infrared region, the magnitude of the monochromatic emissivity ϵ_λ is small and is dependent on free-electron contributions. Emissivity is also a function of the ratio of resistivity to wavelength r/λ , as depicted in Fig. 5-11. At shorter wavelengths, bound-electron contributions become significant, ϵ_λ is larger in magnitude, and it sometimes exhibits a maximum value. In the visible spectrum, common values for ϵ_λ are 0.4 to 0.8 and ϵ_λ decreases slightly as temperature increases. For $0.7 < \lambda < 1.5$ μm , ϵ_λ is approximately independent of temperature. For $\lambda > 8$ μm , ϵ_λ is approximately proportional to the square root of temperature since $\epsilon_\lambda \propto \sqrt{r}$ and $r \propto T$. Here the Drude or Hagen-Rubens relation applies, that is, $\epsilon_{\lambda,n} \approx 0.0365 \sqrt{r/\lambda}$, where r has units of ohm-meters and λ is measured in micrometers.

2. Total emittance is substantially proportional to absolute temperature, and at moderate temperatures $\epsilon_n = 0.058T \sqrt{rT}$, where T is measured in kelvins.

3. The total absorptance of a metal at temperature T_1 with respect to radiation from a black or gray source at temperature T_2 is equal to the emissivity evaluated at the geometric mean of T_1 and T_2 . Figure 5-11 gives values of ϵ_λ and $\epsilon_{\lambda,n}$, and their ratio, as a function of the product rT (solid lines). Although Fig. 5-11 is based on free-electron

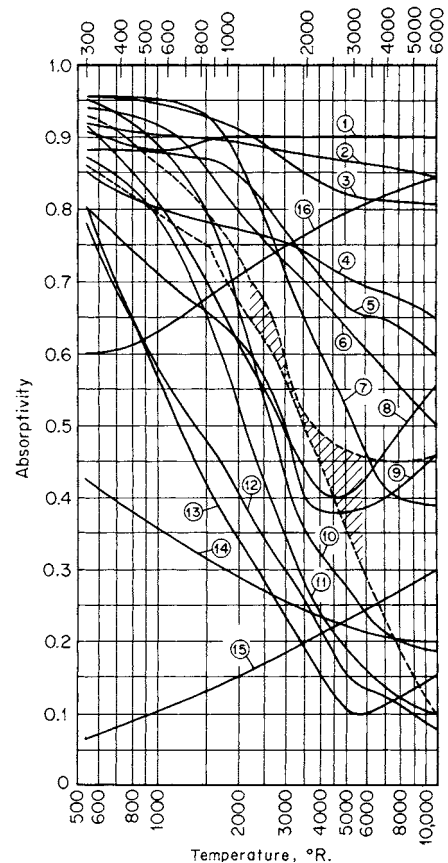


FIG. 5-10 Variation of absorptivity with temperature of radiation source. (1) Slate composition roofing. (2) Linoleum, red brown. (3) Asbestos slate. (4) Soft rubber, gray. (5) Concrete. (6) Porcelain. (7) Vitreous enamel, white. (8) Red brick. (9) Cork. (10) White dutch tile. (11) White chamotte. (12) MgO, evaporated. (13) Anodized aluminum. (14) Aluminum paint. (15) Polished aluminum. (16) Graphite. The two dashed lines bound the limits of data on gray paving brick, asbestos paper, wood, various cloths, plaster of paris, lithopone, and paper. To convert degrees Rankine to kelvins, multiply by $(5.556)(10^{-3})$.

^oIn the literature, *emittance* and *emissivity* are often used interchangeably. NIST (the National Institute of Standards and Technology) recommends use of the suffix *-ivity* for pure materials with optically smooth surfaces, and *-ance* for rough and contaminated surfaces. Most real engineering materials fall into the latter category.

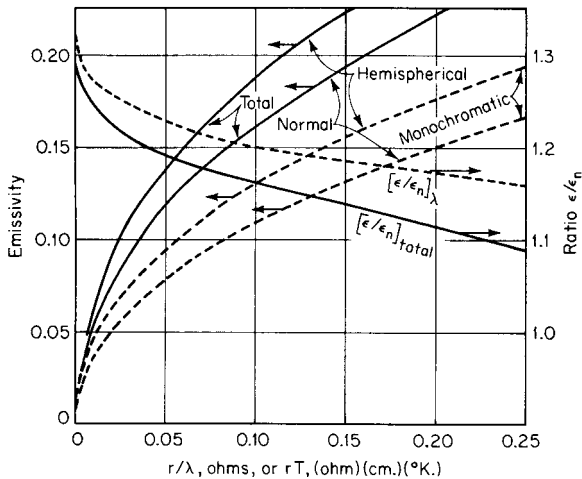


FIG. 5-11 Hemispherical and normal emissivities of metals and their ratio. Dashed lines: monochromatic (spectral) values versus r/λ . Solid lines: total values versus rT . To convert ohm-centimeter-kelvins to ohm-meter-kelvins, multiply by 10^{-2} .

contributions to emissivity in the far infrared, the relations for total emissivity are remarkably good even at high temperatures. Unless extraordinary efforts are taken to prevent oxidation, a metallic surface may exhibit an emissance or absorptance which may be several times that of a polished specimen. For example, the emissance of iron and steel depends strongly on the degree of oxidation and roughness. Clean iron and steel surfaces have an emissance from 0.05 to 0.45 at ambient temperatures and 0.4 to 0.7 at high temperatures. Oxidized and/or roughened iron and steel surfaces have values of emissance ranging from 0.6 to 0.95 at low temperatures to 0.9 to 0.95 at high temperatures.

Refractory Materials For refractory materials, the dependence of emissance and absorptance on grain size and impurity concentrations is quite important.

1. Most refractory materials are characterized by $0.8 < \epsilon_\lambda < 1.0$ for the wavelength region $2 < \lambda < 4 \mu\text{m}$. The monochromatic emissivity ϵ_λ decreases rapidly toward shorter wavelengths for materials that are white in the visible range but demonstrates high values for black materials such as FeO and Cr_2O_3 . Small concentrations of FeO and Cr_2O_3 or other colored oxides, can cause marked increases in the emissance of materials that are normally white. The sensitivity of the emissance of refractory oxides to small additions of absorbing materials is demonstrated by the results of calculations presented in Fig. 5-12. Figure 5-12 shows the emissance of a semi-infinite absorbing-scattering medium as a function of its *albedo* $\omega \equiv K_s/(K_a + K_s)$, where K_a and K_s are the scatter and absorption coefficients, respectively. These results are relevant to the radiative properties of fibrous materials, paints, oxide coatings, refractory materials, and other *particulate* media. They demonstrate that over the relatively small range $1 - \omega = 0.005$ to 0.1 , the hemispherical emissance ϵ_h increases from approximately 0.15 to 1.0. For refractory materials, ϵ_λ varies little with temperature, with the exception of some white oxides which at high temperatures become good emitters in the visible spectrum as a consequence of the induced electronic transitions.

2. For refractory materials at ambient temperatures, the total emissance ϵ is generally high (0.7 to 1.0). Total refractory emissance decreases with increasing temperature, such that a temperature increase from 1000 to 1570°C may result in a 20 to 30 percent reduction in ϵ .

3. Emissance and absorptance increase with increase in grain size over a grain size range of 1 to 200 μm .

4. The ratio ϵ_h/ϵ_n of hemispherical to normal emissivity of polished surfaces varies with refractive index n ; e.g., the ratio decreases from a value of 1.0 when $n = 1.0$ to a value of 0.93 when $n = 1.5$ (common glass) and increases back to 0.96 at $n = 3.0$.

5. As shown in Fig. 5-12, for a surface composed of particulate

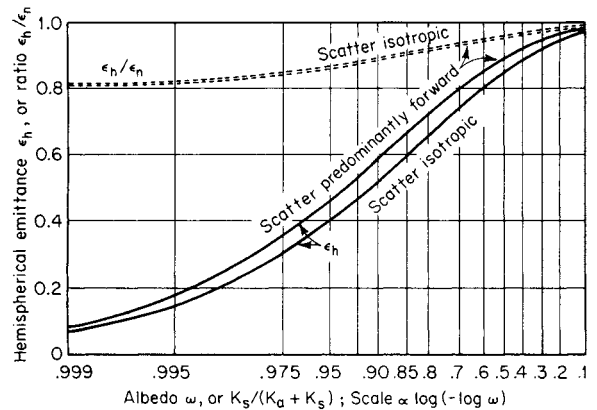


FIG. 5-12 Hemispherical emissance ϵ_h and the ratio of hemispherical to normal emissance ϵ_h/ϵ_n for a semi-infinite absorbing-scattering medium.

matter which scatters isotropically, the ratio ϵ_h/ϵ_n varies from 1.0 when $\omega < 0.1$ to about 0.8 when $\omega = 0.999$.

6. The total absorptance exhibits a decrease with an increase in temperature of the radiation source similar to the decrease in emissance with an increase in the emitter temperature.

Figure 5-10 shows a regular variation of $\alpha_{1,2}$ with T_2 . When T_2 is not very different from T_1 , $\alpha_{1,2} = \epsilon_1(T_2/T_1)^m$. It may be shown that Eq. (5-107b) is then approximated by

$$Q_{1,2} = (1 + m/4)\epsilon_{av} A_1 \sigma(T_1^4 - T_2^4) \quad (5-110)$$

where ϵ_{av} is evaluated at the arithmetic mean of T_1 and T_2 . For metals $m \approx 0.5$ while for nonmetals m is small and negative.

Table 5-4 illustrates values of emissance for materials encountered in engineering practice. It is based on a critical evaluation of early emissivity data. Table 5-4 demonstrates the wide variation possible in the emissivity of a particular material due to variations in surface roughness and thermal pretreatment. With few exceptions the data in Table 5-4 refer to emissances ϵ_n normal to the surface. The hemispherical emissance ϵ_h is usually slightly smaller, as demonstrated by the ratio ϵ_h/ϵ_n depicted in Fig. 5-12. More recent data support the range of emissance values given in Table 5-4 and their dependence on surface conditions. An extensive compilation is provided by Goldsmith, Waterman, and Hirschorn (*Thermophysical Properties of Matter*, Purdue University, Touloukian, ed., Plenum, 1970-1979).

For opaque materials the reflectance ρ is the complement of the absorptance. The directional distribution of the reflected radiation depends on the material, its degree of roughness or grain size, and, if a metal, its state of oxidation. Polished surfaces of homogeneous materials are specular reflectors. In contrast, the intensity of the radiation reflected from a perfectly diffuse or *Lambert surface* is independent of direction. The directional distribution of reflectance of many oxidized metals, refractory materials, and natural products approximates that of a perfectly diffuse reflector. A better model, adequate for many calculation purposes, is achieved by assuming that the total reflectance is the sum of diffuse and specular components ρ_D and ρ_S , as discussed in a subsequent section.

VIEW FACTORS AND DIRECT EXCHANGE AREAS

Consider radiative interchange between two *finite* black surface area elements A_1 and A_2 separated by a transparent medium. Since they are black, the surfaces emit isotropically and totally absorb all incident radiant energy. It is desired to compute the fraction of radiant energy, per unit emissive power E_1 , leaving A_1 in all directions which is intercepted and absorbed by A_2 . The required quantity is defined as the **direct view factor** and is assigned the notation $F_{1,2}$. Since the *net radiant energy interchange* $Q_{1,2} \equiv A_1 F_{1,2} E_1 - A_2 F_{2,1} E_2$ between surfaces A_1 and A_2 must be zero when their temperatures are equal, it follows

TABLE 5-4 Normal Total Emissivity of Various Surfaces

A. Metals and Their Oxides					
Surface	<i>t</i> , °F°	Emissivity*	Surface	<i>t</i> , °F°	Emissivity*
Aluminum			Sheet steel, strong rough oxide layer	75	0.80
Highly polished plate, 98.3% pure	440–1070	0.039–0.057	Dense shiny oxide layer	75	0.82
Polished plate	73	0.040	Cast plate:		
Rough plate	78	0.055	Smooth	73	0.80
Oxidized at 1110°F	390–1110	0.11–0.19	Rough	73	0.82
Aluminum-surfaced roofing	100	0.216	Cast iron, rough, strongly oxidized	100–480	0.95
Calorized surfaces, heated at 1110°F.			Wrought iron, dull oxidized	70–680	0.94
Copper	390–1110	0.18–0.19	Steel plate, rough	100–700	0.94–0.97
Steel	390–1110	0.52–0.57	High temperature alloy steels (see Nickel Alloys).		
Brass			Molten metal		
Highly polished:			Cast iron	2370–2550	0.29
73.2% Cu, 26.7% Zn	476–674	0.028–0.031	Mild steel	2910–3270	0.28
62.4% Cu, 36.8% Zn, 0.4% Pb, 0.3% Al	494–710	0.033–0.037	Lead		
82.9% Cu, 17.0% Zn	530	0.030	Pure (99.96%), unoxidized	260–440	0.057–0.075
Hard rolled, polished:			Gray oxidized	75	0.281
But direction of polishing visible	70	0.038	Oxidized at 390°F.	390	0.63
But somewhat attacked	73	0.043	Mercury	32–212	0.09–0.12
But traces of stearin from polish left on	75	0.053	Molybdenum filament	1340–4700	0.096–0.292
Polished	100–600	0.096	Monel metal, oxidized at 1110°F	390–1110	0.41–0.46
Rolled plate, natural surface	72	0.06	Nickel		
Rubbed with coarse emery	72	0.20	Electroplated on polished iron, then polished	74	0.045
Dull plate	120–660	0.22	Technically pure (98.9% Ni, + Mn), polished	440–710	0.07–0.087
Oxidized by heating at 1110°F	390–1110	0.61–0.59	Electroplated on pickled iron, not polished	68	0.11
Chromium; see Nickel Alloys for Ni-Cr steels	100–1000	0.08–0.26	Wire	368–1844	0.096–0.186
Copper			Plate, oxidized by heating at 1110°F	390–1110	0.37–0.48
Carefully polished electrolytic copper	176	0.018	Nickel oxide	1200–2290	0.59–0.86
Commercial, emiered, polished, but pits remaining	66	0.030	Nickel alloys		
Commercial, scraped shiny but not mirror-like	72	0.072	Chromnickel	125–1894	0.64–0.76
Polished	242	0.023	Nickelin (18–32 Ni; 55–68 Cu; 20 Zn), gray oxidized	70	0.262
Plate, heated long time, covered with thick oxide layer	77	0.78	KA-2S alloy steel (8% Ni; 18% Cr), light silvery, rough, brown, after heating After 42 hr. heating at 980°F.	420–914	0.44–0.36
Plate heated at 1110°F	390–1110	0.57	NCT-3 alloy (20% Ni; 25% Cr.), brown, splotted, oxidized from service	420–980	0.62–0.73
Cuprous oxide	1470–2010	0.66–0.54	NCT-6 alloy (60% Ni; 12% Cr), smooth, black, firm adhesive oxide coat from service	420–980	0.90–0.97
Molten copper	1970–2330	0.16–0.13	Platinum		
Gold			Pure, polished plate	440–1160	0.054–0.104
Pure, highly polished	440–1160	0.018–0.035	Strip	1700–2960	0.12–0.17
Iron and steel			Filament	80–2240	0.036–0.192
Metallic surfaces (or very thin oxide layer):			Wire	440–2510	0.073–0.182
Electrolytic iron, highly polished	350–440	0.052–0.064	Silver		
Polished iron	800–1880	0.144–0.377	Polished, pure	440–1160	0.0198–0.0324
Iron freshly emiered	68	0.242	Polished	100–700	0.0221–0.0312
Cast iron, polished	392	0.21	Steel, see Iron.		
Wrought iron, highly polished	100–480	0.28	Tantalum filament	2420–5430	0.194–0.31
Cast iron, newly turned	72	0.435	Tin—bright tinned iron sheet	76	0.043 and 0.064
Polished steel casting	1420–1900	0.52–0.56	Tungsten		
Ground sheet steel	1720–2010	0.55–0.61	Filament, aged	80–6000	0.032–0.35
Smooth sheet iron	1650–1900	0.55–0.60	Filament	6000	0.39
Cast iron, turned on lathe	1620–1810	0.60–0.70	Zinc		
Oxidized surfaces:			Commercial, 99.1% pure, polished	440–620	0.045–0.053
Iron plate, pickled, then rusted red	68	0.612	Oxidized by heating at 750°F.	750	0.11
Completely rusted	67	0.685	Galvanized sheet iron, fairly bright	82	0.228
Rolled sheet steel	70	0.657	Galvanized sheet iron, gray oxidized	75	0.276
Oxidized iron	212	0.736			
Cast iron, oxidized at 1100°F	390–1110	0.64–0.78			
Steel, oxidized at 1100°F	390–1110	0.79			
Smooth oxidized electrolytic iron	260–980	0.78–0.82			
Iron oxide	930–2190	0.85–0.89			
Rough ingot iron	1700–2040	0.87–0.95			
B. Refractories, Building Materials, Paints, and Miscellaneous					
Asbestos			Carbon		
Board	74	0.96	T-carbon (Gebr. Siemens) 0.9% ash (this started with emissivity at 260°F. of 0.72, but on heating changed to values given)	260–1160	0.81–0.79
Paper	100–700	0.93–0.945	Carbon filament	1900–2560	0.526
Brick			Candle soot	206–520	0.952
Red, rough, but no gross irregularities	70	0.93	Lampblack-waterglass coating	209–362	0.959–0.947
Silica, unglazed, rough	1832	0.80			
Silica, glazed, rough	2012	0.85			
Grog brick, glazed	2012	0.75			
See Refractory Materials below.					

TABLE 5-4 Normal Total Emissivity of Various Surfaces (Concluded)

B. Refractories, Building Materials, Paints, and Miscellaneous					
Surface	$t, ^\circ\text{F}^\circ$	Emissivity ^o	Surface	$t, ^\circ\text{F}^\circ$	Emissivity ^o
Same	260–440	0.957–0.952	Oil paints, sixteen different, all colors	212	0.92–0.96
Thin layer on iron plate	69	0.927	Aluminum paints and lacquers		
Thick coat	68	0.967	10% Al, 22% lacquer body, on rough or smooth surface	212	0.52
Lampblack, 0.003 in. or thicker	100–700	0.945	26% Al, 27% lacquer body, on rough or smooth surface	212	0.3
Enamel, white fused, on iron	66	0.897	Other Al paints, varying age and Al content	212	0.27–0.67
Glass, smooth	72	0.937	Al lacquer, varnish binder, on rough plate	70	0.39
Gypsum, 0.02 in. thick on smooth or blackened plate	70	0.903	Al paint, after heating to 620°F.	300–600	0.35
Marble, light gray, polished	72	0.931	Paper, thin	66	0.924
Oak, planed	70	0.895	Pasted on tinned iron plate	66	0.929
Oil layers on polished nickel (lube oil)	68		On rough iron plate	66	0.944
Polished surface, alone		0.045	On black lacquered plate	66	0.944
+0.001-in. oil		0.27	Plaster, rough lime	50–190	0.91
+0.002-in. oil		0.46	Porcelain, glazed	72	0.924
+0.005-in. oil		0.72	Quartz, rough, fused	70	0.932
Infinitely thick oil layer		0.82	Refractory materials, 40 different	1110–1830	
Oil layers on aluminum foil (linseed oil)			poor radiators		$\left[\begin{matrix} 0.65 \\ 0.70 \\ 0.80 \\ 0.85 \end{matrix} \right] - \left[\begin{matrix} 0.75 \\ 0.85 \\ 0.90 \end{matrix} \right]$
Al foil	212	0.087†	good radiators		
+1 coat oil	212	0.561			
+2 coats oil	212	0.574			
Paints, lacquers, varnishes					
Snowwhite enamel varnish or rough iron plate	73	0.906	Roofing paper	69	0.91
Black shiny lacquer, sprayed on iron	76	0.875	Rubber		
Black shiny shellac on tinned iron sheet	70	0.821	Hard, glossy plate	74	0.945
Black matte shellac	170–295	0.91	Soft, gray, rough (reclaimed)	76	0.859
Black lacquer	100–200	0.80–0.95	Serpentine, polished	74	0.900
Flat black lacquer	100–200	0.96–0.98	Water	32–212	0.95–0.963
White lacquer	100–200	0.80–0.95			

^oWhen two temperatures and two emissivities are given, they correspond, first to first and second to second, and linear interpolation is permissible. $^\circ\text{C} = (^\circ\text{F} - 32)/1.8$.

†Although this value is probably high, it is given for comparison with the data by the same investigator to show the effect of oil layers. See Aluminum, Part A of this table.

thermodynamically that $A_1F_{1,2} = A_2F_{2,1}$. The product of area and view factor $\overline{s_1s_2} \equiv A_1F_{1,2}$, which has the dimensions of area, is termed the **direct surface-to-surface exchange area** for finite black surfaces. Clearly, direct exchange areas are symmetric with respect to their subscripts, that is, $\overline{s_1s_2} = \overline{s_2s_1}$, but view factors are not symmetric unless the associated surface areas are equal. This property is referred to as the **symmetry or reciprocity relation** for direct exchange areas. The shorthand notation $\overline{s_1s_2} \equiv 12 = 21$ for direct exchange areas is often found useful in mathematical developments.

Equation (5-101) may also be restated as

$$\frac{\partial^2 \overline{s_1s_2}}{\partial A_i \partial A_j} = \frac{\cos \phi_i \cos \phi_j}{\pi r^2} \quad (5-111)$$

which leads directly to the required definition of the direct exchange area as a double surface integral

$$\overline{s_1s_2} = \iint_{A_i} \iint_{A_j} \frac{\cos \phi_i \cos \phi_j}{\pi r^2} dA_j dA_i \quad (5-112)$$

All terms in Eq. (5-112) have been previously defined.

Suppose now that Eq. (5-112) is integrated over the entire confining surface of an **enclosure** which has been subdivided into M finite area elements. Each of the M surface **zones** must then satisfy certain **conservation relations** involving *all* the direct exchange areas in the enclosure

$$\sum_{j=1}^M \overline{s_1s_j} = A_1 \quad \text{for } 1 \leq i \leq M \quad (5-113a)$$

or in terms of view factors

$$\sum_{j=1}^M F_{1j} = 1 \quad \text{for } 1 \leq i \leq M \quad (5-113b)$$

Contour integration is commonly used to simplify the evaluation of Eq. (5-112) for specific geometries; see Modest (op. cit., Chap. 4)

or Siegel and Howell (op. cit., Chap. 5). The formulas for two particularly useful view factors involving perpendicular rectangles of area xz and yz with common edge z and equal parallel rectangles of area xy and distance of separation z are given for **perpendicular rectangles** with common dimension z

$$\begin{aligned} (\pi \cdot X) \cdot F_{XY} &= X \tan^{-1} \frac{1}{X} + Y \tan^{-1} \frac{1}{Y} - \sqrt{X^2 + Y^2} \tan^{-1} \sqrt{\frac{1}{X^2 + Y^2}} \\ &+ \frac{1}{4} \ln \left\{ \frac{(1 + X^2)(1 + Y^2)}{1 + X^2 + Y^2} \left[\frac{X^2(1 + X^2 + Y^2)}{(1 + X^2)(X^2 + Y^2)} \right]^{X^2} \left[\frac{Y^2(1 + X^2 + Y^2)}{(1 + Y^2)(X^2 + Y^2)} \right]^{Y^2} \right\} \end{aligned} \quad (5-114a)$$

and for **parallel rectangles**, separated by distance z ,

$$\begin{aligned} \left(\frac{\pi \cdot X \cdot Y}{2} \right) \cdot F_{XY} &= \ln \left[\frac{(1 + X^2)(1 + Y^2)}{1 + X^2 + Y^2} \right]^{1/2} + X\sqrt{1 + Y^2} \tan^{-1} \frac{X}{\sqrt{1 + Y^2}} \\ &+ Y\sqrt{1 + X^2} \tan^{-1} \frac{Y}{\sqrt{1 + X^2}} - X \tan^{-1} X - Y \tan^{-1} Y \end{aligned} \quad (5-114b)$$

In Eqs. (5-114) X and Y are normalized whereby $X = x/z$ and $Y = y/z$ and the corresponding **dimensional** direct surface areas are given by $\overline{s_1s_2} = xzF_{XY}$ and $\overline{s_3s_4} = yzF_{XY}$, respectively.

The exchange area between any two area elements of a sphere is independent of their relative shape and position and is simply the product of the areas, divided by the area of the entire sphere; i.e., any spot on a sphere has equal views of all other spots.

Figure 5-13, curves 1 through 4, shows view factors for selected parallel opposed disks, squares, and 2:1 rectangles and parallel rectangles with one infinite dimension as a function of the ratio of the

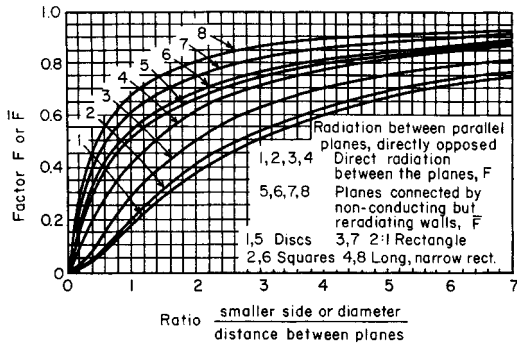


FIG. 5-13 Radiation between parallel planes, directly opposed.

smaller diameter or side to the distance of separation. Curves 2 through 4 of Fig. 5-13, for opposed rectangles, can be computed with Eq. (5-114b). The view factors for two finite coaxial coextensive cylinders of radii $r \leq R$ and height L are shown in Fig. 5-14. The direct view factors for an infinite plane parallel to a system of rows of parallel tubes (see Fig. 5-16) are given as curves 1 and 3 of Fig. 5-15. The view factors for this two-dimensional geometry can be readily calculated by using the **crossed-strings method**.

The crossed-strings method, due to Hottel (*Radiative Transfer*, McGraw-Hill, New York, 1967), is stated as follows: "The exchange area for two-dimensional surfaces, A_1 and A_2 , per unit length (in the infinite dimension) is given by the sum of the lengths of crossed strings from the ends of A_1 to the ends of A_2 less the sum of the uncrossed strings from and to the same points all divided by 2." The strings must be drawn so that all the flux from one surface to the other must cross each of a pair of crossed strings and neither of the pair of uncrossed strings. If one surface can see the other around both sides of an obstruction, two more pairs of strings are involved. The calculation procedure is demonstrated by evaluation of the tube-to-tube view factor for one row of a tube bank, as illustrated in Example 7.

Example 7: The Crossed-Strings Method Figure 5-16 depicts the transverse cross section of two infinitely long, parallel circular tubes of diameter D and center-to-center distance of separation C . Use the crossed-strings method to formulate the tube-to-tube direct exchange area and view factor $\overline{s_1s_2}$ and F_{12} , respectively.

Solution: The circumferential area of each tube is $A_i = \pi D$ per unit length in the infinite dimension for this two-dimensional geometry. Application of the crossed-strings procedure then yields simply

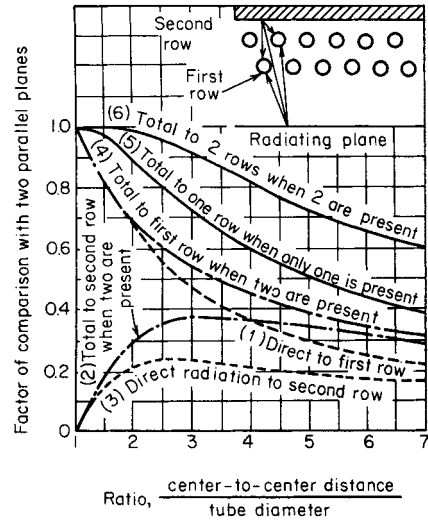


FIG. 5-15 Distribution of radiation to rows of tubes irradiated from one side. Dashed lines: direct view factor F from plane to tubes. Solid lines: total view factor F for black tubes backed by a refractory surface.

$$\overline{s_1s_2} = \frac{2(EFGH - HJ)}{2} = D[\sin^{-1}(1/R) + \sqrt{R^2 - 1} - R]$$

and

$$F_{12} = \overline{s_1s_2}/A_1 = [\sin^{-1}(1/R) + \sqrt{R^2 - 1} - R]/\pi$$

where $EFGH$ and $HJ = C$ are the indicated line segments and $R \equiv C/D \geq 1$. Curve 1 of Fig. 5-15, denoted by $F_{p,1}$, is a function of F_{12} , that is, $F_{p,1} = (\pi/R)(\frac{1}{2} - F_{12})$.

The **Yamauti principle** [Yamauti, *Res. Electrotech Lab. (Tokyo)*, 148 (1924); 194 (1927); 250 (1929)] is stated as follows: *The exchange areas between two pairs of surfaces are equal when there is a one-to-one correspondence for all sets of symmetrically positioned pairs of differential elements in the two surface combinations.* Figure 5-17 illustrates the Yamauti principle applied to surfaces in perpendicular planes having a common edge. With reference to Fig. 5-17, the Yamauti principle states that the diagonally opposed exchange areas are equal, that is, $(1)(4) = (2)(3)$. Figure 5-17 also shows a more complex geometric construction for displaced cylinders for which the Yamauti principle also applies. Collectively the three terms *reciprocity* or *symmetry principle*, *conservation*

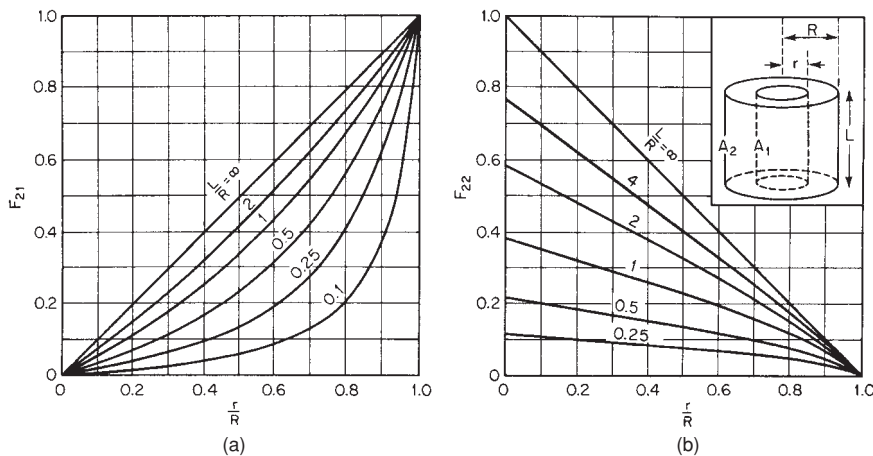


FIG. 5-14 View factors for a system of two concentric coaxial cylinders of equal length. (a) Inner surface of outer cylinder to inner cylinder. (b) Inner surface of outer cylinder to itself.

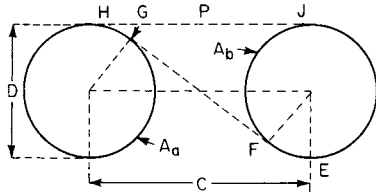


FIG. 5-16 Direct exchange between parallel circular tubes.

principle, and Yamauti principle are referred to as **view factor or exchange area algebra**.

Example 8: Illustration of Exchange Area Algebra Figure 5-17 shows a graphical construction depicting four perpendicular opposed rectangles with a common edge. Numerically evaluate the direct exchange areas and view factors for the diagonally opposed (shaded) rectangles A_1 and A_4 , that is, $\overline{(1)(4)}$, as well as $\overline{(1)(3+4)}$. The dimensions of the rectangular construction are shown in Fig. 5-17 as $x=3$, $y=2$, and $z=1$.

Solution: Using shorthand notation for direct exchange areas, the conservation principle yields

$$\overline{(1+2)(3+4)} = \overline{(1+2)(3)} + \overline{(1+2)(4)} = \overline{(1)(3)} + \overline{(2)(3)} + \overline{(1)(4)} + \overline{(2)(4)}$$

Now by the Yamauti principle we have $\overline{(1)(4)} \equiv \overline{(2)(3)}$. Combination of these two relations yields the first result $\overline{(1)(4)} = [\overline{(1+2)(3+4)} - \overline{(1)(3)} - \overline{(2)(4)}]/2$. For $\overline{(1)(3+4)}$, again conservation yields $\overline{(1)(3+4)} = \overline{(1)(3)} + \overline{(1)(4)}$, and substitution of the expression for $\overline{(1)(4)}$ just obtained yields the second result, that is, $\overline{(1)(3+4)} = [\overline{(1+2)(3+4)} + \overline{(1)(3)} - \overline{(2)(4)}]/2.0$. All three required direct exchange areas in these two relations are readily evaluated from Eq. (5-114a). Moreover, these equations apply to opposed parallel rectangles as well as rectangles with a common edge oriented at any angle. Numerically it follows from Eq. (5-114a) that for $X = \frac{1}{3}$, $Y = \frac{2}{3}$, and $z = 3$ that $\overline{(1+2)(3+4)} = 0.95990$; for $X = 1$, $Y = 2$, and $z = 1$ that $\overline{(1)(3)} = 0.23285$; and for $X = \frac{1}{2}$, $Y = 1$, and $z = 2$ that $\overline{(2)(4)} = 0.585747$. Since $A_1 = 1.0$, this leads to $s_{134} = F_{1,4} = (0.95990 - 0.23285 - 0.584747)/2.0 = 0.07115$ and $s_{13+4} = F_{1,3+4} = (0.95990 + 0.23285 - 0.584747)/2.0 = 0.30400$.

Many literature sources document closed-form algebraic expressions for view factors. Particularly comprehensive references include the compendia by Modest (op. cit., App. D) and Siegel and Howell (op. cit., App. C). The appendices for both of these textbooks also provide a wealth of resource information for radiative transfer. Appendix F of Modest, e.g., references an extensive listing of Fortran computer codes for a variety of radiation calculations which include view factors. These codes are archived in the dedicated Internet web site maintained by the publisher. The textbook by Siegel and Howell also includes an extensive database of view factors archived on a CD-ROM and includes a reference to an author-maintained Internet web site. Other historical sources for view factors include Hottel and Sarofim (op. cit., Chap. 2) and Hamilton and Morgan (NACA-TN 2836, December 1952).

RADIATIVE EXCHANGE IN ENCLOSURES—THE ZONE METHOD

Total Exchange Areas When an enclosure contains reflective surface zones, allowance must be made for not only the radiant energy transferred directly between any two zones but also the additional transfer attendant to however many multiple reflections which occur among the intervening reflective surfaces. Under such circumstances,

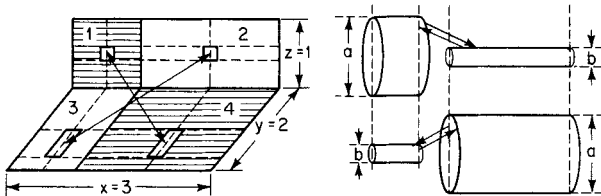


FIG. 5-17 Illustration of the Yamauti principle.

it can be shown that the net radiative flux Q_{ij} between all such surface zone pairs A_i and A_j , making full allowance for all multiple reflections, may be computed from

$$Q_{ij} = \sigma(A_i \mathcal{F}_{ij} T_i^4 - A_j \mathcal{F}_{ji} T_j^4) \quad (5-115)$$

Here, \mathcal{F}_{ij} is defined as the **total surface-to-surface view factor** from A_i to A_j , and the quantity $S_i S_j \equiv A_i \mathcal{F}_{ij}$ is defined as the corresponding **total surface-to-surface exchange area**. In analogy with the direct exchange areas, the total surface-to-surface exchange areas are also symmetric and thus obey reciprocity, that is, $A_i \mathcal{F}_{ij} = A_j \mathcal{F}_{ji}$ or $S_i S_j = S_j S_i$. When applied to an enclosure, total exchange areas and view factors also must satisfy appropriate conservation relations. Total exchange areas are functions of the geometry and radiative properties of the entire enclosure. They are also independent of temperature if all surfaces and any radiatively participating media are gray. The following subsection presents a general matrix method for the explicit evaluation of total exchange areas from direct exchange areas and other enclosure parameters.

In what follows, conventional matrix notation is strictly employed as in $\mathbf{A} = [a_{ij}]$ wherein the scalar subscripts always denote the row and column indices, respectively, and all matrix entities defined here are denoted by boldface notation. Section 3 of this handbook, "Mathematics," provides an especially convenient reference for introductory matrix algebra and matrix computations.

General Matrix Formulation The zone method is perhaps the simplest numerical quadrature of the governing integral equations for radiative transfer. It may be derived from first principles by starting with the equation of transfer for radiation intensity. The zone method always conserves radiant energy since the spatial discretization utilizes macroscopic energy balances involving spatially averaged radiative flux quantities. Because large sets of linear algebraic equations can arise in this process, matrix algebra provides the most compact notation and the most expeditious methods of solution. The mathematical approach presented here is a matrix generalization of the original (scalar) development of the zone method due to Hottel and Sarofim (op. cit.). The present matrix development is abstracted from that introduced by Noble [Noble, J. J., Int. J. Heat Mass Transfer, 18, 261–269 (1975)].

Consider an arbitrary three-dimensional enclosure of total volume V and surface area A which confines an absorbing-emitting medium (gas). Let the enclosure be subdivided (zoned) into M finite surface area and N finite volume elements, each small enough that all such zones are substantially isothermal. The mathematical development in this section is restricted by the following conditions and/or assumptions:

1. The gas temperatures are given a priori.
2. Allowance is made for gas-to-surface radiative transfer.
3. Radiative transfer with respect to the confined gas is either monochromatic or gray. The gray gas absorption coefficient is denoted here by $K(m^{-1})$. In subsequent sections the monochromatic absorption coefficient is denoted by $K_r(\lambda)$.
4. All surface emissivities are assumed to be gray and thus independent of temperature.
5. Surface emission and reflection are isotropic or diffuse.
6. The gas does not scatter.

Noble (op. cit.) has extended the present matrix methodology to the case where the gaseous absorbing-emitting medium also scatters isotropically.

In matrix notation the blackbody emissive powers for all surface and volume zones comprising the zoned enclosure are designated as $\mathbf{E} = [E_i] = [\sigma T_i^4]$, an $M \times 1$ vector, and $\mathbf{E}_g = [E_{g,i}] = [\sigma T_{g,i}^4]$, an $N \times 1$ vector, respectively. Moreover, all surface zones are characterized by three $M \times M$ diagonal matrices for zone area $\mathbf{A} \mathbf{I} = [A_i \delta_{ij}]$, diffuse emissivity $\mathbf{e} \mathbf{I} = [e_i \delta_{ij}]$, and diffuse reflectivity, $\rho \mathbf{I} = [(1 - e_i) \delta_{ij}]$, respectively. Here δ_{ij} is the **Kronecker delta** (that is, $\delta_{ij} = 1$ for $i = j$ and $\delta_{ij} = 0$ for $i \neq j$).

Two arrays of direct exchange areas are now defined; i.e., the matrix $\mathbf{ss} = [s_{ij}]$ is the $M \times M$ array of **direct surface-to-surface exchange areas**, and the matrix $\mathbf{sg} = [s_{ij}^g]$ is the $M \times N$ array of **direct gas-to-surface exchange areas**. Here the scalar elements of \mathbf{ss} and \mathbf{sg} are computed from the integrals

$$s_{ij} = \iint_{A_i} \iint_{A_j} \frac{e^{-Kr}}{\pi r^2} \cos \phi_i \cos \phi_j dA_i dA_j \quad (5-116a)$$

$$\overline{s_i g_j} = \iint_{A_i} \iint_{V_j} K \frac{e^{-Kr}}{\pi r^2} \cos \phi_i dV_j dA_i \quad (5-116b)$$

Equation (5-116a) is a generalization of Eq. (5-112) for the case $K \neq 0$ while $\overline{s_i g_j}$ is a new quantity, which arises *only* for the case $K \neq 0$.

Matrix characterization of the radiative energy balance at each surface zone is facilitated via definition of three $M \times 1$ vectors; the radiative surface fluxes $\mathbf{Q} = [Q_i]$, with units of watts; and the vectors $\mathbf{H} = [H_i]$ and $\mathbf{W} = [W_i]$ both having units of W/m^2 . The arrays \mathbf{H} and \mathbf{W} define the *incident* and *leaving* flux densities, respectively, at each surface zone. The variable \mathbf{W} is also referred to in the literature as the **radiosity** or **exitance**. Since $\mathbf{W} \equiv \epsilon \mathbf{I} \cdot \mathbf{E} + \rho \mathbf{I} \cdot \mathbf{H}$, the radiative flux at each surface zone is also defined in terms of \mathbf{E} , \mathbf{H} , and \mathbf{W} by three equivalent matrix relations, namely,

$$\mathbf{Q} = \mathbf{AI} \cdot [\mathbf{W} - \mathbf{H}] = \epsilon \mathbf{AI} \cdot [\mathbf{E} - \mathbf{H}] = \rho \mathbf{I}^{-1} \cdot \epsilon \mathbf{AI} \cdot [\mathbf{E} - \mathbf{W}] \quad (5-117)$$

where the third form is valid *if and only if the matrix inverse* $\rho \mathbf{I}^{-1}$ *exists*. Two other ancillary matrix expressions are

$$\epsilon \mathbf{AI} \cdot \mathbf{E} = \rho \mathbf{I} \cdot \mathbf{Q} + \epsilon \mathbf{AI} \cdot \mathbf{W} \quad \text{and} \quad \mathbf{AI} \cdot \mathbf{H} = \overline{\mathbf{SS}} \cdot \mathbf{W} + \overline{\mathbf{SG}} \cdot \mathbf{E}_g \quad (5-117a,b)$$

which lead to

$$\epsilon \mathbf{I} \cdot \mathbf{E} = [\mathbf{I} - \rho \mathbf{I} \cdot \mathbf{AI}^{-1} \cdot \overline{\mathbf{SS}}] \cdot \mathbf{W} - \rho \mathbf{I} \cdot \mathbf{AI}^{-1} \cdot \overline{\mathbf{SG}} \cdot \mathbf{E}_g \quad (5-117c)$$

The latter relation is especially useful in radiation pyrometry where true wall temperatures must be computed from wall radiositivities.

Explicit Matrix Solution for Total Exchange Areas For gray or monochromatic transfer, the **primary working relation** for zoning calculations via the matrix method is

$$\mathbf{Q} = \epsilon \mathbf{I} \cdot \mathbf{AI} \cdot \mathbf{E} - \overline{\mathbf{SS}} \cdot \mathbf{E} - \overline{\mathbf{SG}} \cdot \mathbf{E}_g \quad [M \times 1] \quad (5-118)$$

Equation (5-118) makes full allowance for multiple reflections in an enclosure of any degree of complexity. To apply Eq. (5-118) for design or simulation purposes, the gas temperatures must be known and surface boundary conditions must be specified for each and every surface zone in the form of *either* E_i or Q_i . In application of Eq. (5-118), *physically impossible values* of E_i may well result if *physically unrealistic* values of Q_i are specified.

In Eq. (5-118), $\overline{\mathbf{SS}}$ and $\overline{\mathbf{SG}}$ are defined as the *required* arrays of **total surface-to-surface exchange areas** and **total gas-to-surface exchange areas**, respectively. The matrices for total exchange areas are calculated *explicitly* from the corresponding arrays of direct exchange areas and the other enclosure parameters by the following matrix formulas:

$$\text{Surface-to-surface exchange} \quad \overline{\mathbf{SS}} = \epsilon \mathbf{I} \cdot \mathbf{AI} \cdot \mathbf{R} \cdot \overline{\mathbf{ss}} \cdot \epsilon \mathbf{I} \quad [M \times M] \quad (5-118a)$$

$$\text{Gas-to-surface exchange} \quad \overline{\mathbf{SG}} = \epsilon \mathbf{I} \cdot \mathbf{AI} \cdot \mathbf{R} \cdot \overline{\mathbf{sg}} \quad [M \times N] \quad (5-118b)$$

where in Eqs. (5-118), \mathbf{R} is the explicit **inverse reflectivity matrix**, defined as

$$\mathbf{R} = [\mathbf{AI} - \overline{\mathbf{ss}} \cdot \rho \mathbf{I}]^{-1} \quad [M \times M] \quad (5-118c)$$

While the \mathbf{R} matrix is generally not symmetric, the matrix product $\rho \mathbf{I} \cdot \mathbf{R}$ is *always* symmetric. This fact proves useful for error checking.

The most computationally significant aspect of the matrix method is that the inverse reflectivity matrix \mathbf{R} *always exists* for any physically meaningful enclosure problem. More precisely, \mathbf{R} always exists provided that $K \neq 0$. For a transparent medium, \mathbf{R} exists provided that there *formally* exists at least one surface zone A_i such that $\epsilon_i \neq 0$. An important computational corollary of this statement for *transparent media* is that the matrix $[\mathbf{AI} - \overline{\mathbf{ss}}]$ is *always singular* and demonstrates *matrix rank* $M - 1$ (Noble, op. cit.).

Finally, the four matrix arrays $\overline{\mathbf{ss}}$, $\overline{\mathbf{gs}}$, $\overline{\mathbf{SS}}$, and $\overline{\mathbf{SG}}$ of direct and total exchange areas must satisfy **matrix conservation relations**, i.e.,

$$\text{Direct exchange areas} \quad \mathbf{AI} \cdot \mathbf{1}_M = \overline{\mathbf{ss}} \cdot \mathbf{1}_M + \overline{\mathbf{sg}} \cdot \mathbf{1}_N \quad (5-119a)$$

$$\text{Total exchange areas} \quad \epsilon \mathbf{I} \cdot \mathbf{AI} \cdot \mathbf{1}_M = \overline{\mathbf{SS}} \cdot \mathbf{1}_M + \overline{\mathbf{SG}} \cdot \mathbf{1}_N \quad (5-119b)$$

Here $\mathbf{1}_M$ is an $M \times 1$ column vector all of whose elements are unity. If $\epsilon \mathbf{I} = \mathbf{I}$ or equivalently, $\rho \mathbf{I} = \mathbf{0}$, Eq. (5-118c) reduces to $\mathbf{R} = \mathbf{AI}^{-1}$ with

the result that Eqs. (5-118a) and (5-118b) degenerate to simply $\overline{\mathbf{SS}} = \overline{\mathbf{ss}}$ and $\overline{\mathbf{SG}} = \overline{\mathbf{sg}}$. Further, while the array $\overline{\mathbf{SS}}$ is always symmetric, the array $\overline{\mathbf{SG}}$ is generally not square.

For purposes of digital computation, it is good practice to enter all data for direct exchange surface-to-surface areas $\overline{\mathbf{ss}}$ with a precision of *at least five significant figures*. This need arises because all the scalar elements of $\overline{\mathbf{sg}}$ can be calculated *arithmetically* from appropriate direct surface-to-surface exchange areas by using view factor algebra rather than via the definition of the defining integral, Eq. (5-116b). This process often involves small arithmetic differences between two numbers of nearly equal magnitude, and numerical significance is easily lost.

Computer implementation of the matrix method proves straightforward, given the availability of modern software applications. In particular, several especially user-friendly GUI mathematical utilities are available that perform matrix computations using *essentially algebraic notation*. Many simple zoning problems may be solved with spreadsheets. For large M and N , the matrix method can involve management of a large amount of data. Error checks based on symmetry and conservation by calculation of the row sums of the four arrays of direct and total exchange areas then prove indispensable.

Zone Methodology and Conventions For a transparent medium, no more than $\Sigma = M(M - 1)/2$ of the M^2 elements of the $\overline{\mathbf{ss}}$ array are *unique*. Further, surface zones are characterized into two generic types. **Source-sink zones** are defined as those for which temperature is specified and whose radiative flux Q_i is to be determined. For **flux zones**, conversely, these conditions are reversed. When both types of zones are present in an enclosure, Eq. (5-118) may be *partitioned* to produce a more efficient computational algorithm. Let $M = M_s + M_f$ represent the total number of surface zones where M_s is the number of source-sink zones and M_f is the number of flux zones. The flux zones are the *last to be numbered*. Equation (5-118) is then partitioned as follows:

$$\begin{bmatrix} \mathbf{Q}_1 \\ \mathbf{Q}_2 \end{bmatrix} = \begin{bmatrix} \epsilon \mathbf{AI}_{1,1} & \mathbf{0} \\ \mathbf{0} & \epsilon \mathbf{AI}_{2,2} \end{bmatrix} \cdot \begin{bmatrix} \mathbf{E}_1 \\ \mathbf{E}_2 \end{bmatrix} - \begin{bmatrix} \overline{\mathbf{SS}}_{1,1} & \overline{\mathbf{SS}}_{1,2} \\ \overline{\mathbf{SS}}_{2,1} & \overline{\mathbf{SS}}_{2,2} \end{bmatrix} \cdot \begin{bmatrix} \mathbf{E}_1 \\ \mathbf{E}_2 \end{bmatrix} - \begin{bmatrix} \overline{\mathbf{SG}}_1 \\ \overline{\mathbf{SG}}_2 \end{bmatrix} \cdot \mathbf{E}_g \quad (5-120)$$

Here the dimensions of the submatrices $\epsilon \mathbf{AI}_{1,1}$ and $\overline{\mathbf{SS}}_{1,1}$ are both $M_s \times M_s$ and $\overline{\mathbf{SG}}_1$ has dimensions $M_s \times N$. Partition algebra then yields the following two matrix equations for \mathbf{Q}_1 , the $M_s \times 1$ vector of unknown source-sink fluxes and \mathbf{E}_2 , the $M_f \times 1$ vector of unknown emissive powers for the flux zones, i.e.,

$$\mathbf{E}_2 = [\epsilon \mathbf{AI}_{2,2} - \overline{\mathbf{SS}}_{2,2}]^{-1} \cdot [\mathbf{Q}_2 + \overline{\mathbf{SS}}_{2,1} \cdot \mathbf{E}_1 + \overline{\mathbf{SG}}_2 \cdot \mathbf{E}_g] \quad (5-120a)$$

$$\mathbf{Q}_1 = \epsilon \mathbf{AI}_{1,1} \cdot \mathbf{E}_1 - \overline{\mathbf{SS}}_{1,1} \cdot \mathbf{E}_1 - \overline{\mathbf{SS}}_{1,2} \cdot \mathbf{E}_2 - \overline{\mathbf{SG}}_1 \cdot \mathbf{E}_g \quad (5-120b)$$

The inverse matrix in Eq. (5-120a) formally does not exist if there is at least one flux zone such that $\epsilon_i = 0$. However, well-behaved results are usually obtained with Eq. (5-120a) by utilizing a *notional zero*, say, $\epsilon_i \approx 10^{-5}$, to simulate $\epsilon_i = 0$. Computationally, \mathbf{E}_2 is first obtained from Eq. (5-120a) and then substituted into either Eq. (5-120b) or Eq. (5-118).

Surface zones need not be *contiguous*. For example, in a symmetric enclosure, zones on opposite sides of the plane of symmetry may be "lumped" into a single zone for computational purposes. Lumping nonsymmetrical zones is also possible as long as the zone temperatures and emissivities are equal.

An **adiabatic refractory surface** of area A_i and emissivity ϵ_r , for which $Q_r = 0$, proves quite important in practice. A nearly radiatively adiabatic refractory surface occurs when differences between internal conduction and convection and external heat losses through the refractory wall are small compared with the *magnitude* of the *incident* and *leaving* radiation fluxes. For *any* surface zone, the radiant flux is given by $Q = A(W - H) = \epsilon A(E - H)$ and $Q = \epsilon A/\rho(E - W)$ (if $\rho \neq 0$). These equations then lead to the result that if $Q_r = 0$, $E_r = H_r = W_r$, for all $0 \leq \epsilon_r \leq 1$. *Sufficient conditions* for modeling an adiabatic refractory zone are thus *either* to put $\epsilon_r = 0$ or to specify *directly* that $Q_r = 0$ with $\epsilon_r \neq 0$. If $\epsilon_r = 0$, $S_r S_j = 0$ for all $1 \leq j \leq M$ which leads *directly by definition* to $Q_r = 0$. For $\epsilon_r = 0$, the refractory emissive power E_r *never enters the zoning calculations*. For the special case of $K = 0$ and $M_r = 1$, a single (lumped) refractory, with $Q_r = 0$ and $\epsilon_r \neq 0$, $S_r S_j \neq 0$ and the refractory emissive power may be calculated from Eq. (5-120a) as a weighted sum of all *other known blackbody emissive powers* which

characterize the enclosure, i.e.,

$$E_r = \frac{\sum_{j=1}^{M_s} \overline{S_r S_j} E_j}{\sum_{j=1}^{M_s} \overline{S_r S_j}} \quad \text{with } j \neq r \quad (5-121)$$

Equation (5-121) specifically includes those zones which may not have a direct view of the refractory. When $Q_r = 0$, the refractory surface is said to be in **radiative equilibrium** with the entire enclosure. Equation (5-121) is indeterminate if $\epsilon_r = 0$. If $\epsilon_r = 0$, E_r does indeed exist and may be evaluated with use of the statement $E_r = H_r = W_r$. It transpires, however, that E_r is independent of ϵ_r for all $0 \leq \epsilon_r \leq 1$. Moreover, since $W_r = H_r$ when $Q_r = 0$, for all $0 \leq \epsilon_r \leq 1$, the value specified for ϵ_r is irrelevant to radiative transfer in the entire enclosure. In particular it follows that if $Q_r = 0$, then the vectors \mathbf{W} , \mathbf{H} , and \mathbf{Q} for the entire enclosure are also independent of all $0 \leq \epsilon_r \leq 1.0$. A surface zone for which $\epsilon_i = 0$ is termed a **perfect diffuse mirror**. A perfect diffuse mirror is thus also an adiabatic surface zone. The matrix method automatically deals with all options for flux and adiabatic refractory surfaces.

The Limiting Case of a Transparent Medium For the special case of a transparent medium, $K = 0$, many practical engineering applications can be modeled with the zone method. These include combustion-fired muffle furnaces and electrical resistance furnaces. When $K \rightarrow 0$, $\overline{\mathbf{sg}} \rightarrow \mathbf{0}$ and $\overline{\mathbf{SC}} \rightarrow \mathbf{0}$. Equations (5-118) through (5-119) then reduce to three simple matrix relations

$$\mathbf{Q} = \epsilon \mathbf{I} \mathbf{A} \mathbf{I} \mathbf{E} - \overline{\mathbf{SS}} \mathbf{E} \quad (5-122a)$$

$$\overline{\mathbf{SS}} = \epsilon \mathbf{I} \mathbf{A} \mathbf{I} \mathbf{R} \overline{\mathbf{SS}} \epsilon \mathbf{I} \quad (5-122b)$$

with again

$$\mathbf{R} \equiv [\mathbf{A} \mathbf{I} - \overline{\mathbf{SS}} \rho \mathbf{I}]^{-1} \quad (5-122c)$$

The radiant surface flux vector \mathbf{Q} , as computed from Eq. (5-122a), always satisfies the (scalar) conservation condition $\mathbf{1}_M^T \mathbf{Q} = \mathbf{0}$ or $\sum_{i=1}^M Q_i = 0$, which is a statement of the overall radiant energy balance.

The matrix conservation relations also simplify to

$$\mathbf{A} \mathbf{I} \mathbf{I}_M = \overline{\mathbf{SS}} \mathbf{I}_M \quad (5-123a)$$

$$\epsilon \mathbf{I} \mathbf{A} \mathbf{I} \mathbf{I}_M = \overline{\mathbf{SS}} \mathbf{I}_M \quad (5-123b)$$

And the $M \times M$ arrays for all the direct and total view factors can be readily computed from

$$\mathbf{F} = \mathbf{A} \mathbf{I}^{-1} \overline{\mathbf{SS}} \quad (5-124a)$$

and

$$\mathcal{F} = \mathbf{A} \mathbf{I}^{-1} \overline{\mathbf{SS}} \quad (5-124b)$$

where the following matrix conservation relations must also be satisfied,

$$\mathbf{F} \cdot \mathbf{I}_M = \mathbf{I}_M \quad (5-125a)$$

and

$$\mathcal{F} \cdot \mathbf{I}_M = \epsilon \mathbf{I} \cdot \mathbf{I}_M \quad (5-125b)$$

The Two-Zone Enclosure Figure 5-18 depicts four simple enclosure geometries which are particularly useful for engineering calculations characterized by only two surface zones. For $M = 2$, the reflectivity matrix \mathbf{R} is readily evaluated in closed form since an explicit algebraic inversion formula is available for a 2×2 matrix. In this case knowledge of only $\Sigma = 1$ direct exchange area is required. Direct evaluation of Eqs. (5-122) then leads to

$$\overline{\mathbf{SS}} = \begin{bmatrix} \epsilon_1 A_1 - \overline{S_1 S_2} & \overline{S_1 S_2} \\ \overline{S_1 S_2} & \epsilon_2 A_2 - \overline{S_1 S_2} \end{bmatrix} \quad (5-126)$$

where

$$\overline{S_1 S_2} = \frac{1}{\left(\frac{1}{\overline{s_1 s_2}} + \frac{\rho_1}{\epsilon_1 A_1} + \frac{\rho_2}{\epsilon_2 A_2} \right)} \quad (5-127)$$

Equation (5-127) is of general utility for any two-zone system for which $\epsilon_i \neq 0$.

The total exchange areas for the four geometries shown in Fig. 5-18 follow directly from Eqs. (5-126) and (5-127).

1. A planar surface A_1 completely surrounded by a second surface $A_2 > A_1$. Here $F_{1,1} = 0$, $F_{1,2} = 1$, and $\overline{s_1 s_2} = A_1$, resulting in

$$\overline{\mathbf{SS}} = \begin{bmatrix} \epsilon_1 \rho_2 A_1^2 + \epsilon_2 \rho_1 A_1 A_2 & \epsilon_1 \epsilon_2 A_1 A_2 \\ \epsilon_1 \epsilon_2 A_1 A_2 & \epsilon_2 A_2^2 + \epsilon_1 (\rho_2 - \epsilon_2) A_1 A_2 \end{bmatrix} / [\epsilon_1 \rho_2 A_1 + \epsilon_2 A_2]$$

and in particular $\overline{S_1 S_2} = \frac{A_1}{1/\epsilon_1 + (A_1/A_2)(\rho_2/\epsilon_2)}$ (5-127a)

In the limiting case, where A_1 has no negative curvature and is completely surrounded by a very much larger surface A_2 such that $A_1 \ll A_2$, Eq. (5-127a) leads to the even simpler result that $\overline{S_1 S_2} = \epsilon_1 A_1$.

2. Two parallel plates of equal area which are large compared to their distance of separation (infinite parallel plates). Case 2 is a limiting form of case 1 with $A_1 = A_2$. Algebraic manipulation then results in

$$\overline{\mathbf{SS}} = \begin{bmatrix} (\epsilon_1 + \epsilon_2 - 2\epsilon_1\epsilon_2) \cdot A_1 & \epsilon_1 \epsilon_2 A_1 \\ \epsilon_1 \epsilon_2 A_1 & (\epsilon_1 + \epsilon_2 - 2\epsilon_1\epsilon_2) A_1 \end{bmatrix} / [\epsilon_1 + \epsilon_2 - \epsilon_1\epsilon_2]$$

and in particular

$$\overline{S_1 S_2} = \frac{A_1}{1/\epsilon_1 + 1/\epsilon_2 - 1} \quad (5-127b)$$

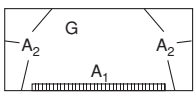

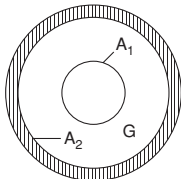
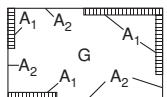
Case 1	Case 2	Case 3	Case 4
			
A planar surface A_1 completely surrounded by a second surface $A_2 > A_1$.	Two infinite parallel plates where $A_1 = A_2$.	Concentric spheres or infinite cylinders where $A_1 < A_2$. Identical to Case 1.	A speckled enclosure with two surface zones.
$\mathbf{F} = \begin{bmatrix} 0 & 1 \\ A_1/A_2 & 1 - A_1/A_2 \end{bmatrix}$	$\mathbf{F} = \begin{bmatrix} 0 & 1 \\ 1 & 0 \end{bmatrix}$	$\mathbf{F} = \begin{bmatrix} 0 & 1 \\ A_1/A_2 & 1 - A_1/A_2 \end{bmatrix}$	$\mathbf{F} = \frac{1}{(A_1 + A_2)} \begin{bmatrix} A_1 & A_2 \\ A_1 & A_2 \end{bmatrix}$

FIG. 5-18 Four enclosure geometries characterized by two surface zones and one volume zone. (Marks' Standard Handbook for Mechanical Engineers, McGraw-Hill, New York, 1999, p. 4-73, Table 4.3.5.)

3. Concentric spheres or cylinders where $A_2 > A_1$. Case 3 is mathematically identical to case 1.

4. A **speckled enclosure** with two surface zones. Here $\mathbf{F} = \frac{1}{A_1 + A_2} \begin{bmatrix} A_1 & A_2 \\ A_1 & A_2 \end{bmatrix}$ such that $\overline{\mathbf{SS}} = \frac{1}{A_1 + A_2} \begin{bmatrix} A_1^2 & A_1 A_2 \\ A_1 A_2 & A_2^2 \end{bmatrix}$ and Eqs.

(5-126) and (5-127) then produce

$$\overline{\mathbf{SS}} = \begin{bmatrix} \epsilon_1^2 A_1^2 & \epsilon_1 \epsilon_2 A_1 A_2 \\ \epsilon_1 \epsilon_2 A_1 A_2 & \epsilon_2^2 A_2^2 \end{bmatrix} / (\epsilon_1 A_1 + \epsilon_2 A_2)$$

with the particular result

$$\overline{S_1 S_2} = \frac{1}{1/(\epsilon_1 A_1) + 1/(\epsilon_2 A_2)} \quad (5-127c)$$

Physically, a two-zone speckled enclosure is characterized by the fact that the view factor from any point on the enclosure surface to the sink zone is identical to that from any other point on the bounding surface. This is only possible when the two zones are "intimately mixed." The seemingly simplistic concept of a speckled enclosure provides a surprisingly useful *default option* in engineering calculations when the *actual* enclosure geometries are quite complex.

Multizone Enclosures [$M \geq 3$] Again assume $K = 0$. The major numerical effort involved in implementation of the zone method is the evaluation of the inverse reflection matrix \mathbf{R} . For $M = 3$, explicit closed-form algebraic formulas *do indeed exist* for the nine scalar elements of the inverse of any arbitrary nonsingular matrix. These formulas are so algebraically complex, however, that it proves impractical to present universal closed-form expressions for the total exchange areas, as has been done for the case $M = 2$. Fortunately, many practical furnace configurations can be idealized with zoning such that only relatively simple *hand calculation procedures are required*. Here the enclosure is modeled with only $M = 3$ surface zones, e.g., a single source, a single sink, and a lumped adiabatic refractory zone. This approach is sometimes termed the **SSR model**. The SSR model assumes that all adiabatic refractory surfaces are *perfect diffuse mirrors*. To implement the SSR procedure, it is necessary to develop *specialized algebraic formulas* and to define a *third black view factor* F_{ij} with an *overbar* as follows.

Refractory Augmented Black View Factors \overline{F}_{ij} Let $M = M_r + M_b$, where M_b is the number of black surface zones and M_r is the number of adiabatic refractory zones. Assume $\epsilon_r = 0$ or $\rho_r = 1$ or, equivalently, that all adiabatic refractory surfaces are *perfect diffuse mirrors*. The view factor \overline{F}_{ij} is then defined as the **refractory augmented black view factor**, i.e., the direct view factor between *any two* black source-sink zones, A_i and A_j , with *full allowance for reflections from all intervening refractory surfaces*. The quantity \overline{F}_{ij} shall be referred to as **\overline{F} -bar**, for expediency.

Consider the special situation where $M_b = 2$, with any number of refractory zones $M_r \geq 1$. By use of appropriate row and column reduction of the reflectivity matrix \mathbf{R} , an especially useful relation can be derived that allows computation of the conventional total exchange area $S_i S_j$ from the *corresponding refractory augmented black view factor* \overline{F}_{ij}

$$\overline{S_1 S_2} = \frac{1}{\left(\frac{\rho_1}{\epsilon_1 A_1} + \frac{\rho_2}{\epsilon_2 A_2} + \frac{1}{A_1 \overline{F}_{1,2}} \right)} \quad (5-128a)$$

or

$$\overline{F}_{1,2} = \frac{1}{\left(\frac{\rho_1}{\epsilon_1} + \left(\frac{A_1}{A_2} \right) \cdot \frac{\rho_2}{\epsilon_2} + \frac{1}{\overline{F}_{1,2}} \right)} \quad (5-128b)$$

where $\epsilon_i \neq 0$. Notice that Eq. (5-128a) appears *deceptively similar* to Eq. (5-127). Collectively, Eqs. (5-128) along with various formulas to compute \overline{F}_{ij} (\overline{F} -bar) are sometimes called the three-zone source/sink/refractory **SSR model**.

The following formulas permit the calculation of \overline{F}_{ij} from requisite *direct* exchange areas. For the special case where the enclosure is divided into *any number of* black source-sink zones, $M_b \geq 2$, and the remainder of the enclosure is lumped together into a single refractory

zone ($M_r = 1$) with total area A_r and uniform average temperature T_r , then the direct refractory augmented exchange area for the black zone pairs is given by

$$A_i \overline{F}_{ij} = A_j \overline{F}_{ji} = \overline{s_i s_j} + \frac{\overline{s_i s_r} \overline{s_r s_j}}{A_r - \overline{s_r s_r}} \quad \text{for } 1 \leq i, j \leq M_b \quad (5-129)$$

For the special case $M_b = 2$ and $M_r = 1$, Eq. (5-129) then simplifies to

$$A_1 \overline{F}_{1,2} = A_2 \overline{F}_{2,1} = \overline{s_1 s_2} + \frac{1}{1/\overline{s_1 s_r} + 1/\overline{s_2 s_r}} \quad (5-130)$$

and if $\overline{s_1 s_r} = \overline{s_2 s_r} = 0$, Eq. (5-130) further reduces to

$$A_1 \overline{F}_{1,2} = \overline{s_1 s_2} + \frac{1}{1/(A_1 - \overline{s_1 s_2}) + 1/(A_2 - \overline{s_2 s_1})} = \frac{A_1 A_2 - (\overline{s_1 s_2})^2}{A_1 + A_2 - 2\overline{s_1 s_2}} \quad (5-131)$$

which necessitates the evaluation of only one direct exchange area. Let the M_r refractory zones be numbered *last*. Then the $M_b \times M_b$ array of refractory augmented direct exchange areas $[A_i \overline{F}_{ij}]$ is symmetric and satisfies and the conservation relation

$$[A_i \overline{F}_{ij}] \cdot \mathbf{1}_{M_b} = \mathbf{A} \mathbf{1}_{M_b} \quad (5-132a)$$

with

$$\overline{\mathbf{F}} \cdot \mathbf{1}_{M_b} = \mathbf{1}_{M_b} \quad (5-132b)$$

Temporarily denote $\overline{S_1 S_2}_R$ as the value of $\overline{S_1 S_2}$ computed from Eq. (5-128a) which assumes $\epsilon_r = 0$. It remains to demonstrate the relationship between $\overline{S_1 S_2}_R$ and the total exchange area $S_1 S_2$ computed from the matrix method for $M = 3$ when zone 3 is an adiabatic refractory for which $Q_3 = 0$ and $\epsilon_3 \neq 0$. Let $\Theta_i = (E_i - E_2)/(E_1 - E_2)$ denote the dimensionless emissive power where $E_1 > E_2$ such that $\Theta_1 = 1$ and $\Theta_2 = 0$. The dimensionless refractory emissive power may then be calculated from Eq. (5-121) as $\Theta_3 = S_3 S_1 / [S_3 S_1 + S_3 S_2]$, which when substituted into Eq. (5-122a) leads to $S_1 S_2_R = \overline{S_1 S_2} + \overline{S_2 S_3} \Theta_3 = \overline{S_1 S_2} + \overline{S_1 S_3} \cdot S_3 S_2 / [S_3 S_1 + S_3 S_2]$. Thus $\overline{S_1 S_2}_R$ is clearly the *refractory-aided* total exchange area between zone 1 and zone 2 and *not* $\overline{S_1 S_2}$ as calculated by the matrix method in general. That is, $\overline{S_1 S_2}_R$ includes not only the radiant energy originating at zone 1 and arriving at zone 2 directly and by reflection from zones 2 and 3, but also radiation originating at zone 1 that is *absorbed* by zone 3 and then wholly reemitted to zone 2; that is, $H_3 = W_3 = E_3$.

Evaluation of any total view factor \mathcal{F}_{ij} using the requisite refractory augmented black view factor \overline{F}_{ij} obviously requires that the latter be readily available and/or capable of calculation. The refractory augmented view factor \overline{F}_{ij} is documented for a few geometrically simple cases and can be calculated or approximated for others. If A_1 and A_2 are equal parallel disks, squares, or rectangles, connected by nonconducting but reradiating refractory surfaces, then \overline{F}_{ij} is given by Fig. 5-13 in curves 5 to 8. Let A_1 represent an infinite plane and A_2 represent one or two rows of infinite parallel tubes. If the only other surface is an adiabatic refractory surface located behind the tubes, $\overline{F}_{2,1}$ is then given by curve 5 or 6 of Fig. 5-15.

Experience has shown that the simple SSR model can yield quite useful results for a host of practical engineering applications without resorting to digital computation. The error due to representation of the source and sink by single zones is often small, even if the views of the enclosure from different parts of the same zone are dissimilar, provided the surface emissivities are near unity. The error is also small if the temperature variation of the refractory is small. Any degree of accuracy can, of course, be obtained via the matrix method for arbitrarily large M and N by using a digital computer. From a computational viewpoint, when $M \geq 4$, the matrix method *must be used*. The matrix method must also be used for finer-scale calculations such as more detailed wall temperature and flux density profiles.

The Electrical Network Analog At each surface zone the *total* radiant flux is proportional to the difference between E_i and W_i , as indicated by the equation $Q_i = (\epsilon_i A_i \rho_i)(E_i - W_i)$. The *net* flux between zones i and j is also given by $Q_{ij} = s_i s_j (W_i - W_j)$, where $Q_i = \sum_{j=1}^M Q_{ij}$, for all $1 \leq i \leq M$, is the *total* heat flux leaving each zone. These relations

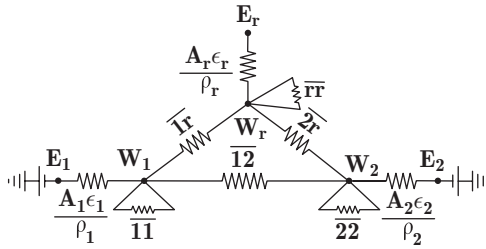


FIG. 5-19 Generalized electrical network analog for a three-zone enclosure. Here A_1 and A_2 are gray surfaces and A_r is a radiatively adiabatic surface. (Hottel, H. C., and A. F. Sarofim, Radiative Transfer, McGraw-Hill, New York, 1967, p. 91.)

suggest a *visual* electrical analog in which E_i and W_i are analogous to voltage potentials. The quantities $\epsilon_r A_r / \rho_r$ and $s_i s_j$ are analogous to conductances (reciprocal impedances), and Q_i or Q_{ij} is analogous to electric currents. Such an electrical analog has been developed by Oppenheim [Oppenheim, A. K., *Trans. ASME*, **78**, 725–735 (1956)].

Figure 5-19 illustrates a generalized electrical network analog for a three-zone enclosure consisting of one refractory zone and two gray zones A_1 and A_2 . The potential points E_i and W_i are separated by conductances $\epsilon_r A_r / \rho_r$. The emissive powers E_1, E_2 represent potential sources or sinks, while W_1, W_2 , and W_r are internal node points. In this construction the nodal point representing each surface is connected to that of every other surface it can see directly. Figure 5-19 can be used to formulate the total exchange area $S_1 S_2$ for the SSR model virtually by inspection. The refractory zone is first characterized by a floating potential such that $E_r = W_r$. Next, the resistance for the parallel “current paths” between the internal nodes W_1 and W_2 is defined by $\frac{1}{A_1 F_{1,2}} \equiv \frac{1}{s_1 s_2 + 1/(1/s_1 s_r + 1/s_2 s_r)}$ which is identical to Eq. (5-130).

Finally, the overall impedance between the source E_1 and the sink E_2 is represented simply by three resistors in series and is thus given by

$$\frac{1}{S_1 S_2} = \frac{\rho_1}{\epsilon_1 A_1} + \frac{1}{A_1 F_{1,2}} + \frac{\rho_2}{\epsilon_2 A_2}$$

or

$$\frac{1}{S_1 S_2} = \frac{1}{\frac{\rho_1}{\epsilon_1 A_1} + \frac{\rho_2}{\epsilon_2 A_2} + \frac{1}{A_1 F_{1,2}}} \quad (5-133)$$

This result is identically that for the SSR model as obtained previously in Eq. (5-128a). This equation is also valid for $M_r \geq 1$ as long as $M_b = 2$. The electrical network analog methodology can be generalized for enclosures having $M > 3$.

Some Examples from Furnace Design The theory of the past several subsections is best understood in the context of two engineering examples involving furnace modeling. The engineering idealization of the **equivalent gray plane concept** is introduced first. Figure 5-20 depicts a common furnace configuration in which the

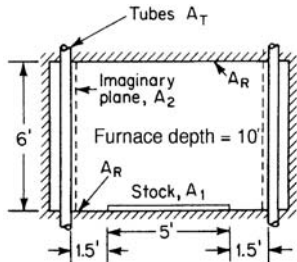


FIG. 5-20 Furnace chamber cross section. To convert feet to meters, multiply by 0.3048.

heating source is two refractory-backed, internally fired tube banks. Clearly the overall geometry for even this common furnace configuration is too complex to be modeled in an expeditious manner by anything other than a *simple engineering idealization*. Thus the furnace shown in Fig. 5-20 is modeled in Example 10, by *partitioning* the entire enclosure into two subordinate furnace compartments. The approach first defines an imaginary gray plane A_2 , located on the inward-facing side of the tube assemblies. Second, the total exchange area between the tubes to this *equivalent* gray plane is calculated, making full allowance for the reflection from the refractory tube backing. The plane-to-tube view factor is then *defined* to be the emissivity of the required equivalent gray plane whose temperature is further assumed to be that of the tubes. This procedure guarantees continuity of the radiant flux *into* the interior radiant portion of the furnace arising from a moderately complicated *external* source.

Example 9 demonstrates classical zoning calculations for radiation pyrometry in furnace applications. Example 10 is a classical furnace design calculation via zoning an enclosure with a *diathermanous* atmosphere and $M = 4$. The latter calculation can only be addressed with the matrix method. The results of Example 10 demonstrate the relative insensitivity of zoning to $M > 3$ and the engineering utility of the SSR model.

Example 9: Radiation Pyrometry A long tunnel furnace is heated by electrical resistance coils embedded in the ceiling. The stock travels on a floor-mounted conveyor belt and has an estimated emissivity of 0.7. The sidewalls are unheated refractories with emissivity 0.55, and the ceiling emissivity is 0.8. The furnace cross section is rectangular with height 1 m and width 2 m. A total radiation pyrometer is sighted on the walls and indicates the following apparent temperatures: ceiling, 1340°C; sidewall readings average about 1145°C; and the load indicates about 900°C. (a) What are the true temperatures of the furnace walls and stock? (b) What is the net heat flux at each surface? (c) How do the matrix method and SSR models compare?

Three-zone model, $M = 3$:

Zone 1: Source (top)

Zone 2: Sink (bottom)

Zone 3: Refractory (lumped sides)

Physical constants:

$$T_0 \equiv 273.15 \text{ K} \quad \sigma \equiv 5.670400 \times 10^{-8} \frac{\text{W}}{\text{m}^2 \cdot \text{K}^4}$$

Enclosure input parameters:

$$H_c := 1 \text{ m} \quad W_c := 2 \text{ m} \quad L_c := 1 \text{ m} \quad A_1 := W_c L_c \quad A_2 := A_1 \quad A_3 := 2H_c L_c$$

$$\epsilon_1 := .8 \quad \epsilon_2 := .7 \quad \epsilon_3 := .55 \quad \rho_1 := 1 - \epsilon_1 \quad \rho_2 := 1 - \epsilon_2 \quad \rho_3 := 1 - \epsilon_3$$

$$\mathbf{AI} := \begin{bmatrix} A_1 & 0 & 0 \\ 0 & A_2 & 0 \\ 0 & 0 & A_3 \end{bmatrix} \quad \mathbf{eI} := \begin{bmatrix} \epsilon_1 & 0 & 0 \\ 0 & \epsilon_2 & 0 \\ 0 & 0 & \epsilon_3 \end{bmatrix} \quad \mathbf{\rho I} := \begin{bmatrix} \rho_1 & 0 & 0 \\ 0 & \rho_2 & 0 \\ 0 & 0 & \rho_3 \end{bmatrix}$$

$$\mathbf{AI} := \begin{bmatrix} 2 & 0 & 0 \\ 0 & 2 & 0 \\ 0 & 0 & 2 \end{bmatrix} \text{m}^2 \quad \mathbf{eI} := \begin{bmatrix} 0.8 & 0 & 0 \\ 0 & 0.7 & 0 \\ 0 & 0 & 0.55 \end{bmatrix} \quad \mathbf{\rho I} := \begin{bmatrix} 0.2 & 0 & 0 \\ 0 & 0.3 & 0 \\ 0 & 0 & 0.45 \end{bmatrix}$$

Compute direct exchange areas by using crossed strings ($\Sigma = 3$):

$$ss_{11} := 0 \quad ss_{22} := 0 \quad ss_{33} := 2(\sqrt{H_c^2 + W_c^2} - W_c)L_c \quad ss_{33} := 0.4721 \text{ m}^2$$

From symmetry and conservation, there are three linear simultaneous results for the off-diagonal elements of \mathbf{ss} :

$$\begin{bmatrix} 12 \\ 13 \\ 23 \end{bmatrix} = \begin{bmatrix} 1 & 1 & 0 \\ 1 & 0 & 1 \\ 0 & 1 & 1 \end{bmatrix}^{-1} \begin{bmatrix} A_1 - 11 \\ A_2 - 22 \\ A_3 - 33 \end{bmatrix} = \frac{1}{2} \begin{bmatrix} 1 & 1 & -1 \\ 1 & -1 & 1 \\ -1 & 1 & 1 \end{bmatrix}$$

$$\times \begin{bmatrix} A_1 - 11 \\ A_2 - 22 \\ A_3 - 33 \end{bmatrix} = \frac{1}{2} \begin{bmatrix} +A_1 + A_2 - A_3 - 11 - 22 + 33 \\ +A_1 - A_2 + A_3 - 11 + 22 - 33 \\ -A_1 + A_2 + A_3 + 11 - 22 - 33 \end{bmatrix}$$

Thus

$$ss_{12} := 0.5 (A_1 + A_2 - A_3 + ss_{33}) \quad ss_{23} := 0.5 (-A_1 + A_2 + A_3 - ss_{33})$$

$$\mathbf{ss} := \begin{bmatrix} ss_{11} & ss_{12} & ss_{13} \\ ss_{12} & ss_{22} & ss_{23} \\ ss_{13} & ss_{23} & ss_{33} \end{bmatrix} \quad \mathbf{ss} := \begin{bmatrix} 0 & 1.2361 & 0.7639 \\ 1.2361 & 0 & 0.7639 \\ 0.7639 & 0.7639 & 0.4721 \end{bmatrix} \text{m}^2 \quad (\mathbf{AI} - \mathbf{ss}) \begin{bmatrix} 1 \\ 1 \\ 1 \end{bmatrix} = \begin{bmatrix} 0 \\ 0 \\ 0 \end{bmatrix} \text{m}^2$$

Compute radiosities W from pyrometer temperature readings:

$$\mathbf{T}_{wc} := \begin{bmatrix} 1340.0 \\ 900.0 \\ 1145.0 \end{bmatrix} C \quad \mathbf{W} := \sigma \left(\mathbf{T}_{wc} \frac{K}{C} + T_0 \right)^4 \quad \mathbf{W} := \begin{bmatrix} 384.0 \\ 107.4 \\ 229.4 \end{bmatrix} \frac{kW}{m^2}$$

Matrix wall flux density relations and heat flux calculations based on W:

$$\mathbf{H} := \mathbf{AI}^{-1}\mathbf{ss}\mathbf{W} \quad \mathbf{Q} := \mathbf{AI}(\mathbf{W} - \mathbf{H}) \quad \mathbf{E} := (\mathbf{eI} - \mathbf{AI})^{-1} \cdot \mathbf{Q} + \mathbf{H}$$

$$\mathbf{H} := \begin{bmatrix} 154.0 \\ 324.9 \\ 241.8 \end{bmatrix} \frac{kW}{m^2} \quad \mathbf{Q} := \begin{bmatrix} 460.0 \\ -435.0 \\ -25.0 \end{bmatrix} kW \quad \mathbf{E} := \begin{bmatrix} 441.5 \\ 14.2 \\ 219.1 \end{bmatrix} \frac{kW}{m^2}$$

The sidewalls act as near-adiabatic surfaces since the heat loss through each sidewall is only about 2.7 percent of the total heat flux originating at the source.

Actual temperatures versus pyrometer readings:

$$\mathbf{T} := \left[\left(\frac{E}{\sigma} \right)^{0.25} - T_0 \right] \frac{C}{K} \quad \mathbf{T} = \begin{bmatrix} 1397.3 \\ 434.1 \\ 1128.9 \end{bmatrix} C \quad \text{versus} \quad \mathbf{T}_{wc} = \begin{bmatrix} 1340.0 \\ 900.0 \\ 1145.0 \end{bmatrix} C$$

Compare SSR model versus matrix method [use Eqs. (5-128a) and (5-130)]: From Eq. (5-130)

$$ssbar_{12} := ss_{1,2} + \frac{1}{\frac{1}{ss_{1,3}} + \frac{1}{ss_{2,3}}} \quad ssbar_{12} = 1.6180 m^2$$

And from Eq. (5-128a)

$$SSR_{12} := \frac{1}{\frac{\rho_1}{\epsilon_1 A_1} + \frac{\rho_2}{\epsilon_2 A_2} + \frac{1}{ssbar_{12}}} \quad SSR_{12} = 1.0446 m^2$$

With the numerical result $Q_{12} := SSR_{12}(E_1 - E_2) \quad Q_{12} = 446.3 kW$

Thus the SSR model produces $Q_{12} = 446.3 kW$ versus the measured value $Q_1 = 460.0 kW$ or a discrepancy of about 3.0 percent. Mathematically the SSR model assumes a value of $\epsilon_3 = 0.0$, which precludes the sidewall heat loss of $Q_3 = -25.0 kW$. This assumption accounts for all of the difference between the two values. It remains to compare SSR_{12} and $SS_{1,2}$ computed by the matrix method.

Compute total exchange areas ($\epsilon_3 = 0.55$):

$$\mathbf{R} := (\mathbf{AI} - \overline{ss}\mathbf{\rho I})^{-1}$$

$$\overline{SS} := \mathbf{eI} - \mathbf{AI} - \mathbf{R}\overline{ss}\mathbf{eI} \quad \overline{SS} = \begin{bmatrix} 0.2948 & 0.8284 & 0.4769 \\ 0.8284 & 0.1761 & 0.3955 \\ 0.4769 & 0.3955 & 0.2277 \end{bmatrix} m^2 \quad (\mathbf{eI} - \mathbf{AI} - \overline{SS}) \begin{bmatrix} 1 \\ 1 \\ 1 \end{bmatrix} = \begin{bmatrix} 0 \\ 0 \\ 0 \end{bmatrix} m^2$$

Clearly SSR_{21} and $SS_{1,2}$ are unequal. But if

$$\Theta_3 := \frac{SS_{3,1}}{SS_{3,1} + SS_{3,2}}$$

define

$$SSA_{12} := SS_{1,2} + SS_{2,3} \cdot \Theta_3$$

and

$$\Theta_3 := 0.5466 \quad SSA_{12} = 1.0446 m^2 \quad E_r := E_2 + (E_1 - E_2) \cdot \Theta_3 \quad E_r = 247.8 \frac{kW}{m^2}$$

Numerically the matrix method predicts $SSA_{12} = 1.0446 m^2$ for $Q_3 = 0$ and $\epsilon_3 = 0.55$, which is identical to $SSR_{1,2}$ for the SSR model. Thus $SSR_{1,2} = SSA_{12}$ is the refractory-aided total exchange area between zone 1 and zone 2. The SSR model also predicts $E_r = 247.8 kW/m^2$ versus the experimental value $E_3 = 219.1 kW/m^2$ (1172.6C vs. 1128.9C), which is also a consequence of the actual 25.0-kW refractory heat loss.

(This example was developed as a MATHCAD 14® worksheet. Mathcad is a registered trademark of Parametric Technology Corporation.)

Example 10: Furnace Simulation via Zoning The furnace chamber depicted in Fig. 5-20 is heated by combustion gases passing through 20 vertical radiant tubes which are backed by refractory sidewalls. The tubes have an outside diameter of $D = 5$ in (12.7 cm) mounted on $C = 12$ in (4.72 cm) centers and a gray body emissivity of 0.8. The interior (radiant) portion of the furnace is a $6 \times 8 \times 10$ ft rectangular parallelepiped with a total surface area of 376 ft² (34.932 m²). A 50-ft² (4.645-m²) sink is positioned centrally on the floor of the furnace. The tube and sink temperatures are measured with embedded thermocouples as 1500 and 1200°F, respectively. The gray refractory emissivity may be taken as 0.5. While all other refractories are assumed to be radiatively adia-

batic, the roof of the furnace is estimated to lose heat to the surroundings with a flux density (W/m²) equal to 5 percent of the source and sink emissive power difference. An estimate of the radiant flux arriving at the sink is required, as well as estimates for the roof and average refractory temperatures in consideration of refractory service life.

Part (a): Equivalent Gray Plane Emissivity Algebraically compute the equivalent gray plane emissivity for the refractory-backed tube bank idealized by the imaginary plane A_2 , depicted in Fig. 5-15.

Solution: Let zone 1 represent one tube and zone 2 represent the effective plane 2, that is, the unit cell for the tube bank. Thus $A_1 = \pi D$ and $A_2 = C$ are the corresponding zone areas, respectively (per unit vertical dimension). This notation is consistent with Example 3. Also put $\epsilon_1 = 0.8$ with $\epsilon_2 = 1.0$ and define $R = C/D = 12/5 = 2.4$. The gray plane effective emissivity is then calculated as the total view factor for the effective plane to tubes, that is, $\mathcal{F}_{2,1} \equiv \bar{\epsilon}_2$. For $R = 2.4$, Fig. 5-15, curve 5, yields the refractory augmented view factor $\bar{\mathcal{F}}_{2,1} \approx 0.81$. Then $\mathcal{F}_{2,1}$ is calculated from Eq. (5-128b) as $\mathcal{F}_{2,1} = \frac{1}{0/1 + (2.4/\pi) \cdot 0.2/0.8 + 1/0.81} \approx 0.702$.

A more accurate value is obtained via the matrix method as $\mathcal{F}_{2,1} = 0.70295$.

Part (b): Radiant Furnace Chamber with Heat Loss

Four-zone model, M = 4: Use matrix method.

Zone 1: Sink (floor)

Zone 2: Source (lumped sides)

Zone 3: Refractory (roof)

Zone 4: Refractory (ends and floor strips)

Physical constants:

$$T_0 \equiv 273.15 K \quad \sigma \equiv 5.6704 \times 10^{-8} \frac{W}{m^2 \cdot K^4}$$

Enclosure input parameters:

$A_1 := 50 ft^2 \quad A_2 := 120 ft^2 \quad A_3 := 80 ft^2 \quad A_4 := 126 ft^2 \quad D := 5 in \quad H := 6 ft$

$\epsilon_1 := .9 \quad \epsilon_2 := .70295 \quad \epsilon_3 := .5 \quad \epsilon_4 := .5 \quad \mathbf{I}_4 := \text{identity}(4)$

$$\mathbf{eI} = \begin{bmatrix} 0.9 & 0 & 0 & 0 \\ 0 & 0.7029 & 0 & 0 \\ 0 & 0 & 0.5 & 0 \\ 0 & 0 & 0 & 0.5 \end{bmatrix} \quad \mathbf{\rho I} := \mathbf{I}_4 - \mathbf{eI} \quad \mathbf{\rho I} = \begin{bmatrix} 0.1 & 0 & 0 & 0 \\ 0 & 0.2971 & 0 & 0 \\ 0 & 0 & 0.5 & 0 \\ 0 & 0 & 0 & 0.5 \end{bmatrix}$$

Compute direct exchange areas: There are $\Sigma = 6$ unique direct exchange areas. These are obtained from Eqs. (5-114) and view factor algebra. The final array of direct exchange areas is:

$$\overline{ss} = \begin{bmatrix} 0 & 1.559 & 1.575 & 1.511 \\ 1.559 & 2.078 & 2.839 & 4.673 \\ 1.575 & 2.839 & 0 & 3.018 \\ 1.511 & 4.673 & 3.018 & 2.503 \end{bmatrix} m^2 \quad \mathbf{AI} = \begin{bmatrix} 4.645 & 0 & 0 & 0 \\ 0 & 11.148 & 0 & 0 \\ 0 & 0 & 7.432 & 0 \\ 0 & 0 & 0 & 11.706 \end{bmatrix} m^2$$

Compute total exchange areas:

$$\mathbf{R} := (\mathbf{AI} - \overline{ss}\mathbf{\rho I})^{-1}$$

$$\overline{SS} := \mathbf{eI} - \mathbf{AI} - \mathbf{R}\overline{ss}\mathbf{eI} \quad \overline{SS} = \begin{bmatrix} 0.405 & 1.669 & 0.955 & 1.152 \\ 1.669 & 2.272 & 1.465 & 2.431 \\ 0.955 & 1.465 & 0.234 & 1.063 \\ 1.152 & 2.431 & 1.063 & 1.207 \end{bmatrix} m^2$$

Check matrix conservation via row-sums:

$$(\mathbf{AI} - \overline{ss}) \begin{bmatrix} 1 \\ 1 \\ 1 \\ 1 \end{bmatrix} = \begin{bmatrix} 0 \\ 0 \\ 0 \\ 0 \end{bmatrix} m^2 \quad (\mathbf{eI} - \mathbf{AI} - \overline{SS}) \begin{bmatrix} 1 \\ 1 \\ 1 \\ 1 \end{bmatrix} = \begin{bmatrix} 0 \\ 0 \\ 0 \\ 0 \end{bmatrix} m^2$$

Emissive power and wall flux input data:

$$\mathbf{T}_F := \begin{bmatrix} 1200 \\ 1500 \\ 32 \\ 32 \end{bmatrix} F \quad \mathbf{T} := \frac{5}{9} (\mathbf{T}_F - 32 F) \frac{C}{F} \quad \mathbf{E} := \sigma \left(\mathbf{T} \frac{K}{C} + T_0 \right)^4$$

$$\mathbf{T} = \begin{bmatrix} 648.9 \\ 815.6 \\ 0.0 \\ 0.0 \end{bmatrix} C \quad \mathbf{E} = \begin{bmatrix} 40.98 \\ 79.66 \\ 0.32 \\ 0.32 \end{bmatrix} \frac{kW}{m^2}$$

$$Q_3 := -0.05 \cdot A_3 (E_2 - E_1) \quad Q_3 = -14.37 kW \quad Q_4 := 0$$

5-30 HEAT AND MASS TRANSFER

Compute refractory emissive powers from known flux inputs Q_3 and Q_4 using partitioned matrix equations [Eq. (5-120b)]:

$$\mathbf{E}_R := \begin{bmatrix} \epsilon_3 A_3 - SS_{3,3} & -SS_{3,4} \\ -SS_{4,3} & \epsilon_4 A_4 - SS_{4,4} \end{bmatrix}^{-1} \cdot \begin{bmatrix} Q_3 + SS_{3,1} E_1 + SS_{3,2} E_2 \\ Q_4 + SS_{4,1} E_1 + SS_{4,2} E_2 \end{bmatrix}$$

$$\mathbf{E}_R = \begin{bmatrix} 60.68 \\ 65.73 \end{bmatrix} \frac{\text{kW}}{\text{m}^2} \quad \mathbf{E} := \begin{bmatrix} E_1 \\ E_2 \\ E_{R1} \\ E_{R2} \end{bmatrix} \quad \mathbf{E} = \begin{bmatrix} 40.98 \\ 79.66 \\ 60.68 \\ 65.73 \end{bmatrix} \frac{\text{kW}}{\text{m}^2}$$

Compute flux values and final zone temperatures:

$$\mathbf{Q} := \epsilon \mathbf{I} \cdot \mathbf{A} \cdot \mathbf{E} - \overline{SS} \cdot \mathbf{E} \quad \mathbf{T} := \left[\left(\frac{\mathbf{E}}{\sigma} \right)^{0.25} - T_0 \right] \frac{\text{C}}{\text{K}}$$

$$\mathbf{Q} = \begin{bmatrix} -111.87 \\ 126.24 \\ -14.37 \\ 0.00 \end{bmatrix} \text{kW} \quad \mathbf{T} = \begin{bmatrix} 648.9 \\ 815.6 \\ 743.9 \\ 764.5 \end{bmatrix} \text{C}$$

Auxiliary calculations for tube area and effective tube emissivity:

$$A_{\text{Tubes}} := 20\pi \cdot D \cdot H \quad \epsilon_{\text{Tubes}} := \frac{Q_2}{A_{\text{Tubes}}(E_2 - E_1)} \quad A_{\text{Tubes}} = 14.59 \text{ m}^2 \quad \epsilon_{\text{Tubes}} = 0.2237$$

Notes: (1) Results for Q and T here are independent of ϵ_3 and ϵ_4 with the exception of T_3 , which is indeed a function of ϵ_3 . (2) The total surface area of the tubes is $A_{\text{Tubes}} = 14.59 \text{ m}^2$. Suppose the tubes were totally surrounded by a black enclosure at the temperature of the sink. The hypothetical emissivity of the tubes would then be $\epsilon_{\text{Tubes}} = 0.224$. (3) A 5 percent roof heat loss is consistent with practical measurement errors. A sensitivity test was performed with $M = 3, 4, \text{ and } 5$ with and without roof heat loss. The SSR model corresponds to $M = 3$ with zero heat loss. For $M = 5$, zone 4 corresponded to the furnace ends and zone 5 corresponded to the floor strips. The results are summarized in the following table. With the exception of the temperature of the floor strips, the computed results are seen to be remarkably insensitive to M .

Effect of Zone Number M on Computed Results

	Zero roof heat loss			5 percent roof heat loss		
	$M = 3$	$M = 4$	$M = 5$	$M = 3$	$M = 4$	$M = 5$
Temperature, °C						
T_3	765.8	762.0	762.4	756.2	743.9	744.3
T_4	NA	765.4	765.0	NA	764.5	761.1
T_5	NA	NA	780.9	NA	NA	776.7
Heat flux, kW						
Q_1	-117.657	-117.275	-116.251	-112.601	-111.870	-110.877
Q_2	117.657	117.275	116.251	126.975	126.244	125.251
Q_3	0.000	0.000	0.000	-14.374	-14.374	-14.374
Q_4	NA	0.000	0.000	NA	0.00	0.00
Q_5	NA	NA	0.000	NA	NA	0.00

(This example was developed as a MATHCAD 14® worksheet. Mathcad is a registered trademark of Parametric Technology Corporation.)

Allowance for Specular Reflection If the assumption that all surface zones are diffuse emitters and reflectors is relaxed, the zoning equations become much more complex. Here, all surface parameters become functions of the *angles of incidence and reflection* of the radiation beams at each surface. In practice, such details of reflectance and emission are seldom known. When they are, the Monte Carlo method of tracing a large number of beams emitted from random positions and in random initial directions is probably the best method of obtaining a solution. Siegel and Howell (op. cit., Chap. 10) and Modest (op. cit., Chap. 20) review the utilization of the Monte Carlo approach to a variety of radiant transfer applications. Among these is the Monte Carlo calculation of direct exchange areas for very complex geometries. Monte Carlo techniques are generally *not used* in practice for simpler engineering applications.

A simple *engineering* approach to specular reflection is the so-called **diffuse plus specular reflection model**. Here the total reflectivity $\rho_i = 1 - \epsilon_i = \rho_{Si} + \rho_{Di}$ is represented as the sum of a *diffuse component*

ρ_{Si} and a *specular component* ρ_{Di} . The method yields analytical results for a number of two surface zone geometries. In particular, the following equation is obtained for exchange between concentric spheres or infinitely long coaxial cylinders for which $A_1 < A_2$:

$$\overline{S_1 S_2} = \frac{A_1}{\left(\frac{1}{\epsilon_1} + \frac{\rho_2}{\epsilon_2} \frac{A_1}{A_2} + \frac{\rho_{S2}}{(1 - \rho_{S2})} [1 - A_1/A_2] \right)} \quad (5-134)$$

For $\rho_{D1} = \rho_{D2} = 0$ (or equivalently $\rho_1 = \rho_{S1}$ with $\rho_2 = \rho_{S2}$), Eq. (5-134) yields the limiting case for wholly specular reflection, i.e.

$$\text{Specular limit} \quad \overline{S_1 S_2} = \frac{A_1}{\left(\frac{1}{\epsilon_1} + \frac{1}{\epsilon_2} - 1 \right)} \quad (5-134a)$$

which is independent of the area ratio, A_1/A_2 . It is important to notice that Eq. (5-124a) is *similar* to Eq. (5-127b) but the emissivities here are defined as $\epsilon_1 \equiv 1 - \rho_{S1}$ and $\epsilon_2 \equiv 1 - \rho_{S2}$. When surface reflection is wholly diffuse [$\rho_{S1} = \rho_{S2} = 0$ or $\rho_1 = \rho_{D1}$ with $\rho_2 = \rho_{D2}$], Eq. (5-134) results in a formula *identical* to Eq. (5-127a), viz.

$$\text{Diffuse limit} \quad \overline{S_1 S_2} = \frac{A_1}{\left[\frac{1}{\epsilon_1} + \left(\frac{A_1}{A_2} \right) \frac{\rho_2}{\epsilon_2} \right]} \quad (5-134b, 5-127a)$$

For the case of (infinite) parallel flat plates where $A_1 = A_2$, Eq. (5-134) leads to a general formula *similar* to Eq. (5-134a) but with the stipulation here that $\epsilon_1 \equiv 1 - \rho_{D1} - \rho_{S1}$ and $\epsilon_2 \equiv 1 - \rho_{D2} - \rho_{S2}$.

Another particularly interesting limit of Eq. (5-134) occurs when $A_2 \gg A_1$, which might represent a small sphere irradiated by an infinite surroundings which can reflect radiation originating at A_1 back to A_1 . That is to say, even though $A_2 \rightarrow \infty$, the "self" total exchange area does not necessarily vanish, to wit

$$\overline{S_1 S_1} = \frac{\epsilon_1^2 \rho_{S2} \cdot A_1}{[1 - \rho_1 \cdot \rho_{S2}]} \quad \text{and} \quad \overline{S_1 S_2} = \frac{\epsilon_1 (1 - \rho_{S2}) \cdot A_1}{[1 - \rho_1 \cdot \rho_{S2}]} \quad (5-134c,d)$$

which again exhibit diffuse and specular limits. The diffuse plus specular reflection model becomes significantly more complex for geometries with $M \geq 3$ where digital computation is usually required.

An Exact Solution to the Integral Equations—The Hohlraum Exact solutions of the fundamental *integral equations* for radiative transfer are available for only a few simple cases. One of these is the evaluation of the emittance from a small aperture, of area A_1 , in the surface of an isothermal spherical cavity of radius R . In German, this geometry is termed a *hohlraum* or hollow space. For this special case the radiosity W is constant over the inner surface of the cavity. It then follows that the ratio W/E is given by

$$W/E = \frac{\epsilon}{1 - \rho [1 - A_1/(4\pi R^2)]} \quad (5-135)$$

where ϵ and $\rho = 1 - \epsilon$ are the diffuse emissivity and reflectivity of the interior cavity surface, respectively. The ratio W/E is the effective emittance of the aperture as sensed by an external narrow-angle receiver (radiometer) viewing the cavity interior. Assume that the cavity is constructed of a rough material whose (diffuse) emissivity is $\epsilon = 0.5$. As a point of reference, if the cavity is to simulate a blackbody emitter to better than 98 percent of an ideal theoretical blackbody, Eq. (5-135) then predicts that the ratio of the aperture to sphere areas $A_1/(4\pi R^2)$ must be less than 2 percent. Equation (5-135) has practical utility in the experimental design of calibration standards for laboratory radiometers.

RADIATION FROM GASES AND SUSPENDED PARTICULATE MATTER

Introduction Flame radiation originates as a result of emission from water vapor and carbon dioxide in the hot gaseous combustion

products and from the presence of particulate matter. The latter includes emission from burning of microscopic and submicroscopic soot particles, and from large suspended particles of coal, coke, or ash. Thermal radiation owing to the presence of water vapor and carbon dioxide is not visible. The characteristic blue color of clean natural gas flames is due to chemiluminescence of the excited intermediates in the flame which contribute negligibly to the radiation from combustion products.

Gas Emissivities Radiant transfer in a gaseous medium is characterized by three quantities; the gas emissivity, gas absorptivity, and gas transmissivity. Gas emissivity refers to radiation originating within a gas volume which is incident on some reference surface. Gas absorptivity and transmissivity, however, refer to the absorption and transmission of radiation from some *external* surface radiation source characterized by some radiation temperature T_1 . The sum of the gas absorptivity and transmissivity must, by definition, be unity. Gas absorptivity may be calculated from an appropriate gas emissivity. The gas emissivity is a function only of the gas temperature T_g while the absorptivity and transmissivity are functions of both T_g and T_1 .

The **standard hemispherical monochromatic gas emissivity** is defined as the direct volume-to-surface exchange area for a hemispherical gas volume to an infinitesimal area element located at the center of the planar base. Consider monochromatic transfer in a *black* hemispherical enclosure of radius R that confines an isothermal volume of gas at temperature T_g . The temperature of the bounding surfaces is T_1 . Let A_2 denote the area of the finite hemispherical surface and dA_1 denote an infinitesimal element of area located at the center of the planar base. The (dimensionless) monochromatic direct exchange area for exchange between the finite hemispherical surface A_2 and dA_1 then follows from direct integration of Eq. (5-116a) as

$$\frac{\partial(\overline{s_1 s_2})_\lambda}{\partial A_1} = \int_{\phi_1=0}^{\pi/2} \frac{e^{-K_\lambda R}}{\pi R^2} \cos\phi_1 \, 2\pi R^2 \sin\phi_1 \, d\phi_1 = e^{-K_\lambda R} \quad (5-136a)$$

and from conservation there results

$$\frac{\partial(\overline{s_1 \bar{g}})_\lambda}{\partial A_1} = 1 - e^{-K_\lambda R} \quad (5-136b)$$

Note that Eq. (5-136b) is identical to the expression for the gas emissivity for a column of path length R . In Eqs. (5-136) the gas absorption coefficient is a function of gas temperature, composition, and wavelength, that is, $K_\lambda = K_\lambda(T, \lambda)$. The net monochromatic radiant flux density at dA_1 due to irradiation from the gas volume is then given by

$$q_{1g,\lambda} = \frac{\partial(\overline{s_1 \bar{g}})_\lambda}{\partial A_1} (E_{1,\lambda} - E_{g,\lambda}) \equiv \alpha_{g,1,\lambda} E_{1,\lambda} - \epsilon_{g,\lambda} E_{g,\lambda} \quad (5-137)$$

In Eq. (5-137), $\epsilon_{g,\lambda}(T, \lambda) = 1 - \exp(-K_\lambda R)$ is defined as the monochromatic or *spectral gas emissivity* and $\alpha_{g,\lambda}(T, \lambda) = \epsilon_{g,\lambda}(T, \lambda)$.

If Eq. (5-137) is integrated with respect to wavelength over the entire EM spectrum, an expression for the *total* flux density is obtained

$$q_{1g} = \alpha_{g,1} E_1 - \epsilon_g E_g \quad (5-138)$$

where
$$\epsilon_g(T_g) = \int_{\lambda=0}^{\infty} \epsilon_\lambda(T_g, \lambda) \cdot \frac{E_{b,\lambda}(T_g, \lambda)}{E_b(T_g)} \, d\lambda \quad (5-138a)$$

and
$$\alpha_{g,1}(T_1, T_g) = \int_{\lambda=0}^{\infty} \alpha_{g,\lambda}(T_g, \lambda) \cdot \frac{E_{b,\lambda}(T_1, \lambda)}{E_b(T_1)} \, d\lambda \quad (5-138b)$$

define the *total* gas emissivity and absorptivity, respectively. The notation used here is analogous to that used for surface emissivity and absorptivity as previously defined. For a *real* gas $\epsilon_g = \alpha_{g,1}$ only if $T_1 = T_g$, while for a *gray* gas mass of arbitrarily shaped volume $\epsilon_g = \alpha_{g,1} = \partial(\overline{s_1 \bar{g}})/\partial A_1$ is independent of temperature. Because $K_\lambda(T, \lambda)$ is also a function of the composition of the radiating species, it is necessary in what follows to define a second absorption coefficient $k_{p,\lambda}$, where $K_\lambda = k_{p,\lambda} p$. Here p is the partial pressure of the radiating species, and $k_{p,\lambda}$, with units of $(\text{atm}\cdot\text{m})^{-1}$, is referred to as the *monochromatic line absorption coefficient*.

Mean Beam Lengths It is always possible to represent the emissivity of an arbitrarily shaped volume of gray gas (and thus the corre-

sponding direct gas-to-surface exchange area) with an equivalent sphere of radius $\bar{R} = L_M$. In this context the hemispherical radius $R = L_M$ is referred to as the **mean beam length** of the arbitrary gas volume. Consider, e.g., an isothermal gas layer at temperature T_g confined by two infinite parallel plates separated by distance L . Direct integration of Eq. (5-116a) and use of conservation yield a closed-form expression for the requisite surface-gas direct exchange area

$$\frac{\partial(\overline{s_1 \bar{g}})}{\partial A_1} = [1 - 2E_3(KL)] \quad (5-139a)$$

where $E_n(z) = \int_{t=1}^{\infty} \frac{e^{-zt}}{t^n} dt$ is defined as the ***n*th-order exponential**

integral which is readily available. Employing the definition of gas emissivity, the **mean beam length** between the plates L_M is then defined by the expression

$$\epsilon_g = [1 - 2E_3(KL)] \equiv 1 - e^{-KL_M} \quad (5-139b)$$

Solution of Eq. (5-139b) yields $KL_M = -\ln[2E_3(KL)]$, and it is apparent that KL_M is a function of KL . Since $E_n(0) = 1/(n-1)$ for $n > 1$, the mean beam length approximation also correctly predicts the gas emissivity as zero when $K = 0$ and $K \rightarrow \infty$.

In the limit $K \rightarrow 0$, power series expansion of both sides of the Eq. (5-139b) leads to $KL_M \rightarrow 2KL \equiv KL_{M0}$, where $L_M \equiv L_{M0} = 2L$. Here L_{M0} is defined as the **optically thin mean beam length** for radiant transfer from the entire *infinite* planar gas layer to a differential element of surface area on one of the plates. The optically thin mean beam length for two infinite parallel plates is thus simply *twice* the plate spacing L . In a similar manner it may be shown that for a sphere of diameter D , $L_{M0} = \frac{3}{8}D$, and for an infinitely long cylinder $L_{M0} = D$. A useful default formula for an arbitrary enclosure of volume V and area A is given by $L_{M0} = 4V/A$. This expression predicts $L_{M0} = \frac{3}{8}R$ for the standard hemisphere of radius R because the optically thin mean beam length is averaged over the *entire* hemispherical enclosure.

Use of the optically thin value of the mean beam length yields values of gas emissivities or exchange areas that are too high. It is thus necessary to introduce a dimensionless constant $\beta \leq 1$ and define some new **average mean beam length** such that $KL_M \equiv \beta KL_{M0}$. For the case of parallel plates, we now require that the mean beam length exactly predict the gas emissivity for a *third* value of KL . In this example we find $\beta = -\ln[2E_3(KL)]/2KL$ and for $KL = 0.193095$ there results $\beta = 0.880$. The value $\beta = 0.880$ is not wholly arbitrary. It also happens to minimize the error defined by the so-called shape correction factor $\phi = [\partial(\overline{s_1 \bar{g}})/\partial A_1]/(1 - e^{-KL_M})$ for all $KL > 0$. The required *average* mean beam length for all $KL > 0$ is then taken simply as $L_M = 0.88L_{M0} = 1.76L$. The error in this approximation is less than 5 percent.

For an arbitrary geometry, the average mean beam length is defined as the radius of a hemisphere of gas which predicts values of the direct exchange area $\overline{s_1 \bar{g}}/A_1 = [1 - \exp(-KL_M)]$, subject to the optimization condition indicated above. It has been found that the error introduced by using average mean beam lengths to approximate direct exchange areas is sufficiently small to be appropriate for many engineering calculations. When $\beta = L_M/L_{M0}$ is evaluated for a large number of geometries, it is found that $0.8 < \beta < 0.95$. It is recommended here that $\beta = 0.88$ be employed in lieu of any further geometric information. For a single-gas zone, all the requisite direct exchange areas can be approximated for engineering purposes in terms of a *single* appropriately defined average mean beam length.

Emissivities of Combustion Products Absorption or emission of radiation by the constituents of gaseous combustion products is determined primarily by vibrational and rotational transitions between the energy levels of the gaseous molecules. Changes in both vibrational and rotational energy states gives rise to *discrete* spectral lines. Rotational lines accompanying vibrational transitions usually overlap, forming a so-called vibration-rotation band. These bands are thus associated with the major vibrational frequencies of the molecules.

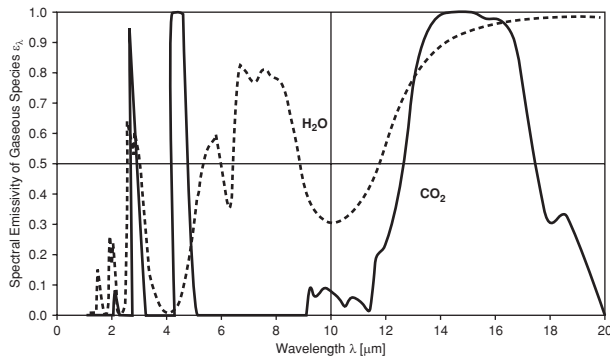


FIG. 5-21 Spectral emittances for carbon dioxide and water vapor after RADCAL. $p_c L = p_w L = 0.36 \text{ atm}\cdot\text{m}$, $T_g = 1500 \text{ K}$.

Each spectral line is characterized by an absorption coefficient $k_{p,\lambda}$ which exhibits a maximum at some central characteristic wavelength or wave number $\eta_0 = 1/\lambda_0$ and is described by a Lorentz² probability distribution. Since the widths of spectral lines are dependent on collisions with other molecules, the absorption coefficient will also depend upon the composition of the combustion gases and the total system pressure. This brief discussion of gas spectroscopy is intended as an introduction to the factors controlling absorption coefficients and thus the factors which govern the empirical correlations to be presented for gas emissivities and absorptivities.

Figure 5-21 shows computed values of the spectral emissivity $\epsilon_{g,\lambda} \equiv \epsilon_{g,\lambda}(T,pL,\lambda)$ as a function of wavelength for an equimolar mixture of carbon dioxide and water vapor for a gas temperature of 1500 K, partial pressure of 0.18 atm, and a path length $L = 2 \text{ m}$. Three principal absorption-emission bands for CO_2 are seen to be centered on 2.7, 4.3, and 15 μm . Two weaker bands at 2 and 9.7 μm are also evident. Three principal absorption-emission bands for water vapor are also identified near 2.7, 6.6, and 20 μm with lesser bands at 1.17, 1.36, and 1.87 μm . The total emissivity ϵ_g and absorptivity $\alpha_{g,1}$ are calculated by integration with respect to wavelength of the spectral emissivities, using Eqs. (5-138) in a manner similar to the development of total surface properties.

Spectral Emissivities Highly resolved spectral emissivities can be generated at ambient temperatures from the HITRAN database (high-resolution transmission molecular absorption) that has been developed for atmospheric models [Rothman, L. S., Chance, K., and Goldman, A., eds., *J. Quant. Spectroscopy & Radiative Trans.*, **82** (1–4), 2003]. This database includes the chemical species: H_2O , CO_2 , O_3 , N_2O , CO , CH_4 , O_2 , NO , SO_2 , NO_2 , NH_3 , HNO_3 , OH , HF , HCl , HBr , ClO , OCS , H_2CO , HOCl , N_2 , HCN , CH_3C , HCl , H_2O_2 , C_2H_2 , C_2H_6 , PH_3 , COF_2 , SF_6 , H_2S , and HCO_2H . These data have been extended to high temperature for CO_2 and H_2O , allowing for the changes in the population of different energy levels and in the line half width [Denison, M. K., and Webb, B. W., *Heat Transfer*, **2**, 19–24 (1994)]. The resolution in the single-line models of emissivities is far greater than that needed in engineering calculations. A number of models are available that average the emissivities over narrow-wavelength regimes or over the entire band. An extensive set of measurements of narrowband parameters performed at NASA (Ludwig, C., et al., *Handbook of Infrared Radiation from Combustion Gases*, NASA SP-3080, 1973) has been used to develop the RADCAL computer code to obtain spectral emissivities for CO_2 , H_2O , CH_4 , CO , and soot (Grosshandler,

²Spectral lines are conventionally described in terms of wave number $\eta = 1/\lambda$, with each line having a peak absorption at wave number η_0 . The Lorentz distribution is defined as $k_{\eta}/S = \frac{b_c}{\pi[b_c^2 + (\eta - \eta_0)^2]}$ where S is the integral of k_{η} over all

wave numbers. The parameter S is known as the integrated line intensity, and b_c is defined as the collision line half-width, i.e., the half-width of the line is one-half of its peak centerline value. The units of k_{η} are $\text{m}^{-1} \text{ atm}^{-1}$.

W. L., "RADCAL," NIST Technical Note 1402, 1993). The exponential wideband model is available for emissions averaged over a band for H_2O , CO_2 , CO , CH_4 , NO , SO_2 , N_2O , NH_3 , and C_2H_2 [Edwards, D. K., and Menard, W. A., *Appl. Optics*, **3**, 621–625 (1964)]. The line and band models have the advantages of being able to account for complexities in determining emissivities of line broadening due to changes in composition and pressure, exchange with spectrally selective walls, and greater accuracy in formulating fluxes in gases with temperature gradients. These models can be used to generate the total emissivities and absorptivities that will be used in this chapter. RADCAL is a command-line FORTRAN code which is available in the public domain on the Internet.

Total Emissivities and Absorptivities Total emissivities and absorptivities for water vapor and carbon dioxide at present are still based on data embodied in the classical **Hottel emissivity charts**. These data have been adjusted with the more recent measurements in RADCAL and used to develop the correlations of emissivities given in Table 5-5. Two empirical correlations which permit hand calculation of emissivities for water vapor, carbon dioxide, and four mixtures of the two gases are presented in Table 5-5. The first section of Table 5-5 provides data for the two constants b and n in the empirical relation

$$\overline{\epsilon_g T_g} = b[pL - 0.015]^n \quad (5-140a)$$

while the second section of Table 5-5 utilizes the four constants in the empirical correlation

$$\log(\overline{\epsilon_g T_g}) = a_0 + a_1 \log(pL) + a_2 \log^2(pL) + a_3 \log^3(pL) \quad (5-140b)$$

In both cases the empirical constants are given for the three temperatures of 1000, 1500, and 2000 K. Table 5-5 also includes some six values for the partial pressure ratios p_w/p_c of water vapor to carbon dioxide, namely, 0, 0.5, 1.0, 2.0, 3.0, and ∞ . These ratios correspond to composition values of $p_c/(p_c + p_w) = 1/(1 + p_w/p_c)$ of 0, 1/3, 1/2, 2/3, 3/4, and unity. For emissivity calculations at other temperatures and mixture compositions, linear interpolation of the constants is recommended.

The absorptivity can be obtained from the emissivity with aid of Table 5-5 by using the following functional equivalence.

$$\overline{\alpha_{g,1} T_1} = [\overline{\epsilon_g T_1}(pL \cdot T_1/T_g)] \left(\frac{T_g}{T_1} \right)^{0.5} \quad (5-141)$$

Verbally, the absorptivity computed from Eq. (5-141) by using the correlations in Table 5-5 is based on a value for gas emissivity ϵ_g calculated at a temperature T_1 and at a partial-pressure path-length product of $(p_c + p_w)LT_1/T_g$. The absorptivity is then equal to this value of gas emissivity multiplied by $(T_g/T_1)^{0.5}$. It is recommended that spectrally based models such as RADCAL (loc. cit.) be used particularly when extrapolating beyond the temperature, pressure, or partial-pressure-length product ranges presented in Table 5-5.

A comparison of the results of the predictions of Table 5-5 with values obtained via the integration of the spectral results calculated from the narrowband model in RADCAL is provided in Fig. 5-22. Here calculations are shown for $p_c L = p_w L = 0.12 \text{ atm}\cdot\text{m}$ and a gas temperature of 1500 K. The RADCAL predictions are 20 percent higher than the measurements at low values of pL and are 5 percent higher at the large values of pL . An extensive comparison of different sources of emissivity data shows that disparities up to 20 percent are to be expected at the current time [Lallemant, N., Sayre, A., and Weber, R., *Prog. Energy Combust. Sci.*, **22**, 543–574, (1996)]. However, smaller errors result for the range of the total emissivity measurements presented in the Hottel emissivity tables. This is demonstrated in Example 11.

Example 11: Calculations of Gas Emissivity and Absorptivity Consider a slab of gas confined between two infinite parallel plates with a distance of separation of $L = 1 \text{ m}$. The gas pressure is 101.325 kPa (1 atm), and the gas temperature is 1500 K (2240°F). The gas is an equimolar mixture of CO_2 and H_2O , each with a partial pressure of 12 kPa ($p_c = p_w = 0.12 \text{ atm}$). The radiative flux to one of its bounding surfaces has been calculated by using RADCAL for two cases. For case (a) the flux to the bounding surface is 68.3 kW/m^2 when the emitting gas is backed by a black surface at an ambient temperature of 300 K (80°F). This (cold) back surface contributes less than 1 percent to the flux. In case (b), the flux is calculated as 106.2 kW/m^2 when the gas is backed by a black surface at a temperature of 1000 K (1340°F). In this example, gas emissivity and

TABLE 5-5 Emissivity-Temperature Product for CO₂-H₂O Mixtures, $\bar{\epsilon}_g T_g$

Limited range for furnaces, valid over 25-fold range of $p_w + p_c L$, 0.046–1.15 m-atm (0.15–3.75 ft-atm)

p_w/p_c	0	1/2	1	2	3	∞
$\frac{p_w}{p_w + p_c}$	0	1/2(0.3–0.42)	1/2(0.42–0.5)	2/3(0.6–0.7)	3/4(0.7–0.8)	1
	CO ₂ only	Corresponding to (CH ₂) _n , covering coal, heavy oils, pitch	Corresponding to (CH ₂) _n , covering distillate oils, paraffins, olefines	Corresponding to CH ₄ , covering natural gas and refinery gas	Corresponding to (CH ₆) _n , covering future high H ₂ fuels	H ₂ O only

Section 1 Constants b and n of $\bar{\epsilon}_g T_g = b(pL - 0.015)^n$, $pL = \text{m-atm}$, $T = \text{K}$

T, K	b	n	b	n	b	n	b	n	b	n	b	n
1000	188	0.209	384	0.33	416	0.34	444	0.34	455	0.35	416	0.400
1500	252	0.256	448	0.38	495	0.40	540	0.42	548	0.42	548	0.523
2000	267	0.316	451	0.45	509	0.48	572	0.51	594	0.52	632	0.640

Section 1 Constants b and n of $\bar{\epsilon}_g T_g = b(pL - 0.05)^n$, $pL = \text{ft-atm}$, $T = \text{°R}$

$T, \text{°R}$	b	n	b	n	b	n	b	n	b	n	b	n
1800	264	0.209	467	0.33	501	0.34	534	0.34	541	0.35	466	0.400
2700	335	0.256	514	0.38	555	0.40	591	0.42	600	0.42	530	0.523
3600	330	0.316	476	0.45	519	0.48	563	0.51	577	0.52	532	0.640

Section 2 Full range, valid over 2000-fold range of $p_w + p_c L$, 0.005–10.0 m-atm (0.016–32.0 ft-atm)
 Constants of $\log_{10} \bar{\epsilon}_g T_g = a_0 + a_1 \log pL + a_2 \log^2 pL + a_3 \log^3 pL$

$\frac{p_w}{p_c}$	$\frac{p_w}{p_w + p_c}$	$pL = \text{m-atm}$, $T = \text{K}$				$pL = \text{ft-atm}$, $T = \text{°R}$					
		T, K	a_0	a_1	a_2	a_3	$T, \text{°R}$	a_0	a_1	a_2	a_3
0	0	1000	2.2661	0.1742	-0.0390	0.0040	1800	2.4206	0.2176	-0.0452	0.0040
		1500	2.3954	0.2203	-0.0433	0.00562	2700	2.5248	0.2695	-0.0521	0.00562
		2000	2.4104	0.2602	-0.0651	-0.00155	3600	2.5143	0.3621	-0.0627	-0.00155
1/2	1/2	1000	2.5754	0.2792	-0.0648	0.0017	1800	2.6691	0.3474	-0.0674	0.0017
		1500	2.6451	0.3418	-0.0685	-0.0043	2700	2.7074	0.4091	-0.0618	-0.0043
		2000	2.6504	0.4279	-0.0674	-0.0120	3600	2.6686	0.4879	-0.0489	-0.0120
1	1/2	1000	2.6090	0.2799	-0.0745	-0.0006	1800	2.7001	0.3563	-0.0736	-0.0006
		1500	2.6862	0.3450	-0.0816	-0.0039	2700	2.7423	0.4561	-0.0756	-0.0039
		2000	2.7029	0.4440	-0.0859	-0.0135	3600	2.7081	0.5210	-0.0650	-0.0135
2	2/3	1000	2.6367	0.2723	-0.0804	0.0030	1800	2.7296	0.3577	-0.0850	0.0030
		1500	2.7178	0.3386	-0.0990	-0.0030	2700	2.7724	0.4384	-0.0944	-0.0030
		2000	2.7482	0.4464	-0.1086	-0.0139	3600	2.7461	0.5474	-0.0871	-0.0139
3	3/4	1000	2.6432	0.2715	-0.0816	0.0052	1800	2.7359	0.3599	-0.0896	0.0052
		1500	2.7257	0.3355	-0.0981	0.0045	2700	2.7811	0.4403	-0.1051	0.0045
		2000	2.7592	0.4372	-0.1122	-0.0065	3600	2.7599	0.5478	-0.1021	-0.0065
∞	1	1000	2.5995	0.3015	-0.0961	0.0119	1800	2.6720	0.4102	-0.1145	0.0119
		1500	2.7083	0.3969	-0.1309	0.0123	2700	2.7238	0.5330	-0.1328	0.0123
		2000	2.7709	0.5099	-0.1646	-0.0165	3600	2.7215	0.6666	-0.1391	-0.0165

NOTE: $p_w/(p_w + p_c)$ of 1/2, 2/3, 3/4, and 3/4 may be used to cover the ranges 0.2–0.4, 0.4–0.6, 0.6–0.7, and 0.7–0.8, respectively, with a maximum error in $\bar{\epsilon}_g$ of 5 percent at $pL = 6.5$ m-atm, less at lower pL 's. Linear interpolation reduces the error generally to less than 1 percent. Linear interpolation or extrapolation on T introduces an error generally below 2 percent, less than the accuracy of the original data.

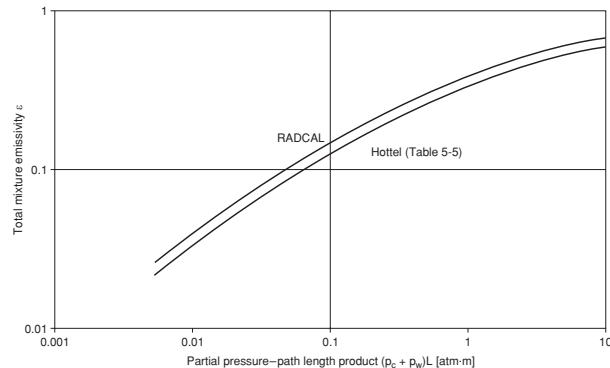


FIG. 5-22 Comparison of Hottel and RADCAL total gas emissivities. Equimolar gas mixture of CO₂ and H₂O with $p_c = p_w = 0.12$ atm and $T_g = 1500$ K.

absorptivity are to be computed from these flux values and compared with values obtained by using Table 5-5.

Case (a): The flux incident on the surface is equal to $\epsilon_g \sigma T_g^4 = 68.3 \text{ kW/m}^2$; therefore, $\epsilon_g = 68,300 / (5.6704 \times 10^{-8} \cdot 1500^4) = 0.238$. To utilize Table 5-5, the mean beam length for the gas is calculated from the relation $L_M = 0.88 L_{M0} = 0.88 \cdot 2L = 1.76$ m. For $T_g = 1500$ K and $(p_c + p_w)L_M = 0.24(1.76) = 0.422$ atm-m, the two-constant correlation in Table 5-5 yields $\epsilon_g = 0.230$ and the four-constant correlation yields $\epsilon_g = 0.234$. These results are clearly in excellent agreement with the predicted value of $\epsilon_g = 0.238$ obtained from RADCAL.

Case (b): The flux incident on the surface (106.2 kW/m^2) is the sum of that contributed by (1) gas emission $\epsilon_g \sigma T_g^4 = 68.3 \text{ kW/m}^2$ and (2) emission from the opposing surface corrected for absorption by the intervening gas using the gas transmissivity, that is, $\tau_{g,1} \sigma T_1^4$ where $\tau_{g,1} = 1 - \alpha_{g,1}$. Therefore $\alpha_{g,1} = [1 - (106,200 - 68,300) / (5.6704 \times 10^{-8} \cdot 1000^4)] = 0.332$. Using Table 5-5, the two-constant and four-constant gas emissivities evaluated at $T_1 = 1000$ K and $pL = 0.4224(1000/1500) = 0.282$ atm-m are $\epsilon_g = 0.2654$ and $\epsilon_g = 0.2707$, respectively. Multiplication by the factor $(T_g/T_1)^{0.5} = (1500/1000)^{0.5} = 1.225$ produces the final values of the two corresponding gas absorptivities $\alpha_{g,1} = 0.325$ and $\alpha_{g,1} = 0.332$, respectively. Again the agreement with RADCAL is excellent.

Other Gases The most extensive available data for gas emissivity are those for carbon dioxide and water vapor because of their importance in the radiation from the products of fossil fuel combustion. Selected data for other species present in combustion gases are provided in Table 5-6.

TABLE 5-6 Total Emissivities of Some Gases

Temperature $P_r L$, atm-ft	1000°R			1600°R			2200°R			2800°R		
	0.01	0.1	1.0	0.01	0.1	1.0	0.01	0.1	1.0	0.01	0.1	1.0
NH ₃ ^a	0.047	0.20	0.61	0.020	0.120	0.44	0.0057	0.051	0.25	(0.001)	(0.015)	(0.14)
SO ₂ ^b	0.020	0.13	0.28	0.013	0.090	0.32	0.0085	0.051	0.27	0.0058	0.043	0.20
CH ₄ ^c	0.0116	0.0518	0.1296	0.0111	0.0615	0.1880	0.0087	0.0608	0.2004	0.00622	0.04702	0.1525
CO ^d	0.0052	0.0167	0.0403	0.0055	0.0196	0.0517	0.0036	0.0145	0.0418	0.00224	0.00986	0.02855
NO ^d	0.0046	0.018	0.060	0.0046	0.021	0.070	0.0019	0.010	0.040	0.0078	0.004	0.025
HCl ^e	0.00022	0.00079	0.0020	0.00036	0.0013	0.0033	0.00037	0.0014	0.0036	0.00029	0.0010	0.0027

NOTE: Figures in this table are taken from plots in Hottel and Sarofim, *Radiative Transfer*, McGraw-Hill, New York, 1967, chap. 6. Values in parentheses are extrapolated. To convert degrees Rankine to kelvins, multiply by (5.556)(10⁻¹). To convert atmosphere-feet to kilopascal-meters, multiply by 30.89.

^aTotal-radiation measurements of Port (Sc.D. thesis in chemical engineering, MIT, 1940) at 1-atm total pressure, $L = 1.68$ ft, T to 2000°R.

^bCalculations of Guerrieri (S.M. thesis in chemical engineering, MIT, 1932) from room-temperature absorption measurements of Coblentz (*Investigations of Infrared Spectra*, Carnegie Institution, Washington, 1905) with poor allowance for temperature.

^cEstimated using Grosshandler, W.L., "RADCAL: A Narrow-Band Model for Radial Calculations in a Combustion Environment," NIST Technical Note 1402, 1993.

^dCalculations of Malkmus and Thompson [*J. Quant. Spectros. Radiat. Transfer*, **2**, 16 (1962)], to $T = 5400$ °R and $PL = 30$ atm-ft.

^eCalculations of Malkmus and Thompson [*J. Quant. Spectros. Radiat. Transfer*, **2**, 16 (1962)], to $T = 5400$ °R and $PL = 300$ atm-ft.

Flames and Particle Clouds

Luminous Flames Luminosity conventionally refers to soot radiation. At atmospheric pressure, soot is formed in locally fuel-rich portions of flames in amounts that usually correspond to less than 1 percent of the carbon in the fuel. Because soot particles are small relative to the wavelength of the radiation of interest in flames (primary particle diameters of soot are of the order of 20 nm compared to wavelengths of interest of 500 to 8000 nm), the incident radiation permeates the particles, and the absorption is proportional to the volume of the particles. In the limit of $r_p/\lambda \ll 1$, the Rayleigh limit, the monochromatic emissivity ϵ_λ is given by

$$\epsilon_\lambda = 1 - \exp(-K \cdot f_v \cdot L/\lambda) \tag{5-142}$$

where f_v is the volumetric soot concentration, L is the path length in the same units as the wavelength λ , and K is dimensionless. The value K will vary with fuel type, experimental conditions, and the temperature history of the soot. The values of K for a wide range of systems are within a factor of about 2 of one another. The single most important variable governing the value of K is the hydrogen/carbon ratio of the soot, and the value of K increases as the H/C ratio decreases. A value of $K = 9.9$ is recommended on the basis of seven studies involving 29 fuels [Mulholland, G. W., and Croarkin, C., *Fire and Materials*, **24**, 227-230 (2000)].

The total emissivity of soot ϵ_s can be obtained by substituting ϵ_λ from Eq. (5-142) for ϵ_λ in Eq. (5-138a) to yield

$$\epsilon_s = \int_{\lambda=0}^{\infty} \epsilon_\lambda \frac{E_{b,\lambda}(T_g, \lambda)}{E_b(T_g)} d\lambda = 1 - \frac{15}{4} [\Psi^{(3)}(1 + K \cdot f_v \cdot L \cdot T/c_2)] \tag{5-143}$$

$$\cong (1 + K \cdot f_v \cdot L \cdot T/c_2)^{-4}$$

Here $\Psi^{(3)}(x)$ is defined as the pentagamma function of x and c_2 (m·K) is again Planck's second constant. The approximate relation in Eq. (5-143) is accurate to better than 1 percent for arguments yielding values of $\epsilon_s < 0.7$. At present, the largest uncertainty in estimating total soot emissivities is in the estimation of the soot volume fraction f_v . Soot forms in the fuel-rich zones of flames. Soot formation rates are a function of fuel type, mixing rate, local equivalence ratio Φ , temperature, and pressure. The equivalence ratio is defined as the quotient of the actual to stoichiometric fuel-to-oxidant ratio $\Phi = [F/O]_{Act}/[F/O]_{Stoich}$. Soot formation increases with the aromaticity or C/H ratio of fuels with benzene, α -methyl naphthalene, and acetylene having a high propensity to form soot and methane having a low soot formation propensity. Oxygenated fuels, such as alcohols, emit little soot. In practical turbulent diffusion flames, soot forms on the fuel side of the flame front. In premixed flames, at a given temperature, the rate of soot formation increases rapidly for $\Phi > 2$. For temperatures above

1500 K, soot burns out rapidly (in less than 0.1s) under fuel-lean conditions, $\Phi < 1$. Because of this rapid soot burnout, soot is usually localized in a relatively small fraction of a furnace or combustor volume. Long, poorly mixed diffusion flames promote soot formation while highly backmixed combustors can burn soot-free. In a typical flame at atmospheric pressure, maximum volumetric soot concentrations are found to be in the range $10^{-7} < f_v < 10^{-6}$. This corresponds to a soot formation of about 1.5 to 15 percent of the carbon in the fuel. When f_v is to be calculated at high pressures, allowance must be made for the significant increase in soot formation with pressure and for the inverse proportionality of f_v with respect to pressure. Great progress is being made in the ability to calculate soot in premixed flames. For example, predicted and measured soot concentration have been compared in a well-stirred reactor operated over a wide range of temperatures and equivalence ratios [Brown, N.J., Revzan, K. L., Frenklach, M., *Twenty-seventh Symposium (International) on Combustion*, pp. 1573-1580, 1998]. Moreover, CFD (computational fluid dynamics) and population dynamics modeling have been used to simulate soot formation in a turbulent non-premixed ethylene-air flame [Zucca, A., Marchisio, D. L., Barresi, A. A., Fox, R. O., *Chem. Eng. Sci.*, 2005]. The importance of soot radiation varies widely between combustors. In large boilers the soot is confined to small volumes and is of only local importance. In gas turbines, cooling the combustor liner is of primary importance so that only small incremental soot radiation is of concern. In high-temperature glass tanks, the presence of soot adds 0.1 to 0.2 to emissivities of oil-fired flames. In natural gas-fired flames, efforts to augment flame emissivities with soot generation have generally been unsuccessful. The contributions of soot to the radiation from pool fires often dominates, and thus the presence of soot in such flames directly impacts the safe separation distances from dikes around oil tanks and the location of flares with respect to oil rigs.

Clouds of Large Black Particles The emissivity ϵ_M of a cloud of black particles with a large perimeter-to-wavelength ratio is

$$\epsilon_M = 1 - \exp[-(a/v)L] \tag{5-144}$$

where a/v is the projected area of the particles per unit volume of space. If the particles have no negative curvature (the particle does not "see" any of itself) and are randomly oriented, $a = a'/4$, where a' is the actual surface area. If the particles are uniform, $a/v = cA = cA'/4$, where A and A' are the projected and total areas of each particle and c is the number concentration of particles. For spherical particles this leads to

$$\epsilon_M = 1 - \exp[-(\pi/4)cd_p^2L] = 1 - \exp(-1.5f_vL/d_p) \tag{5-145}$$

As an example, consider a heavy fuel oil (CH_{1.5}, specific gravity, 0.95) atomized to a mean surface particle diameter of d_p burned with

20 percent excess air to produce coke-residue particles having the original drop diameter and suspended in combustion products at 1204°C (2200°F). The flame emissivity due to the particles along a path of L m, with d_p measured in micrometers, is

$$\epsilon_M = 1 - \exp(-24.3L/d_p) \quad (5-146)$$

For 200- μm particles and $L = 3.05$ m, the particle contribution to emissivity is calculated as 0.31.

Clouds of Nonblack Particles For nonblack particles, emissivity calculations are complicated by multiple scatter of the radiation reflected by each particle. The emissivity ϵ_M of a cloud of gray particles of individual emissivity ϵ_1 can be estimated by the use of a simple modification Eq. (5-144), i.e.,

$$\epsilon_M = 1 - \exp[-\epsilon_1(a/v)L] \quad (5-147)$$

Equation (5-147) predicts that $\epsilon_M \rightarrow 1$ as $L \rightarrow \infty$. This is *impossible* in a scattering system, and use of Eq. (5-147) is restricted to values of the optical thickness $(a/v)L < 2$. Instead, the asymptotic value of ϵ_M is obtained from Fig. 5-12 as $\epsilon_M = \epsilon_b$ ($\lim L \rightarrow \infty$), where the albedo ω is replaced by the particle-surface reflectance $\omega = 1 - \epsilon_1$. Particles with perimeter-to-wavelength ratios of 0.5 to 5.0 can be analyzed, with significant mathematical complexity, by use of the *Mie equations* (Bohren, C. F., and Huffman, D. R., *Absorption and Scattering of Light by Small Particles*, Wiley, 1998).

Combined Gas, Soot, and Particulate Emission In a mixture of emitting species, the emission of each constituent is attenuated on its way to the system boundary by absorption by all other constituents. The transmissivity of a mixture is the product of the transmissivities of its component parts. This statement is a corollary of Beer's law. For present purposes, the transmissivity of "species k " is defined as $\tau_k = 1 - \epsilon_k$. For a mixture of combustion products consisting of carbon dioxide, water vapor, soot, and oil coke or char particles, the total emissivity ϵ_T at any wavelength can therefore be obtained from

$$(1 - \epsilon_T)_\lambda = (1 - \epsilon_C)_\lambda(1 - \epsilon_W)_\lambda(1 - \epsilon_S)_\lambda(1 - \epsilon_M)_\lambda \quad (5-148)$$

where the subscripts denote the four flame species. The total emissivity is then obtained by integrating Eq. (5-148) over the entire EM energy spectrum, taking into account the variability of ϵ_C , ϵ_W , and ϵ_S with respect to wavelength. In Eq. (5-148), ϵ_M is independent of wavelength because absorbing char or coke particles are effectively black-body absorbers. Computer programs for spectral emissivity, such as RADCAL (loc. cit.), perform the integration with respect to wavelength for obtaining total emissivity. Corrections for the overlap of vibration-rotation bands of CO_2 and H_2O are automatically included in the correlations for ϵ_g for mixtures of these gases. The monochromatic soot emissivity is higher at shorter wavelengths, resulting in higher attenuations of the bands at 2.7 μm for CO_2 and H_2O than at longer wavelengths. The following equation is recommended for calculating the emissivity ϵ_{g+s} of a mixture of CO_2 , H_2O , and soot

$$\epsilon_{g+s} = \epsilon_g + \epsilon_s - M \cdot \epsilon_g \epsilon_s \quad (5-149)$$

where M can be represented with acceptable error by the dimensionless function

$$M = 1.12 - 0.27 \cdot (T/1000) + 2.7 \times 10^{-5} f_p \cdot L \quad (5-150)$$

In Eq. (5-150), T has units of kelvins and L is measured in meters. Since coke or char emissivities are gray, their addition to those of the CO_2 , H_2O , and soot follows simply from Eq. (5-148) as

$$\epsilon_T = \epsilon_{g+s} + \epsilon_M - \epsilon_{g+s} \epsilon_M \quad (5-151)$$

with the definition $1 - \epsilon_{g+s} \equiv (1 - \epsilon_C)(1 - \epsilon_W)(1 - \epsilon_S)$.

RADIATIVE EXCHANGE WITH PARTICIPATING MEDIA

Energy Balances for Volume Zones—The Radiation Source Term Reconsider a generalized enclosure with N volume zones confining a gray gas. When the N gas temperatures are *unknown*, an *additional* set of N equations is required in the form of radiant energy

balances for each volume zone. These N equations are given by the *definition* of the N -vector for the **net radiant volume absorption** $\mathbf{S}' = [S'_j]$ for each volume zone

$$\mathbf{S}' = \overline{\mathbf{GS}} \cdot \mathbf{E} + \overline{\mathbf{GG}} \cdot \mathbf{E}_g - 4K\mathbf{VI} \cdot \mathbf{E}_g \quad [N \times 1] \quad (5-152)$$

The radiative source term is a discretized formulation of the *net radiant absorption* for each volume zone which may be incorporated as a *source term* into numerical approximations for the generalized *energy equation*. As such, it permits formulation of energy balances on each zone that may include conductive and convective heat transfer. For $K \rightarrow 0$, $\overline{\mathbf{GS}} \rightarrow 0$, and $\overline{\mathbf{GG}} \rightarrow 0$ leading to $\mathbf{S}' \rightarrow \mathbf{0}_N$. When $K \neq 0$ and $\mathbf{S}' = \mathbf{0}_N$, the gas is said to be in a state of *radiative equilibrium*. In the notation usually associated with the discrete ordinate (DO) and finite volume (FV) methods, see Modest (op. cit., Chap. 16), one would write $S'_i/V_i = K[G - 4E_g] = -\nabla \cdot \vec{q}_r$. Here $H_g = G/4$ is the average flux density incident on a given volume zone from all other surface and volume zones. The DO and FV methods are currently available options as "RTE-solvers" in complex simulations of combustion systems using *computational fluid dynamics* (CFD).^{*}

Implementation of Eq. (5-152) necessitates the definition of two additional *symmetric* $N \times N$ arrays of exchange areas, namely, $\overline{\mathbf{gg}} = [\overline{g_i g_j}]$ and $\overline{\mathbf{GG}} = [\overline{G_i G_j}]$. In Eq. (5-152) $\mathbf{VI} = [V_j \cdot \delta_{ij}]$ is an $N \times N$ diagonal matrix of zone volumes. The total exchange areas in Eq. (5-151) are *explicit* functions of the direct exchange areas as follows:

$$\text{Surface-to-gas exchange} \quad \overline{\mathbf{GS}} = \overline{\mathbf{SG}}^T \quad [N \times M] \quad (5-153a)$$

$$\text{Gas-to-gas exchange} \quad \overline{\mathbf{GG}} = \overline{\mathbf{gg}} + \overline{\mathbf{sg}} \cdot \rho \mathbf{I} \cdot \overline{\mathbf{Rg}} \quad [N \times M] \quad (5-153b)$$

The matrices $\overline{\mathbf{gg}} = [\overline{g_i g_j}]$ and $\overline{\mathbf{GG}} = [\overline{G_i G_j}]$ must also satisfy the following **matrix conservation relations**:

$$\text{Direct exchange areas:} \quad 4K\mathbf{VI} \cdot \mathbf{1}_N = \overline{\mathbf{gs}} \cdot \mathbf{1}_M + \overline{\mathbf{gg}} \cdot \mathbf{1}_N \quad (5-154a)$$

$$\text{Total exchange areas:} \quad 4K\mathbf{VI} \cdot \mathbf{1}_N = \overline{\mathbf{GS}} \cdot \mathbf{1}_M + \overline{\mathbf{GG}} \cdot \mathbf{1}_N \quad (5-154b)$$

The formal integral definition of the direct gas-gas exchange area is

$$\overline{g_i g_j} = \iiint_{V_i} \iiint_{V_j} K^2 \frac{e^{-K_r}}{\pi^2} dV_j dV_i \quad (5-155)$$

Clearly, when $K = 0$, the two direct exchange areas involving a gas zone $\overline{\mathbf{gs}}_i$ and $\overline{\mathbf{gs}}_j$ vanish. Computationally it is *never* necessary to make resort to Eq. (5-155) for calculation of $\overline{g_i g_j}$. This is so because $\overline{s_i g_j}$, $\overline{g_i s_j}$, and $\overline{g_i g_j}$ may *all* be calculated *arithmetically* from appropriate values of $\overline{s_i s_j}$ by using associated conservation relations and view factor algebra.

Weighted Sum of Gray Gas (WSGG) Spectral Model Even in simple engineering calculations, the assumption of a gray gas is almost never a good one. The zone method is now further generalized to make allowance for nongray radiative transfer via incorporation of the **weighted sum of gray gas** (WSGG) spectral model. Hottel has shown that the emissivity $\epsilon_g(T, L)$ of an absorbing-emitting gas mixture containing CO_2 and H_2O of known composition can be approximated by a *weighted sum of P gray gases*

$$\epsilon_g(T, L) \approx \sum_{p=1}^P a_p(T)(1 - e^{-K_p L}) \quad (5-156a)$$

where

$$\sum_{p=1}^P a_p(T) = 1.0 \quad (5-156b)$$

In Eqs. (5-156), K_p is some gray gas absorption coefficient and L is some appropriate path length. In practice, Eqs. (5-156) usually yield acceptable accuracy for $P \leq 3$. For $P = 1$, Eqs. (5-156) degenerate to the case of a single gray gas.

^{*}To further clarify the mathematical differences between zoning and the DO and FV methods recognize that (neglecting scatter) the matrix expressions $\mathbf{H} = \mathbf{AI}^{-1} \cdot \overline{\mathbf{ss}} \cdot \mathbf{W} + \mathbf{AI}^{-1} \cdot \overline{\mathbf{sg}} \cdot \mathbf{E}_g$ and $4K\mathbf{VI} \cdot \mathbf{E}_g = \mathbf{VI}^{-1} \cdot \overline{\mathbf{gs}} \cdot \mathbf{W} + \mathbf{VI}^{-1} \cdot \overline{\mathbf{gg}} \cdot \mathbf{E}_g$ represent spatial discretizations of the integral form(s) of the RTE applied at any point (zone) on the boundary or interior of an enclosure, respectively, for a gray gas.

The Clear plus Gray Gas WSGG Spectral Model In principle, the emissivity of all gases approaches unity for infinite path length L . In practice, however, the gas emissivity may fall considerably short of unity for representative values of pL . This behavior results because of the *band* nature of real gas spectral absorption and emission whereby there is usually no significant overlap between dominant absorption bands. Mathematically, this physical phenomenon is modeled by defining one of the gray gas components in the WSGG spectral model to be *transparent*.

For $P = 2$ and path length L_M , Eqs. (5-156) yield the following expression for the gas emissivity

$$\epsilon_g = a_1(1 - e^{-K_1 L_M}) + a_2(1 - e^{-K_2 L_M}) \quad (5-157)$$

In Eq. (5-157) if $K_1 = 0$ and $a_2 \neq 0$, the limiting value of gas emissivity is $\epsilon_g(T, \infty) \rightarrow a_2$. Put $K_1 = 0$ in Eq. (5-157), $a_g = a_2$, and define $\tau_g = e^{-K_2 L_M}$ as the gray gas transmissivity. Equation (5-157) then simplifies to

$$\epsilon_g = a_g(1 - \tau_g) \quad (5-158)$$

It is important to note in Eq. (5-158) that $0 \leq a_g, \tau_g \leq 1.0$ while $0 \leq \epsilon_g \leq a_g$.

Equation (5-158) constitutes a two-parameter model which may be fitted with only *two* empirical emissivity data points. To obtain the constants a_g and τ_g in Eq. (5-158) at fixed composition and temperature, denote the two emissivity data points as $\epsilon_{g,2} = \epsilon_g(2pL) > \epsilon_{g,1} = \epsilon_g(pL)$ and recognize that $\epsilon_{g,1} = a_g(1 - \tau_g)$ and $\epsilon_{g,2} = a_g(1 - \tau_g^2) = a_g(1 - \tau_g)(1 + \tau_g) = \epsilon_{g,1}(1 + \tau_g)$. These relations lead directly to the final emissivity fitting equations

$$\tau_g = \frac{\epsilon_{g,2}}{\epsilon_{g,1}} - 1 \quad (5-159a)$$

and

$$a_g = \frac{\epsilon_{g,1}}{2 - \epsilon_{g,2}/\epsilon_{g,1}} \quad (5-159b)$$

The clear plus gray WSGG spectral model also readily leads to values for gas *absorptivity* and *transmissivity*, with respect to some appropriate surface radiation source at temperature T_1 , for example,

$$\alpha_{g,1} = a_{g,1}(1 - \tau_g) \quad (5-160a)$$

and

$$\tau_{g,1} = a_{g,1} \tau_g \quad (5-160b)$$

In Eqs. (5-160) the *gray* gas transmissivity τ_g is taken to be identical to that obtained for the gas emissivity ϵ_g . The constant $a_{g,1}$ in Eq. (5-160a) is then obtained with knowledge of *one additional empirical value* for $\alpha_{g,1}$ which may also be obtained from the correlations in Table 5-5. Notice further in the definitions of the three parameters ϵ_g , $\alpha_{g,1}$, and $\tau_{g,1}$ that *all* the temperature dependence is forced into the *two* WSGG constants a_g and $a_{g,1}$.

The *three* clear plus gray WSGG constants a_g , $a_{g,1}$, and τ_g are functions of total pressure, temperature, and mixture composition. It is not necessary to ascribe any particular physical significance to them. Rather, they may simply be visualized as three constants that happen to fit the gas emissivity data. It is noteworthy that *three* constants are far fewer than the number required to calculate gas emissivity data from fundamental spectroscopic data. The two constants a_g and $a_{g,1}$ defined in Eqs. (5-158) and (5-160) can, however, be interpreted *physically* in a particularly simple manner. Suppose the gas absorption spectrum is idealized by *many* absorption bands (boxes), *all* of which are characterized by the *identical* absorption coefficient K . The a 's might then be calculated from the total blackbody energy fraction $F_b(\lambda T)$ defined in Eqs. (5-105) and (5-106). That is, a_g simply represents the total *energy fraction* of the blackbody energy distribution in which the gas *absorbs*. This concept may be further generalized to real gas absorption spectra via the *wideband stepwise gray spectral box model* (Modest, op. cit., Chap. 14).

When $P \geq 3$, exponential curve-fitting procedures for the WSGG spectral model become significantly more difficult for hand computation but are quite routine with the aid of a variety of readily available

mathematical software utilities. The clear plus gray WSGG fitting procedure is demonstrated in Example 8.

The Zone Method and Directed Exchange Areas Spectral dependence of real gas spectral properties is now introduced into the zone method via the WSGG spectral model. It is still assumed, however, that all surface zones are gray isotropic emitters and absorbers.

General Matrix Representation We first define a new set of four **directed exchange areas** $\overleftarrow{\mathbf{SS}}$, $\overleftarrow{\mathbf{SG}}$, $\overleftarrow{\mathbf{GS}}$, and $\overleftarrow{\mathbf{GG}}$ which are denoted by an overarrow. The directed exchange areas are obtained from the total exchange areas for gray gases by simple matrix multiplication using weighting factors derived from the WSGG spectral model. The directed exchange areas are denoted by an overarrow to indicate the "sending" and "receiving" zone. The a -weighting factors for transfer originating at a gas zone $a_{g,i}$ are derived from WSGG gas *emissivity* calculations, while those for transfers originating at a surface zone, a_i are derived from appropriate WSGG gas *absorptivity* calculations. Let $\mathbf{agI}_p = [a_{p,g} \delta_{ij}]$ and $\mathbf{aI}_p = [a_{p,i} \delta_{ij}]$ represent the P [$M \times M$] and [$N \times N$] *diagonal* matrices comprised of the appropriate WSGG a constants. The *directed* exchange areas are then computed from the associated *total* gray gas exchange areas via simple *diagonal* matrix multiplication.

$$\overleftarrow{\mathbf{SS}} = \sum_{p=1}^P \overleftarrow{\mathbf{SS}}_p \cdot \mathbf{aI}_p \quad [M \times M] \quad (5-161a)$$

$$\overleftarrow{\mathbf{SG}} = \sum_{p=1}^P \overleftarrow{\mathbf{SG}}_p \cdot \mathbf{agI}_p \quad [M \times N] \quad (5-161b)$$

$$\overleftarrow{\mathbf{GS}} = \sum_{p=1}^P \overleftarrow{\mathbf{GS}}_p \cdot \mathbf{aI}_p \quad [M \times N] \quad (5-161c)$$

$$\overleftarrow{\mathbf{GG}} = \sum_{p=1}^P \overleftarrow{\mathbf{GG}}_p \cdot \mathbf{agI}_p \quad [N \times N] \quad (5-161d)$$

$$\text{with } \overleftarrow{\mathbf{KI}} = \sum_{p=1}^P \overleftarrow{\mathbf{KI}}_p \cdot \mathbf{agI}_p \quad [N \times N] \quad (5-161e)$$

In contrast to the *total* exchange areas which are always independent of temperature, the four *directed* arrays $\overleftarrow{\mathbf{SS}}$, $\overleftarrow{\mathbf{SG}}$, $\overleftarrow{\mathbf{GS}}$, and $\overleftarrow{\mathbf{GG}}$ are dependent on the temperatures of each and every zone, i.e., as in $a_{p,i} = a_p(T_i)$. Moreover, in contrast to *total* exchange areas, the *directed* arrays $\overleftarrow{\mathbf{SS}}$ and $\overleftarrow{\mathbf{GG}}$ are generally not symmetric and $\overleftarrow{\mathbf{GS}} \neq \overleftarrow{\mathbf{SG}}^T$. Finally, since the directed exchange areas are temperature-*dependent*, iteration may be required to update the \mathbf{aI}_p and \mathbf{agI}_p arrays during the course of a calculation. There is a great deal of latitude with regard to fitting the WSGG a constants in these matrix equations, especially if $N > 1$ and composition variations are to be allowed for in the gas. An extensive discussion of a fitting for $N > 1$ is beyond the scope of this presentation. Details of the fitting procedure, however, are presented in Example 12 in the context of a single-gas zone.

Having formulated the directed exchange areas, the governing matrix equations for the radiative flux equations at each surface zone and the radiant source term are then given as follows:

$$\mathbf{Q} = \epsilon \mathbf{AI} \cdot \mathbf{E} - \overleftarrow{\mathbf{SS}} \cdot \mathbf{E} - \overleftarrow{\mathbf{SG}} \cdot \mathbf{E}_g \quad (5-162a)$$

$$\mathbf{S}' = \overleftarrow{\mathbf{GG}} \cdot \mathbf{E}_g + \overleftarrow{\mathbf{GS}} \cdot \mathbf{E} - 4 \overleftarrow{\mathbf{KI}} \cdot \mathbf{VI} \cdot \mathbf{E}_g \quad (5-162b)$$

or the alternative forms

$$\mathbf{Q} = [\mathbf{EI} \cdot \overleftarrow{\mathbf{SS}} - \overleftarrow{\mathbf{SS}} \cdot \mathbf{EI}] \cdot \mathbf{I}_M + [\mathbf{EI} \cdot \overleftarrow{\mathbf{SG}} - \overleftarrow{\mathbf{SG}} \cdot \mathbf{E}_g \mathbf{I}] \cdot \mathbf{I}_N \quad (5-163a)$$

$$\mathbf{S}' = -[\mathbf{E}_g \mathbf{I} \cdot \overleftarrow{\mathbf{GS}} - \overleftarrow{\mathbf{GS}} \cdot \mathbf{EI}] \cdot \mathbf{I}_M - [\mathbf{E}_g \mathbf{I} \cdot \overleftarrow{\mathbf{GG}} - \overleftarrow{\mathbf{GG}} \cdot \mathbf{E}_g \mathbf{I}] \cdot \mathbf{I}_N \quad (5-163b)$$

It may be *proved* that the \mathbf{Q} and \mathbf{S}' vectors computed from Eqs. (5-162) and (5-163) always *exactly* satisfy the overall (scalar) *radiant* energy balance $\mathbf{I}_M^T \cdot \mathbf{Q} = \mathbf{I}_N^T \cdot \mathbf{S}'$. In words, the total radiant gas emission for all gas zones in the enclosure must always exactly equal the total radiant energy received at all surface zones which comprise the enclosure. In Eqs. (5-162) and (5-163), the following definitions are employed for the *four forward-directed* exchange areas

$$\overrightarrow{\mathbf{SS}} = \overleftarrow{\mathbf{SS}}^T \quad \overrightarrow{\mathbf{SG}} = \overleftarrow{\mathbf{SG}}^T \quad \overrightarrow{\mathbf{GS}} = \overleftarrow{\mathbf{GS}}^T \quad \overrightarrow{\mathbf{GG}} = \overleftarrow{\mathbf{GG}}^T \quad (5-64a,b,c,d)$$

such that formally there are some *eight* matrices of directed exchange areas. The four *backward-directed* arrays of directed exchange areas must satisfy the following conservation relations

$$\overleftarrow{\mathbf{SS}} \cdot \mathbf{I}_M + \overleftarrow{\mathbf{SG}} \cdot \mathbf{I}_N = \boldsymbol{\varepsilon} \mathbf{I} \cdot \mathbf{AI} \cdot \mathbf{I}_M \quad (5-165a)$$

$$4\overleftarrow{\mathbf{KI}} \cdot \mathbf{VI} \cdot \mathbf{I}_N = \overleftarrow{\mathbf{GS}} \cdot \mathbf{I}_M + \overleftarrow{\mathbf{GG}} \cdot \mathbf{I}_N \quad (5-165b)$$

Subject to the restrictions of no scatter and diffuse surface emission and reflection, the above equations are the most general matrix statement possible for the zone method. When $P = 1$, the *directed* exchange areas all reduce to the *total* exchange areas for a single gray gas. If, in addition, $K = 0$, the much simpler case of radiative transfer in a transparent medium results. If, in addition, all surface zones are *black*, the direct, total, and directed exchange areas are all identical.

Allowance for Flux Zones As in the case of a transparent medium, we now distinguish between source and flux surface zones. Let $M = M_s + M_f$ represent the total number of surface zones where M_s is the number of source-sink zones and M_f is the number of flux zones. The flux zones are the *last to be numbered*. To accomplish this, partition the

surface emissive power and flux vectors as $\mathbf{E} = \begin{bmatrix} \mathbf{E}_1 \\ \mathbf{E}_2 \end{bmatrix}$ and $\mathbf{Q} = \begin{bmatrix} \mathbf{Q}_1 \\ \mathbf{Q}_2 \end{bmatrix}$,

where the subscript 1 denotes surface source/sink zones whose emissive power \mathbf{E}_1 is specified a priori, and subscript 2 denotes surface flux zones of unknown emissive power vector \mathbf{E}_2 and known radiative flux vector \mathbf{Q}_2 . Suppose the radiative source vector \mathbf{S}' is *known*. Appropriate partitioning of Eqs. (5-162) then produces

$$\begin{bmatrix} \mathbf{Q}_1 \\ \mathbf{Q}_2 \end{bmatrix} = \begin{bmatrix} \boldsymbol{\varepsilon} \mathbf{AI}_{1,1} & \mathbf{0} \\ \mathbf{0} & \boldsymbol{\varepsilon} \mathbf{AI}_{2,2} \end{bmatrix} \cdot \begin{bmatrix} \mathbf{E}_1 \\ \mathbf{E}_2 \end{bmatrix} + \begin{bmatrix} \overleftarrow{\mathbf{SS}}_{1,2} & \overleftarrow{\mathbf{SS}}_{1,2} \\ \overleftarrow{\mathbf{SS}}_{2,1} & \overleftarrow{\mathbf{SS}}_{2,2} \end{bmatrix} \cdot \begin{bmatrix} \mathbf{E}_1 \\ \mathbf{E}_2 \end{bmatrix} - \begin{bmatrix} \overleftarrow{\mathbf{SG}} \\ \overleftarrow{\mathbf{SG}} \end{bmatrix} \cdot \mathbf{E}_g \quad (5-166a)$$

and

$$\mathbf{S}' = \overleftarrow{\mathbf{GG}} \cdot \mathbf{E}_g + \begin{bmatrix} \overleftarrow{\mathbf{GS}}_1 & \overleftarrow{\mathbf{GS}}_2 \end{bmatrix} \begin{bmatrix} \mathbf{E}_1 \\ \mathbf{E}_2 \end{bmatrix} - 4\overleftarrow{\mathbf{KI}} \cdot \mathbf{VI} \cdot \mathbf{E}_g \quad (5-166b)$$

where the definitions of the matrix partitions follow the conventions with respect to Eq. (5-120). Simultaneous solution of the *two* unknown vectors in Eqs. (5-166) then yields

$$\mathbf{E}_2 = \mathbf{RP} \cdot \begin{bmatrix} \overleftarrow{\mathbf{SS}}_{2,1} + \overleftarrow{\mathbf{SG}}_2 \cdot \mathbf{PP} \cdot \overleftarrow{\mathbf{GS}}_1 \\ \overleftarrow{\mathbf{SS}}_{2,2} + \overleftarrow{\mathbf{SG}}_2 \cdot \mathbf{PP} \cdot \mathbf{S}' \end{bmatrix} \cdot \mathbf{E}_1 + \mathbf{RP} \cdot \begin{bmatrix} \mathbf{Q}_2 - \overleftarrow{\mathbf{SG}}_2 \cdot \mathbf{PP} \cdot \mathbf{S}' \end{bmatrix} \quad (5-167a)$$

and

$$\mathbf{E}_g = \mathbf{PP} \cdot \begin{bmatrix} \overleftarrow{\mathbf{GS}}_1 & \overleftarrow{\mathbf{GS}}_2 \end{bmatrix} \begin{bmatrix} \mathbf{E}_1 \\ \mathbf{E}_2 \end{bmatrix} - \mathbf{PP} \cdot \mathbf{S}' \quad (5-167b)$$

where two auxiliary inverse matrices \mathbf{RP} and \mathbf{PP} are defined as

$$\mathbf{PP} = [4\overleftarrow{\mathbf{KI}} \cdot \mathbf{VI} - \overleftarrow{\mathbf{GG}}]^{-1} \quad (5-168a)$$

$$\mathbf{RP} = [\boldsymbol{\varepsilon} \mathbf{AI}_{2,2} - \overleftarrow{\mathbf{SS}}_{2,2} - \overleftarrow{\mathbf{SG}}_2 \cdot \mathbf{PP} \cdot \overleftarrow{\mathbf{GS}}_2]^{-1} \quad (5-168b)$$

The emissive power vectors \mathbf{E} and \mathbf{E}_g are then both *known* quantities for purposes of subsequent calculation.

Algebraic Formulas for a Single Gas Zone As shown in Fig. 5-10, the three-zone system with $M = 2$ and $N = 1$ can be employed to simulate a surprisingly large number of useful engineering geometries. These include two infinite parallel plates confining an absorbing-emitting medium; *any* two-surface zone system where a nonconvex surface zone is completely surrounded by a second zone (this includes concentric spheres and cylinders), and the speckled two-surface enclosure. As in the case of a transparent medium, the inverse reflectivity matrix \mathbf{R} is capable of explicit matrix inversion for $M = 2$. This allows derivation of *explicit* algebraic equations for all the required *directed* exchange areas for the clear plus gray WSGG spectral model with $M = 1$ and 2 and $N = 1$.

The Limiting Case $M = 1$ and $N = 1$ The directed exchange areas for this special case correspond to a single well-mixed gas zone completely surrounded by a single surface zone A_1 . Here the reflectivity matrix is a 1×1 scalar quantity which follows directly from the

general matrix equations as $\mathbf{R} = [1/(A_1 - \overline{s_1 s_1} \cdot \rho_1)]$. There are *two* WSGG clear plus gray constants a_1 and a_g , and only *one* unique directed exchange area which satisfies the conservation relation $\overline{s_1 s_1} + \overline{s_1 g} = A_1$. The only two physically meaningful directed exchange areas are those between the surface zone A_1 and the gas zone

$$\overleftarrow{S_1 G} = \frac{a_g \cdot \boldsymbol{\varepsilon}_1 A_1 \cdot \overline{s_1 g}}{\boldsymbol{\varepsilon}_1 \cdot A_1 + \rho_1 \cdot \overline{s_1 g}} \quad (5-169a)$$

$$\overleftarrow{G S_1} = \frac{a_1 \cdot \boldsymbol{\varepsilon}_1 A_1 \cdot \overline{s_1 g}}{\boldsymbol{\varepsilon}_1 \cdot A_1 + \rho_1 \cdot \overline{s_1 g}} \quad (5-169b)$$

The total radiative flux Q_1 at surface A_1 and the radiative source term $Q_1 = S$ are given by

$$Q_1 = \overleftarrow{G S_1} \cdot E_1 - \overleftarrow{S_1 G} \cdot E_g \quad (5-169)$$

Directed Exchange Areas for $M = 2$ and $N = 1$ For this case there are *four* WSGG constants, i.e., a_1 , a_2 , a_g , and τ_g . There is one required value of K that is readily obtained from the equation $K = -\ln(\tau_g)/L_{0g}$, where $\tau_g = \exp(-KL_{0g})$. For an enclosure with $M = 2$, $N = 1$, and $K \neq 0$, only *three* unique direct exchange areas are required because conservation stipulates $A_1 = \overline{s_1 s_2} + \overline{s_1 s_2} + \overline{s_1 g}$ and $A_2 = \overline{s_1 s_2} + \overline{s_2 s_2} + \overline{s_2 g}$. For $M = 2$ and $N = 1$, the matrix Eqs. (5-118) readily lead to the *general* gray gas matrix solution for $\overleftarrow{\mathbf{SS}}$ and $\overleftarrow{\mathbf{SG}}$ with $K \neq 0$ as

$$\overleftarrow{\mathbf{SS}} = \begin{bmatrix} \boldsymbol{\varepsilon}_1 A_1 - \overline{S_1 S_2} - \overline{S_1 G} & \overline{S_1 S_2} \\ \overline{S_1 S_1} & \boldsymbol{\varepsilon}_2 A_2 - \overline{S_1 S_2} - \overline{S_2 G} \end{bmatrix} \quad (5-170a)$$

where

$$\overline{S_1 S_2} = \boldsymbol{\varepsilon}_1 \boldsymbol{\varepsilon}_2 A_1 A_2 \overline{s_1 s_2} / \det \mathbf{R}^{-1} \quad (5-170b)$$

$$\text{and } \overleftarrow{\mathbf{SG}} = \begin{bmatrix} \boldsymbol{\varepsilon}_1 A_1 [(A_2 - \rho_2 \cdot \overline{s_2 s_2}) \cdot \overline{s_1 g} + \rho_2 \cdot \overline{s_1 s_2} \cdot \overline{s_2 g}] \\ \boldsymbol{\varepsilon}_2 A_2 [(A_1 - \rho_1 \cdot \overline{s_1 s_1}) \cdot \overline{s_2 g} + \rho_1 \cdot \overline{s_1 s_2} \cdot \overline{s_1 g}] \end{bmatrix} / \det \mathbf{R}^{-1} \quad (5-170c)$$

with $\overleftarrow{\mathbf{GS}} = \overleftarrow{\mathbf{SG}}^T$ and the indicated determinate of \mathbf{R}^{-1} is evaluated algebraically as

$$\det \mathbf{R}^{-1} = (A_1 - \overline{s_1 s_1} \cdot \rho_1) \cdot (A_2 - \overline{s_2 s_2} \cdot \rho_2) - \rho_1 \cdot \rho_2 \cdot \overline{s_1 s_2}^2 \quad (5-170d)$$

For the WSGG clear gas components we denote $\overleftarrow{\mathbf{SS}} \Big|_{K=0} \equiv \overleftarrow{\mathbf{SS}}_0$ and $\overleftarrow{\mathbf{SG}} \Big|_{K=0} \equiv \overleftarrow{\mathbf{SG}}_0 = \mathbf{0}$. Finally the WSGG arrays of directed exchange areas are computed simply from a -weighted sums of the gray gas total exchange areas as

$$\overleftarrow{\mathbf{SS}} = \overleftarrow{\mathbf{SS}}_0 \cdot \begin{bmatrix} 1 - a_1 & 0 \\ 0 & 1 - a_2 \end{bmatrix} + \overleftarrow{\mathbf{SS}} \cdot \begin{bmatrix} a_1 & 0 \\ 0 & a_2 \end{bmatrix}$$

$$\overleftarrow{\mathbf{SG}} = \overleftarrow{\mathbf{SG}} \cdot a_g \quad (5-171a,b,c)$$

$$\overleftarrow{\mathbf{GS}} = \overleftarrow{\mathbf{GS}} \cdot \begin{bmatrix} a_1 & 0 \\ 0 & a_2 \end{bmatrix} \neq \overleftarrow{\mathbf{SG}}^T$$

and finally

$$\overleftarrow{\mathbf{GG}} = a_g \cdot 4KV - \overleftarrow{\mathbf{GS}} \cdot \begin{bmatrix} 1 \\ 1 \end{bmatrix} \quad (5-171d)$$

The results of this development may be further expanded into algebraic form with the aid of Eq. (5-127) to yield the following

$$\overleftarrow{S_2 S_1} = \frac{\boldsymbol{\varepsilon}_1 \boldsymbol{\varepsilon}_2 A_1 A_2 \overline{s_2 s_1} (1 - a_1)}{\boldsymbol{\varepsilon}_1 \boldsymbol{\varepsilon}_1 A_1 A_2 + (\boldsymbol{\varepsilon}_1 A_1 \rho_2 + \boldsymbol{\varepsilon}_2 A_2 \rho_1) \overline{s_2 s_1} + \rho_1 \rho_2 \overline{s_1 s_2}^2} + \frac{\boldsymbol{\varepsilon}_1 \boldsymbol{\varepsilon}_2 A_1 A_2 \overline{s_2 s_1} a_1}{\det \mathbf{R}^{-1}} \quad (5-171e)$$

$$\overleftarrow{\mathbf{SG}} = \begin{bmatrix} \boldsymbol{\varepsilon}_1 A_1 [(A_2 - \rho_2 \cdot \overline{s_2 s_2}) \cdot \overline{s_1 g} + \rho_2 \cdot \overline{s_1 s_2} \cdot \overline{s_2 g}] a_g \\ \boldsymbol{\varepsilon}_2 A_2 [(A_1 - \rho_1 \cdot \overline{s_1 s_1}) \cdot \overline{s_2 g} + \rho_1 \cdot \overline{s_1 s_2} \cdot \overline{s_1 g}] a_g \end{bmatrix} / \det \mathbf{R}^{-1} \quad (5-171f)$$

and

$$\overleftarrow{\mathbf{GS}} = \begin{bmatrix} \overleftarrow{G S_1} & \overleftarrow{G S_2} \end{bmatrix} \quad (5-171g)$$

whose matrix elements are given by $\overleftarrow{GS}_1 \equiv \epsilon_1 A_1 [(A_2 - \rho_2 \overleftarrow{s_1 s_1}) \cdot \overleftarrow{s_1 g} + \rho_2 \overleftarrow{s_1 s_2} \cdot \overleftarrow{s_2 g}] / \det \mathbf{R}^{-1}$ and $\overleftarrow{GS}_2 \equiv \epsilon_2 A_2 [(A_1 - \rho_1 \overleftarrow{s_1 s_1}) \cdot \overleftarrow{s_2 g} + \rho_1 \overleftarrow{s_1 s_2} \cdot \overleftarrow{s_1 g}] / \det \mathbf{R}^{-1}$. Derivation of the scalar (algebraic) forms for the directed exchange areas here is done primarily for pedagogical purposes. Computationally, the only advantage is to obviate the need for a digital computer to evaluate a $[2 \times 2]$ matrix inverse.

Allowance for an Adiabatic Refractory with $N = 1$ and $M = 2$
 Put $N = 1$ and $M = 2$, and let zone 2 represent the refractory surface. Let $Q_2 = 0$ and $\epsilon_2 \neq 0$, and it then follows that we may define a refractory-aided directed exchange area $\overleftarrow{S}_1 G_R$ by

$$\overleftarrow{S}_1 G_R = \overleftarrow{S}_1 G + \frac{\overleftarrow{S}_1 S_2 \cdot \overleftarrow{S}_2 G}{\overleftarrow{S}_1 S_2 + \overleftarrow{S}_2 G} \quad (5-172a)$$

Assuming radiative equilibrium, the emissive power of the refractory may also be calculated from the companion equation

$$E_2 = \frac{\overleftarrow{S}_2 S_1 \cdot E_1 + \overleftarrow{S}_2 G \cdot E_g}{\overleftarrow{S}_2 S_1 + \overleftarrow{S}_2 G} \quad (5-172b)$$

In this circumstance, *all* the radiant energy originating in the gas volume is transferred to the *sole* sink zone A_1 . Equation (5-172a) is thus tantamount to the statement that $Q_1 = S'$ or that the net emission from the source ultimately must arrive at the sink. Notice that if $\epsilon_1 = 0$, Eq. (5-172a) leads to a physically incongruous statement since *all* the directed exchange areas would vanish and *no sink* would exist. Even for the simple case of $M = 2, N = 1$, the algebraic complexity of Eqs. (5-171) suggests that *numerical matrix manipulation* of directed exchange areas is to be preferred rather than calculations using algebraic formulas.

Engineering Approximations for Directed Exchange Areas
 Use of the preceding equations for directed exchange areas with $M = 2, N = 1$ and the WSGG clear plus gray gas spectral approximation requires knowledge of three independent direct exchange areas. It also formally requires evaluation of three WSGG weighting constants $a_1, a_2,$ and a_g with respect to the three temperatures $T_1, T_2,$ and T_g . Further simplifications may be made by assuming that radiant transfer for the *entire* enclosure is characterized by the *single* mean beam length $L_M = 0.88 \cdot 4 \cdot V/A$. The requisite direct exchange areas are then approximated by

$$\overleftarrow{SS} = \tau_g \begin{bmatrix} A_1 \cdot F_{1,1} & A_1 \cdot F_{1,2} \\ A_2 \cdot F_{2,1} & A_2 \cdot F_{2,2} \end{bmatrix} \quad (5-173a)$$

with
$$\overleftarrow{sg} = (1 - \tau_g) \begin{bmatrix} A_1 \\ A_2 \end{bmatrix} \quad (5-173b)$$

and for the particular case of a speckled enclosure

$$\overleftarrow{SS} = \frac{\tau_g}{A_1 + A_2} \begin{bmatrix} A_1^2 & A_1 \cdot A_2 \\ A_1 \cdot A_2 & A_2^2 \end{bmatrix} \quad (5-174a)$$

also with
$$\overleftarrow{sg} = (1 - \tau_g) \begin{bmatrix} A_1 \\ A_2 \end{bmatrix} \quad (5-174b)$$

where again τ_g is obtained from the WSGG fit of gas emissivity. These approximate formulas clearly obviate the need for *exact* values of the direct exchange areas and may be used in conjunction with Eqs. (5-171).

For engineering calculations, an additional simplification is sometimes warranted. Again characterize the system by a single mean beam length $L_M = 0.88 \cdot 4 \cdot V/A$ and employ the *identical* value of $\tau_g = KL_M$ for all surface-gas transfers. The three a constants *might* then be obtained by a WSGG data-fitting procedure for gas emissivity and gas absorptivity which utilizes the three different temperatures $T_g, T_1,$ and T_2 . For engineering purposes we choose a simpler method, however. First calculate values of ϵ_g and $\alpha_{g,1}$ for gas temperature T_g with respect to the *dominant* (sink) temperature T_1 . The *net* radiative flux between an isothermal gas mass at temperature T_g and a black isothermal bounding surface A_1 at temperature T_1 (the sink) is given by Eq. (5-138) as

$$Q_{1,g} = A_1 \sigma (\alpha_{g,1} T_1^4 - \epsilon_g T_g^4) \quad (5-175)$$

It is clear that transfer from the gas to the surface and transfer from the surface into the gas are characterized by two different constants of proportionality, ϵ_g and $\alpha_{g,1}$. To allow for the difference between gas emissivity and absorptivity, it proves convenient to introduce a single *mean gas emissivity* defined by

$$\sigma [\epsilon_g T_g^4 - \alpha_{g,1} T_1^4] = \epsilon_m \sigma (T_g^4 - T_1^4) \quad (5-176a)$$

or
$$\epsilon_m \equiv \frac{\epsilon_g - \alpha_{g,1} (T_1/T_g)^4}{1 - (T_1/T_g)^4} \quad (5-176b)$$

The calculation then proceeds by computing *two* values of ϵ_m at the given T_g and T_1 temperature pair and the two values of pL_M and $2pL_M$. We thereby obtain the expression $\epsilon_m = a_m (1 - \tau_m)$. It is then assumed that $a_1 = a_2 = a_g = a_m$ for use in Eqs. (5-171). This simplification may be used for $M > 2$ as long as $N = 1$. This simplification is illustrated in Example 12.

Example 12: WSGG Clear plus Gray Gas Emissivity Calculations
 Methane is burned to completion with 20 percent excess air (50 percent relative humidity at 298 K or 0.0088 mol water/mol dry air) in a furnace chamber of floor dimensions 3×10 m and height 5 m. The entire surface area of the enclosure is a gray sink with emissivity of 0.8 at temperature 1000 K. The confined gas is well stirred at a temperature of 1500 K. Evaluate the clear plus gray WSGG constants and the mean effective gas emissivity, and calculate the average radiative flux density to the enclosure surface.

Two-zone model, $M = 1, N = 1$: A single volume zone completely surrounded by a single sink surface zone.

Function definitions:

Gas emissivity: $\epsilon_g F(T_g, pL, b, n) := b \cdot (pL - 0.015)^n + T_g$
 Eq. (5-140a)

Gas absorptivity: $\alpha_g 1F(T_g, T_1, pL, b, n)$
 Eq. (5-141)

$$:= \frac{\epsilon_g F(T_1, pL \cdot T_1 + T_g, b, n) \cdot T_1 \cdot (T_g + T_1)^{0.5}}{T_1}$$

Mean effective gas emissivity: $\epsilon_{gm}(\epsilon_g, \alpha_g, T_g, T_1) := \frac{\epsilon_g - \alpha_g (T_1 + T_g)^4}{1 - (T_1 + T_g)^4}$
 Eq. (5-176a)

Physical constants: $\sigma \equiv 5.670400 \times 10^{-8} \frac{W}{m^2 \cdot K^4}$

Enclosure input parameters:

$T_g := 1500 \text{ K} \quad T_1 := 1000 \text{ K} \quad A_1 := 190 \text{ m}^2 \quad V := 150 \text{ m}^3$

$\epsilon_1 := 0.8 \quad \rho_1 := 1 - \epsilon_1 \quad \rho_1 = 0.2$

$E_1 := \sigma T_1^4 \quad E_g := \sigma T_g^4 \quad E_1 = 56.70 \frac{kW}{m^2} \quad E_g = 287.06 \frac{kW}{m^2}$

Stoichiometry yields the following mole table:

Mole Table: Basis 1.0 mol Methane

Species	MW	Moles in	Mass in	Moles out	Y out
CH ₄	16.04	1.00000	16.04	0.00000	0.00000
O ₂	32.00	2.40000	76.80	0.40000	0.03193
N ₂	28.01	9.02857	252.93	9.02857	0.72061
CO ₂	44.01	0.00000	0.00	1.00000	0.07981
H ₂ O	18.02	0.10057	1.81	2.10057	0.16765
Totals	27.742	12.52914	347.58	1.52914	1.00000

$p_W := .16765 \text{ atm} \quad p_C := 0.07981 \text{ atm} \quad p := p_W + p_C \quad p = 0.2475 \text{ atm}$
 $p_W + p_C = 2.101$

The mean beam length is approximated by

$$L_M := 0.88 \cdot 4 \cdot V \div A_1 \quad L_M = 2.7789 \text{ m}$$

and $pL_M := p \cdot L_M \quad pL_M = 0.6877 \text{ atm} \cdot \text{m} \quad pL_M = 0.6877$

The gas emissivities and absorptivities are then calculated from the two constant correlation in Table 5-5 (column 5 with $p_w/p_c = 2.0$) as follows:

$\epsilon_{g1} := \epsilon_g F(1500, pL_M, 540, .42) \quad \epsilon_{g1} = 0.3048$

$$\begin{aligned}\varepsilon_{g2} &:= \varepsilon_{gF}(1500, 2pL_M, 540, .42) & \varepsilon_{g2} &= 0.4097 \\ \alpha_{g11} &:= \alpha_{g1F}(1500, 1000, pL_M, 444, .34) & \alpha_{g11} &= 0.4124 \\ \alpha_{g12} &:= \alpha_{g1F}(1500, 1000, 2pL_M, 444, .34) & \alpha_{g12} &= 0.5250\end{aligned}$$

Case (a): Compute Flux Density Using Exact Values of the WSGG Constants

$$\begin{aligned}\tau_g &:= \frac{\varepsilon_{g2}}{\varepsilon_{g1}} - 1 & a_g &:= \frac{\varepsilon_{g1}}{1 - \tau_g} & \varepsilon_g &:= a_g \cdot (1 - \tau_g) & a_{g1} &:= \frac{\alpha_{g11}}{1 - \tau_g} \\ \tau_g &= 0.3442 & a_g &= 0.4647 & \varepsilon_g &= 0.3048 & a_{g1} &= 0.6289\end{aligned}$$

and the WSGG gas absorption coefficient (which is necessary for calculation of direct exchange areas) is calculated as $K_1 := \frac{-\ln \tau_g}{L_M}$ or $K_1 = 0.3838 \frac{1}{m}$

Compute directed exchange areas:
Eqs. (5-169)

$$\begin{aligned}s1g &:= (1 - \tau_g) \cdot A_1 & s1g &= 124.61 \text{ m}^2 \\ DS1G &:= \frac{a_g \cdot \varepsilon_1 \cdot A_1 \cdot s1g}{\varepsilon_1 \cdot A_1 + \rho_1 \cdot s1g} & DGS1 &:= \frac{a_{g1} \cdot \varepsilon_1 \cdot A_1 \cdot s1g}{\varepsilon_1 \cdot A_1 + \rho_1 \cdot s1g} \\ DS1G &= 49.75 \text{ m}^2 & DGS1 &= 67.32 \text{ m}^2\end{aligned}$$

And finally the gas to sink flux density is computed as

$$Q_1 := DGS1 \cdot E_1 - DS1G \cdot E_g \quad Q_1 = -10464.0 \text{ kW} \quad \frac{Q_1}{A_1} = -55.07 \frac{\text{kW}}{\text{m}^2}$$

Case (b): Compute the Flux Density Using Mean Effective Gas Emissivity Approximation

$$\begin{aligned}\varepsilon_{gm1} &:= \varepsilon_{gm}(\varepsilon_{g1}, \alpha_{g11}, T_g, T_1) & \varepsilon_{gm1} &= 0.2783 \\ \varepsilon_{gm2} &:= \varepsilon_{gm}(\varepsilon_{g2}, \alpha_{g12}, T_g, T_1) & \varepsilon_{gm2} &= 0.3813 \\ \tau_m &:= \frac{\varepsilon_{gm2}}{\varepsilon_{gm1}} - 1 & a_m &:= \frac{\varepsilon_{gm1}}{1 - \tau_m} & \varepsilon_m &:= a_m \cdot (1 - \tau_m) \\ \tau_m &= 0.3701 & a_m &= 0.4418 & \varepsilon_m &= 0.2783 & s1g_m &:= (1 - \tau_m) \cdot A_1 \\ S1G_m &:= \frac{\varepsilon_1 \cdot a_m \cdot s1g_m \cdot A_1}{\varepsilon_1 \cdot A_1 + \rho_1 \cdot s1g_m} & S1G_m &= 45.68 \text{ m}^2 & s1g_m &= 119.67 \text{ m}^2 \\ q_{1m} &:= \frac{S1G_m \cdot (E_1 - E_g)}{A_1} & q_{1m} &= -55.38 \frac{\text{kW}}{\text{m}^2} \\ \text{compared with } \frac{Q_1}{A_1} &= -55.07 \frac{\text{kW}}{\text{m}^2}\end{aligned}$$

The computed flux densities are nearly equal because there is a *single* sink zone A_1 . (This example was developed as a MATHCAD 14[®] worksheet. Mathcad is a registered trademark of Parametric Technology Corporation.)

ENGINEERING MODELS FOR FUEL-FIRED FURNACES

Modern digital computation has evolved methodologies for the design and simulation of fuel-fired combustion chambers and furnaces which incorporate virtually *all* the transport phenomena, chemical kinetics, and thermodynamics studied by chemical engineers. Nonetheless, there still exist many furnace design circumstances where such computational sophistication is not always appropriate. Indeed, a practical need still exists for simple engineering models for purposes of conceptual process design, cost estimation, and the correlation of test performance data. In this section, the zone method is used to develop perhaps the simplest **computational template** available to address some of these practical engineering needs.

Input/Output Performance Parameters for Furnace Operation The term **firing density** is typically used to define the basic *operational input parameter* for fuel-fired furnaces. In practice, firing density is often defined as the input fuel feed rate per unit area (or volume) of furnace heat-transfer surface. Thus defined, the firing density is a *dimensional quantity*. Since the feed enthalpy rate H_f is

proportional to the feed rate, we employ the sink area A_1 to define a **dimensionless firing density** as $\bar{N}_{FD} = H_f / \sigma T_{Ref}^4 \cdot A_1$ where T_{Ref} is some characteristic reference temperature. In practice, gross furnace *output performance* is often described by using one of several *furnace efficiencies*. The most common is the **gas or gas-side furnace efficiency** η_g , defined as the total enthalpy transferred to furnace internals divided by the total available feed enthalpy. Here the total available feed enthalpy is defined to include the lower heating value (LHV) of the fuel plus any air preheat above an arbitrary ambient datum temperature. Under certain conditions the definition of furnace efficiency reduces to some variant of the simple equation $\eta_g = (T_{Ref} - T_{out}) / (T_{Ref} - T_0)$ where again T_{Ref} is some reference temperature appropriate to the system in question.

The Long Plug Flow Furnace (LPFF) Model If a combustion chamber of cross-sectional area A_{Duct} and perimeter P_{Duct} is sufficiently long in the direction of flow, compared to its mean hydraulic radius, $L \gg R_h = A_{Duct} / P_{Duct}$, the radiative flux from the gas to the bounding surfaces can sometimes be adequately characterized by the *local* gas temperature. The physical rationale for this is that the *magnitudes* of the opposed upstream and downstream radiative fluxes through a cross section transverse to the direction of flow are sufficiently large as to substantially balance each other. Such a situation is not unusual in engineering practice and is referred to as the *long furnace approximation*. As a result, the radiative flux from the gas to the bounding surface may then be approximated using *two-dimensional* directed exchange areas, $\overleftarrow{S_1G} / A_1 \equiv \frac{\partial(S_1G)}{\partial A_1}$, calculated using methods as described previously.

Consider a duct of length L and perimeter P , and assume plug flow in the direction of flow z . Further assume high-intensity mixing at the entrance end of the chamber such that combustion is *complete* as the combustion products enter the duct. The duct then acts as a long heat exchanger in which heat is transferred to the walls at constant temperature T_1 by the combined effects of radiation and convection. Subject to the long furnace approximation, a differential energy balance on the duct then yields

$$\dot{m} \bar{C}_p \frac{dT_g}{dz} = P \left[\frac{\overleftarrow{S_1G}}{A_1} \sigma (T_g^4 - T_1^4) + h(T_g - T_1) \right] \quad (5-177)$$

where \dot{m} is the mass flow rate and \bar{C}_p is the heat capacity per unit mass. Equation (5-177) is nonlinear with respect to temperature. To solve Eq. (5-177), first linearize the convective heat-transfer term in the right-hand side with the approximation $\Delta T = T_2 - T_1 \approx (T_2^3 - T_1^3) / 4T_{1,2}^2$ where $T_{1,2} = (T_1 + T_2) / 2$. This linearization underestimates ΔT by no more than 5 percent when $T_2 / T_1 < 1.59$. Integration of Eq. (5-177) then leads to the solution

$$\ln \left[\frac{(T_{g,out} - T_1)(T_{g,in} + T_1)}{(T_{g,out} + T_1)(T_{g,in} - T_1)} \right] + 2.0 \tan^{-1} \left[\frac{(T_{g,in} - T_{g,out}) \cdot T_1}{(T_1^2 + T_{g,in} \cdot T_{g,out})} \right] = - \frac{4}{D_{eff}} \quad (5-178)$$

The LPFF model is described by only two dimensionless parameters, namely an *effective* firing density and a dimensionless sink temperature, viz.,

$$D_{eff} = \frac{N_{FD}}{\left(\frac{\overleftarrow{S_1G}}{A_1} \right) + N_{CR}} \quad \text{and} \quad \Theta_1 = T_1 / T_{g,in} \quad (5-178a,b)$$

Here the dimensionless firing density, N_{FD} , and a dimensionless convection-radiation number N_{CR} are defined as

$$N_{FD} = \frac{\dot{m} \bar{C}_p}{\sigma T_1^3 A_1} \quad \text{and} \quad N_{CR} = \frac{h}{4\sigma T_{g,1}^3} \quad (5-178c,d)$$

where $A_1 = PL$ is the duct surface area (the sink area), and $\bar{T}_{g,1} = (T_g + T_1) / 2$ is treated as a constant. This definition of the effective dimensionless firing density, D_{eff} , clearly delineates the relative

roles of radiation and convective heat transfer since radiation and convection are identified as *parallel (electrical) conductances*.

In analogy with a conventional heat exchanger, Eq. (5-178) displays two asymptotic limits. First define

$$\eta_f = \frac{T_{g,\text{in}} - T_{g,\text{out}}}{T_{g,\text{in}} - T_1} = 1 - \frac{T_{g,\text{out}} - T_1}{T_{g,\text{in}} - T_1} \quad (5-179)$$

as the efficiency of the long furnace. The two asymptotic limits with respect to firing density are then given by

$$D_{\text{eff}} \ll 1, \quad T_{g,\text{out}} \rightarrow T_1 \quad \eta_f \rightarrow 1 \quad (5-179a)$$

and

$$D_{\text{eff}} \gg 1, \quad T_{g,\text{out}} \rightarrow T_{g,\text{in}}$$

$$\eta_f \rightarrow \frac{4}{D_{\text{eff}} \left[1 - \frac{R-1}{R+1} - 2 \frac{R-1}{R^2+1} \right]} \quad (5-179b)$$

where $R \equiv T_{g,\text{in}}/T_1 = 1/\Theta_1$.

For low firing rates, the exit temperature of the furnace gases approaches that of the sink, i.e., sufficient residence time is provided for nearly complete heat removal from the gases. When the combustion chamber is overfired, only a small fraction of the available feed enthalpy heat is removed within the furnace. The exit gas temperature then remains essentially that of the inlet temperature, and the furnace efficiency tends asymptotically to zero.

It is important to recognize that the two-dimensional exchange area $\frac{\overline{S}_1 \overline{G}}{A_1} \equiv \frac{\partial(\overline{S}_1 \overline{G})}{\partial A_1}$ in the definition of D_{eff} can represent a *lumped* two-

dimensional exchange area of somewhat arbitrary complexity. This quantity also contains *all* the information concerning furnace geometry and gas and surface emissivities. To compare the relative importance of radiation with respect to convection, suppose $h = 10 \text{ Btu}/(\text{hr-ft}^2 \cdot ^\circ\text{R}) = 0.057 \text{ kW}/(\text{K} \cdot \text{m}^2)$ and $T_{g,1} = 1250 \text{ K}$, which leads to the numerical value $N_{\text{CR}} = 0.128$; or, in general, N_{CR} is of order 0.1 or less. The importance of the radiation contribution is estimated by bounding the magnitude of the dimensionless directed exchange area. For the case of a single gas zone completely surrounded by a black enclosure, Eq. (5-169) reduces to simply $\overline{S}_1 \overline{G}/A_1 = \epsilon_g \leq 1.0$, and it is evident that the magnitude of the radiation contribution never exceeds unity. At high temperatures, radiative effects can easily dominate other modes of heat transfer by an order of magnitude or more. When mean beam length calculations are employed, use $L_M/D = 0.94$ for a cylindrical cross section of diameter D , and

$$L_{M0} = \frac{2H \cdot W}{H + W}$$

for a rectangular duct of height H and width W .

The Well-Stirred Combustion Chamber (WSCC) Model
Many combustion chambers utilize high-momentum feed conditions with associated high-intensity mixing. The **well-stirred combustion chamber (WSCC) model** assumes a single gas zone and high-intensity mixing. Moreover, combustion and heat transfer are visualized to occur *simultaneously* within the combustion chamber. The WSCC model is characterized by some *six* temperatures which are listed in rank order as T_0 , T_{air} , T_1 , T_e , T_g , and T_f . Even though the combustion chamber is well mixed, it is *arbitrarily* assumed that the gas temperature within the enclosure T_g is *not necessarily equal* to the gas exit temperature T_e . Rather the two temperatures are related by the simple relation $\Delta T_{ge} \equiv T_g - T_e$, where $\Delta T_{ge} \approx 170 \text{ K}$ (as a representative value) is introduced as an *adjustable parameter* for purposes of data fitting and to make allowance for nonideal mixing. In addition, T_0 is the ambient temperature, T_{air} is the air preheat temperature, and T_f is a *pseudoadiabatic flame temperature*, as shall be explained in the following development. The condition $\Delta T_{ge} \equiv 0$ is intended to simulate a perfect continuous well-stirred reactor (CSTR).

Dimensional WSCC Approach A macroscopic enthalpy balance on the well-stirred combustion chamber is written as

$$-\Delta H = H_{\text{in}} - H_{\text{out}} = Q_{\text{Rad}} + Q_{\text{Con}} + Q_{\text{Ref}} \quad (5-180)$$

Here $Q_{\text{Rad}} = \overline{S}_1 \overline{G}_R \sigma (T_g^4 - T_1^4)$ represents radiative heat transfer to the sink (with due allowance for the presence of any refractory surfaces). And the two terms $Q_{\text{Con}} = h_1 A_1 (T_g - T_1)$ and $Q_{\text{Ref}} = U A_R (T_g - T_0)$ formulate the convective heat transfer to the sink and *through* the refractory, respectively.

Formulation of the left-hand side of Eq. (5-180) requires representative thermodynamic data and information on the combustion stoichiometry. In particular, the former includes the lower heating value of the fuel, the temperature-dependent molal heat capacity of the inlet and outlet streams, and the air preheat temperature T_{air} . It proves especially convenient now to introduce the definition of a pseudoadiabatic flame temperature T_f , which is *not* the true adiabatic flame temperature, but rather is an adiabatic flame temperature based on the average heat capacity of the combustion products over the temperature interval $T_0 < T < T_e$. The calculation of T_f does not allow for dissociation of chemical species and is a surrogate for the total enthalpy content of the input fuel-air mixture. It also proves to be an especially convenient system *reference temperature*. Details for the calculation of T_f are illustrated in Example 13.

In terms of this particular definition of the pseudoadiabatic flame temperature T_f , the total enthalpy change and gas efficiency are given simply as

$$\Delta H = \dot{H}_f - \dot{m} \cdot \overline{C}_{P,\text{Prod}} (T_e - T_0) = \dot{m} \overline{C}_{P,\text{Prod}} (T_f - T_e) \quad (5-181a,b)$$

where $\dot{H}_f \equiv \dot{m} \cdot \overline{C}_{P,\text{Prod}} (T_f - T_0)$ and $T_e = T_g - \Delta T_{ge}$. This particular definition of T_f leads to an especially convenient formulation of furnace efficiency

$$\eta_g = Q/\dot{H}_f = \frac{\dot{m} \cdot \overline{C}_{P,\text{Prod}} (T_f - T_e)}{\dot{m} \cdot \overline{C}_{P,\text{Prod}} (T_f - T_0)} = \frac{T_f - T_e}{T_f - T_0} \quad (5-182)$$

In Eq. (5-182), \dot{m} is the total mass flow rate and $\overline{C}_{P,\text{Prod}}$ [J/(kg·K)] is defined as the average heat capacity of the product stream over the temperature interval $T_0 < T < T_e$.

The final overall enthalpy balance is then written as

$$\dot{m} \cdot \overline{C}_{P,\text{Prod}} (T_f - T_e) = \overline{S}_1 \overline{G}_R \sigma (T_g^4 - T_1^4) + h_1 A_1 (T_g - T_1) + U A_R (T_g - T_0) \quad (5-183)$$

with $T_e = T_g - \Delta T_{ge}$.

Equation (5-183) is a nonlinear algebraic equation which may be solved by a variety of iterative methods. The *sole* unknown quantity, however, in Eq. (5-183) is the *gas* temperature T_g . It should be recognized, in particular, that T_f , T_e , $\overline{C}_{P,\text{Prod}}$, and the directed exchange area are all explicit functions of T_g . The method of solution of Eq. (5-183) is demonstrated in some detail in Example 13.

Dimensionless WSCC Approach In Eq. (5-183), assume the convective heat loss through the refractory is negligible, and linearize the convective heat transfer to the sink. These approximations lead to the result

$$\dot{m} \cdot \overline{C}_{P,\text{Prod}} (T_f - T_g + \Delta T_{ge}) = \overline{S}_1 \overline{G}_R \sigma (T_g^4 - T_1^4) + h_1 A_1 (T_g - T_1) / 4 \overline{T}_{g,1}^3 \quad (5-184)$$

where $\overline{T}_{g,1} = (T_g + T_1)/2$ is some characteristic average temperature which is taken as constant. Now normalize all temperatures based on the pseudoadiabatic temperature as in $\Theta_i = T_i/T_f$. Equation (5-184) then leads to the dimensionless equation

$$D_{\text{eff}} (1 - \Theta_g + \Delta^\circ) = (\Theta_g^4 - \Theta_1^4) \quad (5-185)$$

where again $D_{\text{eff}} = N_{\text{FD}} / (\overline{S}_1 \overline{G}/A_1 + N_{\text{CR}})$ is defined *exactly* as in the case of the LPFF model, with the proviso that the WSCC dimensionless firing density is defined here as $N_{\text{FD}} = \dot{m} \overline{C}_{P,\text{Prod}} / (\sigma T_f^3 A_1)$. The dimensionless furnace efficiency follows directly from Eq. (5-182) as

$$\eta_g = \frac{1 - \Theta_e}{1 - \Theta_0} = \frac{1 - \Theta_g + \Delta^\circ}{1 - \Theta_0} \quad (5-186a)$$

We also define a **reduced furnace efficiency** η'_g

$$\eta'_g \equiv (1 - \Theta_0)\eta_g = 1 - \Theta_g + \Delta^\circ \tag{5-186b}$$

Since Eq. (5-186b) may be rewritten as $\Theta_g = (1 + \Delta^\circ - \eta'_g)$, combination of Eqs. (5-185) and (5-186b) then yields the final result

$$D_{\text{eff}}\eta'_g = (1 + \Delta^\circ - \eta'_g)^4 - \Theta_1^4 \tag{5-187}$$

Equation (5-187) provides an *explicit* relation between the modified furnace efficiency and the effective firing density directly in which the gas temperature is eliminated.

Equation (5-187) has two asymptotic limits

$$\begin{aligned} D_{\text{eff}} \ll 1 \quad \Theta_g &\rightarrow \Theta_1 \\ \eta'_g &\rightarrow 1 - \Theta_1 + \Delta^\circ \end{aligned} \tag{5-188a}$$

and

$$\begin{aligned} D_{\text{eff}} \gg 1 \quad \Theta_g &\rightarrow 1 + \Delta^\circ \quad \text{and} \quad \Theta_e \rightarrow 1 \\ \eta'_g &\rightarrow \frac{(1 + \Delta^\circ)^4 - \Theta_1^4}{D_{\text{eff}} + 4(1 + \Delta^\circ)^3} \end{aligned} \tag{5-188b}$$

Figure 5-23 is a plot of η'_g versus D_{eff} computed from Eq. (5-187) for the case $\Delta^\circ = 0$.

The asymptotic behavior of Eq. (5-189) mirrors that of the LPPF model. Here, however, for low firing densities, the exit temperature of the furnace exit gases approaches $\Theta_e = \Theta_1 - \Delta^\circ$ rather than the sink temperature. Moreover, for $D_{\text{eff}} \ll 1$ the reduced furnace efficiency adopts the constant value $\eta'_g = 1 - \Theta_e = 1 + \Delta^\circ - \Theta_1$. Again at very high firing rates, only a very small fraction of the available feed enthalpy heat is recovered within the furnace. Thus the exit gas temperature remains nearly unchanged from the pseudoadiabatic flame temperature $[T_e \approx T_f]$ and the gas-side efficiency necessarily approaches zero.

Example 13: WSCC Furnace Model Calculations Consider the furnace geometry and combustion stoichiometry described in Example 12. The end-fired furnace is 3 m wide, 5 m tall, and 10 m long. Methane at a firing rate of 2500 kg/h is burned to completion with 20 percent excess air which is preheated to 600°C. The speckled furnace model is to be used. The sink (zone 1)

occupies 60 percent of the total interior furnace area and is covered with two rows of 5-in (0.127-m) tubes mounted on equilateral centers with a center-to-center distance of twice the tube diameter. The sink temperature is 1000 K, and the tube emissivity is 0.7. Combustion products discharge from a 10-m² duct in the roof which is also tube-screen covered and is to be considered part of the sink. The refractory (zone 2) with emissivity 0.6 is radiatively adiabatic but demonstrates a small convective heat loss to be calculated with an overall heat transfer coefficient U . Compute all unknown furnace temperatures, the gas-side furnace efficiency, and the mean heat flux density through the tube surface. Use the *dimensional* solution approach for the well-stirred combustor model and compare computed results with the *dimensionless* WSCC and LPPF models. Computed values for mean equivalent gas emissivity obtained from Eq. (5-174b) and Table 5-5 for $T_g = 2000$ K for $L_M = 2.7789$ m and $T_1 = 1000$ K are found to be

$T_g = 1500$ K	$a_m = 0.44181$	$\tau_m = 0.37014$	$\epsilon_m = 0.27828$
$T_g = 2000$ K	$a_m = 0.38435$	$\tau_m = 0.41844$	$\epsilon_m = 0.22352$

Over this temperature range the gas emissivity may be calculated by linear interpolation. Additional heat-transfer and thermodynamic data are supplied in context.

Three-zone speckled furnace model, M = 2, N = 1:

Zone 1: Sink (60 percent of total furnace area)

Zone 2: Refractory surface (40 percent of total furnace area)

Physical constants:

$$\sigma = 5.670400 \times 10^{-8} \frac{\text{W}}{\text{m}^2 \cdot \text{K}^4}$$

Linear interpolation function for mean effective gas emissivity constants:

$$\text{LINTF}(T, Y_2, Y_1) := \frac{Y_1 \cdot (2000 \text{ K} - T) + Y_2 \cdot (T - 1500 \text{ K})}{500 \text{ K}} \quad (1500 \text{ K} < T < 2000 \text{ K})$$

Enclosure input parameters:

$$V_{\text{tot}} := 150 \text{ m}^3 \quad A_{\text{tot}} := 190 \text{ m}^2 \quad C_1 := 0.6 \quad C_2 := 1 - C_1$$

$$A_1 := C_1 \cdot A_{\text{tot}} \quad A_2 := C_2 \cdot A_{\text{tot}} \quad D_{\text{tube}} := .127 \text{ m}$$

Direct exchange areas for WSCC clear gas component (temperature independent):

$$F := \begin{pmatrix} C_1 & C_2 \\ C_1 & C_2 \end{pmatrix} \quad AI := \begin{pmatrix} A_1 & 0 \\ 0 & A_2 \end{pmatrix} \quad ss1 := AI \cdot F \quad ss1 = \begin{pmatrix} 68.40 & 45.60 \\ 45.60 & 30.40 \end{pmatrix} \text{m}^2$$

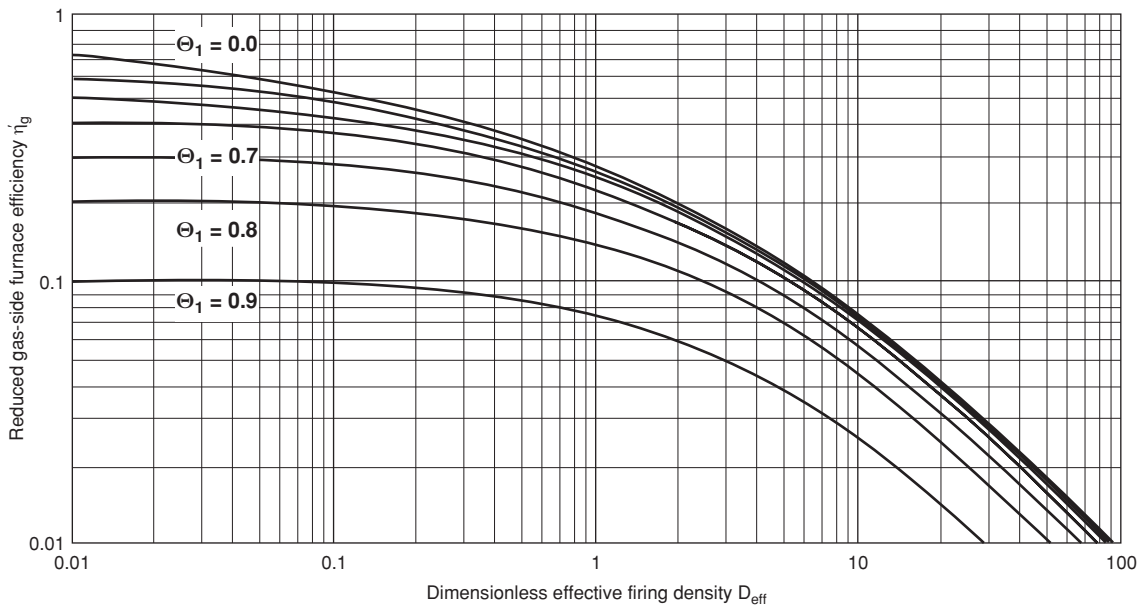


FIG. 5-23 Reduced gas-side furnace efficiency versus effective firing density for well-stirred combustion chamber model. $\Delta^\circ = 0$, $\Theta_1 = 0.0, 0.4, 0.5, 0.6, 0.7, 0.8, 0.9$.

5-42 HEAT AND MASS TRANSFER

Equivalent gray plane emissivity calculations for sink:

$$\epsilon_{\text{tube}} := 0.7 \quad F_{\text{bar}} := 0.987 \quad (\text{from Fig. 5-13, curve 6 with ratio} = 2.0)$$

$$\epsilon_{1,\text{eq}} := \frac{1}{\left(\frac{1}{\epsilon_1} - 1\right) + 2 \cdot \frac{D_{\text{tube}}}{2 \cdot \pi \cdot D_{\text{tube}}} \cdot \left(\frac{1}{\epsilon_{\text{tube}}} - 1\right) + \frac{1}{F_{\text{bar}}}} \quad \epsilon_{1,\text{eq}} = 0.86988$$

$$\epsilon_1 := \epsilon_{1,\text{eq}} \quad \epsilon_2 := 0.6 \quad \epsilon I := \begin{pmatrix} \epsilon_1 & 0 \\ 0 & \epsilon_2 \end{pmatrix} \quad \rho I := \text{identity}(2) - \epsilon I$$

Total exchange areas for WSGG clear gas component:

$$R1 := (AI - ss1 \cdot \rho I)^{-1} \quad SS1 := \epsilon I \cdot AI \cdot R1 \cdot ss1 \cdot \epsilon I \quad SS1 = \begin{pmatrix} 67.93 & 31.24 \\ 31.24 & 14.36 \end{pmatrix} \text{m}^2$$

Temperature and emissive power input data:

$$T_1 := 1000.0 \text{ K} \quad T_{\text{air}} := 873.15 \text{ K}$$

$$T_0 := 298.15 \text{ K} \quad \Delta T_{\text{gr}} := 170 \text{ K} \quad E_1 := \sigma \cdot T_1^4 \quad E_1 = 56.704 \frac{\text{kW}}{\text{m}^2}$$

Mean beam length calculations:

$$L_{M0} := 4 \cdot \frac{V_{\text{tot}}}{A_{\text{tot}}} \quad L_{M0} = 3.1579 \text{ m} \quad L_M := 0.88 L_{M0} \quad L_M = 2.7789 \text{ m}$$

Stoichiometric and thermodynamic input data:

$$\text{MCH}_{4,\text{dot}} := 2500 \frac{\text{kg}}{\text{h}} \quad \text{MW}_{\text{CH}_4} := 16.04 \frac{\text{g}}{\text{mol}} \quad \text{MW}_{\text{in}} := 27.742 \frac{\text{g}}{\text{mol}}$$

$$\Sigma \text{Mols} := 12.52914 \quad \text{LHV} := 191760 \frac{\text{cal}}{\text{mol}} \quad \text{MCP}_{\text{air}} := 7.31 \frac{\text{cal}}{\text{mol} \cdot \text{K}}$$

$$\text{MCP}(T) := \left[7.01 + 0.875 \left(\frac{T}{1000 \text{ K}} \right) \right] \frac{\text{cal}}{\text{mol} \cdot \text{K}} \quad (800 \text{ K} < T < 1200 \text{ K})$$

M_{dot} is the total mass flowrate and $\text{NCH}_{4,\text{dot}}$ is the molal flowrate of CH_4 .

$$M_{\text{dot}} := \frac{\text{MCH}_{4,\text{dot}} \cdot \text{MW}_{\text{in}} \cdot \Sigma \text{Mols}}{\text{MW}_{\text{CH}_4}} \quad \text{NCH}_{4,\text{dot}} := \frac{\text{MCH}_{4,\text{dot}}}{\text{MW}_{\text{CH}_4}}$$

$$M_{\text{dot}} = 54174.5 \frac{\text{kg}}{\text{h}} \quad \text{NCH}_{4,\text{dot}} = 155860.3 \frac{\text{mol}}{\text{h}}$$

Overall refractory heat-transfer coefficient:

$$D_r := 0.343 \text{ m} \quad k_r := 0.00050 \frac{\text{kW}}{\text{m} \cdot \text{K}}$$

$$h_0 := 0.0114 \frac{\text{kW}}{\text{m}^2 \cdot \text{K}} \quad h_0 = 2.0077 \frac{\text{Btu}}{\text{h} \cdot \text{ft}^2 \cdot \text{R}} \quad h_1 := 0.0170 \frac{\text{kW}}{\text{m}^2 \cdot \text{K}}$$

$$h_1 = 2.9939 \frac{\text{Btu}}{\text{h} \cdot \text{ft}^2 \cdot \text{R}} \quad U := \frac{1}{\frac{1}{h_0} + \frac{1}{h_1} + \frac{D_r}{k_r}}$$

$$U = 0.001201 \frac{\text{kW}}{\text{m}^2 \cdot \text{K}} \quad U = 0.2115 \frac{\text{Btu}}{\text{h} \cdot \text{ft}^2 \cdot \text{R}}$$

START OF ITERATION LOOP: Successive Substitution with T_g as the Trial Variable

$$\text{Assume } T_g := 1759.1633222447 \text{ K} \quad T_r := T_g - \Delta T_{\text{gr}} \quad T_e = 1589.2 \text{ K}$$

$$E_g := \sigma \cdot T_g^4 \quad E_g = 543.05 \frac{\text{kW}}{\text{m}^2}$$

Compute temperature-dependent mean effective gas emissivity via linear interpolation:

$$\tau_m := \text{LINTF}(T_g, 0.37014, 0.418442) \quad a_m := \text{LINTF}(T_g, 0.44181, 0.38435)$$

$$\tau_m = 0.3934 \quad a_m = 0.4141 \quad \epsilon_m := a_m \cdot (1 - \tau_m) \quad \epsilon_m = 0.2512$$

Compare interpolated value:

$$\epsilon_{\text{com}} := \text{LINTF}(T_g, 0.27828, 0.22352) \quad \epsilon_{\text{com}} = 0.2519$$

Direct and total exchange areas for WSGG gray gas component:

$$ss2 := \tau_m \cdot ss1 \quad sg2 := (AI - ss2) \begin{bmatrix} 1 \\ 1 \end{bmatrix} \quad R2 := (AI - ss2 \cdot \rho I)^{-1}$$

$$ss2 = \begin{pmatrix} 26.91 & 17.94 \\ 17.94 & 11.96 \end{pmatrix} \text{m}^2 \quad sg2 = \begin{pmatrix} 69.15 \\ 46.10 \end{pmatrix} \text{m}^2 \quad SS2 := \epsilon I \cdot AI \cdot R2 \cdot ss2 \cdot \epsilon I$$

Compute directed exchange areas:

$$DSS := (1 - a_m) \cdot SS1 + a_m \cdot SS2 \quad DSG := a_m \cdot \epsilon I \cdot AI \cdot R2 \cdot sg2$$

Refractory augmented directed gas-sink exchange area:

$$\text{DS1GR} := \text{DSG}_1 + \frac{\text{DSS}_{1,2} \cdot \text{DSG}_2}{\text{DSS}_{1,2} + \text{DSG}_2} \quad \text{DS1GR} = 35.59 \text{ m}^2 \quad \text{Eq. (5-172a)}$$

Compute refractory temperature (T_2); assume radiative equilibrium:

$$\text{Equation (5-172b): } E_2 := \frac{\text{DSS}_{2,1} \cdot E_1 + \text{DSG}_{2,1} \cdot E_g}{\text{DSS}_{2,1} + \text{DSG}_{2,1}}$$

$$E_2 = 231.24 \frac{\text{kW}}{\text{m}^2}$$

$$T_2 := \left(\frac{E_2}{\sigma} \right)^{0.25} \quad T_2 = 1421.1 \text{ K}$$

Enthalpy balance: Basis: 1 mole CH_4 :

$$h_{\text{in}} := \text{LHV} + (\Sigma \text{Mols} - 1) \cdot \text{MCP}_{\text{air}} \cdot (T_{\text{air}} - T_0) \quad h_{\text{in}} = 240219.9 \frac{\text{cal}}{\text{mol}}$$

Compute pseudoadiabatic flame temperature T_f :

$$T_f := T_0 + \frac{h_{\text{in}}}{\Sigma \text{Mols} \cdot \text{MCP}(T_e)} \quad h_{\text{out}} := \Sigma \text{Mols} \cdot \text{MCP}(T_e) \cdot (T_e - T_0)$$

$$T_f = 2580.5 \text{ K} \quad h_{\text{out}} = 135880.8 \frac{\text{cal}}{\text{mol}}$$

$$H_{\text{in}} := \text{NCH}_{4,\text{dot}} \cdot h_{\text{in}} \quad H_{\text{out}} := \text{NCH}_{4,\text{dot}} \cdot h_{\text{out}} \quad \Delta H := H_{\text{out}} - H_{\text{in}}$$

$$H_{\text{in}} = 43543.59 \text{ kW} \quad H_{\text{out}} = 24630.51 \text{ kW} \quad \Delta H = -18913.08 \text{ kW}$$

Overall enthalpy balance:

$$Q1_g := \text{DS1GR} \cdot (E_g - E_1) \quad Q1_g = 17308.45 \text{ kW}$$

$$Q1_{\text{Con}} := h_1 \cdot A_1 \cdot (T_g - T_1) \quad Q1_{\text{Con}} = 1471.26 \text{ kW}$$

$$Q2_{\text{Con}} := U \cdot A_2 \cdot (T_g - T_0) \quad Q2_{\text{Con}} = 133.37 \text{ kW}$$

$$\text{ERROR} := Q1_g + Q1_{\text{Con}} + Q2_{\text{Con}} + \Delta H \quad \% \text{ERROR}1 := 100 \frac{\text{ERROR}}{\Delta H}$$

$$\text{ERROR} = -0.0000 \text{ kW} \quad \% \text{ERROR}1 = 0.00000$$

$$T_{\text{gcalc}} := \left[\frac{\text{DS1GR} \cdot E_1 - (\Delta H + Q1_{\text{Con}} + Q2_{\text{Con}})}{\text{DS1GR} \cdot \sigma} \right]^{0.25} \quad T_{\text{gcalc}} = 1759.16332 \text{ K}$$

Average assumed and calculated temperatures for next iteration

$$T_{\text{gnew}} := \frac{T_g + T_{\text{gcalc}}}{2} \quad T_{\text{gnew}} = 1759.1633222935 \text{ K} \quad \text{Go to Start}$$

END OF ITERATION LOOP: Final Gas Temperature $T_g = 1759.16 \text{ K}$

$$\eta_g := \frac{H_{\text{in}} - H_{\text{out}}}{H_{\text{in}}} \quad \text{or} \quad \eta_{1g} := \frac{T_f - T_e}{T_f - T_0} \quad \eta_g = 0.43435 \quad \eta_{1g} = 0.43435$$

Heat flux density calculations:

$$q_1 := \frac{Q1_g + Q1_{\text{Con}}}{A_1} \quad q_{\text{tube}} := q_1 \cdot \left(2 \cdot \frac{D_{\text{tube}}}{2 \cdot \pi \cdot D_{\text{tube}}} \right)$$

$$q_1 = 164.7 \frac{\text{kW}}{\text{m}^2} \quad q_{\text{tube}} = 52.44 \frac{\text{kW}}{\text{m}^2}$$

Note: This example was also solved with $\Delta T_{\text{gr}} = 0$. The results were as follows: $T_f = 2552.8 \text{ K}$, $T_r = T_e = 1707.1 \text{ K}$, $T_2 = 1381.1 \text{ K}$, $\eta_g = 37.51$ percent, $D_{\text{eff}} = 0.53371$, and $\Delta H = 16332.7 \text{ kW}$. The WSCC model with $\Delta T_{\text{gr}} = 0$ predicts a lower performance bound.

Compare dimensionless WSCC model:

$$\Theta_0 := \frac{T_0}{T_f} \quad \Theta_1 := \frac{T_1}{T_f} \quad \Delta T_{\text{star}} := \frac{\Delta T_{\text{gr}}}{T_f}$$

$$T_{\text{gl}} := \frac{T_1 + T_g}{2}$$

$$\Theta_0 = 0.1155 \quad \Theta_1 = 0.3875 \quad \Delta T_{star} = 0.06588 \quad T_{g1} = 1379.58 \text{ K}$$

$$C_{pProd} := \frac{MCp(T_c)}{MW_{in}} \quad C_{pProd} = 0.000352 \text{ kW} \cdot \frac{\text{h}}{\text{kg} \cdot \text{K}}$$

$$N_{FD} := M_{dot} \frac{C_{pProd}}{\sigma T_g^3 A_1} \quad N_{CR} := \frac{h_1}{4 \sigma T_{g1}^3} \quad D_{eff} := \frac{N_{FD}}{\frac{DSIGR}{A_1} + N_{CR}}$$

$$N_{FD} = 0.17176 \quad N_{CR} = 0.02855 \quad D_{eff} = 0.50409 \quad \frac{DSIGR}{A_1} = 0.31218$$

$$\eta_{prime} := \eta_g (1 - \Theta_0) \quad D1_{eff} := \frac{(1 + \Delta T_{star} - \eta_{prime})^4 - \Theta_1^4}{\eta_{prime}}$$

$$D1_{eff} = 0.50350 \quad \text{versus} \quad D_{eff} = 0.50409$$

This small discrepancy is due to linearization and neglect of convective refractory heat losses in the dimensionless WSCC model.

Compare dimensionless LPFF model:

$$R_{in} := \frac{1}{\Theta_1} \quad R_{in} = 2.58050$$

Trial and error calculation to match effective firing densities:
Assume:

$$T_{out} := 1000.13763 \text{ K} \quad R_{out} := \frac{T_{out}}{T_1} \quad R_{out} = 1.00014 \quad \frac{4}{D_{eff}} = 7.93513$$

$$CLong := -\ln \left[\frac{(R_{out} - 1)(R_{in} + 1)}{(R_{in} - 1)(R_{out} + 1)} \right] - 2 \cdot \text{atan} \left(\frac{R_{in} - R_{out}}{1 + R_{in} R_{out}} \right) \quad CLong = 7.93514$$

$$\eta_{L_f} := \frac{R_{in} - R_{out}}{R_{in} - 1} \quad \eta_{L_f} = 0.99991292 \quad \text{versus} \quad \eta_g = 0.43435$$

Note: The long plug flow furnace Model is so efficient that it would be grossly underfired using the computed WSCC effective firing density. Of the two models, the LPFF model always predicts an upper theoretical performance limit.

(This example was developed as a MATHCAD 14® worksheet. Mathcad is registered trademark of Parametric Technology Corporation.)

WSCC Model Utility and More Complex Zoning Models

Despite its simplicity, the WSCC construct has a wide variety of practical uses and is of significant pedagogical value. Here an engineering situation of inordinate complexity is described by the definition of only eight dimensionless quantities D_{eff} , N_{FD} , $\hat{S}_i G_R/A_1$, N_{CR} , η_g , Δ^* , Θ_0 , and Θ_1 . The first three are related by the simple algebraic definition $D_{eff} = N_{FD}/(\hat{S}_i G_R/A_1 + N_{CR})$. These dimensionless quantities con-

tain all the physical input information for the model, namely, furnace parameters and geometry, radiative properties of the combustion products, and the stoichiometry and thermodynamics of the combustion process. The WSCC model leads to a dimensionless two-dimensional plot of *reduced* effective furnace efficiency versus dimensionless effective firing density (Fig. 5-23), which is characterized by only two additional parameters, namely, Δ^* and Θ_1 .

Of the models presented here, the WSCC model with $\Delta T_{ge} = 0$ produces the lowest furnace efficiencies. The long furnace model usually produces the highest furnace efficiency. This is really not a fair statement because two distinctly different pieces of process equipment are compared. In this regard, a more appropriate definition of the dimensionless firing density for the LPFF model might be $N'_{FD} = \dot{m} \bar{C}_p / (\sigma T_{g,in}^3 A_1)$. It may be counterintuitive, but the WSCC and LPFF models *generally do not* characterize the extreme conditions for the performance of combustors as in the case of chemical reactors.

Figure 5-23 has been used to correlate furnace performance data for a multitude of industrial furnaces and combustors. Typical operational domains for a variety of fuel-fired industrial furnaces are summarized in Table 5-7. The WSCC approach (or "speckled" furnace model) is a classic contribution to furnace design methodology which was first due to Hottel [op. cit.]. The WSCC model provides a simple *furnace design template* which leads to a host of more complex furnace models. These models include an obvious extension to a tanks-in-series model as well as multizone models utilizing empirical cold-flow velocity patterns. For more information on practical furnace design models, reference is made to Hottel and Sarofim (op. cit., Chap. 14). Qualitative aspects of process equipment have been treated in some detail elsewhere (Baukal, C. E., ed., *The John Zink Combustion Handbook*, CRC Press, Boca Raton, Fla., 2001).

TABLE 5-7 Operational Domains for Representative Process Furnaces and Combustors

Domain	Furnace or combustor type	Dimensionless sink temperature	Dimensionless firing density
A	Oil processing furnaces; radiant section of oil tube stills and cracking coils	$\Theta_1 \approx 0.4$	$0.1 < D_{eff} < 1.0$
B	Domestic boiler combustion chambers	$\Theta_1 \approx 0.2$	$0.5 < D_{eff} < 1.1$
C	Glass furnaces	$0.7 < \Theta_1 < 0.8$	$0.035 < D_{eff} < 0.8$
D	Soaking pits	$\Theta_1 \approx 0.6$	$0.7 < D_{eff} < 1.1$
E	Gas-turbine combustors	$0.4 < \Theta_1 < 0.7$	$4.0 < D_{eff} < 25.0$

MASS TRANSFER

GENERAL REFERENCES: Bird, Stewart, and Lightfoot, *Transport Phenomena*, 2d ed., Wiley, New York, 2002. Cussler, *Diffusion: Mass Transfer in Fluid Systems*, 2d ed., Cambridge University Press, Cambridge, 1997. Danner and Daubert, *Manual for Predicting Chemical Process Design Data*, AIChE, New York, 1983. Daubert and Danner, *Physical and Thermodynamic Properties of Pure Chemicals*, Taylor and Francis, Bristol, Pa., 1989–1995. Gammon, Marsh, and Dewan, *Transport Properties and Related Thermodynamic Data of Binary Mixtures*, AIChE, New York, Part 1, 1993; Part 2, 1994. Geankoplis, *Transport Processes and Separation Process Principles*, 5th ed., Prentice-Hall PTR, Upper Saddle River, N.J., 2003. Kirwan, "Mass Transfer Principles," Chap. 2 in Rousseau, R. W. (ed.), *Handbook of Separation Process Technology*, Wiley, New York, 1987. McCabe, Smith, and Harriott, *Unit Operations of Chemical Engineering*, 7th ed., McGraw-Hill, New York, 2006. Middleman, *An Introduction to Mass and Heat Transfer*, Wiley, New York, 1997. Poling, Prausnitz, and O'Connell, *The Properties of Gases and Liquids*, 5th ed., McGraw-Hill, New York, 2001. Schwartzberg and Chao, *Food Technol.*, **36**(2), 73 (1982). Sherwood, Pigford, and Wilke, *Mass Transfer*, McGraw-Hill, New York, 1975. Skelland, *Diffusional Mass Transfer*, Wiley, New York, 1974. Taylor and Krishna, *Multicomponent Mass Transfer*, Wiley, New York, 1993. Thompson, *Introduction to Transport Phenomena*, Prentice-Hall PTR, Upper Saddle River, N.J., 1999. Treybal, *Mass-Transfer Operations*, 3d ed., McGraw-Hill, New York, 1980.

REFERENCES FOR DIFFUSIVITIES, TABLES 5-10, 5-13 TO 5-15

- Asfour and Dullien, *Chem. Eng. Sci.*, **41**, 1891 (1986).
- Blanc, *J. Phys.*, **7**, 825 (1908).
- Bosse and Bart, *Ind. Eng. Chem. Res.*, **45**, 1822 (2006).
- Brokaw, *Ind. Eng. Chem. Process Des. and Dev.*, **8**, 2, 240 (1969).
- Caldwell and Babb, *J. Phys. Chem.*, **60**, 51 (1956).
- Catchpole and King, *Ind. Eng. Chem. Res.*, **33**, 1828 (1994).
- Chen and Chen, *Chem. Eng. Sci.*, **40**, 1735 (1985).
- Cullinan, *AIChE J.*, **31**, 1740–1741 (1985).
- Cussler, *AIChE J.*, **26**, 1 (1980).
- Fuller, Schettler, and Giddings, *Ind. Eng. Chem.*, **58**, 18 (1966).
- Hayduk and Laudie, *AIChE J.*, **20**, 3, 611 (1974).
- Hayduk and Minhas, *Can. J. Chem. Eng.*, **60**, 195 (1982).
- He and Yu, *Ind. Eng. Chem. Res.*, **36**, 4430 (1997).
- Lee and Thodos, *Ind. Eng. Chem. Fundam.*, **22**, 17–26 (1983).
- Lee and Thodos, *Ind. Eng. Chem. Res.*, **27**, 992–997 (1988).
- Leffler and Cullinan, *Ind. Eng. Chem. Fundam.*, **9**, 84, 88 (1970).
- Liu and Ruckenstein, *Ind. Eng. Chem. Res.*, **36**, 888 (1997) and corrections **37**, 3524 (1998).
- Mathur and Thodos, *AIChE J.*, **11**, 613 (1965).
- Matthews and Akgerman, *AIChE J.*, **33**, 881 (1987).

20. Rathbun and Babb, *Ind. Eng. Chem. Proc. Des. Dev.*, **5**, 273 (1966).
 21. Riazi and Whitson, *Ind. Eng. Chem. Res.*, **32**, 3081 (1993).
 22. Siddiqi and Lucas, *Can. J. Chem. Eng.*, **64**, 839 (1986).
 23. Smith and Taylor, *Ind. Eng. Chem. Fundam.*, **22**, 97 (1983).
 24. Sridhar and Potter, *AIChE J.*, **23**, 4, 590 (1977).
 25. Sun and Chen, *Ind. Eng. Chem. Res.*, **26**, 815 (1987).
 26. Tyn and Calus, *J. Chem. Eng. Data*, **20**, 310 (1975).
 27. Úmesi and Danner, *Ind. Eng. Chem. Process Des. Dev.*, **20**, 662 (1981).
 28. Vignes, *Ind. Eng. Chem. Fundam.*, **5**, 184 (1966).
 29. Wilke, *Chem. Eng. Prog.*, **46**, 2, 95 (1950).
 30. Wilke and Chang, *AIChE J.*, **1**, 164 (1955).
 31. Wilke and Lee, *Ind. Eng. Chem.*, **47**, 1253 (1955).
- REFERENCES FOR DIFFUSIVITIES IN POROUS SOLIDS, TABLE 5-16**
32. Ruthven, *Principles of Adsorption and Adsorption Processes*, Wiley, 1984.
 33. Satterfield, *Mass Transfer in Heterogeneous Catalysis*, MIT Press, 1970.
 34. Suzuki, *Adsorption Engineering*, Kodansha—Elsevier, 1990.
 35. Yang, *Gas Separation by Adsorption Processes*, Butterworths, 1987.
- REFERENCES FOR TABLES 5-17 TO 5-24**
36. Bahmanyar, et al., *Chem. Eng. Rsch. Des.*, **68**, 74 (1990).
 37. Baier et al., *Chem. Eng. Sci.*, **54**, 343 (1999).
 38. Beenackers and van Swaij, *Chem. Eng. Sci.*, **48**, 3109 (1993).
 39. Bird, Stewart, and Lightfoot, *Transport Phenomena*, Wiley, 1960.
 40. Blatt et al. (eds.), (ed.), *Membrane Science and Technology*, **47**, Plenum, 1970.
 41. Bocquet et al., *AIChE J.*, **51**, 1067 (2005).
 42. Bolles and Fair, *Institution Chem. Eng. Symp. Ser.*, **56**, 3/35 (1979).
 43. Bolles and Fair, *Chem. Eng.*, **89**(14), 109 (July 12, 1982).
 44. Bravo and Fair, *Ind. Eng. Chem. Process Des. Dev.*, **21**, 162 (1982).
 45. Bravo, Rocha and Fair, *Hydrocarbon Processing*, 91 (Jan. 1985).
 46. Brian and Hales, *AIChE J.*, **15**, 419 (1969).
 47. Calderbank and Moo-Young, *Chem. Eng. Sci.*, **16**, 39 (1961).
 48. Cavatorta, Bohm, and Chiappori de del Giorgio, *AIChE J.*, **45**, 938 (1999).
 49. Chaumat et al., *Chem. Eng. Sci.*, **60**, 5930 (2005).
 50. Chen, Lin, and Liu, *Ind. Eng. Chem. Res.*, **44**, 7868 (2005).
 51. Chilton and Colburn, *Ind. Eng. Chem.*, **26**, 1183 (1934).
 52. Chowdhia, Foutch, and Lee, *Ind. Eng. Chem. Res.*, **42**, 1485 (2003).
 53. Colburn, *Trans. AIChE*, **29**, 174 (1933).
 54. Cornell, Knapp, and Fair, *Chem. Eng. Prog.*, **56**(7), 68 (1960).
 55. Cornet and Kaloo, *Proc. 3rd Int'l. Congr. Metallic Corrosion—Moscow*, **3**, 83 (1966).
 56. Crause and Nieuwoudt, *Ind. Eng. Chem. Res.*, **38**, 4928 (1999).
 57. Deckwer et al., *Biotech. Bioeng.* (1981).
 58. Dudukovic, Milosevic, and Pjanovic, *AIChE J.*, **42**, 269 (1996).
 59. Dwivedi and Upadhyay, *Ind. Eng. Chem. Process Des. Develop.*, **16**, 1657 (1977).
 60. Eisenberg, Tobias, and Wilke, *Chem. Eng. Prog. Symp. Sec.*, **51**(16), 1 (1955).
 61. El-Shazly et al., *Ind. Eng. Chem. Res.*, **41**, 5516 (2002).
 62. Elzinga and Banchemo, *Chem. Eng. Progr. Symp. Ser.*, **55**(29), 149 (1959).
 63. Fair, "Distillation" in Rousseau (ed.), *Handbook of Separation Process Technology*, Wiley, 1987.
 64. Fan, Yang, and Wen, *AIChE J.*, **6**, 482 (1960).
 65. Garner and Suckling, *AIChE J.*, **4**, 114 (1958).
 66. Geankoplis, *Transport Processes and Unit Operations*, 4th ed., Prentice Hall, 2003.
 67. Gibilaro et al., *Chem. Eng. Sci.*, **40**, 1811 (1985).
 68. Gilliland and Sherwood, *Ind. Eng. Chem.*, **26**, 516 (1934).
 69. Costick et al., *Ind. Eng. Chem. Res.*, **42**, 3626 (2003).
 70. Griffith, *Chem. Eng. Sci.*, **12**, 198 (1960).
 71. Guedes de Carvalho and Alves, *AIChE J.*, **45**, 2495 (1999).
 72. Gupta and Thodos, *AIChE J.*, **9**, 751 (1963).
 73. Gupta and Thodos, *Ind. Eng. Chem. Fundam.*, **3**, 218 (1964).
 74. Harriott, *AIChE J.*, **8**, 93 (1962).
 75. Hassan et al., *Ind. Eng. Chem. Res.*, **44**, 5761 (2005).
 76. Heertjes, Holve, and Talsma, *Chem. Eng. Sci.*, **3**, 122 (1954).
 77. Hines and Maddox, *Mass Transfer: Fundamentals and Applications*, Prentice-Hall, 1985.
 78. Hoffer et al., *Chem. Eng. Sci.*, **59**, 259 (2004).
 79. Houwing, Billiet, and van der Wielin, *AIChE J.*, **49**, 1158 (2003).
 80. Hsiung and Thodos, *Int. J. Heat Mass Transfer*, **20**, 331 (1977).
 81. Hsu, Sato, and Sage, *Ind. Eng. Chem.*, **46**, 870 (1954).
 82. Hughmark, *Ind. Eng. Chem. Fundam.*, **6**, 408 (1967).
 83. Johnson, Besic, and Hamielec, *Can. J. Chem. Eng.*, **47**, 559 (1969).
 84. Johnstone and Pigford, *Trans. AIChE*, **38**, 25 (1942).
 85. Kafesjian, Plank, and Gerhard, *AIChE J.*, **7**, 463 (1961).
 86. Kelly and Swenson, *Chem. Eng. Prog.*, **52**, 263 (1956).
 87. King, *Separation Processes*, 2d ed., McGraw-Hill (1980).
 88. Kirwan, "Mass Transfer Principles" in Rousseau, *Handbook of Separation Process Technology*, Wiley, 1987.
 89. Klein, Ward, and Lacey, "Membrane Processes—Dialysis and Electro-Dialysis" in Rousseau, *Handbook of Separation Process Technology*, Wiley, 1987.
 90. Kohl, "Absorption and Stripping" in Rousseau, *Handbook of Separation Process Technology*, Wiley, 1987.
 91. Kojima et al., *J. Chem. Engng. Japan*, **20**, 104 (1987).
 92. Koloini, Sopic, and Zumer, *Chem. Eng. Sci.*, **32**, 637 (1977).
 93. Kreutzer et al., *Ind. Eng. Chem. Res.*, **44**, 9646 (2005).
 94. Lancia, Musmarra, and Pepe, *Ind. Eng. Chem. Res.*, **36**, 3859 (1997).
 95. Larachi et al., *Ind. Eng. Chem. Res.*, **42**, 222 (2003).
 96. Lau et al., *Ind. Eng. Chem. Res.*, **43**, 1302 (2004).
 97. Lee, *Biochemical Engineering*, Prentice-Hall, 1992.
 98. Lee and Foster, *Appl. Catal.*, **63**, 1 (1990).
 99. Lee and Holder, *Ind. Eng. Chem. Res.*, **34**, 906 (1995).
 100. Lee and Lueptow, *Separ. Sci. Technol.*, **39**, 539 (2004).
 101. Levich, *Physicochemical Hydrodynamics*, Prentice-Hall, 1962.
 102. Levins and Gastonbury, *Trans. Inst. Chem. Eng.*, **50**, 32, 132 (1972).
 103. Linton and Sherwood, *Chem. Eng. Prog.*, **46**, 258 (1950).
 104. Ludwig, *Applied Process Design for Chemical and Petrochemical Plants*, 2d ed., vol. 2, Gulf Pub. Co., 1977.
 105. McCabe, Smith, and Harriott, *Unit Operations of Chemical Engineering*, 7th ed., McGraw-Hill, 2005.
 106. Nelson and Galloway, *Chem. Eng. Sci.*, **30**, 7 (1975).
 107. Notter and Sleicher, *Chem. Eng. Sci.*, **26**, 161 (1971).
 108. Ohashi et al., *J. Chem. Eng. Japan*, **14**, 433 (1981).
 109. Onda, Takeuchi, and Okumoto, *J. Chem. Eng. Japan*, **1**, 56 (1968).
 110. Pangarkar et al., *Ind. Eng. Chem. Res.*, **41**, 4141 (2002).
 111. Pasternak and Gauvin, *AIChE J.*, **7**, 254 (1961).
 112. Pasternak and Gauvin, *Can. J. Chem. Eng.*, **38**, 35 (April 1960).
 113. Patil, Deshmukh, and Joshi, *Ind. Eng. Chem. Res.*, **43**, 2765 (2004).
 114. Pekdemir, Davies, and Sara, *Ind. Eng. Chem. Res.*, **37**, 1560 (1998).
 115. Perez and Sandall, *AIChE J.*, **20**, 770 (1974).
 116. Petrovic and Thodos, *Ind. Eng. Chem. Fundam.*, **7**, 274 (1968).
 117. Pinczewski and Sideman, *Chem. Eng. Sci.*, **29**, 1969 (1974).
 118. Prasad and Sirkar, *AIChE J.*, **34**, 177 (1988).
 119. Rahman and Streat, *Chem. Eng. Sci.*, **36**, 293 (1981).
 120. Ramirez and Davis, *AIChE J.*, **45**, 1355 (1999).
 121. Ranz and Marshall, *Chem. Eng. Prog.*, **48**, 141, 173 (1952).
 122. Reiss, *Ind. Eng. Chem. Process Des. Develop.*, **6**, 486 (1967).
 123. Riet, *Ind. Eng. Chem. Process Des. Dev.*, **18**, 357 (1979).
 124. Rocha, Bravo, and Fair, *Ind. Eng. Chem. Res.*, **35**, 1660 (1996).
 125. Rowe, *Chem. Eng. Sci.*, **30**, 7 (1975).
 126. Rowe, Claxton, and Lewis, *Trans. Inst. Chem. Eng. London*, **43**, 14 (1965).
 127. Ruckenstein and Rajagopalan, *Chem. Eng. Commun.*, **4**, 15 (1980).
 128. Ruthven, *Principles of Adsorption and Adsorption Processes*, Wiley, 1984.
 129. Sanger and Deckwer, *Chem. Eng. J.*, **22**, 179 (1981).
 130. Satterfield, *AIChE J.*, **21**, 209 (1975).
 131. Schluter and Deckwer, *Chem. Eng. Sci.*, **47**, 2357 (1992).
 132. Schmitz, Steiff, and Weinspach, *Chem. Engng. Technol.*, **10**, 204 (1987).
 133. Schugerl et al., *Adv. Biochem. Eng.*, **8**, 63 (1978).
 134. Scott and Lobato, *Ind. Eng. Chem. Res.*, **42**, 5697 (2003).
 135. Sedahmed, Zatout, and Zewail, *Ind. Eng. Chem. Res.*, **37**, 3481 (1998).
 136. Shah et al., *AIChE J.*, **28**, 353 (1982).
 137. Sherwood et al., *Ind. Eng. Chem. Fundam.*, **4**, 113 (1965).
 138. Sherwood, Pigford, and Wilke, *Mass Transfer*, McGraw-Hill, 1975.
 139. Siegel, Sparrow, and Hallman, *Appl. Sci. Res. Sec. A*, **7**, 386 (1958).
 140. Sissom and Pitts, *Elements of Transport Phenomena*, McGraw-Hill, 1972.
 141. Skelland, *Diffusional Mass Transfer*, Wiley (1974).
 142. Skelland and Cornish, *AIChE J.*, **9**, 73 (1963).
 143. Skelland and Moeti, *Ind. Eng. Chem. Res.*, **29**, 2258 (1990).
 144. Skelland and Tedder, "Extraction—Organic Chemicals Processing" in Rousseau, *Handbook of Separation Process Technology*, Wiley, 1987, pp. 405–466.
 145. Skelland and Wellek, *AIChE J.*, **10**, 491, 789 (1964).
 146. Slater, "Rate Coefficients in Liquid-Liquid Extraction Systems" in Godfrey and Slater, *Liquid-Liquid Extraction Equipment*, Wiley, 1994, pp. 45–94.
 147. Steinberger and Treybal, *AIChE J.*, **6**, 227 (1960).
 148. Taniguchi and Kimura, *AIChE J.*, **47**, 1967 (2000).
 149. Taylor and Krishna, *Multicomponent Mass Transfer*, Wiley, 1993.
 150. Tokarz, Millies, and Mewes, *AIChE J.*, **47**, 799 (2001).
 151. Tournie, Laguerie, and Couderc, *Chem. Eng. Sci.*, **34**, 1247 (1979).
 152. Treybal, *Mass Transfer Operations*, 3d ed., McGraw-Hill, 1980.

153. Vandu, Liu, and Krishna, *Chem. Eng. Sci.*, **60**, 6430 (2005).
154. Von Karman, *Trans. ASME*, **61**, 705 (1939).
155. Wakao and Funazkri, *Chem. Eng. Sci.*, **33**, 1375 (1978).
156. Wang, Yuan, and Yu, *Ind. Eng. Chem. Res.*, **44**, 8715 (2005).
157. Wankat, *Separation Process Engineering*, 2d ed., Prentice-Hall, 2007.
158. Wilson and Geankoplis, *Ind. Eng. Chem. Fundam.*, **5**, 9 (1966).
159. Wright and Glasser, *AIChE J.*, **47**, 474 (2001).
160. Yagi and Yoshida, *Ind. Eng. Chem. Process Des. Dev.*, **14**, 488 (1975).
161. Yapici and Ozbahar, *Ind. Eng. Chem. Res.*, **37**, 643 (1998).
162. Zaki, Nirdosh, and Sedahmed, *Ind. Eng. Chem. Res.*, **41**, 3307 (2002).

INTRODUCTION

This part of Sec. 5 provides a concise guide to solving problems in situations commonly encountered by chemical engineers. It deals with diffusivity and mass-transfer coefficient estimation and common flux equations, although material balances are also presented in typical coordinate systems to permit a wide range of problems to be formulated and solved.

Mass-transfer calculations involve transport properties, such as diffusivities, and other empirical factors that have been found to relate mass-transfer rates to measured “driving forces” in myriad geometries and conditions. The context of the problem dictates whether the fundamental or more applied coefficient should be used. One key distinction is that, whenever there is flow parallel to an interface through which mass transfer occurs, the relevant coefficient is an empirical combination of properties and conditions. Conversely, when diffusion occurs in stagnant media or in creeping flow without transverse velocity gradients, ordinary diffusivities may be suitable for solving the problem. In either case, it is strongly suggested to employ data, whenever available, instead of relying on correlations.

Units employed in diffusivity correlations commonly followed the cgs system. Similarly, correlations for mass transfer correlations used the cgs or English system. In both cases, only the most recent correlations employ SI units. Since most correlations involve other properties and physical parameters, often with mixed units, they are repeated here as originally stated. Common conversion factors are listed in Table 1-4.

Fick's First Law This law relates flux of a component to its composition gradient, employing a constant of proportionality called a diffusivity. It can be written in several forms, depending on the units and frame of reference. Three that are related but not identical are

$$vJ_A = -D_{AB} \frac{dc_A}{dz} \approx mJ_A = -cD_{AB} \frac{dx_A}{dz} \approx mJ_A = -\rho D_{AB} \frac{dw_A}{dz} \quad (5-189)$$

The first equality (on the left-hand side) corresponds to the molar flux with respect to the volume average velocity, while the equality in the center represents the molar flux with respect to the molar average velocity and the one on the right is the mass flux with respect to the mass average velocity. These must be used with consistent flux expressions for fixed coordinates and for N_C components, such as:

$$N_A = vJ_A + c_A \sum_{i=1}^{N_C} N_i \bar{V}_i = mJ_A + x_A \sum_{i=1}^{N_C} N_i = \frac{mJ_A + w_A \sum_{i=1}^{N_C} n_i}{M_A} \quad (5-190)$$

In each case, the term containing the summation accounts for *conveyance*, which is the amount of component A carried by the net flow in the direction of diffusion. Its impact on the total flux can be as much as 10 percent. In most cases it is much less, and it is frequently ignored. Some people refer to this as the “convective” term, but that conflicts with the other sense of convection which is promoted by flow perpendicular to the direction of flux.

Mutual Diffusivity, Mass Diffusivity, Interdiffusion Coefficient Diffusivity is denoted by D_{AB} and is defined by Fick's first law as the ratio of the flux to the concentration gradient, as in Eq. (5-189). It is analogous to the thermal diffusivity in Fourier's law and to the kinematic viscosity in Newton's law. These analogies are flawed because both heat and momentum are conveniently defined with respect to fixed coordinates, irrespective of the direction of transfer or its magnitude, while mass diffusivity most commonly requires infor-

mation about bulk motion of the medium in which diffusion occurs. For liquids, it is common to refer to the limit of infinite dilution of A in B using the symbol, D_{AB}° .

When the flux expressions are consistent, as in Eq. (5-190), the diffusivities in Eq. (5-189) are identical. As a result, experimental diffusivities are often measured under constant volume conditions but may be used for applications involving open systems. It turns out that the two versions are very nearly equivalent for gas-phase systems because there is negligible volume change on mixing. That is not usually true for liquids, however.

Self-Diffusivity Self-diffusivity is denoted by D_{AA} and is the measure of mobility of a species in itself; for instance, using a small concentration of molecules tagged with a radioactive isotope so they can be detected. Tagged and untagged molecules presumably do not have significantly different properties. Hence, the solution is ideal, and there are practically no gradients to “force” or “drive” diffusion. This kind of diffusion is presumed to be purely statistical in nature.

In the special case that A and B are similar in molecular weight, polarity, and so on, the self-diffusion coefficients of pure A and B will be approximately equal to the mutual diffusivity, D_{AB} . Second, when A and B are the less mobile and more mobile components, respectively, their self-diffusion coefficients can be used as rough lower and upper bounds of the mutual diffusion coefficient. That is, $D_{AA} \leq D_{AB} \leq D_{BB}$. Third, it is a common means for evaluating diffusion for gases at high pressure. Self-diffusion in liquids has been studied by many [Easteal, *AIChE J.* **30**, 641 (1984), Ertl and Dullien, *AIChE J.* **19**, 1215 (1973), and Vadovic and Colver, *AIChE J.* **18**, 1264 (1972)].

Tracer Diffusivity Tracer diffusivity, denoted by $D_{A'B}$ is related to both mutual and self-diffusivity. It is evaluated in the presence of a second component B , again using a tagged isotope of the first component. In the dilute range, tagging A merely provides a convenient method for indirect composition analysis. As concentration varies, tracer diffusivities approach mutual diffusivities at the dilute limit, and they approach self-diffusivities at the pure component limit. That is, at the limit of dilute A in B , $D_{A'B} \rightarrow D_{AB}^\circ$ and $D_{B'A} \rightarrow D_{B'B}^\circ$; likewise at the limit of dilute B in A , $D_{B'A} \rightarrow D_{BA}^\circ$ and $D_{A'B} \rightarrow D_{AA}^\circ$.

Neither the tracer diffusivity nor the self-diffusivity has much practical value except as a means to understand ordinary diffusion and as order-of-magnitude estimates of mutual diffusivities. Darken's equation [Eq. (5-230)] was derived for tracer diffusivities but is often used to relate mutual diffusivities at moderate concentrations as opposed to infinite dilution.

Mass-Transfer Coefficient Denoted by k_c , k_x , K , and so on, the mass-transfer coefficient is the ratio of the flux to a concentration (or composition) difference. These coefficients generally represent rates of transfer that are much greater than those that occur by diffusion alone, as a result of convection or turbulence at the interface where mass transfer occurs. There exist several principles that relate that coefficient to the diffusivity and other fluid properties and to the intensity of motion and geometry. Examples that are outlined later are the film theory, the surface renewal theory, and the penetration theory, all of which pertain to idealized cases. For many situations of practical interest like investigating the flow inside tubes and over flat surfaces as well as measuring external flow through banks of tubes, in fixed beds of particles, and the like, correlations have been developed that follow the same forms as the above theories. Examples of these are provided in the subsequent section on mass-transfer coefficient correlations.

Problem Solving Methods Most, if not all, problems or applications that involve mass transfer can be approached by a systematic course of action. In the simplest cases, the unknown quantities are obvious. In more complex (e.g., multicomponent, multiphase, multi-dimensional, nonisothermal, and/or transient) systems, it is more subtle to resolve the known and unknown quantities. For example, in multicomponent systems, one must know the fluxes of the components before predicting their effective diffusivities and vice versa. More will be said about that dilemma later. Once the known and unknown quantities are resolved, however, a combination of conservation equations, definitions, empirical relations, and properties are

Nomenclature and Units—Mass Transfer

Symbols	Definition	SI units	U.S. Customary units
a	Effective interfacial mass transfer area per unit volume	m^2/m^3	ft^2/ft^3
A_s	Cross-sectional area of vessel	m^2 or cm^2	ft^2
A'	Constant (see Table 5-24-K)		
a_p	See a		
c	Concentration = P/RT for an ideal gas	mol/m^3 or mol/l or $gequiv/l$	$lbmol/ft^3$
c_i	Concentration of component $i = x, c$ at gas-liquid interface	mol/m^3 or mol/l or $gequiv/l$	$lbmol/ft^3$
c_p	Specific heat	$kJ/(kg \cdot K)$	$Btu/(lb \cdot ^\circ F)$
d	Characteristic length	m or cm	ft
d_b	Bubble diameter	m	ft
d_c	Column diameter	m or cm	ft
d_{drop}	Sauter mean diameter	m	ft
d_{imp}	Impeller diameter	m	ft
d_{pore}	Pore diameter	m or cm	ft
$D_{A,A}$	Self-diffusivity (= D_A at $x_A = 1$)	m^2/s or cm^2/s	ft^2/h
D_{AB}	Mutual diffusivity	m^2/s or cm^2/s	ft^2/h
D_{AB}^∞	Mutual diffusivity at infinite dilution of A in B	m^2/s or cm^2/s	ft^2/h
D_{eff}	Effective diffusivity within a porous solid = $\epsilon_p D/\tau$	m^2/s	ft^2/h
D_K	Knudson diffusivity for gases in small pores	m^2/s or cm^2/s	ft^2/h
D_L	Liquid phase diffusion coefficient	m^2/s	ft^2/h
D_s	Surface diffusivity	m^2/s or cm^2/s	ft^2/h
E	Energy dissipation rate/mass		
E_s	Activation energy for surface diffusion	J/mol or cal/mol	
f	Friction factor for fluid flow	Dimensionless	Dimensionless
F	Faraday's constant	$96,487$ Coulomb/gequiv	
g	Acceleration due to gravity	m/s^2	ft/h^2
g_c	Conversion factor	1.0	4.17×10^8 lb ft/[lbf-h ²]
G	Gas-phase mass flux	$kg/(s \cdot m^2)$	$lb/(h \cdot ft^2)$
G_a	Dry air flux	$kg/(s \cdot m^2)$	$lb/(h \cdot ft^2)$
G_M	Molar gas-phase mass flux	$kmol/(s \cdot m^2)$	$(lbmol)/(h \cdot ft^2)$
h'	Heat transfer coefficient	$W/(m^2 \cdot K) = J/(s \cdot m^2 \cdot K)$	$Btu/(h \cdot ft^2 \cdot ^\circ F)$
h_T	Total height of tower packing	m	ft
H	Compartment height	m	ft
H	Henry's law constant	$kPa/(mole-fraction solute in liquid phase)$	$(lbf/in^2)/(mole-fraction solute in liquid phase)$
H'	Henry's law constant	$kPa/[kmol/(m^3 \text{ solute in liquid phase})]$	$(lbf/in^2)/[(lbmol)/(ft^3 \text{ solute in liquid phase})]$ or $atm/[(lbmole)/(ft^3 \text{ solute in liquid phase})]$
H_G	Height of one transfer unit based on gas-phase resistance	m	ft
H_{OG}	Height of one overall gas-phase mass-transfer unit	m	ft
H_L	Height of one transfer unit based on liquid-phase resistance	m	ft
H_{OL}	Height of one overall liquid-phase mass-transfer unit	m	ft
HTU	Height of one transfer unit (general)	m	ft
j_D	Chilton-Colburn factor for mass transfer, Eq. (5-289)	Dimensionless	Dimensionless
j_H	Chilton-Colburn factor for heat transfer	Dimensionless	Dimensionless
j_M	See j_D		
m_{JA}	Mass flux of A by diffusion with respect to the mean mass velocity	$kmol/(m^2 \cdot s)$ or $mol/(cm^2 \cdot s)$	$lbmol/(ft^2 \cdot h)$
M_{JA}	Molar flux of A by diffusion with respect to mean molar velocity	$kmol/(m^2 \cdot s)$ or $mol/(cm^2 \cdot s)$	$lbmol/(ft^2 \cdot h)$
v_{JA}	Molar flux of A with respect to mean volume velocity	$kmol/(m^2 \cdot s)$	$lbmol/(ft^2 \cdot h)$
J_{si}	Molar flux by surface diffusion	$kmol/(m^2 \cdot s)$ or $gmol/(cm^2 \cdot s)$	$lbmol/(ft^2 \cdot h)$
k	Boltzmann's constant	8.9308×10^{-10} gequiv ohm/s	
k	Film mass transfer coefficient	m/s or cm/s	ft/hr
k	Thermal conductivity	$(J \cdot m)/(s \cdot m^2 \cdot K)$	$Btu/(h \cdot ft \cdot ^\circ F)$
k'	Mass-transfer coefficient for dilute systems	$kmol/[(s \cdot m^2)(kmol/m^3)]$ or m/s	$lbmol/[(h \cdot ft^2)(lbmol/ft^3)]$ or ft/hr
k_G	Gas-phase mass-transfer coefficient for dilute systems	$kmol/[(s \cdot m^2)(kPa \text{ solute partial pressure})]$	$lbmol/[(h \cdot ft^2)lbf/in^2 \text{ solute partial pressure}]$
K_G	Gas-phase mass-transfer coefficient for dilute systems	$kmol/[(s \cdot m^2)(mole fraction in gas)]$	$lbmol/[(h \cdot ft^2)(mole fraction in gas)]$
k_{GA}	Volumetric gas-phase mass-transfer coefficient for concentrated systems	$kmol/[(s \cdot m^3)(mole fraction)]$	$(lbmol)/[(h \cdot ft^3)(mole fraction)]$
\bar{k}_{GA}	Overall volumetric gas-phase mass-transfer coefficient for concentrated systems	$kmol/(s \cdot m^3)$	$lbmol/(h \cdot ft^3)$
\bar{k}_L^0	Liquid phase mass transfer coefficient for pure absorption (no reaction)	$kmol/(s \cdot m^2)$	$lbmol/(h \cdot ft^2)$
k_L	Liquid-phase mass-transfer coefficient for dilute systems	$kmol/[(s \cdot m^2)(mole-fraction solution in liquid)]$	$(lbmol)/[(h \cdot ft^2)(mole-fraction solute in liquid)]$
k'_L	Liquid-phase mass-transfer coefficient for dilute systems	$kmol/[(s \cdot m^2)(kmol/m^3)]$ or m/s	$(lbmol)/[(h \cdot ft^2)(lbmol/ft^3)]$ or ft/h
\bar{k}_L	Liquid-phase mass-transfer coefficient for concentrated systems	$kmol/(s \cdot m^2)$	$lbmol/(h \cdot ft^2)$
k_{LA}	Volumetric liquid-phase mass-transfer coefficient for dilute systems	$kmol/[(s \cdot m^3)(mole fraction)]$	$(lbmol)/[(h \cdot ft^3)(mole fraction)]$
K	Overall mass transfer coefficient	m/s or cm/s	ft/h
K	α/R = specific conductance	ohm/cm	
K_G	Overall gas-phase mass-transfer coefficient for dilute systems	$kmol/[(s \cdot m^2)(mole fraction)]$	$(lbmol)/[(h \cdot ft^2)(mole fraction)]$

Nomenclature and Units—Mass Transfer (Continued)

Symbols	Definition	SI units	U.S. Customary units
\hat{K}_G	Overall gas-phase mass-transfer coefficient for concentrated systems	kmol/(s·m ²)	lbmol/(h·ft ²)
$K_{G,a}$	Overall volumetric gas-phase mass-transfer dilute systems	kmol/[(s·m ³)(mole-fraction solute in gas)]	(lbmol)/[(h·ft ³)(mole-fraction solute in gas)]
$K'_{G,a}$	Overall volumetric gas-phase mass-transfer dilute systems	kmol/[(s·m ³)(kPa solute partial pressure)]	(lbmol)/[(h·ft ³)(lbf/in ² solute partial pressure)]
$(Ka)_H$	Overall enthalpy mass-transfer coefficient	kmol/[(s·m ²)(mole fraction)]	lb/[(h·ft ²)(lb water/lb dry air)]
K_L	Overall liquid-phase mass-transfer coefficient	kmol/[(s·m ²)(mole fraction)]	(lbmol)/[(h·ft ²)(mole fraction)]
\hat{K}_L	Liquid-phase mass-transfer coefficient for concentrated systems	kmol/(s·m ²)	(lbmol)/(h·ft ²)
$K_{L,a}$	Overall volumetric liquid-phase mass-transfer coefficient for dilute systems	kmol/[(s·m ³)(mole-fraction solute in liquid)]	(lbmol)/[(h·ft ³)(mole-fraction solute in liquid)]
$\hat{K}'_{L,a}$	Overall volumetric liquid-phase mass-transfer coefficient for concentrated systems	kmol/(s·m ³)	(lbmol)/(h·ft ³)
L	Liquid-phase mass flux	kg/(s·m ²)	lb/(h·ft ²)
L_M	Molar liquid-phase mass flux	kmol/(s·m ²)	(lbmol)/(h·ft ²)
m	Slope of equilibrium curve = dy/dx (mole-fraction solute in gas)/(mole-fraction solute in liquid)	Dimensionless	Dimensionless
m	Molality of solute	mol/1000 g solvent	
M_i	Molecular weight of species i	kg/kmol or g/mol	lb/lbmol
M	Mass in a control volume V	kg or g	lb
$ n_+ , n_- $	Valences of cationic and anionic species	Dimensionless	Dimensionless
n'	See Table 5-24-K	Dimensionless	Dimensionless
n_A	Mass flux of A with respect to fixed coordinates	kg/(s·m ²)	lb/(h·ft ²)
N	Impeller speed	Revolution/s	Revolution/min
N'	Number deck levels	Dimensionless	Dimensionless
N_A	Interphase mass-transfer rate of solute A per interfacial area with respect to fixed coordinates	kmol/(s·m ²)	(lbmol)/(h·ft ²)
N_c	Number of components	Dimensionless	Dimensionless
N_{Fr}	Froude Number ($d_{imp} N^2/g$)	Dimensionless	Dimensionless
N_{Gr}	Grashof number ($\frac{g x^3}{(\mu/\rho)^2} \left(\frac{\rho_\infty}{\rho_s} - 1 \right)$)	Dimensionless	Dimensionless
N_{OG}	Number of overall gas-phase mass-transfer units	Dimensionless	Dimensionless
N_{OL}	Number of overall liquid-phase mass-transfer units	Dimensionless	Dimensionless
NTU	Number of transfer units (general)	Dimensionless	Dimensionless
N_{Kn}	Knudson number = l/d_{pore}	Dimensionless	Dimensionless
N_{Pr}	Prandtl number ($c_p \mu/k$)	Dimensionless	Dimensionless
N_{Re}	Reynolds number (Gd/μ_G)	Dimensionless	Dimensionless
N_{Sc}	Schmidt number ($\mu_G/\rho_G D_{AB}$) or ($\mu_L/\rho_L D_L$)	Dimensionless	Dimensionless
N_{Sh}	Sherwood number ($k_c R T d / D_{AB} p_T$), see also Tables 5-17 to 5-24	Dimensionless	Dimensionless
N_{St}	Stanton number (k_c / G_M) or (k_L / L_M)	Dimensionless	Dimensionless
N_{We}	Weber number ($\rho N^2 d_{imp}^3 / \sigma$)	Dimensionless	Dimensionless
p	Solute partial pressure in bulk gas	kPa	lbf/in ²
$p_{B,M}$	Log mean partial pressure difference of stagnant gas B	Dimensionless	Dimensionless
p_i	Solute partial pressure at gas-liquid interface	kPa	lbf/in ²
p_T	Total system pressure	kPa	lbf/in ²
P	Pressure	Pa	lbf/in ² or atm
P	Power	Watts	
P_c	Critical pressure	Pa	lbf/in ² or atm
Per	Perimeter/area	m ⁻¹	ft ⁻¹
Q	Volumetric flow rate	m ³ /s	ft ³ /h
r_A	Radius of dilute spherical solute	Å	
R	Gas constant	8.314 J/mol K = 8.314 Pa m ³ /(mol K) = 82.057 atm cm ³ /mol K	10.73 ft ³ psia/lbmol·h
R	Solution electrical resistance	ohm	
R_i	Radius of gyration of the component i molecule	Å	
s	Fractional surface-renewal rate	s ⁻¹	h ⁻¹
S	Tower cross-sectional area = $\pi d^2/4$	m ²	ft ²
t	Contact time	s	h
t_f	Formation time of drop	s	h
T	Temperature	K	°R
T_b	Normal boiling point	K	°R
T_c	Critical temperature	K	°R
T_r	Reduced temperature = T/T_c	Dimensionless	Dimensionless
u, v	Fluid velocity	m/s or cm/s	ft/h
u_o	Blowing or suction velocity	m/s	ft/h
u_∞	Velocity away from object	m/s	ft/h
u_L	Superficial liquid velocity in vertical direction	m/s	ft/h
v_s	Slip velocity	m/s	ft/h
v_T	Terminal velocity	m/s	ft/h
v_{TS}	Stokes law terminal velocity	m/s	ft/h
V	Packed volume in tower	m ³	ft ³
V	Control volume	m ³ or cm ³	ft ³
V_b	Volume at normal boiling point	m ³ /kmol or cm ³ /mol	ft ³ /lbmol
V_i	Molar volume of i at its normal boiling point	m ³ /kmol or cm ³ /mol	ft ³ /lbmol
\bar{v}_i	Partial molar volume of i	m ³ /kmol or cm ³ /mol	ft ³ /lbmol

5-48 HEAT AND MASS TRANSFER

Nomenclature and Units—Mass Transfer (Concluded)

Symbols	Definition	SI units	U.S. Customary units
V_{mli}	Molar volume of the liquid-phase component i at the melting point	m^3/kmol or cm^3/mol	ft^3/lbmol
V_{tower}	Tower volume per area	m^3/m^2	ft^3/ft^2
w	Width of film	m	ft
x	Length along plate	m	ft
x	Mole-fraction solute in bulk-liquid phase	$(\text{kmol solute})/(\text{kmol liquid})$	$(\text{lbmol solute})/(\text{lb mol liquid})$
x_A	Mole fraction of component A	$\text{kmole A}/\text{kmole fluid}$	$\text{lbmol A}/\text{lb mol fluid}$
x^o	Mole-fraction solute in bulk liquid in equilibrium with bulk-gas solute concentration y	$(\text{kmol solute})/(\text{kmol liquid})$	$(\text{lbmol solute})/(\text{lbmol liquid})$
x_{BM}	Logarithmic-mean solvent concentration between bulk liquid and interface values	$(\text{kmol solvent})/(\text{kmol liquid})$	$(\text{lbmol solvent})/(\text{lbmol liquid})$
x_{BM}^o	Logarithmic-mean inert-solvent concentration between bulk-liquid value and value in equilibrium with bulk gas	$(\text{kmol solvent})/(\text{kmol liquid})$	$(\text{lbmol solvent})/(\text{lbmol liquid})$
x_i	Mole-fraction solute in liquid at gas-liquid interface	$(\text{kmol solute})/(\text{kmol liquid})$	$(\text{lbmol solute})/(\text{lbmol liquid})$
y	Mole-fraction solute in bulk-gas phase	$(\text{kmol solute})/(\text{kmol gas})$	$(\text{lbmol solute})/(\text{lbmol gas})$
y_{BM}	Logarithmic-mean inert-gas concentration [Eq. (5-275)]	$(\text{kmol inert gas})/(\text{kmol gas})$	$(\text{lbmol inert gas})/(\text{lbmol gas})$
y_{BM}^o	Logarithmic-mean inert-gas concentration	$(\text{kmol inert gas})/(\text{kmol gas})$	$(\text{lbmol inert gas})/(\text{lbmol gas})$
y_i	Mole fraction solute in gas at interface	$(\text{kmol solute})/(\text{kmol gas})$	$(\text{lbmol solute})/(\text{lbmol gas})$
y_i^o	Mole-fraction solute in gas at interface in equilibrium with the liquid-phase interfacial solute concentration x_i	$(\text{kmol solute})/(\text{kmol gas})$	$(\text{lbmol solute})/(\text{lbmol gas})$
z	Direction of unidimensional diffusion	m	ft
Greek Symbols			
α	$1 + N_B/N_A$	Dimensionless	Dimensionless
α	Conductance cell constant (measured)	cm^{-1}	
β	$M_A^{1/2} p_c^{1/3} / T_c^{5/6}$	Dimensionless	Dimensionless
δ	Effective thickness of stagnant-film layer	m	ft
ϵ	Fraction of discontinuous phase in continuous phase for two-phase flow	Dimensionless	Dimensionless
ϵ	Void fraction available for gas flow or fractional gas holdup	m^3/m^3	ft^3/ft^3
ϵ_A	Characteristic Lennard-Jones energy	Dimensionless	Dimensionless
ϵ_{AB}	$(\epsilon_A \epsilon_B)^{1/2}$	Dimensionless	Dimensionless
γ_i	Activity coefficient of solute i	Dimensionless	Dimensionless
γ_{\pm}	Mean ionic activity coefficient of solute	Dimensionless	Dimensionless
λ_+, λ_-	Infinite dilution conductance of cation and anion	$\text{cm}^2/(\text{equiv-ohm})$	
Λ	$1000 \text{ K}/C = \lambda_+ + \lambda_- = \Lambda_o + f(C)$	$\text{cm}^2/\text{ohm gequiv}$	
Λ_o	Infinite dilution conductance	$\text{cm}^2/\text{gequiv ohm}$	
μ_i	Dipole moment of i	Debeyes	
μ_i	Viscosity of pure i	cP or Pa s	$\text{lb}/(\text{h-ft})$
μ_G	Gas-phase viscosity	$\text{kg}/(\text{s-m})$	$\text{lb}/(\text{h-ft})$
μ_L	Liquid-phase viscosity	$\text{kg}/(\text{s-m})$	$\text{lb}/(\text{h-ft})$
ν	Kinematic viscosity = ρ/μ	m^2/s	ft^2/h
ρ	Density of A	kg/m^3 or g/cm^3	lb/ft^3
ρ_c	Critical density of A	kg/m^3 or g/cm^3	lb/ft^3
ρ_c	Density continuous phase	kg/m^3	lb/ft^3
ρ_G	Gas-phase density	kg/m^3	lb/ft^3
$\bar{\rho}_L$	Average molar density of liquid phase	kmol/m^3	$(\text{lbmol})/\text{ft}^3$
ρ_p	Particle density	kg/m^3 or g/cm^3	lb/ft^3
ρ_r	Reduced density = ρ/ρ_c	Dimensionless	Dimensionless
ψ_i	Parachor of component $i = V_i \sigma^{1/4}$		
ψ	Parameter, Table 5-24-G	Dimensionless	Dimensionless
σ	Interfacial tension	dyn/cm	lb/ft
σ_i	Characteristic length	\AA	
σ_i	Surface tension of component i	dyn/cm	
σ_{AB}	Binary pair characteristic length = $(\sigma_A + \sigma_B)/2$	\AA	
τ	Intraparticle tortuosity	Dimensionless	Dimensionless
ω	Pitzer's acentric factor = $-[1.0 + \log_{10}(P^o/P_c)]$	Dimensionless	
ω	Rotational velocity	Radians/s	
Ω	Diffusion collision integral = $f(kT/\epsilon_{AB})$	Dimensionless	Dimensionless
Subscripts			
A	Solute component in liquid or gas phase		
B	Inert-gas or inert-solvent component		
G	Gas phase		
m	Mean value		
L	Liquid phase		
super	Superficial velocity		
Superscript			
o	At equilibrium		

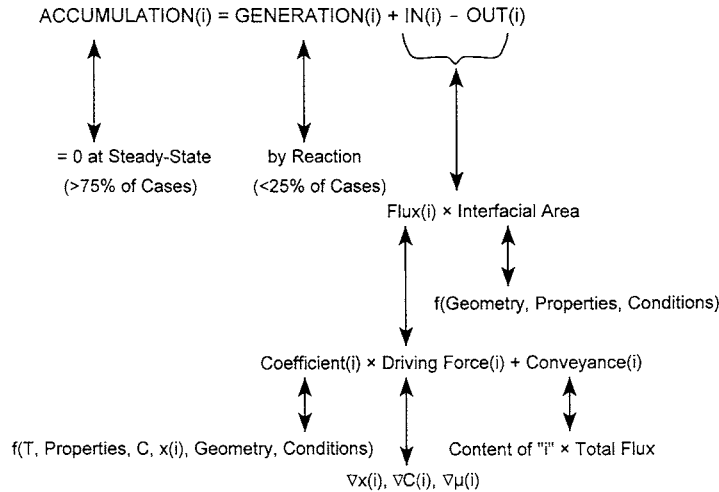


FIG. 5-24 Flowchart illustrating problem solving approach using mass-transfer rate expressions in the context of mass conservation.

applied to arrive at an answer. Figure 5-24 is a flowchart that illustrates the primary types of information and their relationships, and it applies to many mass-transfer problems.

CONTINUITY AND FLUX EXPRESSIONS

Material Balances Whenever mass-transfer applications involve equipment of specific dimensions, flux equations alone are inadequate to assess results. A material balance or continuity equation must also be used. When the geometry is simple, macroscopic balances suffice. The following equation is an overall mass balance for such a unit having N_m bulk-flow ports and N_n ports or interfaces through which diffusive flux can occur:

$$\frac{dM}{dt} = \sum_{i=1}^{N_m} m_i + \sum_{i=1}^{N_n} n_i A_{cs_i} \tag{5-191}$$

where M represents the mass in the unit volume V at any time t ; m_i is the mass flow rate through the i th port; and n_i is the mass flux through the i th port, which has a cross-sectional area of A_{cs_i} . The corresponding balance equation for individual components includes a reaction term:

$$\frac{dM_j}{dt} = \sum_{i=1}^{N_m} m_{ij} + \sum_{i=1}^{N_n} n_{ij} A_{cs_i} + r_j V \tag{5-192}$$

For the j th component, $m_{ij} = m_i w_{ij}$ is the component mass flow rate in stream i ; w_{ij} is the mass fraction of component j in stream i ; and r_j is the net reaction rate (mass generation minus consumption) per unit volume V that contains mass M . If it is inconvenient to measure mass flow rates, the product of density and volumetric flow rate is used instead.

In addition, most situations that involve mass transfer require material balances, but the pertinent area is ambiguous. Examples are packed columns for absorption, distillation, or extraction. In such

cases, flow rates through the discrete ports (nozzles) must be related to the mass-transfer rate in the packing. As a result, the mass-transfer rate is determined via flux equations, and the overall material balance incorporates the stream flow rates m_i and integrated fluxes. In such instances, it is common to begin with the most general, differential material balance equations. Then, by eliminating terms that are negligible, the simplest applicable set of equations remains to be solved. Table 5-8 provides material balances for Cartesian, cylindrical, and spherical coordinates. The generic form applies over a unit cross-sectional area and constant volume:

$$\frac{\partial \rho_j}{\partial t} = -\nabla \cdot n_j + r_j \tag{5-193a}$$

where $n_j = \rho v_j$. Applying Fick's law and expressing composition as concentration gives

$$\frac{\partial c_j}{\partial t} = -v \cdot \nabla c_j + D_j \nabla^2 c_j + r_j \tag{5-193b}$$

Flux Expressions: Simple Integrated Forms of Fick's First Law Simplified flux equations that arise from Eqs. (5-189) and (5-190) can be used for unidimensional, steady-state problems with binary mixtures. The boundary conditions represent the compositions x_{A_L} and x_{A_R} at the left-hand and right-hand sides of a hypothetical layer having thickness Δz . The principal restriction of the following equations is that the concentration and diffusivity are assumed to be constant. As written, the flux is positive from left to right, as depicted in Fig. 5-25.

1. Equimolar counterdiffusion ($N_A = -N_B$)

$$N_A = M J_A = -D_{AB} c \frac{dx_A}{dz} = \frac{D_{AB}}{\Delta z} c (x_{A_L} - x_{A_R}) \tag{5-197}$$

TABLE 5-8 Continuity Equation in Various Coordinate Systems

Coordinate System	Equation
Cartesian	$\frac{\partial \rho_j}{\partial t} = -\left(\frac{\partial n_{x_j}}{\partial x} + \frac{\partial n_{y_j}}{\partial y} + \frac{\partial n_{z_j}}{\partial z}\right) + r_j$ (5-194)
Cylindrical	$\frac{\partial \rho_j}{\partial t} = -\left(\frac{1}{r} \frac{\partial m_{r_j}}{\partial r} + \frac{1}{r} \frac{\partial n_{\theta_j}}{\partial \theta} + \frac{\partial n_{z_j}}{\partial z}\right) + r_j$ (5-195)
Spherical	$\frac{\partial \rho_j}{\partial t} = -\left(\frac{1}{r^2} \frac{\partial r^2 n_{r_j}}{\partial r} + \frac{1}{r \sin \theta} \frac{\partial n_{\theta_j} \sin \theta}{\partial \theta} + \frac{1}{r \sin \theta} \frac{\partial n_{\phi_j}}{\partial \phi}\right) + r_j$ (5-196)

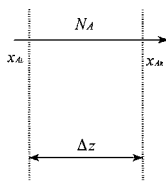


FIG. 5-25 Hypothetical film and boundary conditions.

2. Unimolar diffusion ($N_A \neq 0, N_B = 0$)

$$N_A = M J_A + x_A N_A = \frac{D_{AB}}{\Delta z} c \ln \frac{1 - x_{A_R}}{1 - x_{A_L}} \quad (5-198)$$

3. Steady state diffusion ($N_A \neq -N_B \neq 0$)

$$N_A = M J_A + x_A (N_A + N_B) = \frac{N_A}{N_A + N_B} \frac{D_{AB}}{\Delta z} c \ln \frac{\frac{N_A}{N_A + N_B} - x_{A_R}}{\frac{N_A}{N_A + N_B} - x_{A_L}} \quad (5-199)$$

The unfortunate aspect of the last relationship is that one must know a priori the ratio of the fluxes to determine the magnitudes. It is not possible to solve simultaneously the pair of equations that apply for components A and B because the equations are not independent.

Stefan-Maxwell Equations Following Eq. (5-190), a simple and intuitively appealing flux equation for applications involving N_c components is

$$N_i = -c D_{im} \nabla x_i + x_i \sum_{j=1}^{N_c} N_j \quad (5-200)$$

In the late 1800s, the development of the kinetic theory of gases led to a method for calculating multicomponent gas diffusion (e.g., the flux of each species in a mixture). The methods were developed simultaneously by Stefan and Maxwell. The problem is to determine the diffusion coefficient D_{im} . The Stefan-Maxwell equations are simpler in principle since they employ binary diffusivities:

$$\nabla x_i = \sum_{j=1}^{N_c} \frac{1}{c D_{ij}} (x_i N_j - x_j N_i) \quad (5-201)$$

If Eqs. (5-200) and (5-201) are combined, the multicomponent diffusion coefficient may be assessed in terms of binary diffusion coefficients [see Eq. (5-214)]. For gases, the values D_{ij} of this equation are approximately equal to the binary diffusivities for the ij pairs. The Stefan-Maxwell diffusion coefficients may be negative, and the method may be applied to liquids, even for electrolyte diffusion [Kraaijeveld, Wesselingh, and Kuiken, *Ind. Eng. Chem. Res.*, **33**, 750 (1994)]. Approximate solutions have been developed by linearization [Toor, H.L., *AIChE J.*, **10**, 448 and 460 (1964); Stewart and Prober, *Ind. Eng. Chem. Fundam.*, **3**, 224 (1964)]. Those differ in details but yield about the same accuracy. More recently, efficient algorithms for solving the equations exactly have been developed (see Taylor and Krishna, Krishnamurthy and Taylor [*Chem. Eng. J.*, **25**, 47 (1982)], and Taylor and Webb [*Comput. Chem. Eng.*, **5**, 61 (1981)]).

Useful studies of multicomponent diffusion were presented by Vrentas and Vrentas [*Ind. Eng. Chem. Res.*, **44**, 1112 (2005)], Curtis

and Bird [*Ind. Eng. Chem. Res.*, **38**, 2515 (1999)], and Amundson, Pan, and Paulson [*AIChE J.*, **48**, 813 (2003)]. Vrentas and Vrentas treated only ternary mixtures, such as restrictions due to the entropy inequality, application of the Onsager reciprocal relations, and stability. Curtis and Bird reconciled the multicomponent Fick's law approach with the more elegant Stefan-Maxwell theory. They also provided interrelationships of multicomponent diffusivities devised for various situations, i.e., binary, ternary, and quaternary mixtures. Amundson et al. presented numerical methods for coping with mixtures having four or more components, which are nearly intractable via the analytical S-M method, due to the difficult inversion. Related studies were performed by Ghorayeb and Firoozabadi [*AIChE J.*, **46**, 883 (2000)] and Firoozabadi, Ghorayeb, and Saukla [*AIChE J.*, **46**, 892 (2000)]. The former covered ordinary molecular diffusion as well as pressure and thermal diffusion for multicomponent mixtures. The latter covered thermal diffusion in multicomponent mixtures.

DIFFUSIVITY ESTIMATION—GASES

Whenever measured values of diffusivities are available, they should be used. Typically, measurement errors are less than those associated with predictions by empirical or even semitheoretical equations. A few general sources of data are Sec. 2 of this handbook; e.g., experimental values for gas mixtures are listed in Table 2-371. Estimation methods for some gaseous applications appear in Eqs. (2-150) through (2-154). Other pertinent references are Schwartzberg and Chao; Poling et al.; Gammon et al.; and Daubert and Danner. Many other more restricted sources are listed under specific topics later in this subsection.

Before using diffusivities from either data or correlations, it is a good idea to check their reasonableness with respect to values that have been commonly observed in similar situations. Table 5-9 is a compilation of several rules of thumb. These values are not authoritative; they simply represent guidelines based on experience.

Diffusivity correlations for gases are outlined in Table 5-10. Specific parameters for individual equations are defined in the specific text regarding each equation. References are given at the beginning of the "Mass Transfer" subsection. The errors reported for Eqs. (5-202) through (5-205) were compiled by Poling et al., who compared the predictions with 68 experimental values of D_{AB} . Errors cited for Eqs. (5-206) to (5-212) were reported by the authors.

Binary Mixtures—Low Pressure—Nonpolar Components Many evaluations of correlations are available [Elliott and Watts, *Can. J. Chem.*, **50**, 31 (1972); Lugg, *Anal. Chem.*, **40**, 1072 (1968); Marrero and Mason, *AIChE J.*, **19**, 498 (1973)]. The differences in accuracy of the correlations are minor, and thus the major concern is ease of calculation. The Fuller-Schettler-Giddings equation is usually the simplest correlation to use and is recommended by Poling et al.

Chapman-Enskog (Bird et al.) and Wilke and Lee [31] The inherent assumptions of these equations are quite restrictive (i.e., low density, spherical atoms), and the intrinsic potential function is empirical. Despite that, they provide good estimates of D_{AB} for many polyatomic gases and gas mixtures, up to about 1000 K and a maximum of 70 atm. The latter constraint is because observations for many gases indicate that $D_{AB}P$ is constant up to 70 atm.

The characteristic length is $\sigma_{AB} = (\sigma_A + \sigma_B)/2$ in Å. In order to estimate Ω_D for Eq. (5-202) or (5-203), two empirical equations are

TABLE 5-9 Rules of Thumb for Diffusivities (See Cussler, Poling et al., Schwartzberg and Chao)

Continuous phase	D_i magnitude		D_i range		Comments
	m ² /s	cm ² /s	m ² /s	cm ² /s	
Gas at atmospheric pressure	10 ⁻⁵	0.1	10 ⁻⁴ –10 ⁻⁶	1–10 ⁻²	Accurate theories exist, generally within ±10%; $D_i P \cong \text{constant}$; $D_i \propto T^{1.66 \text{ to } 2.0}$
Liquid	10 ⁻⁹	10 ⁻⁵	10 ⁻⁸ –10 ⁻¹⁰	10 ⁻⁴ –10 ⁻⁶	Approximate correlations exist, generally within ±25%
Liquid occluded in solid matrix	10 ⁻¹⁰	10 ⁻⁶	10 ⁻⁸ –10 ⁻¹²	10 ⁻⁴ –10 ⁻⁸	Hard cell walls: $D_{\text{eff}}/D_i = 0.1$ to 0.2. Soft cell walls: $D_{\text{eff}}/D_i = 0.3$ to 0.9
Polymers and glasses	10 ⁻¹²	10 ⁻⁸	10 ⁻¹⁰ –10 ⁻¹⁴	10 ⁻⁶ –10 ⁻¹⁰	Approximate theories exist for dilute and concentrated limits; strong composition dependence
Solid	10 ⁻¹⁴	10 ⁻¹⁰	10 ⁻¹⁰ –10 ⁻³⁴	10 ⁻⁶ –10 ⁻³⁰	Approximate theories exist; strong temperature dependence

TABLE 5-10 Correlations of Diffusivities for Gases

Authors*	Equation	Error, %
1. Binary Mixtures—Low Pressure—Nonpolar		
Chapman-Enskog	$D_{AB} = \frac{0.001858T^{3/2} M_{AB}^{1/2}}{P\sigma_{AB}^2 \Omega_D}$ (5-202)	7.3
Wilke-Lee [31]	$D_{AB} = \frac{(0.00217 - 0.0005M_{AB}^{1/2}) T^{3/2} M_{AB}^{1/2}}{P\sigma_{AB}^2 \Omega_D}$ (5-203)	7.0
Fuller-Schettler-Giddings [10]	$D_{AB} = \frac{0.001T^{1.75} M_{AB}^{1/2}}{P [(\sum v)_A^{1/3} + (\sum v)_B^{1/3}]^2}$ (5-204)	5.4
2. Binary Mixtures—Low Pressure—Polar		
Brokaw [4]	$D_{AB} = \frac{0.001858T^{3/2} M_{AB}^{1/2}}{P\sigma_{AB}^2 \Omega_D}$ (5-205)	9.0
3. Self-Diffusivity		
Mathur-Thodos [18]	$D_{AA} = \frac{10.7 \times 10^{-5} T_r}{\beta \rho_r} \{ \rho_r \leq 1.5 \}$ (5-206)	5
Lee-Thodos [14]	$D_{AA} = \frac{0.77 \times 10^{-5} T_r}{\rho_r \delta} \{ \rho_r \leq 1 \}$ (5-207)	0.5
Lee-Thodos [15]	$D_{AA} = \frac{(0.007094G + 0.001916)^{2.5} T_r}{\delta}, [\rho_r > 1, G < 1]$ (5-208)	17
4. Supercritical Mixtures		
Sun and Chen [25]	$D_{AB} = \frac{1.23 \times 10^{-10} T}{\mu^{0.799} V_{CA}^{0.49}}$ (5-209)	5
Catchpole and King [6]	$D_{AB} = 5.152 D_c T_r \frac{(\rho_r^{-0.667} - 0.4510) (1 + M_A/M_B) R}{(1 + (V_{cB}/V_{cA})^{0.333})^2}$ (5-210)	10
Liu and Ruckenstein [17]	$D_{AB} = \frac{kT}{f\pi\mu_A\sigma_{AB}} \left[\frac{1}{1 + \frac{2}{3} \left(1 - \frac{1}{2} \theta_{AB}^{\infty}\right)^{1/2}} + \frac{\sigma_{AB}}{3\sigma_A} \right]$ (5-211)	5.7
	$D_{AB} = \alpha(V_A^k - \beta) \sqrt{\frac{T}{M_B}}, \alpha = 10^{-5} \left[0.56392 + 2.1417 \exp\left(\frac{-0.95088 \sqrt{M_A V_{CA}}}{P_{CA}}\right) \right]$ (5-212)	6.9
	$\beta = 8.9061 + 0.93858 \frac{\sqrt{M_A V_{CA}}}{P_{CA}}$	
	$k = \frac{2}{3} [1 - 0.28 \exp(-0.3 \sqrt{M_A \rho_{v,1}})]$	

*References are listed at the beginning of the "Mass Transfer" subsection.

available. The first is:

$$\Omega_D = (44.54T^{0-4.909} + 1.911T^{0-1.575})^{0.10} \quad (5-213a)$$

where $T^{\circ} = kT/\epsilon_{AB}$ and $\epsilon_{AB} = (\epsilon_A \epsilon_B)^{1/2}$. Estimates for σ_i and ϵ_i are given in Table 5-11. This expression shows that Ω_D is proportional to temperature roughly to the -0.49 power at low temperatures and to the

-0.16 power at high temperature. Thus, gas diffusivities are proportional to temperatures to the 2.0 power and 1.66 power, respectively, at low and high temperatures. The second is:

$$\Omega_D = \frac{A}{T^{\circ B}} + \frac{C}{\exp(DT^{\circ})} + \frac{E}{\exp(FT^{\circ})} + \frac{G}{\exp(HT^{\circ})} \quad (5-213b)$$

TABLE 5-11 Estimates for ϵ_i and σ_i (K, Å, atm, cm³, mol)

Critical point	$\epsilon/k = 0.75 T_c$	$\sigma = 0.841 V_c^{1/3}$ or $2.44 (T_c/P_c)^{1/3}$
Critical point	$\epsilon/k = 65.3 T_c \rho_c^{-3.6}$	$\sigma = \frac{1.866 V_c^{1/3}}{\rho_c^{1.2}}$
Normal boiling point	$\epsilon/k = 1.15 T_b$	$\sigma = 1.18 V_b^{1/3}$
Melting point	$\epsilon/k = 1.92 T_m$	$\sigma = 1.222 V_m^{1/3}$
Acentric factor	$\epsilon/k = (0.7915 + 0.1693 \omega) T_c$	$\sigma = (2.3551 - 0.087 \omega) \left(\frac{T_c}{P_c}\right)^{1/3}$

NOTE: These values may not agree closely, so usage of a consistent basis is suggested (e.g., data at the normal boiling point).

TABLE 5-12 Atomic Diffusion Volumes for Use in Estimating D_{AB} by the Method of Fuller, Schettler, and Giddings [10]

Atomic and Structural Diffusion-Volume Increments, v_i (cm ³ /mol)			
C	16.5	(Cl)	19.5
H	1.98	(S)	17.0
O	5.48	Aromatic ring	-20.2
(N)	5.69	Heterocyclic ring	-20.2
Diffusion Volumes for Simple Molecules, Σv_i (cm ³ /mol)			
H ₂	7.07	CO	18.9
D ₂	6.70	CO ₂	26.9
He	2.88	N ₂ O	35.9
N ₂	17.9	NH ₃	14.9
O ₂	16.6	H ₂ O	12.7
Air	20.1	(CCl ₂ F ₂)	114.8
Ar	16.1	(SF ₆)	69.7
Kr	22.8	(Cl ₂)	37.7
(Xe)	37.9	(Br ₂)	67.2
Ne	5.59	(SO ₂)	41.1

Parentheses indicate that the value listed is based on only a few data points.

where $A = 1.06036$, $B = 0.15610$, $C = 0.1930$, $D = 0.47635$, $E = 1.03587$, $F = 1.52996$, $G = 1.76474$, and $H = 3.89411$.

Fuller, Schettler, and Giddings [10] The parameters and constants for this correlation were determined by regression analysis of 340 experimental diffusion coefficient values of 153 binary systems. Values of Σv_i used in this equation are in Table 5-12.

Binary Mixtures—Low Pressure—Polar Components The Brokaw [4] correlation was based on the Chapman-Enskog equation, but σ_{AB}^* and Ω_D^* were evaluated with a modified Stockmayer potential for polar molecules. Hence, slightly different symbols are used. That potential model reduces to the Lennard-Jones 6-12 potential for interactions between nonpolar molecules. As a result, the method should yield accurate predictions for polar as well as nonpolar gas mixtures. Brokaw presented data for 9 relatively polar pairs along with the prediction. The agreement was good: an average absolute error of 6.4 percent, considering the complexity of some of the gas pairs [e.g., (CH₃)₂O and CH₃Cl]. Despite that, Poling, (op. cit.) found the average error was 9.0 percent for combinations of mixtures (including several polar-nonpolar gas pairs), temperatures and pressures. In this equation, Ω_D is calculated as described previously, and other terms are:

$$\begin{aligned}\Omega_{D^*} &= \Omega_D + 0.19 \delta_{AB}^2/T^\circ & T^\circ &= kT/\epsilon_{AB} \\ \sigma_{AB}^* &= (\sigma_A \sigma_B)^{1/2} & \sigma_i^* &= [1.585 V_{bi}/(1 + 1.3 \delta_i^2)]^{1/3} \\ \delta_{AB} &= (\delta_A \delta_B)^{1/2} & \delta_i &= 1.94 \times 10^3 \mu_i^2/V_{bi} T_{bi} \\ \epsilon_{AB} &= (\epsilon_A \epsilon_B)^{1/2} & \epsilon_i/k &= 1.18 (1 + 1.3 \delta_i^2) T_{bi}\end{aligned}$$

Binary Mixtures—High Pressure Of the various categories of gas-phase diffusion, this is the least studied. This is so because of the effects of diffusion being easily distorted by even a slight pressure gradient, which is difficult to avoid at high pressure. Harstad and Bellan [Ind. Eng. Chem. Res. 43, 645 (2004)] developed a corresponding-states expression that extends the Chapman-Enskog method, covered earlier. They express the diffusivity at high pressure by accounting for the reduced temperature, and they suggest employing an equation of state and shifting from $D_{AB}^o = f(T, P)$ to $D_{AB} = g(T, V)$.

Self-Diffusivity Self-diffusivity is a property that has little intrinsic value, e.g., for solving separation problems. Despite that, it reveals quite a lot about the inherent nature of molecular transport, because the effects of discrepancies of other physical properties are eliminated, except for those that constitute isotopic differences, which are necessary to ascertain composition differences. Self-diffusivity has been studied extensively under high pressures, e.g., greater than 70 atm. There are few accurate estimation methods for mutual diffusivities at such high pressures, because composition measurements are difficult.

The general observation for gas-phase diffusion $D_{AB} P = \text{constant}$, which holds at low pressure, is not valid at high pressure. Rather, $D_{AB} P$ decreases as pressure increases. In addition, composition effects, which frequently are negligible at low pressure, are very significant at high pressure.

Liu and Ruckenstein [Ind. Eng. Chem. Res. 36, 3937 (1997)] studied self-diffusion for both liquids and gases. They proposed a semiempirical equation, based on hard-sphere theory, to estimate self-diffusivities. They extended it to Lennard-Jones fluids. The necessary energy parameter is estimated from viscosity data, but the molecular collision diameter is estimated from diffusion data. They compared their estimates to 26 pairs, with a total of 1822 data points, and achieved a relative deviation of 7.3 percent.

Zielinski and Hanley [AIChE J. 45, 1 (1999)] developed a model to predict multicomponent diffusivities from self-diffusion coefficients and thermodynamic information. Their model was tested by estimated experimental diffusivity values for ternary systems, predicting drying behavior of ternary systems, and reconciling ternary self-diffusion data measured by pulsed-field gradient NMR.

Mathur and Thodos [18] showed that for reduced densities less than unity, the product $D_{AB} \rho$ is approximately constant at a given temperature. Thus, by knowing the value of the product at low pressure, it is possible to estimate its value at a higher pressure. They found at higher pressures the density increases, but the product $D_{AB} \rho$ decreases rapidly. In their correlation, $\beta = M_A^{1/2} P_C^{1/3} / T_C^{5/6}$.

Lee and Thodos [14] presented a generalized treatment of self-diffusivity for gases (and liquids). These correlations have been tested for more than 500 data points each. The average deviation of the first is 0.51 percent, and that of the second is 17.2 percent. $\delta = M_A^{1/2} / P_C^{1/2} V_C^{5/6}$, s/cm^2 , and where $G = (X^\circ - X)/(X^\circ - 1)$, $X = \rho_r / T_r^{0.1}$, and $X^\circ = \rho_r / T_r^{0.1}$ evaluated at the solid melting point.

Lee and Thodos [15] expanded their earlier treatment of self-diffusivity to cover 58 substances and 975 data points, with an average absolute deviation of 5.26 percent. Their correlation is too involved to repeat here, but those interested should refer to the original paper.

Liu, Silva, and Macedo [Chem. Eng. Sci. 53, 2403 (1998)] present a theoretical approach incorporating hard-sphere, square-well, and Lennard-Jones models. They compared their resulting estimates to estimates generated via the Lee-Thodos equation. For 2047 data points with nonpolar species, the Lee-Thodos equation was slightly superior to the Lennard-Jones fluid-based model, that is, 5.2 percent average deviation versus 5.5 percent, and much better than the square-well fluid-based model (10.6 percent deviation). For over 467 data points with polar species, the Lee-Thodos equation yielded 36 percent average deviation, compared with 25 percent for the Lennard-Jones fluid-based model, and 19 percent for the square-well fluid-based model.

Silva, Liu, and Macedo [Chem. Eng. Sci. 53, 2423 (1998)] present an improved theoretical approach incorporating slightly different Lennard-Jones models. For 2047 data points with nonpolar species, their best model yielded 4.5 percent average deviation, while the Lee-Thodos equation yielded 5.2 percent, and the prior Lennard-Jones fluid-based model produced 5.5 percent. The new model was much better than all the other models for over 424 data points with polar species, yielding 4.3 percent deviation, while the Lee-Thodos equation yielded 34 percent and the Lennard-Jones fluid-based model yielded 23 percent.

Supercritical Mixtures DeBenedetti and Reid [AIChE J., 32, 2034 (1986) and 33, 496 (1987)] showed that conventional correlations based on the Stokes-Einstein relation (for liquid phase) tend to overpredict diffusivities in the supercritical state. Nevertheless, they observed that the Stokes-Einstein group $D_{AB} \mu / T$ was constant. Thus, although no general correlation applies, only one data point is necessary to examine variations of fluid viscosity and/or temperature effects. They explored certain combinations of aromatic solids in SF₆ and CO₂.

Sun and Chen [25] examined tracer diffusion data of aromatic solutes in alcohols up to the supercritical range and found their data correlated with average deviations of 5 percent and a maximum deviation of 17 percent for their rather limited set of data.

Catchpole and King [6] examined binary diffusion data of near-critical fluids in the reduced density range of 1 to 2.5 and found that their data correlated with average deviations of 10 percent and a maximum deviation of 60 percent. They observed two classes of behavior. For the first, no correction factor was required ($R = 1$). That class was comprised of alcohols as solvents with aromatic or aliphatic solutes, or

carbon dioxide as a solvent with aliphatics except ketones as solutes, or ethylene as a solvent with aliphatics except ketones and naphthalene as solutes. For the second class, the correction factor was $R = X^{0.17}$. The class was comprised of carbon dioxide with aromatics; ketones and carbon tetrachloride as solutes; and aliphatics (propane, hexane, dimethyl butane), sulfur hexafluoride, and chlorotrifluoromethane as solvents with aromatics as solutes. In addition, sulfur hexafluoride combined with carbon tetrachloride, and chlorotrifluoromethane combined with 2-propanone were included in that class. In all cases, $X = (1 + (V_{CA}/V_{CB})^{1/3})^2 / (1 + M_A/M_B)$ was in the range of 1 to 10.

Liu and Ruckenstein [17] presented a semiempirical equation to estimate diffusivities under supercritical conditions that is based on the Stokes-Einstein relation and the long-range correlation, respectively. The parameter $2\theta_{AB}^*$ was estimated from the Peng-Robinson equation of state. In addition, $f = 2.72 - 0.3445 T_{CB}/T_{CA}$ for most solutes, but for C_5 through C_{14} linear alkanes, $f = 3.046 - 0.786 T_{CB}/T_{CA}$. In both cases T_{ci} is the species critical temperature. They compared their estimates to 33 pairs, with a total of 598 data points, and achieved lower deviations (5.7 percent) than the Sun-Chen correlation (13.3 percent) and the Catchpole-King equation (11.0 percent).

He and Yu [13] presented a semiempirical equation to estimate diffusivities under supercritical conditions that is based on hard-sphere theory. It is limited to $\rho_r \geq 0.21$, where the reduced density is $\rho_r = \rho_A(T, P)/\rho_{CA}$. They compared their estimates to 107 pairs, with a total of 1167 data points, and achieved lower deviations (7.8 percent) than the Catchpole-King equation (9.7 percent), which was restricted to $\rho_r \geq 1$.

Silva and Macedo [Ind. Eng. Chem. Res. 37, 1490 (1998)] measured diffusivities of ethers in CO_2 under supercritical conditions and compared them to the Wilke-Chang [Eq. (5-218)], Tyn-Calus [Eq. (5-219)], Catchpole-King [Eq. (5-210)], and their own equations. They found that the Wilke-Chang equation provided the best fit.

Gonzalez, Bueno, and Medina [Ind. Eng. Chem. Res. 40, 3711 (2001)] measured diffusivities of aromatic compounds in CO_2 under supercritical conditions and compared them to the Wilke-Chang [Eq. (5-218)], Hayduk-Minhas [Eq. (5-226)], and other equations. They recommended the Wilke-Chang equation (which yielded a relative error of 10.1 percent) but noted that the He-Yu equation provided the best fit (5.5 percent).

Low-Pressure/Multicomponent Mixtures These methods are outlined in Table 5-13. Stefan-Maxwell equations were discussed earlier. Smith and Taylor [23] compared various methods for predicting multicomponent diffusion rates and found that Eq. (5-214) was superior among the effective diffusivity approaches, though none is very good. They also found that linearized and exact solutions are roughly equivalent and accurate.

Blanc [3] provided a simple limiting case for dilute component i diffusing in a stagnant medium (i.e., $N \approx 0$), and the result, Eq. (5-215), is known as Blanc's law. The restriction basically means that the compositions of all the components, besides component i , are relatively large and uniform.

Wilke [29] obtained solutions to the Stefan-Maxwell equations. The first, Eq. (5-216), is simple and reliable under the same conditions as Blanc's law. This equation applies when component i diffuses through

a stagnant mixture. It has been tested and verified for diffusion of toluene in hydrogen + air + argon mixtures and for diffusion of ethyl propionate in hydrogen + air mixtures [Fairbanks and Wilke *Ind. Eng. Chem.*, 42, 471 (1950)]. When the compositions vary from one boundary to the other, Wilke recommends that the arithmetic average mole fractions be used. Wilke also suggested using the Stefan-Maxwell equation, which applies when the fluxes of two or more components are significant. In this situation, the mole fractions are arithmetic averages of the boundary conditions, and the solution requires iteration because the ratio of fluxes is not known a priori.

DIFFUSIVITY ESTIMATION—LIQUIDS

Many more correlations are available for diffusion coefficients in the liquid phase than for the gas phase. Most, however, are restricted to binary diffusion at infinite dilution D_{AB}^0 or to self-diffusivity D_{AA} . This reflects the much greater complexity of liquids on a molecular level. For example, gas-phase diffusion exhibits negligible composition effects and deviations from thermodynamic ideality. Conversely, liquid-phase diffusion almost always involves volumetric and thermodynamic effects due to composition variations. For concentrations greater than a few mole percent of A and B , corrections are needed to obtain the true diffusivity. Furthermore, there are many conditions that do not fit any of the correlations presented here. Thus, careful consideration is needed to produce a reasonable estimate. Again, if diffusivity data are available at the conditions of interest, then they are strongly preferred over the predictions of any correlations. Experimental values for liquid mixtures are listed in Table 2-325.

Stokes-Einstein and Free-Volume Theories The starting point for many correlations is the Stokes-Einstein equation. This equation is derived from continuum fluid mechanics and classical thermodynamics for the motion of large spherical particles in a liquid. For this case, the need for a molecular theory is cleverly avoided. The Stokes-Einstein equation is (Bird et al.)

$$D_{AB} = \frac{kT}{6\pi r_A \mu_B} \quad (5-217)$$

where A refers to the solute and B refers to the solvent. This equation is applicable to very large unhydrated molecules ($M > 1000$) in low-molecular-weight solvents or where the molar volume of the solute is greater than $500 \text{ cm}^3/\text{mol}$ (Reddy and Doraiswamy, *Ind. Eng. Chem. Fundam.*, 6, 77 (1967); Wilke and Chang [30]). Despite its intellectual appeal, this equation is seldom used "as is." Rather, the following principles have been identified: (1) The diffusion coefficient is inversely proportional to the size $r_A \approx V_A^{1/3}$ of the solute molecules. Experimental observations, however, generally indicate that the exponent of the solute molar volume is larger than one-third. (2) The term $D_{AB}\mu_B/T$ is approximately constant only over a 10-to-15 K interval. Thus, the dependence of liquid diffusivity on properties and conditions does not generally obey the interactions implied by that grouping. For example, Robinson, Edmister, and Dullien [*Ind. Eng. Chem. Fundam.*, 5, 75 (1966)] found that $\ln D_{AB} \propto -1/T$. (3) Finally, pressure does not affect liquid-phase diffusivity much, since μ_B and V_A are only weakly pressure-dependent. Pressure does have an impact at very high levels.

TABLE 5-13 Relationships for Diffusivities of Multicomponent Gas Mixtures at Low Pressure

Authors*	Equation
Stefan-Maxwell, Smith and Taylor [23]	$D_{im} = \left[1 - x_i \left(\sum_{j=1}^{NC} N_j \right) / N_i \right] \sum_{j=1}^{NC} \left[\left(x_j - \frac{x_i N_i}{N_i} \right) / D_{ij} \right] \quad (5-214)$
Blanc [2]	$D_{im} = \left(\sum_{j=1}^{NC} \frac{x_j}{D_{ij}} \right)^{-1} \quad (5-215)$
Wilke [29]	$D_{im} = \left(\sum_{j=1, j \neq i}^{NC} \frac{x_j}{D_{ij}} \right)^{-1} \quad (5-216)$

*References are listed at the beginning of the "Mass Transfer" subsection.

Another advance in the concepts of liquid-phase diffusion was provided by Hildebrand [*Science*, **174**, 490 (1971)] who adapted a theory of viscosity to self-diffusivity. He postulated that $D_{A'A}^{\circ} = B(V - V_{ms})/V_{ms}$, where $D_{A'A}^{\circ}$ is the self-diffusion coefficient, V is the molar volume, and V_{ms} is the molar volume at which fluidity is zero (i.e., the molar volume of the solid phase at the melting temperature). The difference ($V - V_{ms}$) can be thought of as the free volume, which increases with temperature; and B is a proportionality constant.

Ertl and Dullien (ibid.) found that Hildebrand's equation could not fit their data with B as a constant. They modified it by applying an empirical exponent n (a constant greater than unity) to the volumetric ratio. The new equation is not generally useful, however, since there is no means for predicting n . The theory does identify the free volume as an important physical variable, since $n > 1$ for most liquids implies that diffusion is more strongly dependent on free volume than is viscosity.

Dilute Binary Nonelectrolytes: General Mixtures These correlations are outlined in Table 5-14.

Wilke-Chang [30] This correlation for D_{AB}° is one of the most widely used, and it is an empirical modification of the Stokes-Einstein equation. It is not very accurate, however, for water as the solute. Otherwise, it applies to diffusion of very dilute A in B . The average absolute error for 251 different systems is about 10 percent. Φ_B is an association factor of solvent B that accounts for hydrogen bonding.

Component B	Φ_B
Water	2.26
Methanol	1.9
Ethanol	1.5
Propanol	1.2
Others	1.0

The value of Φ_B for water was originally stated as 2.6, although when the original data were reanalyzed, the empirical best fit was 2.26. Random comparisons of predictions with 2.26 versus 2.6 show no consistent advantage for either value, however. Kooijman [*Ind. Eng. Chem. Res.* **41**, 3326 (2002)] suggests replacing V_A with $\theta_A V_{A^*}$, in which $\theta_A = 1$ except when $A = \text{water}$, $\theta_A = 4.5$. This modification leads to an overall error of 8.7 percent for 41 cases he compared. He suggests retaining $\Phi_B = 2.6$ when $B = \text{water}$. It has been suggested to replace the exponent of 0.6 with 0.7 and to use an association factor of 0.7 for systems containing aromatic hydrocarbons. These modifications, however, are not recommended by Umesi and Danner [27]. Lees and Sarram [*J. Chem. Eng. Data*, **16**, 41 (1971)] present a comparison of the association parameters. The average absolute error for 87 different solutes in water is 5.9 percent.

Tyn-Calus [26] This correlation requires data in the form of molar volumes and parachors $\psi_i = V_i \sigma_i^{1/4}$ (a property which, over moderate temperature ranges, is nearly constant), measured at the same temperature (not necessarily the temperature of interest). The parachors for the components may also be evaluated at different temperatures from each other. Quale [*Chem. Rev.* **53**, 439 (1953)] has compiled values of ψ_i for many chemicals. Group contribution methods are available for estimation purposes (Poling et al.). The following suggestions were made by Poling et al.: The correlation is constrained to cases in which $\mu_B < 30$ cP. If the solute is water or if the solute is an organic acid and the solvent is not water or a short-chain alcohol, dimerization of the solute A should be assumed for purposes of estimating its volume and parachor. For example, the appropriate values for water as solute at 25°C are $V_W = 37.4$ cm³/mol and $\psi_W = 105.2$ cm³g^{1/4}/s^{1/2}/mol. Finally, if the solute is nonpolar, the solvent volume and parachor should be multiplied by $\delta\mu_B$. According to Kooijman (ibid.), if the Brock-Bird method (described in Poling et al.) is used to

TABLE 5-14 Correlations for Diffusivities of Dilute, Binary Mixtures of Nonelectrolytes in Liquids

Authors ^a	Equation	Error
1. General Mixtures		
Wilke-Chang [30]	$D_{AB}^{\circ} = \frac{7.4 \times 10^{-8} (\Phi_B M_B)^{1/2} T}{\mu_B V_A^{0.6}} \quad (5-218)$	20%
Tyn-Calus [26]	$D_{AB}^{\circ} = \frac{8.93 \times 10^{-8} (V_A/V_B^2)^{1/6} (\psi_B/\psi_A)^{0.6} T}{\mu_B} \quad (5-219)$	10%
Umesi-Danner [27]	$D_{AB}^{\circ} = \frac{2.75 \times 10^{-8} (R_B/R_A^{2/3}) T}{\mu_B} \quad (5-220)$	16%
Siddiqi-Lucas [22]	$D_{AB}^{\circ} = \frac{9.89 \times 10^{-8} V_B^{0.265} T}{V_A^{0.45} \mu_B^{0.907}} \quad (5-221)$	13%
2. Gases in Low Viscosity Liquids		
Sridhar-Potter [24]	$D_{AB}^{\circ} = D_{BB} \left(\frac{V_{cB}}{V_{cA}} \right)^{2/3} \left(\frac{V_B}{V_{mB}} \right) \quad (5-222)$	18%
Chen-Chen [7]	$D_{AB}^{\circ} = 2.018 \times 10^{-9} \frac{(\beta V_{cB})^{2/3} (RT_{cB})^{1/2}}{M_A^{1/6} (M_B V_{cA})^{1/3}} (V_f - 1) \left(\frac{T}{T_{cA}} \right)^{1/2} \quad (5-223)$	6%
3. Aqueous Solutions		
Hayduk-Laudie [11]	$D_{AW}^{\circ} = \frac{13.16 \times 10^{-5}}{\mu_w^{1.14} V_A^{0.589}} \quad (5-224)$	18%
Siddiqi-Lucas [22]	$D_{AW}^{\circ} = 2.98 \times 10^{-7} V_A^{-0.5473} \mu_w^{-1.026} T \quad (5-225)$	13%
4. Hydrocarbon Mixtures		
Hayduk-Minhas [12]	$D_{AB}^{\circ} = 13.3 \times 10^{-8} T^{1.47} \mu_B^{(10.2/V_A - 0.791)} V_A^{-0.71} \quad (5-226)$	5%
Matthews-Akgerman [19]	$D_{AB}^{\circ} = 32.88 M_A^{-0.61} V_D^{-1.04} T^{0.5} (V_B - V_D) \quad (5-227)$	5%
Riazi-Whitson [21]	$D_{AB} = 1.07 \frac{(\rho D_{AB})^{\circ}}{\rho} \left(\frac{\mu}{\mu^{\circ}} \right)^{-0.27 - 0.38 \omega + (-0.05 + 0.1 \omega) P} \quad (5-228)$	15%

^aReferences are listed at the beginning of the "Mass Transfer" subsection.

estimate the surface tension, the error is only increased by about 2 percent, relative to employing experimentally measured values.

Umesi-Danner [27] They developed an equation for nonaqueous solvents with nonpolar and polar solutes. In all, 258 points were involved in the regression. R_i is the radius of gyration in Å of the component molecule, which has been tabulated by Passut and Danner [*Chem. Eng. Progress Symp. Ser.*, **140**, 30 (1974)] for 250 compounds. The average absolute deviation was 16 percent, compared with 26 percent for the Wilke-Chang equation.

Siddiqi-Lucas [22] In an impressive empirical study, these authors examined 1275 organic liquid mixtures. Their equation yielded an average absolute deviation of 13.1 percent, which was less than that for the Wilke-Chang equation (17.8 percent). Note that this correlation does not encompass aqueous solutions; those were examined and a separate correlation was proposed, which is discussed later.

Binary Mixtures of Gases in Low-Viscosity, Nonelectrolyte Liquids **Sridhar and Potter [24]** derived an equation for predicting gas diffusion through liquid by combining existing correlations. Hildebrand had postulated the following dependence of the diffusivity for a gas in a liquid: $D_{AB}^0 = D_{B'B}(V_{cB}/V_{cA})^{2/3}$, where $D_{B'B}$ is the solvent self-diffusion coefficient and V_{cA} is the critical volume of component i , respectively. To correct for minor changes in volumetric expansion, Sridhar and Potter multiplied the resulting equation by V_B/V_{mB} , where V_{mB} is the molar volume of the liquid B at its melting point and $D_{B'B}$ can be estimated by the equation of Ertl and Dullien (see p. 5-54). Sridhar and Potter compared experimentally measured diffusion coefficients for twenty-seven data points of eleven binary mixtures. Their average absolute error was 13.5 percent, but Chen and Chen [7] analyzed about 50 combinations of conditions and 3 to 4 replicates each and found an average error of 18 percent. This correlation does not apply to hydrogen and helium as solutes. However, it demonstrates the usefulness of self-diffusion as a means to assess mutual diffusivities and the value of observable physical property changes, such as molar expansion, to account for changes in conditions.

Chen-Chen [7] Their correlation was based on diffusion measurements of 50 combinations of conditions with 3 to 4 replicates each and exhibited an average error of 6 percent. In this correlation, $V_r = V_B/[0.9724(V_{mB} + 0.04765)]$ and V_{mB} is the liquid molar volume at the melting point, as discussed previously. Their association parameter β [which is different from the definition of that symbol in Eq. (5-229)] accounts for hydrogen bonding of the solvent. Values for acetonitrile and methanol are: $\beta = 1.58$ and 2.31, respectively.

Dilute Binary Mixtures of a Nonelectrolyte in Water The correlations that were suggested previously for general mixtures, unless specified otherwise, may also be applied to diffusion of miscellaneous solutes in water. The following correlations are restricted to the present case, however.

Hayduk and Laudie [11] They presented a simple correlation for the infinite dilution diffusion coefficients of nonelectrolytes in water. It has about the same accuracy as the Wilke-Chang equation (about 5.9 percent). There is no explicit temperature dependence, but the 1.14 exponent on μ_w compensates for the absence of T in the numerator. That exponent was misprinted (as 1.4) in the original article and has been reproduced elsewhere erroneously.

Siddiqi and Lucas [227] These authors examined 658 aqueous liquid mixtures in an empirical study. They found an average absolute deviation of 19.7 percent. In contrast, the Wilke-Chang equation gave 35.0 percent and the Hayduk-Laudie correlation gave 30.4 percent.

Dilute Binary Hydrocarbon Mixtures **Hayduk and Minhas [12]** presented an accurate correlation for normal paraffin mixtures that was developed from 58 data points consisting of solutes from C_5 to C_{32} and solvents from C_5 to C_{16} . The average error was 3.4 percent for the 58 mixtures.

Matthews and Akgerman [19] The free-volume approach of Hildebrand was shown to be valid for binary, dilute liquid paraffin mixtures (as well as self-diffusion), consisting of solutes from C_8 to C_{16} and solvents of C_6 and C_{12} . The term they referred to as the "diffusion volume" was simply correlated with the critical volume, as $V_D = 0.308 V_c$. We can infer from Table 5-11 that this is approximately related to the volume at the melting point as $V_D = 0.945 V_m$. Their correlation was valid for diffusion of linear alkanes at temperatures

up to 300°C and pressures up to 3.45 MPa. Matthews, Rodden, and Akgerman [*J. Chem. Eng. Data*, **32**, 317 (1987)] and Erkey and Akgerman [*AIChE J.*, **35**, 443 (1989)] completed similar studies of diffusion of alkanes, restricted to n -hexadecane and n -octane, respectively, as the solvents.

Riasi and Whitson [21] They presented a generalized correlation in terms of viscosity and molar density that was applicable to both gases and liquids. The average absolute deviation for gases was only about 8 percent, while for liquids it was 15 percent. Their expression relies on the Chapman-Enskog correlation [Eq. (5-202)] for the low-pressure diffusivity and the Stiel-Thodos [*AIChE J.*, **7**, 234 (1961)] correlation for low-pressure viscosity:

$$\mu^0 = \frac{x_A \mu_A^0 M_A^{1/2} + x_B \mu_B^0 M_B^{1/2}}{x_A M_A^{1/2} + x_B M_B^{1/2}}$$

where $\mu_i^0 \xi_i = 3.4 \times 10^{-4} T_{r,i}^{0.94}$ for $T_{r,i} < 1.5$ or $\mu_i^0 \xi_i = 1.778 \times 10^{-4} (4.58 T_{r,i} - 1.67)^{0.58}$ for $T_{r,i} > 1.5$. In these equations, $\xi_i = T_{c,i}^{1/6} P_{c,i}^{2/3} M_i^{1/2}$, and units are in cP, atm, K, and mol. For dense gases or liquids, the Chung et al. [*Ind. Eng. Chem. Res.*, **27**, 671 (1988)] or Jossi-Stiel-Thodos [*AIChE J.*, **8**, 59 (1962)] correlation may be used to estimate viscosity. The latter is:

$$(\mu - \mu^0) \xi + 10^{-4} = (0.1023 + 0.023364 \rho_r + 0.058533 \rho_r^2 - 0.040758 \rho_r^3 + 0.093324 \rho_r^4)$$

$$\text{where } \xi = \frac{(x_A T_{cA} + x_B T_{cB})^{1/6}}{(x_A M_A + x_B M_B)^{1/2} (x_A P_{cA} + x_B P_{cB})}$$

$$\text{and } \rho_r = (x_A V_{cA} + x_B V_{cB}) \rho.$$

Dilute Binary Mixtures of Nonelectrolytes with Water as the Solute **Olander [AIChE J., **7**, 175 (1961)] modified the Wilke-Chang equation to adapt it to the infinite dilution diffusivity of water as the solute. The modification he recommended is simply the division of the right-hand side of the Wilke-Chang equation by 2.3. Unfortunately, neither the Wilke-Chang equation nor that equation divided by 2.3 fit the data very well. A reasonably valid generalization is that the Wilke-Chang equation is accurate if water is very insoluble in the solvent, such as pure hydrocarbons, halogenated hydrocarbons, and nitro-hydrocarbons. On the other hand, the Wilke-Chang equation divided by 2.3 is accurate for solvents in which water is very soluble, as well as those that have low viscosities. Such solvents include alcohols, ketones, carboxylic acids, and aldehydes. Neither equation is accurate for higher-viscosity liquids, especially diols.**

Dilute Dispersions of Macromolecules in Nonelectrolytes The Stokes-Einstein equation has already been presented. It was noted that its validity was restricted to large solutes, such as spherical macromolecules and particles in a continuum solvent. The equation has also been found to predict accurately the diffusion coefficient of spherical latex particles and globular proteins. Corrections to Stokes-Einstein for molecules approximating spheroids is given by Tanford *Physical Chemistry of Macromolecules*, Wiley, New York, (1961). Since solute-solute interactions are ignored in this theory, it applies in the dilute range only.

Hiss and Cussler [AIChE J., **19, 698 (1973)] Their basis is the diffusion of a small solute in a fairly viscous solvent of relatively large molecules, which is the opposite of the Stokes-Einstein assumptions. The large solvent molecules investigated were not polymers or gels but were of moderate molecular weight so that the macroscopic and microscopic viscosities were the same. The major conclusion is that $D_{AB}^0 \mu^{2/3} = \text{constant}$ at a given temperature and for a solvent viscosity from 5×10^{-3} to 5 Pa·s or greater (5 to 5×10^3 cP). This observation is useful if D_{AB}^0 is known in a given high-viscosity liquid (oils, tars, etc.). Use of the usual relation of $D_{AB}^0 \propto 1/\mu$ for such an estimate could lead to large errors.**

Concentrated, Binary Mixtures of Nonelectrolytes Several correlations that predict the composition dependence of D_{AB} are summarized in Table 5-15. Most are based on known values of D_{AB}^0 and D_{BA}^0 . In fact, a rule of thumb states that, for many binary systems, D_{AB}^0 and D_{BA}^0 bound the D_{AB} vs. x_A curve. Cullinan's [8] equation predicts diffusivities even in lieu of values at infinite dilution, but requires accurate density, viscosity, and activity coefficient data.

TABLE 5-15 Correlations of Diffusivities for Concentrated, Binary Mixtures of Nonelectrolyte Liquids

Authors*	Equation
Caldwell-Babb [5]	$D_{AB} = (x_A D_{BA}^{\circ} + x_B D_{AB}^{\circ}) \beta_A$ (5-231)
Rathbun-Babb [20]	$D_{AB} = (x_A D_{BA}^{\circ} + x_B D_{AB}^{\circ}) \beta_A^n$ (5-232)
Vignes [28]	$D_{AB} = D_{AB}^{\circ} D_{BA}^{\circ} \beta_A$ (5-233)
Leffler-Cullinan [16]	$D_{AB} \mu_{mix} = (D_{AB}^{\circ} \mu_B)^{x_B} (D_{BA}^{\circ} \mu_A)^{x_A} \beta_A$ (5-234)
Cussler [9]	$D_{AB} = D_0 \left[1 + \frac{K}{x_A x_B} \left(\frac{\partial \ln x_A}{\partial \ln a_A} - 1 \right) \right]^{-1/2}$ (5-235)
Cullinan [8]	$D_{AB} = \frac{kT}{2\pi \mu_{mix} (V/A)^{1/3}} \left[\frac{2\pi x_A x_B \beta_A}{1 + \beta_A (2\pi x_A x_B - 1)} \right]^{1/2}$ (5-236)
Asfour-Dullien [1]	$D_{AB} = \left(\frac{D_{AB}^{\circ}}{\mu_B} \right)^{x_B} \left(\frac{D_{BA}^{\circ}}{\mu_A} \right)^{x_A} \zeta \mu \beta_A$ (5-237)
Siddiqi-Lucas [22]	$D_{AB} = (C_B \bar{V}_B D_{AB}^{\circ} + C_A \bar{V}_A D_{BA}^{\circ}) \beta_A$ (5-238)
Bosse and Bart no. 1 [3]	$D_{AB} = (D_{AB}^{\circ})^{x_B} (D_{BA}^{\circ})^{x_A} \exp \left(-\frac{g^E}{RT} \right)$ (5-239)
Bosse and Bart no. 2 [3]	$\mu D_{AB} = (\mu_B D_{AB}^{\circ})^{x_B} (\mu_A D_{BA}^{\circ})^{x_A} \exp \left(-\frac{g^E}{RT} \right)$ (5-240)

Relative errors for the correlations in this table are very dependent on the components of interest and are cited in the text. *See the beginning of the "Mass Transfer" subsection for references.

Since the infinite dilution values D_{AB}° and D_{BA}° are generally unequal, even a thermodynamically ideal solution like $\gamma_A = \gamma_B = 1$ will exhibit concentration dependence of the diffusivity. In addition, non-ideal solutions require a thermodynamic correction factor to retain the true "driving force" for molecular diffusion, or the gradient of the chemical potential rather than the composition gradient. That correction factor is:

$$\beta_A = 1 + \frac{\partial \ln \gamma_A}{\partial \ln x_A} \quad (5-229)$$

Caldwell and Babb [5] Darken [*Trans. Am. Inst. Mining Met. Eng.*, **175**, 184 (1948)] observed that solid-state diffusion in metallurgical applications followed a simple relation. His equation related the tracer diffusivities and mole fractions to the mutual diffusivity:

$$D_{AB} = (x_A D_B + x_B D_A) \beta_A \quad (5-230)$$

Caldwell and Babb used virtually the same equation to evaluate the mutual diffusivity for concentrated mixtures of common liquids.

Van Geet and Adamson [*J. Phys. Chem.*, **68**, 238 (1964)] tested that equation for the *n*-dodecane (*A*) and *n*-octane (*B*) system and found the average deviation of D_{AB} from experimental values to be -0.68 percent. In addition, that equation was tested for benzene + bromobenzene, *n*-hexane + *n*-dodecane, benzene + CCl_4 , octane + decane, heptane + cetane, benzene + diphenyl, and benzene + nitromethane with success. For systems that depart significantly from thermodynamic ideality, it breaks down, sometimes by a factor of eight. For example, in the binary systems acetone + CCl_4 , acetone + chloroform, and ethanol + CCl_4 , it is not accurate. Thus, it can be expected to be fairly accurate for nonpolar hydrocarbons of similar molecular weight but not for polar-polar mixtures. Siddiqi, Krahn, and Lucas [*J. Chem. Eng. Data*, **32**, 48 (1987)] found that this relation was superior to those of Vignes and Leffler and Cullinan for a variety of mixtures. Umesi and Danner [27] found an average absolute deviation of 13.9 percent for 198 data points.

Rathbun and Babb [20] suggested that Darken's equation could be improved by raising the thermodynamic correction factor β_A to a power, *n*, less than unity. They looked at systems exhibiting negative deviations from Raoult's law and found $n = 0.3$. Furthermore, for polar-nonpolar mixtures, they found $n = 0.6$. In a separate study, Siddiqi and Lucas [22] followed those suggestions and found an average absolute error of 3.3 percent for nonpolar-nonpolar mixtures, 11.0 percent for polar-nonpolar mixtures, and 14.6 percent for polar-polar mixtures. Siddiqi, Krahn, and Lucas (ibid.) examined a few other mixtures and

found that $n = 1$ was probably best. Thus, this approach is, at best, highly dependent on the type of components being considered.

Vignes [28] empirically correlated mixture diffusivity data for 12 binary mixtures. Later Ertl, Ghai, and Dollon [*AIChE J.*, **20**, 1 (1974)] evaluated 122 binary systems, which showed an average absolute deviation of only 7 percent. None of the latter systems, however, was very nonideal.

Leffler and Cullinan [16] modified Vignes' equation using some theoretical arguments to arrive at Eq. (5-234), which the authors compared to Eq. (5-233) for the 12 systems mentioned above. The average absolute maximum deviation was only 6 percent. Umesi and Danner [27], however, found an average absolute deviation of 11.4 percent for 198 data points. For normal paraffins, it is not very accurate. In general, the accuracies of Eqs. (5-233) and (5-234) are not much different, and since Vignes' is simpler to use, it is suggested. The application of either should be limited to nonassociating systems that do not deviate much from ideality ($0.95 < \beta_A < 1.05$).

Cussler [9] studied diffusion in concentrated associating systems and has shown that, in associating systems, it is the size of diffusing clusters rather than diffusing solutes that controls diffusion. D_0 is a reference diffusion coefficient discussed hereafter; a_A is the activity of component A; and K is a constant. By assuming that D_0 could be predicted by Eq. (5-233) with $\beta = 1$, K was found to be equal to 0.5 based on five binary systems and validated with a sixth binary mixture. The limitations of Eq. (5-235) using D_0 and K defined previously have not been explored, so caution is warranted. Gurkan [*AIChE J.*, **33**, 175 (1987)] showed that K should actually be closer to 0.3 (rather than 0.5) and discussed the overall results.

Cullinan [8] presented an extension of Cussler's cluster diffusion theory. His method accurately accounts for composition and temperature dependence of diffusivity. It is novel in that it contains no adjustable constants, and it relates transport properties and solution thermodynamics. This equation has been tested for six very different mixtures by Rollins and Knaebel [*AIChE J.*, **37**, 470 (1991)], and it was found to agree remarkably well with data for most conditions, considering the absence of adjustable parameters. In the dilute region (of either A or B), there are systematic errors probably caused by the breakdown of certain implicit assumptions (that nevertheless appear to be generally valid at higher concentrations).

Asfour and Dullien [1] developed a relation for predicting alkane diffusivities at moderate concentrations that employs:

$$\zeta = \left(\frac{V_{fm}}{V_{fxA} V_{fxB}} \right)^{2/3} \frac{M_{xA} M_{xB}}{M_m} \quad (5-241)$$

where $V_{f_i} = V_{\beta_i}^0$; the fluid free volume is $V_{f_i} = V_i - V_{m_i}$ for $i = A, B$, and m , in which V_{m_i} is the molar volume of the liquid at the melting point and

$$V_{m,m} = \left(\frac{x_A^2}{V_{m,A}} + \frac{2x_A x_B}{V_{m,AB}} + \frac{x_B^2}{V_{m,B}} \right)^{-1}$$

and

$$V_{m,AB} = \left[\frac{V_{m,A}^{1/3} + V_{m,B}^{1/3}}{2} \right]^3$$

and μ is the mixture viscosity; M_m is the mixture mean molecular weight; and β_A is defined by Eq. (5-229). The average absolute error of this equation is 1.4 percent, while the Vignes equation and the Lefler-Cullinan equation give 3.3 percent and 6.2 percent, respectively.

Siddiqi and Lucas [22] suggested that component volume fractions might be used to correlate the effects of concentration dependence. They found an average absolute deviation of 4.5 percent for nonpolar-nonpolar mixtures, 16.5 percent for polar-nonpolar mixtures, and 10.8 percent for polar-polar mixtures.

Bosse and Bart added a term to account for excess Gibbs free energy, involved in the activation energy for diffusion, which was previously omitted. Doing so yielded minor modifications of the Vignes and Lefler-Cullinan equations [Eqs. (5-233) and (5-234), respectively]. The UNIFAC method was used to assess the excess Gibbs free energy. Comparing predictions of the new equations with data for 36 pairs and 326 data points yielded relative deviations of 7.8 percent and 8.9 percent, respectively, but which were better than the closely related Vignes (12.8 percent) and Lefler-Cullinan (10.4 percent) equations.

Binary Electrolyte Mixtures When electrolytes are added to a solvent, they dissociate to a certain degree. It would appear that the solution contains at least three components: solvent, anions, and cations. If the solution is to remain neutral in charge at each point (assuming the absence of any applied electric potential field), the anions and cations diffuse effectively as a single component, as for molecular diffusion. The diffusion of the anionic and cationic species in the solvent can thus be treated as a binary mixture.

Nernst-Haskell The theory of dilute diffusion of salts is well developed and has been experimentally verified. For dilute solutions of a single salt, the well-known Nernst-Haskell equation (Poling et al.) is applicable:

$$D_{AB}^0 = \frac{RT}{F^2} \frac{\left| \frac{1}{n_+} + \frac{1}{n_-} \right|}{\frac{1}{\lambda_+^0} + \frac{1}{\lambda_-^0}} = 8.9304 \times 10^{-10} T \frac{\left| \frac{1}{n_+} + \frac{1}{n_-} \right|}{\frac{1}{\lambda_+^0} + \frac{1}{\lambda_-^0}} \quad (5-242)$$

where D_{AB}^0 = diffusivity based on molarity rather than normality of dilute salt A in solvent B, cm^2/s .

The previous definitions can be interpreted in terms of ionic-species diffusivities and conductivities. The latter are easily measured and depend on temperature and composition. For example, the equivalent conductance Λ is commonly tabulated in chemistry handbooks as the limiting (infinite dilution) conductance Λ_0 , and at standard concentrations, typically at 25°C. $\Lambda = 1000K/C = \lambda_+ + \lambda_- = \Lambda_0 + f(C)$, ($\text{cm}^2/\text{ohm gequiv}$); $K = \alpha/R$ = specific conductance, (ohm cm^{-1}); C = solution concentration, (gequiv/ℓ); α = conductance cell constant (measured), (cm^{-1}); R = solution electrical resistance, which is measured (ohm); and $f(C)$ = a complicated function of concentration. The resulting equation of the electrolyte diffusivity is

$$D_{AB} = \frac{|\lambda_{+}| + |\lambda_{-}|}{(|\lambda_{-}|/D_{+}) + (|\lambda_{+}|/D_{-})} \quad (5-243)$$

where $|\lambda_{\pm}|$ represents the magnitude of the ionic charge and where the cationic or anionic diffusivities are $D_{\pm} = 8.9304 \times 10^{-10} T \lambda_{\pm} / |\lambda_{\pm}| \text{ cm}^2/\text{s}$. The coefficient is $kN_0/F^2 = R/F^2$. In practice, the equivalent conductance of the ion pair of interest would be obtained and supplemented with conductances of permutations of those ions and one independent cation and anion. This would allow determination of all the ionic conductances and hence the diffusivity of the electrolyte solution.

Gordon [J. Phys. Chem. **5**, 522 (1937)] Typically, as the concentration of a salt increases from infinite dilution, the diffusion coefficient

decreases rapidly from D_{AB}^0 . As concentration is increased further, however, D_{AB} rises steadily, often becoming greater than D_{AB}^0 . Gordon proposed the following empirical equation, which is applicable up to concentrations of $2N$:

$$D_{AB} = D_{AB}^0 \frac{1}{C_B \bar{V}_B} \frac{\mu_B}{\mu} \left(1 + \frac{\ln \gamma_{\pm}}{\ln m} \right) \quad (5-244)$$

where D_{AB}^0 is given by the Nernst-Haskell equation. References that tabulate γ_{\pm} as a function of m , as well as other equations for D_{AB} , are given by Poling et al.

Morgan, Ferguson, and Scovazzo [Ind. Eng. Chem. Res. **44**, 4815 (2005)] They studied diffusion of gases in ionic liquids having moderate to high viscosity (up to about 1000 cP) at 30°C. Their range was limited, and the empirical equation they found was

$$D_{AB} = 3.7 \times 10^{-3} \left(\frac{1}{\mu_B^{0.59} V_{A0} \rho_B^2} \right) \quad (5-245)$$

which yielded a correlation coefficient of 0.975. Of the estimated diffusivities 90 percent were within ± 20 percent of the experimental values. The exponent for viscosity approximately confirmed the observation of Hiss and Cussler (ibid).

Multicomponent Mixtures No simple, practical estimation methods have been developed for predicting multicomponent liquid-diffusion coefficients. Several theories have been developed, but the necessity for extensive activity data, pure component and mixture volumes, mixture viscosity data, and tracer and binary diffusion coefficients have significantly limited the utility of the theories (see Poling et al.).

The generalized Stefan-Maxwell equations using binary diffusion coefficients are not easily applicable to liquids since the coefficients are so dependent on conditions. That is, in liquids, each D_{ij} can be strongly composition dependent in binary mixtures and, moreover, the binary D_{ij} is strongly affected in a multicomponent mixture. Thus, the convenience of writing multicomponent flux equations in terms of binary coefficients is lost. Conversely, they apply to gas mixtures because each D_{ij} is practically independent of composition by itself and in a multicomponent mixture (see Taylor and Krishna for details).

One particular case of multicomponent diffusion that has been examined is the dilute diffusion of a solute in a homogeneous mixture (e.g., of A in B + C). Umesi and Danner [27] compared the three equations given below for 49 ternary systems. All three equations were equivalent, giving average absolute deviations of 25 percent.

Perkins and Geankoplis [Chem. Eng. Sci., **24**, 1035 (1969)]

$$D_{am} \mu_m^{0.8} = \sum_{\substack{j=1 \\ j \neq A}}^n x_j D_{Aj}^0 \mu_j^{0.8} \quad (5-246)$$

Cullinan [Can. J. Chem. Eng. **45**, 377 (1967)] This is an extension of Vignes' equation to multicomponent systems:

$$D_{am} = \prod_{\substack{j=1 \\ j \neq A}}^n (D_{Aj}^0)^{x_j} \quad (5-247)$$

Lefler and Cullinan [16] They extended their binary relation to an arbitrary multicomponent mixture, as follows:

$$D_{am} \mu_m = \prod_{\substack{j=1 \\ j \neq A}}^n (D_{Aj}^0 \mu_j)^{x_j} \quad (5-248)$$

where D_{Aj} is the dilute binary diffusion coefficient of A in j; D_{am} is the dilute diffusion of A through m; x_j is the mole fraction; μ_j is the viscosity of component j; and μ_m is the mixture viscosity.

Akita [Ind. Eng. Chem. Fundam., **10**, 89 (1981)] Another case of multicomponent dilute diffusion of significant practical interest is that of gases in aqueous electrolyte solutions. Many gas-absorption processes use electrolyte solutions. Akita presents experimentally tested equations for this case.

Graham and Dranoff [Ind. Eng. Chem. Fundam., **21**, 360 and 365 (1982)] They studied multicomponent diffusion of electrolytes in ion exchangers. They found that the Stefan-Maxwell interaction coefficients reduce to limiting ion tracer diffusivities of each ion.

Pinto and Graham [AIChE J. **32**, 291 (1986) and **33**, 436 (1987)] They studied multicomponent diffusion in electrolyte solutions. They focused on the Stefan-Maxwell equations and corrected for solvation effects. They achieved excellent results for 1-1 electrolytes in water at 25°C up to concentrations of 4M.

Anderko and Lencka [Ind. Eng. Chem. Res. **37**, 2878 (1998)] These authors present an analysis of self-diffusion in multicomponent aqueous electrolyte systems. Their model includes contributions of long-range (Coulombic) and short-range (hard-sphere) interactions. Their mixing rule was based on equations of nonequilibrium thermodynamics. The model accurately predicts self-diffusivities of ions and gases in aqueous solutions from dilute to about 30 mol/kg water. It makes it possible to take single-solute data and extend them to multicomponent mixtures.

DIFFUSION OF FLUIDS IN POROUS SOLIDS

Diffusion in porous solids is usually the most important factor controlling mass transfer in adsorption, ion exchange, drying, heterogeneous catalysis, leaching, and many other applications. Some of the applications of interest are outlined in Table 5-16. Applications of these equations are found in Secs. 16, 22, and 23.

Diffusion within the largest cavities of a porous medium is assumed to be similar to ordinary or bulk diffusion except that it is hindered by the pore walls (see Eq. 5-249). The tortuosity τ that expresses this hindrance has been estimated from geometric arguments. Unfortunately,

measured values are often an order of magnitude greater than those estimates. Thus, the effective diffusivity D_{eff} (and hence τ) is normally determined by comparing a diffusion model to experimental measurements. The normal range of tortuosities for silica gel, alumina, and other porous solids is $2 \leq \tau \leq 6$, but for activated carbon, $5 \leq \tau \leq 65$.

In small pores and at low pressures, the mean free path ℓ of the gas molecule (or atom) is significantly greater than the pore diameter d_{pore} . Its magnitude may be estimated from

$$\ell = \frac{3.2 \mu}{P} \left(\frac{RT}{2\pi M} \right)^{1/2} \text{ m}$$

As a result, collisions with the wall occur more frequently than with other molecules. This is referred to as the Knudsen mode of diffusion and is contrasted with ordinary or bulk diffusion, which occurs by intermolecular collisions. At intermediate pressures, both ordinary diffusion and Knudsen diffusion may be important [see Eqs. (5-252) and (5-253)].

For gases and vapors that adsorb on the porous solid, surface diffusion may be important, particularly at high surface coverage [see Eqs. (5-254) and (5-257)]. The mechanism of surface diffusion may be viewed as molecules hopping from one surface site to another. Thus, if adsorption is too strong, surface diffusion is impeded, while if adsorption is too weak, surface diffusion contributes insignificantly to the overall rate. Surface diffusion and bulk diffusion usually occur in parallel [see Eqs. (5-258) and (5-259)]. Although D_s is expected to be less than D_{eff} , the solute flux due to surface diffusion may be larger

TABLE 5-16 Relations for Diffusion in Porous Solids

Mechanism	Equation	Applies to	References°
Bulk diffusion in pores	$D_{eff} = \frac{\epsilon_p D}{\tau}$ (5-249)	Gases or liquids in large pores. $N_{Kn} = \ell/d_{pore} < 0.01$	[33]
Knudsen diffusion	$D_K = 48.5 d_{pore} \left(\frac{T}{M} \right)^{1/2}$ in m^2/s (5-250) $D_{K,eff} = \frac{\epsilon_p D_K}{\tau}$	Dilute (low pressure) gases in small pores. $N_{Kn} = \ell/d_{pore} > 10$	Geankoplis, [34, 35]
	$N_i = -D_K \frac{dC_i}{dz}$ (5-251)	" " " "	
Combined bulk and Knudsen diffusion	$D_{eff} = \left(\frac{1 - \alpha X_A}{D_{eff}} + \frac{1}{D_{K,eff}} \right)^{-1}$ (5-252) $\alpha = 1 + \frac{N_B}{N_A}$	" " " " $N_A \neq N_B$	Geankoplis, [32, 35]
	$D_{eff} = \left(\frac{1}{D_{eff}} + \frac{1}{D_{K,eff}} \right)^{-1}$ (5-253)	$N_A = N_B$	
Surface diffusion	$J_{si} = -D_{s,eff} \rho_p \left(\frac{dq_i}{dz} \right)$ (5-254) $D_{s,eff} = \frac{\epsilon_p D_s}{\tau}$ (5-255)	Adsorbed gases or vapors " " " "	[32, 34, 35]
	$D_{s0} = \frac{D_{s0=0}}{(1 - \theta)}$ (5-256)	θ = fractional surface coverage ≤ 0.6	
	$D_s = D'_s(q) \exp\left(\frac{-E_s}{RT}\right)$ (5-257)	" " " "	
Parallel bulk and surface diffusion	$J = -\left[D_{eff} \left(\frac{dp_i}{dz} \right) + D_{s,eff} \rho_p \left(\frac{dq_i}{dz} \right) \right]$ (5-258)	" " " "	[34]
	$J = -D_{app} \left(\frac{dp_i}{dz} \right)$ (5-259)	" " " "	
	$D_{app} = D_{eff} + D_{s,eff} \rho_p \left(\frac{dq_i}{dp_i} \right)$ (5-260)	" " " "	

°See the beginning of the "Mass Transfer" subsection for references.

than that due to bulk diffusion if $\partial q_i/\partial z \gg \partial C_i/\partial z$. This can occur when a component is strongly adsorbed and the surface coverage is high. For all that, surface diffusion is not well understood. The references in Table 5-16 should be consulted for further details.

INTERPHASE MASS TRANSFER

Transfer of material between phases is important in most separation processes in which two phases are involved. When one phase is pure, mass transfer in the pure phase is not involved. For example, when a pure liquid is being evaporated into a gas, only the gas-phase mass transfer need be calculated. Occasionally, mass transfer in one of the two phases may be neglected even though pure components are not involved. This will be the case when the resistance to mass transfer is much larger in one phase than in the other. Understanding the nature and magnitudes of these resistances is one of the keys to performing reliable mass transfer. In this section, mass transfer between gas and liquid phases will be discussed. The principles are easily applied to the other phases.

Mass-Transfer Principles: Dilute Systems When material is transferred from one phase to another across an interface that separates the two, the resistance to mass transfer in each phase causes a concentration gradient in each, as shown in Fig. 5-26 for a gas-liquid interface. The concentrations of the diffusing material in the two phases immediately adjacent to the interface generally are unequal, even if expressed in the same units, but usually are assumed to be related to each other by the laws of thermodynamic equilibrium. Thus, it is assumed that the thermodynamic equilibrium is reached at the gas-liquid interface almost immediately when a gas and a liquid are brought into contact.

For systems in which the solute concentrations in the gas and liquid phases are dilute, the rate of transfer may be expressed by equations which predict that the rate of mass transfer is proportional to the difference between the bulk concentration and the concentration at the gas-liquid interface. Thus

$$N_A = k'_G(p - p_i) = k'_L(c_i - c) \tag{5-261}$$

where N_A = mass-transfer rate, k'_G = gas-phase mass-transfer coefficient, k'_L = liquid-phase mass-transfer coefficient, p = solute partial pressure in bulk gas, p_i = solute partial pressure at interface, c = solute concentration in bulk liquid, and c_i = solute concentration in liquid at interface.

The mass-transfer coefficients k'_G and k'_L by definition are equal to the ratios of the molar mass flux N_A to the concentration driving forces $(p - p_i)$ and $(c_i - c)$ respectively. An alternative expression for the rate of transfer in dilute systems is given by

$$N_A = k_C(y - y_i) = k_L(x_i - x) \tag{5-262}$$

where N_A = mass-transfer rate, k_C = gas-phase mass-transfer coefficient, k_L = liquid-phase mass-transfer coefficient, y = mole-fraction

solute in bulk-gas phase, y_i = mole-fraction solute in gas at interface, x = mole-fraction solute in bulk-liquid phase, and x_i = mole-fraction solute in liquid at interface.

The mass-transfer coefficients defined by Eqs. (5-261) and (5-262) are related to each other as follows:

$$k_C = k'_G p_T \tag{5-263}$$

$$k_L = k'_L \bar{\rho}_L \tag{5-264}$$

where p_T = total system pressure employed during the experimental determinations of k'_G values and $\bar{\rho}_L$ = average molar density of the liquid phase. The coefficient k_C is relatively independent of the total system pressure and therefore is more convenient to use than k'_G , which is inversely proportional to the total system pressure.

The above equations may be used for finding the interfacial concentrations corresponding to any set of values of x and y provided the ratio of the individual coefficients is known. Thus

$$(y - y_i)/(x_i - x) = k_L/k_C = k'_L \bar{\rho}_L / k'_G p_T = L_M H_C / G_M H_L \tag{5-265}$$

where L_M = molar liquid mass velocity, G_M = molar gas mass velocity, H_L = height of one transfer unit based on liquid-phase resistance, and H_C = height of one transfer unit based on gas-phase resistance. The last term in Eq. (5-265) is derived from Eqs. (5-284) and (5-286).

Equation (5-265) may be solved graphically if a plot is made of the equilibrium vapor and liquid compositions and a point representing the bulk concentrations x and y is located on this diagram. A construction of this type is shown in Fig. 5-27, which represents a gas-absorption situation.

The interfacial mole fractions y_i and x_i can be determined by solving Eq. (5-265) simultaneously with the equilibrium relation $y_i^\circ = F(x_i)$ to obtain y_i and x_i . The rate of transfer may then be calculated from Eq. (5-262).

If the equilibrium relation $y_i^\circ = F(x_i)$ is sufficiently simple, e.g., if a plot of y_i° versus x_i is a straight line, not necessarily through the origin, the rate of transfer is proportional to the difference between the bulk concentration in one phase and the concentration (in that same phase) which would be in equilibrium with the bulk concentration in the second phase. One such difference is $y - y^\circ$, and another is $x^\circ - x$. In this case, there is no need to solve for the interfacial compositions, as may be seen from the following derivation.

The rate of mass transfer may be defined by the equation

$$N_A = K_C(y - y^\circ) = k_C(y - y_i) = k_L(x_i - x) = K_L(x^\circ - x) \tag{5-266}$$

where K_C = overall gas-phase mass-transfer coefficient, K_L = overall liquid-phase mass-transfer coefficient, y° = vapor composition in equilibrium with x , and x° = liquid composition in equilibrium with vapor of composition y . This equation can be rearranged to the formula

$$\frac{1}{K_C} = \frac{1}{k_C} \left(\frac{y - y^\circ}{y - y_i} \right) = \frac{1}{k_C} + \frac{1}{k_C} \left(\frac{y_i - y^\circ}{y - y_i} \right) = \frac{1}{k_C} + \frac{1}{k_L} \left(\frac{y_i - y^\circ}{x_i - x} \right) \tag{5-267}$$

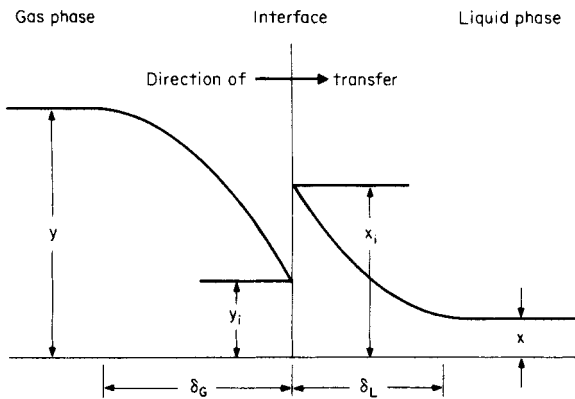


FIG. 5-26 Concentration gradients near a gas-liquid interface.

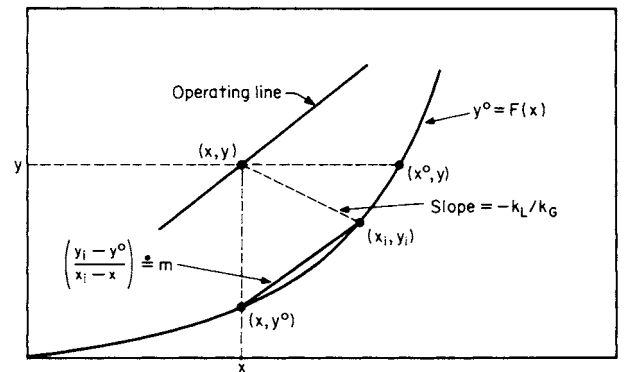


FIG. 5-27 Identification of concentrations at a point in a countercurrent absorption tower.

5-60 HEAT AND MASS TRANSFER

in view of Eq. (5-265). Comparison of the last term in parentheses with the diagram of Fig. 5-27 shows that it is equal to the slope of the chord connecting the points (x, y°) and (x_i, y_i) . If the equilibrium curve is a straight line, then this term is the slope m . Thus

$$1/K_G = (1/k_G + m/k_L) \quad (5-268)$$

When Henry's law is valid ($p_A = Hx_A$ or $p_A = H'c_A$), the slope m can be computed according to the relationship

$$m = H/p_T = H'\bar{v}_L/p_T \quad (5-269)$$

where m is defined in terms of mole-fraction driving forces compatible with Eqs. (5-262) through (5-268), i.e., with the definitions of k_L , k_G , and K_G .

If it is desired to calculate the rate of transfer from the overall concentration difference based on bulk-liquid compositions ($x^\circ - x$), the appropriate overall coefficient K_L is related to the individual coefficients by the equation

$$1/K_L = [1/k_L + 1/(mk_G)] \quad (5-270)$$

Conversion of these equations to a k'_G, k'_L basis can be accomplished readily by direct substitution of Eqs. (5-263) and (5-264).

Occasionally one will find k'_L or K'_L values reported in units (SI) of meters per second. The correct units for these values are $\text{kmol}/[(s \cdot \text{m}^2)(\text{kmol}/\text{m}^3)]$, and Eq. (5-264) is the correct equation for converting them to a mole-fraction basis.

When k'_G and K'_G values are reported in units (SI) of $\text{kmol}/[(s \cdot \text{m}^2)(\text{kPa})]$, one must be careful in converting them to a mole-fraction basis to multiply by the total pressure actually employed in the original experiments and *not* by the total pressure of the system to be designed. This conversion is valid for systems in which Dalton's law of partial pressures ($p = yp_T$) is valid.

Comparison of Eqs. (5-268) and (5-270) shows that for systems in which the equilibrium line is straight, the overall mass transfer coefficients are related to each other by the equation

$$K_L = mK_G \quad (5-271)$$

When the equilibrium curve is not straight, there is no strictly logical basis for the use of an overall transfer coefficient, since the value of m will be a function of position in the apparatus, as can be seen from Fig. 5-27. In such cases the rate of transfer must be calculated by solving for the interfacial compositions as described above.

Experimentally observed rates of mass transfer often are expressed in terms of overall transfer coefficients even when the equilibrium lines are curved. This procedure is empirical, since the theory indicates that in such cases the rates of transfer may not vary in direct proportion to the overall bulk concentration differences ($y - y^\circ$) and ($x^\circ - x$) at all concentration levels even though the rates may be proportional to the concentration difference in each phase taken separately, i.e., $(x_i - x)$ and $(y - y_i)$.

In most types of separation equipment such as packed or spray towers, the interfacial area that is effective for mass transfer cannot be accurately determined. For this reason it is customary to report experimentally observed rates of transfer in terms of transfer coefficients based on a unit volume of the apparatus rather than on a unit of interfacial area. Such volumetric coefficients are designated as K_{Ca} , k_{La} , etc., where a represents the interfacial area per unit volume of the apparatus. Experimentally observed variations in the values of these volumetric coefficients with variations in flow rates, type of packing, etc., may be due as much to changes in the effective value of a as to changes in k . Calculation of the overall coefficients from the individual volumetric coefficients is made by means of the equations

$$1/K_{Ca} = (1/k_{Ca} + m/k_{La}) \quad (5-272)$$

$$1/K_{La} = (1/k_{La} + 1/mk_{Ca}) \quad (5-273)$$

Because of the wide variation in equilibrium, the variation in the values of m from one system to another can have an important effect on the overall coefficient and on the selection of the type of equipment to use. For example, if m is large, the liquid-phase part of the overall resistance might be extremely large where k_L might be relatively small. This kind of reasoning must be applied with caution, however, since species with different equilibrium characteristics are separated under different

operating conditions. Thus, the effect of changes in m on the overall resistance to mass transfer may partly be counterbalanced by changes in the individual specific resistances as the flow rates are changed.

Mass-Transfer Principles: Concentrated Systems When solute concentrations in the gas and/or liquid phases are large, the equations derived above for dilute systems no longer are applicable. The correct equations to use for concentrated systems are as follows:

$$N_A = \hat{k}_G(y - y_i)/y_{BM} = \hat{k}_L(x_i - x)/x_{BM} \\ = \hat{K}_G(y - y^\circ)/y_{BM}^\circ = \hat{K}_L(x^\circ - x)/x_{BM}^\circ \quad (5-274)$$

where ($N_B = 0$)

$$y_{BM} = \frac{(1 - y) - (1 - y_i)}{\ln [(1 - y)/(1 - y_i)]} \quad (5-275)$$

$$y_{BM}^\circ = \frac{(1 - y) - (1 - y^\circ)}{\ln [(1 - y)/(1 - y^\circ)]} \quad (5-276)$$

$$x_{BM} = \frac{(1 - x) - (1 - x_i)}{\ln [(1 - x)/(1 - x_i)]} \quad (5-277)$$

$$x_{BM}^\circ = \frac{(1 - x) - (1 - x^\circ)}{\ln [(1 - x)/(1 - x^\circ)]} \quad (5-278)$$

and where \hat{k}_G and \hat{k}_L are the gas-phase and liquid-phase mass-transfer coefficients for concentrated systems and \hat{K}_G and \hat{K}_L are the overall gas-phase and liquid-phase mass-transfer coefficients for concentrated systems. These coefficients are defined later in Eqs. (5-281) to (5-283).

The factors y_{BM} and x_{BM} arise from the fact that, in the diffusion of a solute through a second stationary layer of insoluble fluid, the resistance to diffusion varies in proportion to the concentration of the insoluble stationary fluid, approaching zero as the concentration of the insoluble fluid approaches zero. See Eq. (5-198).

The factors y_{BM}° and x_{BM}° cannot be justified on the basis of mass-transfer theory since they are based on overall resistances. These factors therefore are included in the equations by analogy with the corresponding film equations.

In dilute systems the logarithmic-mean insoluble-gas and nonvolatile-liquid concentrations approach unity, and Eq. (5-274) reduces to the dilute-system formula. For equimolar counter diffusion (e.g., binary distillation), these log-mean factors should be omitted. See Eq. (5-197).

Substitution of Eqs. (5-275) through (5-278) into Eq. (5-274) results in the following simplified formula:

$$N_A = \hat{k}_G \ln [(1 - y_i)/(1 - y)] \\ = \hat{K}_G \ln [(1 - y^\circ)/(1 - y)] \\ = \hat{k}_L \ln [(1 - x)/(1 - x_i)] \\ = \hat{K}_L \ln [(1 - x^\circ)/(1 - x^\circ)] \quad (5-279)$$

Note that the units of \hat{k}_G , \hat{K}_G , \hat{k}_L , and \hat{K}_L are all identical to each other, i.e., $\text{kmol}/(s \cdot \text{m}^2)$ in SI units.

The equation for computing the interfacial gas and liquid compositions in concentrated systems is

$$(y - y_i)/(x_i - x) = \hat{k}_L y_{BM} / \hat{k}_G x_{BM} \\ = L_M H_C y_{BM} / G_M H_L x_{BM} = k_L / k_G \quad (5-280)$$

This equation is identical to the one for dilute systems since $\hat{k}_G = k_G y_{BM}$ and $\hat{k}_L = k_L x_{BM}$. Note, however, that when \hat{k}_G and \hat{k}_L are given, the equation must be solved by trial and error, since x_{BM} contains x_i and y_{BM} contains y_i .

The overall gas-phase and liquid-phase mass-transfer coefficients for concentrated systems are computed according to the following equations:

$$\frac{1}{\hat{K}_G} = \frac{y_{BM}}{y_{BM}^\circ} \frac{1}{\hat{k}_G} + \frac{x_{BM}}{y_{BM}^\circ} \frac{1}{\hat{k}_L} \left(\frac{y_i - y^\circ}{x_i - x} \right) \quad (5-281)$$

$$\frac{1}{\hat{K}_L} = \frac{x_{BM}}{x_{BM}^\circ} \frac{1}{\hat{k}_L} + \frac{y_{BM}}{x_{BM}^\circ} \frac{1}{\hat{k}_G} \left(\frac{x^\circ - x_i}{y - y_i} \right) \quad (5-282)$$

When the equilibrium curve is a straight line, the terms in parentheses can be replaced by the slope m or $1/m$ as before. In this case the

overall mass-transfer coefficients for concentrated systems are related to each other by the equation

$$\hat{K}_L = m \hat{K}_G (x_{BM}^\circ / y_{BM}^\circ) \quad (5-283)$$

All these equations reduce to their dilute-system equivalents as the inert concentrations approach unity in terms of mole fractions of inert concentrations in the fluids.

HTU (Height Equivalent to One Transfer Unit) Frequently the values of the individual coefficients of mass transfer are so strongly dependent on flow rates that the quantity obtained by dividing each coefficient by the flow rate of the phase to which it applies is more nearly constant than the coefficient itself. The quantity obtained by this procedure is called the height equivalent to one transfer unit, since it expresses in terms of a single length dimension the height of apparatus required to accomplish a separation of standard difficulty.

The following relations between the transfer coefficients and the values of HTU apply:

$$H_G = G_M / k_G a y_{BM} = G_M / \hat{K}_G a \quad (5-284)$$

$$H_{OG} = G_M / K_G a y_{BM}^\circ = G_M / \hat{K}_G a \quad (5-285)$$

$$H_L = L_M / k_L a x_{BM} = L_M / \hat{K}_L a \quad (5-286)$$

$$H_{OL} = L_M / K_L a x_{BM}^\circ = L_M / \hat{K}_L a \quad (5-287)$$

The equations that express the addition of individual resistances in terms of HTUs, applicable to either dilute or concentrated systems, are

$$H_{OG} = \frac{y_{BM}}{y_{BM}^\circ} H_G + \frac{m G_M}{L_M} \frac{x_{BM}}{y_{BM}^\circ} H_L \quad (5-288)$$

$$H_{OL} = \frac{x_{BM}}{x_{BM}^\circ} H_L + \frac{L_M}{m G_M} \frac{y_{BM}}{x_{BM}^\circ} H_G \quad (5-289)$$

These equations are strictly valid only when m , the slope of the equilibrium curve, is constant, as noted previously.

NTU (Number of Transfer Units) The NTU required for a given separation is closely related to the number of theoretical stages or plates required to carry out the same separation in a stagewise or plate-type apparatus. For equimolar counterdiffusion, such as in a binary distillation, the number of overall gas-phase transfer units N_{OG} required for changing the composition of the vapor stream from y_1 to y_2 is

$$N_{OG} = \int_{y_2}^{y_1} \frac{dy}{y - y^\circ} \quad (5-290)$$

When diffusion is in one direction only, as in the absorption of a soluble component from an insoluble gas,

$$N_{OG} = \int_{y_2}^{y_1} \frac{y_{BM}^\circ dy}{(1 - y)(y - y^\circ)} \quad (5-291)$$

The total height of packing required is then

$$h_T = H_{OG} N_{OG} \quad (5-292)$$

When it is known that H_{OG} varies appreciably within the tower, this term must be placed inside the integral in Eqs. (5-290) and (5-291) for accurate calculations of h_T . For example, the packed-tower design equation in terms of the overall gas-phase mass-transfer coefficient for absorption would be expressed as follows:

$$h_T = \int_{y_2}^{y_1} \left[\frac{G_M}{K_G a y_{BM}^\circ} \right] \frac{y_{BM}^\circ dy}{(1 - y)(y - y^\circ)} \quad (5-293)$$

where the first term under the integral can be recognized as the HTU term. Convenient solutions of these equations for special cases are discussed later.

Definitions of Mass-Transfer Coefficients \hat{K}_G and \hat{K}_L The mass-transfer coefficient is defined as the ratio of the molar mass flux N_A to the concentration driving force. This leads to many different ways of defining these coefficients. For example, gas-phase mass-transfer rates may be defined as

$$N_A = k_G (y - y_i) = k'_G (p - p_i) = \hat{k}_G (y - y_i) / y_{BM} \quad (5-294)$$

where the units (SI) of k_G are $\text{kmol}/[(\text{s}\cdot\text{m}^2)(\text{mole fraction})]$, the units of

k'_G are $\text{kmol}/[(\text{s}\cdot\text{m}^2)(\text{kPa})]$, and the units of \hat{k}_G are $\text{kmol}/(\text{s}\cdot\text{m}^2)$. These coefficients are related to each other as follows:

$$k_G = k_C y_{BM} = k'_G p_T y_{BM} \quad (5-295)$$

where p_T is the total system pressure (it is assumed here that Dalton's law of partial pressures is valid).

In a similar way, liquid-phase mass-transfer rates may be defined by the relations

$$N_A = k_L (x_i - x) = k'_L (c_i - c) = \hat{k}_L (x_i - x) / x_{BM} \quad (5-296)$$

where the units (SI) of k_L are $\text{kmol}/[(\text{s}\cdot\text{m}^2)(\text{mole fraction})]$, the units of k'_L are $\text{kmol}/[(\text{s}\cdot\text{m}^2)(\text{kmol}/\text{m}^3)]$ or meters per second, and the units of \hat{k}_L are $\text{kmol}/(\text{s}\cdot\text{m}^2)$. These coefficients are related as follows:

$$\hat{k}_L = k_L x_{BM} = k'_L \bar{\rho}_L x_{BM} \quad (5-297)$$

where $\bar{\rho}_L$ is the molar density of the liquid phase in units (SI) of kilomoles per cubic meter. Note that, for dilute solutions where $x_{BM} \doteq 1$, k_L and \hat{k}_L will have identical numerical values. Similarly, for dilute gases $\hat{k}_G \doteq k_G$.

Simplified Mass-Transfer Theories In certain simple situations, the mass-transfer coefficients can be calculated from first principles. The film, penetration, and surface-renewal theories are attempts to extend these theoretical calculations to more complex situations. Although these theories are often not accurate, they are useful to provide a physical picture for variations in the mass-transfer coefficient.

For the special case of steady-state unidirectional diffusion of a component through an inert-gas film in an ideal-gas system, the rate of mass transfer is derived as

$$N_A = \frac{D_{AB} p_T}{RT \delta_C} \frac{(y - y_i)}{y_{BM}} = \frac{D_{AB} p_T}{RT \delta_C} \ln \frac{1 - y_i}{1 - y} \quad (5-298)$$

where D_{AB} is the diffusion coefficient or "diffusivity," δ_C is the "effective" thickness of a stagnant-gas layer which would offer a resistance to molecular diffusion equal to the experimentally observed resistance, and R is the gas constant. [Nernst, *Z. Phys. Chem.*, **47**, 52 (1904); Whitman, *Chem. Mat. Eng.*, **29**, 149 (1923), and Lewis and Whitman, *Ind. Eng. Chem.*, **16**, 1215 (1924)].

The film thickness δ_C depends primarily on the hydrodynamics of the system and hence on the Reynolds number and the Schmidt number. Thus, various correlations have been developed for different geometries in terms of the following dimensionless variables:

$$N_{Sh} = \hat{k}_C R T d / D_{AB} p_T = f(N_{Re}, N_{Sc}) \quad (5-299)$$

where N_{Sh} is the Sherwood number, N_{Re} ($= Gd/\mu_C$) is the Reynolds number based on the characteristic length d appropriate to the geometry of the particular system; and N_{Sc} ($= \mu_C/\rho_C D_{AB}$) is the Schmidt number.

According to this analysis one can see that for gas-absorption problems, which often exhibit unidirectional diffusion, the most appropriate driving-force expression is of the form $(y - y_i)/y_{BM}$, and the most appropriate mass-transfer coefficient is therefore \hat{k}_G . This concept is to be found in all the key equations for the design of mass-transfer equipment.

The Sherwood-number relation for gas-phase mass-transfer coefficients as represented by the film diffusion model in Eq. (5-299) can be rearranged as follows:

$$N_{Sh} = (\hat{k}_G / G_M) N_{Re} N_{Sc} = N_{St} N_{Re} N_{Sc} = f(N_{Re}, N_{Sc}) \quad (5-300)$$

where $N_{St} = \hat{k}_G / G_M = k'_G p_{BM} / G_M$ is known as the Stanton number. This equation can now be stated in the alternative functional forms

$$N_{St} = \hat{k}_G / G_M = g(N_{Re}, N_{Sc}) \quad (5-301)$$

$$j_D = N_{St} \cdot N_{Sc}^{2/3} \quad (5-302)$$

where j is the Chilton-Colburn "j factor" for mass transfer (discussed later).

The important point to note here is that the gas-phase mass-transfer coefficient \hat{k}_G depends principally upon the transport properties of the fluid (N_{Sc}) and the hydrodynamics of the particular system involved (N_{Re}). It also is important to recognize that specific mass-transfer correlations can be derived only in conjunction with the

investigator's particular assumptions concerning the numerical values of the effective interfacial area a of the packing.

The stagnant-film model discussed previously assumes a steady state in which the local flux across each element of area is constant; i.e., there is no accumulation of the diffusing species within the film. Higbie [*Trans. Am. Inst. Chem. Eng.*, **31**, 365 (1935)] pointed out that industrial contactors often operate with repeated brief contacts between phases in which the contact times are too short for the steady state to be achieved. For example, Higbie advanced the theory that in a packed tower the liquid flows across each packing piece in laminar flow and is remixed at the points of discontinuity between the packing elements. Thus, a fresh liquid surface is formed at the top of each piece, and as it moves downward, it absorbs gas at a decreasing rate until it is mixed at the next discontinuity. This is the basis of penetration theory.

If the velocity of the flowing stream is uniform over a very deep region of liquid (total thickness, $\delta_T \gg \sqrt{Dt}$), the time-averaged mass-transfer coefficient according to penetration theory is given by

$$k'_L = 2\sqrt{D_L/\pi t} \quad (5-303)$$

where k'_L = liquid-phase mass-transfer coefficient, D_L = liquid-phase diffusion coefficient, and t = contact time.

In practice, the contact time t is not known except in special cases in which the hydrodynamics are clearly defined. This is somewhat similar to the case of the stagnant-film theory in which the unknown quantity is the thickness of the stagnant layer δ (in film theory, the liquid-phase mass-transfer coefficient is given by $k'_L = D_L/\delta$).

The penetration theory predicts that k'_L should vary by the square root of the molecular diffusivity, as compared with film theory, which predicts a first-power dependency on D . Various investigators have reported experimental powers of D ranging from 0.5 to 0.75, and the Chilton-Colburn analogy suggests a $2/3$ power.

Penetration theory often is used in analyzing absorption with chemical reaction because it makes no assumption about the depths of penetration of the various reacting species, and it gives a more accurate result when the diffusion coefficients of the reacting species are not equal. When the reaction process is very complex, however, penetration theory is more difficult to use than film theory, and the latter method normally is preferred.

Danckwerts [*Ind. Eng. Chem.*, **42**, 1460 (1951)] proposed an extension of the penetration theory, called the surface renewal theory, which allows for the eddy motion in the liquid to bring masses of fresh liquid continually from the interior to the surface, where they are exposed to the gas for finite lengths of time before being replaced. In his development, Danckwerts assumed that every element of fluid has an equal chance of being replaced regardless of its age. The Danckwerts model gives

$$k'_L = \sqrt{Ds} \quad (5-304)$$

where s = fractional rate of surface renewal.

Note that both the penetration and the surface-renewal theories predict a square-root dependency on D . Also, it should be recognized that values of the surface-renewal rate s generally are not available, which presents the same problems as do δ and t in the film and penetration models.

The predictions of correlations based on the film model often are nearly identical to predictions based on the penetration and surface-renewal models. Thus, in view of its relative simplicity, the film model normally is preferred for purposes of discussion or calculation. It should be noted that none of these theoretical models has proved adequate for making a priori predictions of mass-transfer rates in packed towers, and therefore empirical correlations such as those outlined later in Table 5-24 must be employed.

Mass-Transfer Correlations Because of the tremendous importance of mass transfer in chemical engineering, a very large number of studies have determined mass-transfer coefficients both empirically and theoretically. Some of these studies are summarized in Tables 5-17 to 5-24. Each table is for a specific geometry or type of contactor, starting with flat plates, which have the simplest geometry (Table 5-17); then wetted wall columns (Table 5-18); flow in pipes and ducts (Table 5-19); submerged objects (Table 5-20); drops and

bubbles (Table 5-21); agitated systems (Table 5-22); packed beds of particles for adsorption, ion exchange, and chemical reaction (Table 5-23); and finishing with packed bed two-phase contactors for distillation, absorption and other unit operations (Table 5-24). Although extensive, these tables are not meant to be encyclopedic, but a variety of different configurations are shown to provide a flavor of the range of correlations available. These correlations include transfer to or from one fluid and either a second fluid or a solid. Many of the correlations are for k_L and k_G values obtained from dilute systems where $x_{BM} \approx 1.0$ and $y_{BM} \approx 1.0$. The most extensive source for older mass-transfer correlations in a variety of geometries is Skelland (*Diffusional Mass Transfer*, 1974). The extensive review of bubble column systems (see Table 5-21) by Shah et al. [*AIChE J.*, **28**, 353 (1982)] includes estimation of bubble size, gas holdup, interfacial area $k_L a$, and liquid dispersion coefficient. For correlations for particle-liquid mass transfer in stirred tanks (part of Table 5-22) see the review by Pangarkar et al. [*Ind. Eng. Chem. Res.*, **41**, 4141 (2002)]. For mass transfer in distillation, absorption, and extraction in packed beds (Table 5-24), see also the appropriate sections in this handbook and the review by Wang, Yuan, and Yu [*Ind. Eng. Chem. Res.*, **44**, 8715 (2005)]. For simple geometries, one may be able to determine a theoretical (T) form of the mass-transfer correlation. For very complex geometries, only an empirical (E) form can be found. In systems of intermediate complexity, semiempirical (S) correlations where the form is determined from theory and the coefficients from experiment are often useful. Although the major limitations and constraints in use are usually included in the tables, obviously many details cannot be included in this summary form. Readers are strongly encouraged to check the references before using the correlations in important situations. Note that even authoritative sources occasionally have typographical errors in the fairly complex correlation equations. Thus, it is a good idea to check several sources, including the original paper. The references will often include figures comparing the correlations with data. These figures are very useful since they provide a visual picture of the scatter in the data.

Since there are often several correlations that are applicable, how does one choose the correlation to use? First, the engineer must determine which correlations are closest to the current situation. This involves recognizing the similarity of geometries, which is often challenging, and checking that the range of parameters in the correlation is appropriate. For example, the Bravo, Rocha, and Fair correlation for distillation with structured packings with triangular cross-sectional channels (Table 5-24-H) uses the Johnstone and Pigford correlation for rectification in vertical wetted wall columns (Table 5-18-F). Recognizing that this latter correlation pertains to a rather different application and geometry was a nontrivial step in the process of developing a correlation. If several correlations appear to be applicable, check to see if the correlations have been compared to each other and to the data. When a detailed comparison of correlations is not available, the following heuristics may be useful:

1. Mass-transfer coefficients are derived from models. They must be employed in a similar model. For example, if an arithmetic concentration difference was used to determine k , that k should only be used in a mass-transfer expression with an arithmetic concentration difference.
2. Semiempirical correlations are often preferred to purely empirical or purely theoretical correlations. Purely empirical correlations are dangerous to use for extrapolation. Purely theoretical correlations may predict trends accurately, but they can be several orders of magnitude off in the value of k .
3. Correlations with broader data bases are often preferred.
4. The analogy between heat and mass transfer holds over wider ranges than the analogy between mass and momentum transfer. Good heat transfer data (without radiation) can often be used to predict mass-transfer coefficients.
5. More recent data is often preferred to older data, since end effects are better understood, the new correlation often builds on earlier data and analysis, and better measurement techniques are often available.
6. With complicated geometries, the product of the interfacial area per volume and the mass-transfer coefficient is required. Correlations of ka_p or of HTU are more accurate than individual correlations of k and

TABLE 5-17 Mass-Transfer Correlations for a Single Flat Plate or Disk—Transfer to or from Plate to Fluid

Situation	Correlation	Comments E = Empirical, S = Semiempirical, T = Theoretical	References°
<p>A. Laminar, local, flat plate, forced flow</p> <p>Laminar, average, flat plate, forced flow</p> <p><i>j</i>_D-factors</p>	$N_{Sh,x} = \frac{k'x}{D} = 0.323(N_{Re,x})^{1/2}(N_{Sc})^{1/3}$ <p>Coefficient 0.323 is a better fit.</p> $N_{Sh,avg} = \frac{k'_m L}{D} = 0.664(N_{Re,L})^{1/2}(N_{Sc})^{1/3}$ <p>Coefficient 0.664 is a better fit.</p> <p><i>k</i>'_m is mean mass-transfer coefficient for dilute systems.</p> $j_D = j_H = \frac{f}{2} = 0.664(N_{Re,L})^{-1/2}$	<p>[T] Low M.T. rates. Low mass-flux, constant property systems. <i>N</i>_{Sh,x} is local <i>k</i>. Use with arithmetic difference in concentration. Coefficient 0.323 is Blasius' approximate solution.</p> <p>$N_{Re,x} = \frac{xu_\infty \rho}{\mu}$, <i>x</i> = length along plate</p> <p>$N_{Re,L} = \frac{Lu_\infty \rho}{\mu}$, 0.664 (Polhausen)</p> <p>is a better fit for <i>N</i>_{Sc} > 0.6, <i>N</i>_{Re,x} < 3 × 10⁵.</p> <p>[S] Analogy. <i>N</i>_{Sc} = 1.0, <i>f</i> = drag coefficient. <i>j</i>_D is defined in terms of <i>k</i>'_m.</p>	<p>[77] p. 183 [87] p. 526 [138] p. 79 [140] p. 518</p> <p>[141] p. 110</p> <p>[91] p. 480</p> <p>[141] p. 271</p>
<p>B. Laminar, local, flat plate, blowing or suction and forced flow</p>	$N_{Sh,x} = \frac{k'x}{D} = (\text{Slope})_{y=0} (N_{Re,x})^{1/2}(N_{Sc})^{1/3}$	<p>[T] Blowing is positive. Other conditions as above.</p> <p>$\frac{u_o}{u_\infty} \sqrt{N_{Re,x}}$</p> <p>$\frac{u_\infty}{(\text{Slope})_{y=0}}$ 0.6 0.5 0.25 0.0 -2.5</p> <p>0.01 0.06 0.17 0.332 1.64</p>	<p>[77] p. 185</p> <p>[140] p. 271</p>
<p>C. Laminar, local, flat plate, natural convection vertical plate</p>	$N_{Sh,x} = \frac{k'x}{D} = 0.508 N_{Sc}^{1/2} (0.952 + N_{Sc})^{-1/4} N_{Gr}^{1/4}$ $N_{Gr} = \frac{gx^3}{(\mu/\rho)^2} \left(\frac{\rho_\infty}{\rho_0} - 1 \right)$	<p>[T] Low MT rates. Dilute systems, Δ<i>p</i>/ρ << 1. <i>N</i>_{Gr}, <i>N</i>_{Sc} < 10⁹. Use with arithmetic concentration difference. <i>x</i> = length from plate bottom.</p>	<p>[141] p. 120</p>
<p>D. Laminar, stationary disk</p> <p>Laminar, spinning disk</p>	$N_{Sh} = \frac{k'd_{\text{disk}}}{D} = \frac{8}{\pi}$ $N_{Sh} = \frac{k'd_{\text{disk}}}{D} = 0.879 N_{Re}^{1/2} N_{Sc}^{1/3}$ <p><i>N</i>_{Re} < ~ 10⁴</p>	<p>[T] Stagnant fluid. Use arithmetic concentration difference.</p> <p>[T] Asymptotic solution for large <i>N</i>_{Sc}. <i>u</i> = ω<i>d</i>_{disk/2}, ω = rotational speed, rad/s. Rotating disks are often used in electrochemical research.</p>	<p>[138] p. 240</p> <p>[101] p. 60</p> <p>[138] p. 240</p>
<p>E. Laminar, inclined, plate</p>	$N_{Sh,avg} = 0.783 N_{Re, \text{film}}^{1/3} N_{Sc}^{1/3} \left(\frac{x^3 \rho^3 g \sin \alpha}{\mu^2} \right)^{2/9}$ $N_{Re, \text{film}} = \frac{4Q\rho}{\mu^2} < 2000$ $N_{Sh,avg} = \frac{k'_m x}{D}$ $\delta_{\text{film}} = \left(\frac{3\mu Q}{w\rho g \sin \alpha} \right)^{1/3} = \text{film thickness}$	<p>[T] Constant-property liquid film with low mass-transfer rates. Use arithmetic concentration difference. Newtonian fluid. Solute does not penetrate past region of linear velocity profile. Differences between theory and experiment. <i>w</i> = width of plate, δ_{<i>j</i>} = film thickness, α = angle of inclination, <i>x</i> = distance from start soluble surface.</p>	<p>[141] p. 130 [138] p. 209</p>
<p>F. Turbulent, local flat plate, forced flow</p> <p>Turbulent, average, flat plate, forced flow</p>	$N_{Sh,x} = \frac{k'x}{D} = 0.0292 N_{Re,x}^{0.8}$ $N_{Sh,avg} = \frac{k'L}{D} = 0.0365 N_{Re,L}^{0.8}$	<p>[S] Low mass-flux with constant property system. Use with arithmetic concentration difference. <i>N</i>_{Sc} = 1.0, <i>N</i>_{Re,x} > 10⁵</p> <p>Based on Prandtl's 1/7-power velocity law,</p> $\frac{u}{u_\infty} = \left(\frac{y}{\delta} \right)^{1/7}$	<p>[77] p. 191 [138] p. 201 [141] p. 221</p>
<p>G. Laminar and turbulent, flat plate, forced flow</p>	$j_D = j_H = \frac{f}{2} = 0.037 N_{Re,L}^{0.2}$ $j_D = (k_C/G_M) N_{Sc}^{2/3}$ $j_H = (h'/C_p G) N_{Pr}^{2/3}$	<p>[E] Chilton-Colburn analogies, <i>N</i>_{Sc} = 1.0, (gases), <i>f</i> = drag coefficient. Corresponds to item 5-17-F and refers to same conditions. 8000 < <i>N</i>_{Re} < 300,000. Can apply analogy, <i>j</i>_D = <i>f</i>/2, to entire plate (including laminar portion) if average values are used.</p>	<p>[77] p. 193 [88] p. 112 [138] p. 201 [141] p. 271 [80] [53]</p>

5-64 HEAT AND MASS TRANSFER

TABLE 5-17 Mass-Transfer Correlations for a Single Flat Plate or Disk—Transfer to or from Plate to Fluid (Concluded)

Situation	Correlation	Comments E = Empirical, S = Semiempirical, T = Theoretical	References ^o
H. Laminar and turbulent, flat plate, forced flow	$N_{Sh,avg} = 0.037N_{Sc}^{1/3}(N_{Re,L}^{0.8} - 15,500)$ to $N_{Re,L} = 320,000$ $N_{Sh,avg} = 0.037N_{Sc}^{1/3}$ $\times \left(N_{Re,L}^{0.8} - N_{Re,Cr}^{0.8} + \frac{0.664}{0.037} N_{Re,Cr}^{1/2} \right)$ in range 3×10^5 to 3×10^6 .	[E] Use arithmetic concentration difference. $N_{Sh,avg} = \frac{k_m L}{D}$, $N_{Sc} > 0.5$ Entrance effects are ignored. $N_{Re,Cr}$ is transition laminar to turbulent.	[88] p. 112 [138] p. 201
I. Turbulent, local flat plate, natural convection, vertical plate Turbulent, average, flat plate, natural convection, vertical plate	$N_{Sh,x} = \frac{k'x}{D} = 0.0299N_{Gr}^{2/5}N_{Sc}^{7/15}$ $\times (1 + 0.494N_{Sc}^{2/3})^{-2/5}$ $N_{Sh,avg} = 0.0249N_{Gr}^{2/5}N_{Sc}^{7/15} \times (1 + 0.494N_{Sc}^{2/3})^{-2/5}$ $N_{Gr} = \frac{gx^3}{(\mu/\rho)^2} \left(\frac{\rho_\infty}{\rho_0} - 1 \right), \quad N_{Sh,avg} = \frac{k_m L}{D}$	[S] Low solute concentration and low transfer rates. Use arithmetic concentration difference. $N_{Gr} > 10^{10}$ Assumes laminar boundary layer is small fraction of total.	[141] p. 225
J. Perforated flat disk Perforated vertical plate. Natural convection.	$N_{Sh} = 0.059N_{Sc}^{0.35}N_{Gr}^{0.35} \left(\frac{d_h}{d} \right)^{0.04}$ Characteristic length = disk diameter d $N_{Sh} = 0.1N_{Sc}^{1/3}N_{Gr}^{1/3}$ Characteristic length = L , electrode height	[E] $6 \times 10^9 < N_{Sc}N_{Gr} < 10^{12}$ and $1943 < N_{Sc} < 2168$ d_h = hole diameter [E] $1 \times 10^{10} < N_{Sc}N_{Gr} < 5 \times 10^{13}$ and $1939 < N_{Sc} < 2186$ Average deviation $\pm 10\%$	[162]
K. Turbulent, vertical plate	$N_{Sh,avg} = \frac{k'_m x}{D} = 0.327N_{Re,fil}^{2/9}N_{Sc}^{1/3} \left(\frac{x^3 \rho^2 g}{\mu^2} \right)^{2/9}$ $\delta_{film} = 0.172 \left(\frac{Q^2}{w^2 g} \right)^{1/3}$	[E] See 5-17-E for terms. $N_{Re,fil} = \frac{4Q\rho}{w\mu^2} > 2360$ Solute remains in laminar sublayer.	[141] p. 229
L. Cross-corrugated plate (turbulence promoter for membrane systems)	$N_{Sh} = cN_{Re}^a N_{Sc}^c$	[E] Entrance turbulent channel For parallel flow and corrugations: $N_{Sc} = 1483$, $a = 0.56$, $c = 0.268$ $N_{Sc} = 4997$, $a = 0.50$, $c = 0.395$ Corrugations perpendicular to flow: $N_{Sc} = 1483$, $a = 0.57$, $c = 0.368$ $N_{Sc} = 4997$, $a = 0.52$, $c = 0.487$	[134]
M. Turbulent, spinning disk	$N_{Sh} = \frac{k'd_{disk}}{D} = 5.6N_{Re}^{1.1}N_{Sc}^{1/3}$ $6 \times 10^5 < N_{Re} < 2 \times 10^6$ $120 < N_{Sc} < 1200$	[E] Use arithmetic concentration difference. $u = \omega d_{disk}/2$ where ω = rotational speed, radians/s. $N_{Re} = \rho \omega d^2 / 2\mu$.	[55] [138] p. 241
N. Mass transfer to a flat plate membrane in a stirred vessel	$N_{Sh} = \frac{k'd_{tank}}{D} = aN_{Re}^b N_{Sc}^c$ $N_{Re} = \frac{\omega d_{tank}^2 \rho}{\mu}$ a depends on system. $a = 0.0443$ [40]; b is often 0.65–0.70 [89]. If	[E] Use arithmetic concentration difference. ω = stirrer speed, radians/s. Useful for laboratory dialysis, R.O., U.F., and microfiltration systems. $b = 0.785$ [40]. c is often 0.33 but other values have been reported [89].	[40] [89] p. 965
O. Spiral type RO (seawater desalination)	$N_{Sh} = 0.210 N_{Re}^{2/3} N_{Sc}^{1/4}$ Or with slightly larger error, $N_{Sh} = 0.080 N_{Re}^{0.875} N_{Sc}^{1/4}$	[E] Polyamide membrane. $p = 6.5$ MPa and TDS rejection = 99.8%. Recovery ratio 40%.	[148]

^oSee the beginning of the “Mass Transfer” subsection for references.

TABLE 5-18 Mass-Transfer Correlations for Falling Films with a Free Surface in Wetted Wall Columns—Transfer between Gas and Liquid

Situation	Correlation	Comments E = Empirical, S = Semiempirical, T = Theoretical	References*
A. Laminar, vertical wetted wall column	$N_{Sh,avg} = \frac{K'_m x}{D} \approx 3.41 \frac{x}{\delta_{film}}$ (first term of infinite series) $\delta_{film} = \left(\frac{3\mu Q}{w\rho g} \right)^{1/3} = \text{film thickness}$ $N_{Re, film} = \frac{4Q\rho}{w\mu} < 20$	[T] Low rates M.T. Use with log mean concentration difference. Parabolic velocity distribution in films. w = film width (circumference in column) Derived for flat plates, used for tubes if $r_{tube} \left(\frac{\rho g}{2\sigma} \right)^{1/2} > 3.0$. σ = surface tension If $N_{Re, film} > 20$, surface waves and rates increase. An approximate solution $D_{apparent}$ can be used. Ripples are suppressed with a wetting agent good to $N_{Re} = 1200$.	[138] p. 78 [141] p. 137 [152] p. 50
B. Turbulent, vertical wetted wall column	$N_{Sh,avg} = \frac{K'_m d_t}{D} = 0.023 N_{Re}^{0.83} N_{Sc}^{0.44}$ A coefficient 0.0163 has also been reported using $N_{Re'}$, where $v = v$ of gas relative to liquid film.	[E] Use with log mean concentration difference for correlations in B and D. N_{Re} is for gas. N_{Sc} for vapor in gas. $2000 < N_{Re} \leq 35,000$, $0.6 \leq N_{Sc} \leq 2.5$. Use for gases, d_t = tube diameter.	[68] [77] p. 181 [138] p. 211 [141] p. 265 [149] p. 212 [152] p. 71 [58]
Better fit	$N_{Sh,avg} = 0.0318 N_{Re}^{0.790} N_{Sc}^{0.5}$	[S] Reevaluated data	
C. Turbulent, very short column	$N_{Sh} = 0.00283 N_{Re,g}^{0.5} N_{Sc,g}^{0.06} N_{Re,liq}$ $N_{Sh} = k_g(d_{tube} - 2\delta)/D$ $N_{Re,g} = \rho_g u_g (d_{tube} - 2\delta)/\mu_g$ $N_{Re,liq} = \rho_{liq} Q_{liq} / [\pi \mu (d_{tube} - 2\delta)]$	[E] Evaporation data $N_{Sh,g} = 11$ to 65 , $N_{Re,g} = 2400$ to 9100 $N_{Re,liq} = 110$ to 480 , $N_{Sc,g} = 0.62$ to 1.93 δ = film thickness	[56]
D. Turbulent, vertical wetted wall column with ripples	$N_{Sh,avg} = \frac{K'_m d_t}{D} = 0.00814 N_{Re}^{0.83} N_{Sc}^{0.44} \left(\frac{4Q\rho}{w\mu} \right)^{0.15}$ $30 \leq \left(\frac{4Q\rho}{w\mu} \right) < 1200$ $N_{Sh,avg} = \frac{K'_m d_t}{D} = 0.023 N_{Re}^{0.8} N_{Sc}^{1/3}$	[E] For gas systems with rippling. Fits 5-18-B for $\left(\frac{4Q\rho}{w\mu} \right) = 1000$ [E] "Rounded" approximation to include ripples. Includes solid-liquid mass-transfer data to find $1/3$ coefficient on N_{Sc} . May use $N_{Re}^{0.83}$. Use for liquids. See also Table 5-19.	[85] [138] p. 213
E. Turbulent, with ripples	$N_{Sh} = \left(\frac{2}{\pi} \right)^{0.5} N_{Re,\epsilon}^{0.5} N_{Sc}^{0.5}$ $N_{Re,\epsilon} = \dot{\epsilon} L^2 / \nu$	[E] $\dot{\epsilon}$ = dilation rate of surface = $\frac{\partial v_x^c}{\partial x} + \frac{\partial v_y^c}{\partial y}$	[150]
F. Rectification in vertical wetted wall column with turbulent vapor flow, Johnstone and Pigford correlation	$N_{Sh,avg} = \frac{k'_c d_{col} p_{BM}}{D_c p} = 0.0328 (N'_{Re})^{0.77} N_{Sc}^{0.33}$ $3000 < N'_{Re} < 40,000, 0.5 < N_{Sc} < 3$ $N'_{Re} = \frac{d_{col} v_{rel} \rho_v}{\mu_v}, v_{rel} = \text{gas velocity relative to liquid film} = \frac{3}{2} u_{avg} \text{ in film}$	[E] Use logarithmic mean driving force at two ends of column. Based on four systems with gas-side resistance only. p_{BM} = logarithmic mean partial pressure of nondiffusing species B in binary mixture. p = total pressure Modified form is used for structured packings (See Table 5-24-H).	[84] [138] p. 214 [156]

*See the beginning of the "Mass Transfer" subsection for references.

a_p , since the measurements are simpler to determine the product ka_p or HTU.

7. Finally, if a mass-transfer coefficient looks too good to be true, it probably is incorrect.

To determine the mass-transfer rate, one needs the interfacial area in addition to the mass-transfer coefficient. For the simpler geometries, determining the interfacial area is straightforward. For packed beds of particles a , the interfacial area per volume can be estimated as shown in Table 5-23-A. For packed beds in distillation, absorption, and so on in Table 5-24, the interfacial area per volume is included with the mass-transfer coefficient in the correlations for HTU. For agitated liquid-liquid systems, the interfacial area can be estimated

from the dispersed phase holdup and mean drop size correlations. Godfrey, Obi, and Reeve [*Chem. Engr. Prog.* **85**, 61 (Dec. 1989)] summarize these correlations. For many systems, $\bar{d}_{drop}/d_{imp} = (\text{const})N_{We}^{-0.6}$ where $N_{We} = \rho_c N^2 d_{imp}^3 / \sigma$. Piché, Grandjean, and Larachi [*Ind. Eng. Chem. Res.* **41**, 4911 (2002)] developed two correlations for reconciling the gas-liquid mass-transfer coefficient and interfacial area in randomly packed towers. The correlation for the interfacial area was a function of five dimensionless groups, and yielded a relative error of 22.5 percent for 325 data points. That equation, when combined with a correlation for N_{Sh} as a function of four dimensionless groups, achieved a relative error of 24.4 percent, for 3455 data points for the product $k'_c a$.

TABLE 5-19 Mass-Transfer Correlations for Flow in Pipes and Ducts—Transfer Is from Wall to Fluid

Situation	Correlation	Comments E = Empirical, S = Semiempirical, T = Theoretical	References°																		
A. Tubes, laminar, fully developed parabolic velocity profile, developing concentration profile, constant wall concentration	$N_{Sh} = \frac{k'd_t}{D} = 3.66 + \frac{0.0668(d_t/x)N_{Re}N_{Sc}}{1 + 0.04[(d_t/x)N_{Re}N_{Sc}]^{2/3}}$	[T] Use log mean concentration difference. For $\frac{x/d_t}{N_{Re}N_{Sc}} < 0.10$, $N_{Re} < 2100$. x = distance from tube entrance. Good agreement with experiment at values $10^4 > \frac{\pi}{4} \frac{d_t}{x} N_{Re}N_{Sc} > 10$	[77] p. 176 [87] p. 525 [141] p. 159																		
Fully developed concentration profile	$N_{Sh} = \frac{k'd_t}{D} = 3.66$	[T] $\frac{x/d_t}{N_{Re}N_{Sc}} > 0.1$	[141] p. 165																		
B. Tubes, approximate solution	$N_{Sh,x} = \frac{k'd_t}{D} = 1.077 \left(\frac{d_t}{x}\right)^{1/3} (N_{Re}N_{Sc})^{1/3}$ $N_{Sh,avg} = \frac{k'd_t}{D} = 1.615 \left(\frac{d_t}{L}\right)^{1/3} (N_{Re}N_{Sc})^{1/3}$	[T] For arithmetic concentration difference. $\frac{W}{\rho D x} > 400$ Leveque's approximation: Concentration BL is thin. Assume velocity profile is linear. High mass velocity. Fits liquid data well.	[141] p. 166																		
C. Tubes, laminar, uniform plug velocity, developing concentration profile, constant wall concentration	$N_{Sh,avg} = \frac{1}{2} \frac{d_t}{L} N_{Re}N_{Sc} \left[\frac{1 - 4 \sum_{j=1}^{\infty} a_j^{-2} \exp\left(\frac{-2a_j^2(x/r_i)}{N_{Re}N_{Sc}}\right)}{1 + 4 \sum_{j=1}^{\infty} a_j^{-2} \exp\left(\frac{-2a_j^2(x/r_i)}{N_{Re}N_{Sc}}\right)} \right]$ Graetz solution for heat transfer written for M.T.	[T] Use arithmetic concentration difference. Fits gas data well, for $\frac{W}{D \rho x} < 50$ (fit is fortuitous). $N_{Sh,avg} = (k'_m d_t)/D$. $a_1 = 2.405$, $a_2 = 5.520$, $a_3 = 8.654$, $a_4 = 11.792$, $a_5 = 14.931$. Graphical solutions are in references.	[103] [141] p. 150																		
D. Laminar, fully developed parabolic velocity profile, constant mass flux at wall	$N_{Sh} = \left[\frac{11}{48} - \frac{1}{2} \sum_{j=1}^{\infty} \frac{\exp[-\lambda_j^2(x/r_i)/(N_{Re}N_{Sc})]}{C_j \lambda_j^4} \right]^{-1}$ <table style="margin-left: auto; margin-right: auto;"> <tr> <td>j</td> <td>λ_j^2</td> <td>C_j</td> </tr> <tr> <td>1</td> <td>25.68</td> <td>7.630×10^{-3}</td> </tr> <tr> <td>2</td> <td>83.86</td> <td>2.058×10^{-3}</td> </tr> <tr> <td>3</td> <td>174.2</td> <td>0.901×10^{-3}</td> </tr> <tr> <td>4</td> <td>296.5</td> <td>0.487×10^{-3}</td> </tr> <tr> <td>5</td> <td>450.9</td> <td>0.297×10^{-3}</td> </tr> </table>	j	λ_j^2	C_j	1	25.68	7.630×10^{-3}	2	83.86	2.058×10^{-3}	3	174.2	0.901×10^{-3}	4	296.5	0.487×10^{-3}	5	450.9	0.297×10^{-3}	[T] Use log mean concentration difference. $N_{Re} < 2100$ $N_{Sh,x} = \frac{k'd_t}{D}$ $N_{Re} = \frac{vd_t \rho}{\mu}$	[139] [141] p. 167
j	λ_j^2	C_j																			
1	25.68	7.630×10^{-3}																			
2	83.86	2.058×10^{-3}																			
3	174.2	0.901×10^{-3}																			
4	296.5	0.487×10^{-3}																			
5	450.9	0.297×10^{-3}																			
E. Laminar, alternate	$N_{Sh} = 4.36 + \frac{0.023(d_t/L)N_{Re}N_{Sc}}{1 + 0.0012(d_t/L)N_{Re}N_{Sc}}$	[T] $N_{Sh} = \frac{k'd_t}{D}$, Use log mean concentration difference. $N_{Re} < 2100$	[77] p. 176																		
F. Laminar, fully developed concentration and velocity profile	$N_{Sh} = \frac{k'd_t}{D} = \frac{48}{11} = 4.3636$	[T] Use log mean concentration difference. $N_{Re} < 2100$	[141] p. 167																		
G. Vertical tubes, laminar flow, forced and natural convection	$N_{Sh,avg} = 1.62N_{Gz}^{1/3} \left[1 \pm 0.0742 \frac{(N_{Gr}N_{Sc}d/L)^{3/4}}{N_{Gz}} \right]^{1/3}$	[T] Approximate solution. Use minus sign if forced and natural convection oppose each other. Good agreement with experiment. $N_{Gz} = \frac{N_{Re}N_{Sc}d}{L}$, $N_{Gr} = \frac{g\Delta\rho d^3}{\rho\nu^2}$	[127]																		
H. Hollow-fiber extraction inside fibers	$N_{Sh} = 0.5N_{Gz}$, $N_{Gz} < 6$ $N_{Sh} = 1.62N_{Gz}^{0.5}$, $N_{Gz} \geq 6$	[E] Use arithmetic concentration difference.	[41]																		
I. Tubes, laminar, RO systems	$N_{Sh,avg} = \frac{k'_m d_t}{D} = 1.632 \left(\frac{ud_t^2}{DL} \right)^{1/3}$	Use arithmetic concentration difference. Thin concentration polarization layer, not fully developed. $N_{Re} < 2000$, L = length tube.	[40]																		
J. Tubes and parallel plates, laminar RO	Graphical solutions for concentration polarization. Uniform velocity through walls.	[T]	[137]																		
K. Rotating annulus for reverse osmosis	For nonvortical flow: $N_{Sh} = 2.15 \left[N_{Tb} \left(\frac{d}{r_i} \right)^{0.5} \right]^{0.18} N_{Sc}^{1/3}$ For vortical flow: $N_{Sh} = 1.05 \left[N_{Tb} \left(\frac{d}{r_i} \right)^{0.5} \right]^{1/3} N_{Sc}^{1/3}$	[E,S] N_{Tb} = Taylor number = $r_i \omega d / \nu$ r_i = inner cylinder radius ω = rotational speed, rad/s d = gap width between cylinders	[100]																		

TABLE 5-19 Mass-Transfer Correlations for Flow in Pipes and Ducts—Transfer Is from Wall to Fluid (Continued)

Situation	Correlation	Comments E = Empirical, S = Semiempirical, T = Theoretical	References°
L. Parallel plates, laminar, parabolic velocity, developing concentration profile, constant wall concentration	Graphical solution	[T] Low transfer rates.	[141] p. 176
L'. 5-19-L, fully developed	$N_{Sh} = \frac{k'(2h)}{D} = 7.6$	[T] h = distance between plates. Use log mean concentration difference. $\frac{N_{Re} N_{Sc}}{x/(2h)} < 20$	[141] p. 177
M. Parallel plates, laminar, parabolic velocity, developing concentration profile, constant mass flux at wall	Graphical solution	[T] Low transfer rates.	[141] p. 176
N. 5-19-M, fully developed	$N_{Sh} = \frac{k'(2h)}{D} = 8.23$	[T] Use log mean concentration difference. $\frac{N_{Re} N_{Sc}}{x/(2h)} < 20$	[141] p. 177
O. Laminar flow, vertical parallel plates, forced and natural convection	$N_{Sh,avg} = 1.47 N_{Gz}^{1/3} \left[1 \pm 0.0989 \frac{(N_{Gr} N_{Sc} h/L)^{3/4}}{N_{Gz}} \right]^{1/3}$	[T] Approximate solution. Use minus sign if forced and natural convection oppose each other. Good agreement with experiment. $N_{Gz} = \frac{N_{Re} N_{Sc} h}{L}, N_{Gr} = \frac{g \Delta \rho h^3}{\rho \nu^2}$	[127]
P. Parallel plates, laminar, RO systems	$N_{Sh,avg} = \frac{k'(2H_p)}{D} = 2.354 \left(\frac{u H_p^2}{DL} \right)^{1/3}$	Thin concentration polarization layer. Short tubes, concentration profile not fully developed. Use arithmetic concentration difference.	[40]
Q. Tubes, turbulent	$N_{Sh,avg} = \frac{k'_m d_t}{D} = 0.023 N_{Re}^{0.83} N_{Sc}^{1/3}$ $2100 < N_{Re} < 35,000$ $0.6 < N_{Sc} < 3000$ $N_{Sh,avg} = \frac{k'_m d_t}{D} = 0.023 N_{Re}^{0.83} N_{Sc}^{0.44}$ $2000 < N_{Re} < 35,000$ $0.6 < N_{Sc} < 2.5$	[E] Use with log mean concentration difference at two ends of tube. Good fit for liquids. From wetted wall column and dissolution data—see Table 5-18-B. [E] Evaporation of liquids. Use with log mean concentration difference. Better fit for gases.	[77] p. 181 [103] [152] p. 72 [68][77] p. 181 [88] p. 112 [138] p. 211
R. Tubes, turbulent	$N_{Sh} = \frac{k' d_t}{D} = 0.0096 N_{Re}^{0.913} N_{Sc}^{0.346}$	[E] $430 < N_{Sc} < 100,000$. Dissolution data. Use for high N_{Sc} .	[105] p. 668
S. Tubes, turbulent, smooth tubes, Reynolds analogy	$N_{Sh} = \frac{k' d_t}{D} = \left(\frac{f}{2} \right) N_{Re} N_{Sc}$ f = Fanning friction factor	[T] Use arithmetic concentration difference. N_{Sc} near 1.0 Turbulent core extends to wall. Of limited utility.	[66] p. 474 [77] p. 171 [141] p. 239 [149] p. 250
T. Tubes, turbulent, smooth tubes, Chilton-Colburn analogy	$j_D = j_H \leq \frac{f}{2}$ If $\frac{f}{2} = 0.023 N_{Re}^{-0.2}, j_D = \frac{N_{Sh}}{N_{Re} N_{Sc}^{1/3}} = 0.023 N_{Re}^{-0.2}$ $N_{Sh} = \frac{k' d_t}{D}$, Sec. 5-17-G $j_D = j_H = f(N_{Re}, \text{ geometry and B.C.})$	[E] Use log-mean concentration difference. Relating j_D to $f/2$ approximate. N_{Re} and N_{Sc} near 1.0. Low concentration. Results about 20% lower than experiment. $3 \times 10^4 < N_{Re} < 10^6$ [E] Good over wide ranges.	[39] pp. 400, 647 [51][53] [141] p. 264 [149] p. 251 [66] p. 475 [39] p. 647 [51]
U. Tubes, turbulent, smooth tubes, constant surface concentration, Prandtl analogy	$N_{Sh} = \frac{k' d_t}{D} = \frac{(f/2) N_{Re} N_{Sc}}{1 + 5\sqrt{f/2}(N_{Sc} - 1)}$ $\frac{f}{2} = 0.04 N_{Re}^{-0.25}$	[T] Use arithmetic concentration difference. Improvement over Reynolds analogy. Best for N_{Sc} near 1.0.	[77] p. 173 [141] p. 241

TABLE 5-19 Mass-Transfer Correlations for Flow in Pipes and Ducts—Transfer Is from Wall to Fluid (Concluded)

Situation	Correlation	Comments E = Empirical, S = Semiempirical, T = Theoretical	References*
V. Tubes, turbulent, smooth tubes, Constant surface concentration, Von Karman analogy	$N_{Sh} = \frac{(f/2)N_{Re}N_{Sc}}{1 + 5\sqrt{f/2} \left\{ (N_{Sc} - 1) + \ln \left[1 + \frac{5}{6}(N_{Sc} - 1) \right] \right\}}$ $\frac{f}{2} = 0.04 N_{Re}^{-0.25}$	[T] Use arithmetic concentration difference. $N_{Sh} = k'd_t/D$. Improvement over Prandtl, $N_{Sc} < 25$.	[77] p. 173 [141] p. 243 [149] p. 250 [154]
W. Tubes, turbulent, smooth tubes, constant surface concentration	For $0.5 < N_{Sc} < 10$: $N_{Sh,avg} = 0.0097 N_{Re}^{9/10} N_{Sc}^{1/2} \times (1.10 + 0.44 N_{Sc}^{-1/3} - 0.70 N_{Sc}^{-1/6})$ For $10 < N_{Sc} < 1000$: $N_{Sh,avg}$ $= \frac{0.0097 N_{Re}^{9/10} N_{Sc}^{1/2} (1.10 + 0.44 N_{Sc}^{-1/3} - 0.70 N_{Sc}^{-1/6})}{1 + 0.064 N_{Sc}^{1/2} (1.10 + 0.44 N_{Sc}^{-1/3} - 0.70 N_{Sc}^{-1/6})}$ For $N_{Sc} > 1000$: $N_{Sh,avg} = 0.0102 N_{Re}^{9/10} N_{Sc}^{1/3}$	[S] Use arithmetic concentration difference. Based on partial fluid renewal and an infrequently replenished thin fluid layer for high N_{Sc} . Good fit to available data. $N_{Re} = \frac{u_{bulk} d_t}{\nu}$ $N_{Sh,avg} = \frac{k'_{avg} d_t}{D}$	[77] p. 179 [117]
X. Turbulent flow, tubes	$N_{St} = \frac{N_{Sh}}{N_{Pe}} = \frac{N_{Sh}}{N_{Re} N_{Sc}} = 0.0149 N_{Re}^{-0.12} N_{Sc}^{-2/3}$	[E] Smooth pipe data. Data fits within 4% except at $N_{Sc} > 20,000$, where experimental data is underpredicted. $N_{Sc} > 100$, $10^5 > N_{Re} > 2100$	[107]
Y. Turbulent flow, noncircular ducts	Use correlations with $d_{eq} = \frac{4 \text{ cross-sectional area}}{\text{wetted perimeter}}$	Can be suspect for systems with sharp corners. Parallel plates: $d_{eq} = 4 \frac{2hw}{2w + 2h}$	[141] p. 289
Z. Decaying swirling flow in pipe	$N_{Sh,avg} = 0.3508 N_{Sc}^{1/2} N_{Re}^{0.759} (x/d)^{-0.400} \times (1 + \tan\theta)^{0.271}$ $N_{Re} = 1730 \text{ to } 8650, N_{Sc} = 1692$	[E,S] x = axial distance, d = diameter, θ = vane angle (15° to 60°) Regression coefficient = 0.9793. Swirling increases mass transfer.	[161]

*See the beginning of the "Mass Transfer" subsection for references.

Effects of Total Pressure on k_C and k_L . The influence of total system pressure on the rate of mass transfer from a gas to a liquid or to a solid has been shown to be the same as would be predicted from stagnant-film theory as defined in Eq. (5-298), where

$$\hat{k}_C = D_{AB} p_T / RT \delta_C \quad (5-305)$$

Since the quantity $D_{AB} p_T$ is known to be relatively independent of the pressure, it follows that the rate coefficients \hat{k}_C , $k_C y_{BM}$, and $K_C p_T y_{BM}$ ($= k_C p_{BM}$) do not depend on the total pressure of the system, subject to the limitations discussed later.

Investigators of tower packings normally report $k'_C a$ values measured at very low inlet-gas concentrations, so that $y_{BM} = 1$, and at total pressures close to 100 kPa (1 atm). Thus, the correct rate coefficient for use in packed-tower designs involving the use of the driving force $(y - y_i)/y_{BM}$ is obtained by multiplying the reported $k'_C a$ values by the value of p_T employed in the actual test unit (e.g., 100 kPa) and *not* the total pressure of the system to be designed.

From another point of view one can correct the reported values of $k'_C a$ in $\text{kmol}/[(s \cdot \text{m}^3)(\text{kPa})]$, valid for a pressure of 101.3 kPa (1 atm), to some other pressure by dividing the quoted values of $k'_C a$ by the design pressure and multiplying by 101.3 kPa, i.e., $(k'_C a \text{ at design pressure } p_T) = (k'_C a \text{ at } 1 \text{ atm}) \times 101.3/p_T$.

One way to avoid a lot of confusion on this point is to convert the experimentally measured $k'_C a$ values to values of $\hat{k}_C a$ straightaway, before beginning the design calculations. A design based on the rate coefficient $\hat{k}_C a$ and the driving force $(y - y_i)/y_{BM}$ will be independent of the total system pressure with the following limitations: caution should be employed in assuming that $\hat{k}_C a$ is independent of total pressure for systems having significant vapor-phase non-idealities, for systems that operate in the vicinity of the critical

point, or for total pressures higher than about 3040 to 4050 kPa (30 to 40 atm).

Experimental confirmations of the relative independence of \hat{k}_C with respect to total pressure have been widely reported. Deviations do occur at extreme conditions. For example, Bretsznajder (*Prediction of Transport and Other Physical Properties of Fluids*, Pergamon Press, Oxford, 1971, p. 343) discusses the effects of pressure on the $D_{AB} p_T$ product and presents experimental data on the self-diffusion of CO_2 which show that the D - p product begins to decrease at a pressure of approximately 8100 kPa (80 atm). For reduced temperatures higher than about 1.5, the deviations are relatively modest for pressures up to the critical pressure. However, deviations are large near the critical point (see also p. 5-52). The effect of pressure on the gas-phase viscosity is also negligible for pressures below about 5060 kPa (50 atm).

For the liquid-phase mass-transfer coefficient k_L , the effects of total system pressure can be ignored for all practical purposes. Thus, when using \hat{k}_C and \hat{k}_L for the design of gas absorbers or strippers, the primary pressure effects to consider will be those which affect the equilibrium curves and the values of m . If the pressure changes affect the hydrodynamics, then \hat{k}_C , \hat{k}_L , and a can all change significantly.

Effects of Temperature on k_C and k_L . The Stanton-number relationship for gas-phase mass transfer in packed beds, Eq. (5-301), indicates that for a given system geometry the rate coefficient \hat{k}_C depends only on the Reynolds number and the Schmidt number. Since the Schmidt number for a gas is approximately independent of temperature, the principal effect of temperature upon \hat{k}_C arises from changes in the gas viscosity with changes in temperature. For normally encountered temperature ranges, these effects will be small owing to the fractional powers involved in Reynolds-number terms (see Tables 5-17 to 5-24). It thus can be concluded that for all

TABLE 5-20 Mass-Transfer Correlations for Flow Past Submerged Objects

Situation	Correlation	Comments E = Empirical, S = Semiempirical, T = Theoretical	References ^a												
A. Single sphere	$N_{Sh} = \frac{k'_C p_{BLM} R T d_s}{PD} = \frac{2r}{r - r_s}$ <table border="1" style="margin-left: auto; margin-right: auto;"> <tr> <td>r/r_s</td> <td>2</td> <td>5</td> <td>10</td> <td>50</td> <td>∞ (asymptotic limit)</td> </tr> <tr> <td>N_{Sh}</td> <td>4.0</td> <td>2.5</td> <td>2.22</td> <td>2.04</td> <td>2.0</td> </tr> </table>	r/r_s	2	5	10	50	∞ (asymptotic limit)	N_{Sh}	4.0	2.5	2.22	2.04	2.0	[T] Use with log mean concentration difference. r = distance from sphere, r_s , d_s = radius and diameter of sphere. No convection.	[141] p. 18
r/r_s	2	5	10	50	∞ (asymptotic limit)										
N_{Sh}	4.0	2.5	2.22	2.04	2.0										
B. Single sphere, creeping flow with forced convection	$N_{Sh} = \frac{k'd}{D} = [4.0 + 1.21(N_{Re} N_{Sc})^{2/3}]^{1/2}$ $N_{Sh} = \frac{k'd}{D} = a(N_{Re} N_{Sc})^{1/3}$ $a = 1.00 \pm 0.01$	[T] Use with log mean concentration difference. Average over sphere. Numerical calculations. ($N_{Re} N_{Sc}$) < 10,000 N_{Re} < 1.0. Constant sphere diameter. Low mass-transfer rates. [T] Fit to above ignoring molecular diffusion. 1000 < ($N_{Re} N_{Sc}$) < 10,000.	[46][88] p. 114 [105] [138] p. 214 [101] p. 80 [138] p. 215												
C. Single spheres, molecular diffusion, and forced convection, low flow rates	$N_{Sh} = 2.0 + AN_{Re}^{1/2} N_{Sc}^{1/3}$ $A = 0.5 \text{ to } 0.62$ <p style="margin-left: 40px;">$A = 0.60.$</p> <p style="margin-left: 40px;">$A = 0.95.$</p> <p style="margin-left: 40px;">$A = 0.95.$</p> <p style="margin-left: 40px;">$A = 0.544.$</p>	[E] Use with log mean concentration difference. Average over sphere. Frössling Eq. ($A = 0.552$), $2 \leq N_{Re} \leq 800$, $0.6 \leq N_{Sc} \leq 2.7$. N_{Sh} lower than experimental at high N_{Re} . [E] Ranz and Marshall $2 \leq N_{Re} \leq 200$, $0.6 \leq N_{Sc} \leq 2.5$. Modifications recommended [110] See also Table 5-23-O. [E] Liquids $2 \leq N_{Re} \leq 2,000$. Graph in Ref. 138, p. 217–218. [E] $100 \leq N_{Re} \leq 700$; $1,200 \leq N_{Sc} \leq 1525$. [E] Use with arithmetic concentration difference. $N_{Sc} = 1$; $50 \leq N_{Re} \leq 350$.	[39] [77], p. 194 [88] p. 114 [141] p. 276 [39] p. 409, 647 [121] [110] [138] p. 217 [141] p. 276 [65][66] p. 482 [138] p. 217 [126][141] p. 276 [81][141] p. 276												
D. Same as 5-20-C	$N_{Sh} = \frac{k'd_s}{D} = 2.0 + 0.575 N_{Re}^{1/2} N_{Sc}^{0.35}$	[E] Use with log mean concentration difference. $N_{Sc} \leq 1$, $N_{Re} < 1$.	[70][141] p. 276												
E. Same as 5-20-C	$N_{Sh} = \frac{k'd_s}{D} = 2.0 + 0.552 N_{Re}^{0.53} N_{Sc}^{1/3}$	[E] Use with log mean concentration difference. $1.0 < N_{Re} \leq 48,000$ Gases: $0.6 \leq N_{Sc} \leq 2.7$.	[66] p. 482												
F. Single spheres, forced concentration, any flow rate	$N_{Sh} = \frac{k'_L d_s}{D} = 2.0 + 0.59 \left[\frac{E^{1/3} d_p^{4/3} \rho}{\mu} \right]^{0.57} N_{Sc}^{1/3}$ <p style="margin-left: 40px;">Energy dissipation rate per unit mass of fluid (ranges $570 < N_{Sc} < 1420$):</p> $E = \left(\frac{C_{Dr}}{2} \right) \left(\frac{v_r^3}{d_p} \right) \frac{m^2}{s^3}$	[S] Correlates large amount of data and compares to published data. v_r = relative velocity between fluid and sphere, m/s. C_{Dr} = drag coefficient for single particle fixed in fluid at velocity v_r . See 5-23-F for calculation details and applications. $2 < \left(\frac{E^{1/3} d_p^{4/3} \rho}{\mu} \right) < 63,000$	[108]												
G. Single spheres, forced convection, high flow rates, ignoring molecular diffusion	$N_{Sh} = \frac{k'd_s}{D} = 0.347 N_{Re}^{0.62} N_{Sc}^{1/3}$ $N_{Sh} = \frac{k'd_s}{D} = 0.33 N_{Re}^{0.6} N_{Sc}^{1/3}$ $N_{Sh} = \frac{k'd_s}{D} = 0.43 N_{Re}^{0.56} N_{Sc}^{1/3}$ $N_{Sh} = \frac{k'd_s}{D} = 0.692 N_{Re}^{0.514} N_{Sc}^{1/3}$	[E] Use with arithmetic concentration difference. Liquids, $2000 < N_{Re} < 17,000$. High N_{Sc} , graph in Ref. 138, p. 217–218. [E] $1500 \leq N_{Re} \leq 12,000$. [E] $200 \leq N_{Re} \leq 4 \times 10^4$, “air” $\leq N_{Sc} \leq$ “water.” [E] $500 \leq N_{Re} \leq 5000$.	[66] p. 482 [147] [138] p. 217 [141] p. 276 [141] p. 276 [112] [141] p. 276												
H. Single sphere immersed in bed of smaller particles. For gases.	$N_{Sh,avg} = \frac{k d_1}{D'} = \epsilon \left[4 + \frac{4}{5} N_{Pe'}^{2/3} + \frac{4}{\pi} N_{Pe'} \right] \left(1 + \frac{1}{9} N_{Pe'} \right)^{1/2}$ <p style="margin-left: 40px;">Limit $N_{Pe'} \rightarrow 0, N_{Sh,avg} = 2\epsilon$</p>	[T] Compared to experiment. $N_{Pe'} = \frac{u_c d_1}{D'}$, $D' = D/\tau$, D = molecular diffusivity, d_1 = diameter large particle, τ = tortuosity. Arithmetic conc. difference fluid flow in inert bed follows Darcy's law.	[71]												
I. Single cylinders, perpendicular flow	$N_{Sh} = \frac{k'd_s}{D} = AN_{Re}^{1/2} N_{Sc}^{1/3}, A = 0.82$ <p style="margin-left: 40px;">$A = 0.74$</p> <p style="margin-left: 40px;">$A = 0.582$</p> $\hat{j}_D = 0.600(N_{Re})^{-0.487}$ $N_{Sh} = \frac{k'd_{cyl}}{D}$	[E] $100 < N_{Re} \leq 3500$, $N_{Sc} = 1560$. [E] $120 \leq N_{Re} \leq 6000$, $N_{Sc} = 2.44$. [E] $300 \leq N_{Re} \leq 7600$, $N_{Sc} = 1200$. [E] Use with arithmetic concentration difference. $50 \leq N_{Re} \leq 50,000$; gases, $0.6 \leq N_{Sc} \leq 2.6$; liquids; $1000 \leq N_{Sc} \leq 3000$. Data scatter $\pm 30\%$.	[141] p. 276 [141] p. 276 [142] [141] p. 276 [66] p. 486												

5-70 HEAT AND MASS TRANSFER

TABLE 5-20 Mass-Transfer Correlations for Flow Past Submerged Objects (Concluded)

Situation	Correlation	Comments E = Empirical, S = Semiempirical, T = Theoretical	References ^o
J. Rotating cylinder in an infinite liquid, no forced flow	$j_D = \frac{k'}{v} N_{Sc}^{0.644} = 0.0791 N_{Re}^{-0.30}$ <p>Results presented graphically to $N_{Re} = 241,000$.</p> $N_{Re} = \frac{v d_{cyl} \rho}{\mu} \text{ where } v = \frac{\omega d_{cyl}}{2} = \text{peripheral velocity}$	<p>[E] Used with arithmetic concentration difference. Useful geometry in electrochemical studies.</p> <p>$112 < N_{Re} \leq 100,000$. $835 < N_{Sc} < 11490$</p> <p>k' = mass-transfer coefficient, cm/s; ω = rotational speed, radian/s.</p>	<p>[60]</p> <p>[138] p. 238</p>
K. Stationary or rotating cylinder for air	<p>Stationary:</p> $N_{Sh,avg} = AN_{Re}^c Sc^{1/3}$ <p>$2.0 \times 10^4 \leq N_{Re} \leq 2.5 \times 10^5$; $d/H = 0.3$, $Tu = 0.6\%$</p> <p>$A = 0.0539$, $c = 0.771$ [114]</p> <p>A and c depend on geometry [37]</p> <p>Rotating in still air:</p> $N_{Sh,avg} = 0.169 N_{Re, \omega}^{2/3}$ <p>$1.0E4 \leq N_{Re, \omega} \leq 1.0E5$; $N_{Sc} \approx 2.0$; $N_{Gr} \approx 2.0 \times 10^6$</p>	<p>[E] Reasonable agreement with data of other investigators. d = diameter of cylinder; H = height of wind tunnel, Tu of = turbulence level, $N_{Re, \omega}$ = rotational Reynold's number = $u_{\omega} d \rho / \mu$, u_{ω} = cylinder surface velocity. Also correlations for two-dimensional slot jet flow [114]. For references to other correlations see [37].</p>	<p>[37]</p> <p>[114]</p>
L. Oblate spheroid, forced convection	$j_D = \frac{N_{Sh}}{N_{Re} N_{Sc}^{1/3}} = 0.74 N_{Re}^{-0.5}$ $N_{Re} = \frac{d_{ch} v \rho}{\mu}, d_{ch} = \frac{\text{total surface area}}{\text{perimeter normal to flow}}$ <p>e.g., for cube with side length a, $d_{ch} = 1.27a$.</p> $N_{Sh} = \frac{k' d_{ch}}{D}$	<p>[E] Used with arithmetic concentration difference.</p> <p>$120 \leq N_{Re} \leq 6000$; standard deviation 2.1%.</p> <p>Eccentricities between 1:1 (spheres) and 3:1. Oblate spheroid is often approximated by drops.</p>	<p>[141] p. 284</p> <p>[142]</p>
M. Other objects, including prisms, cubes, hemispheres, spheres, and cylinders; forced convection	$j_D = 0.692 N_{Re,p}^{-0.486}, N_{Re,p} = \frac{v d_{ch} \rho}{\mu}$ <p>Terms same as in 5-20-J.</p>	<p>[E] Used with arithmetic concentration difference. Agrees with cylinder and oblate spheroid results, $\pm 15\%$. Assumes molecular diffusion and natural convection are negligible.</p> <p>$500 \leq N_{Re,p} \leq 5000$. Turbulent.</p>	<p>[88] p. 115</p> <p>[141] p. 285</p> <p>[111] [112]</p>
N. Other objects, molecular diffusion limits	$N_{Sh} = \frac{k' d_{ch}}{D} = A$	<p>[T] Use with arithmetic concentration difference. Hard to reach limits in experiments. Spheres and cubes $A = 2$, tetrahedrons $A = 2\sqrt{6}$ octahedrons $2\sqrt{2}$.</p>	<p>[88] p. 114</p>
O. Shell side of microporous hollow fiber module for solvent extraction	$N_{Sh} = \beta [d_h (1 - \phi) / L] N_{Re}^{0.6} N_{Sc}^{0.33}$ $N_{Sh} = \frac{\bar{K} d_h}{D}$ $N_{Re} = \frac{d_h v \rho}{\mu}, \bar{K} = \text{overall mass-transfer coefficient}$ <p>$\beta = 5.8$ for hydrophobic membrane.</p> <p>$\beta = 6.1$ for hydrophilic membrane.</p>	<p>[E] Use with logarithmic mean concentration difference.</p> <p>d_h = hydraulic diameter</p> $= \frac{4 \times \text{cross-sectional area of flow}}{\text{wetted perimeter}}$ <p>ϕ = packing fraction of shell side. L = module length.</p> <p>Based on area of contact according to inside or outside diameter of tubes depending on location of interface between aqueous and organic phases. Can also be applied to gas-liquid systems with liquid on shell side.</p>	<p>[118]</p>

See Table 5-23 for flow in packed beds.

^oSee the beginning of the "Mass Transfer" subsection for references.

TABLE 5-21 Mass-Transfer Correlations for Drops, Bubbles, and Bubble Columns

Conditions	Correlations	Comments E = Empirical, S = Semiempirical, T = Theoretical	References*																																																	
A. Single liquid drop in immiscible liquid, drop formation, discontinuous (drop) phase coefficient	$\hat{k}_{d,f} = A \left(\frac{\rho_d}{M_d} \right)_{av} \left(\frac{D_d}{\pi t_f} \right)^{1/2}$ $A = \frac{24}{7} \text{ (penetration theory)}$ $A = 1.31 \text{ (semiempirical value)}$ $A = \left[\frac{24}{7} (0.8624) \right] \text{ (extension by fresh surface elements)}$	<p>[T,S] Use arithmetic mole fraction difference.</p> <p>Fits some, but not all, data. Low mass transfer rate. M_d = mean molecular weight of dispersed phase; t_f = formation time of drop. $k_{L,d}$ = mean dispersed liquid phase M.T. coefficient kmole/[s·m² (mole fraction)].</p>	[141] p. 399																																																	
B. Same as 5-21-A	$\hat{k}_{d,f} = 0.0432$ $\times \frac{d_p}{t_f} \left(\frac{\rho_d}{M_d} \right)_{av} \left(\frac{u_o}{d_p g} \right)^{0.089} \left(\frac{d_p^2}{t_f D_d} \right)^{-0.334} \left(\frac{\mu_d}{\sqrt{\rho_d d_p \sigma g_c}} \right)^{-0.601}$	<p>[E] Use arithmetic mole fraction difference. Based on 23 data points for 3 systems. Average absolute deviation 26%. Use with surface area of drop after detachment occurs. u_o = velocity through nozzle; σ = interfacial tension.</p>	[141] p. 401 [144] p. 434																																																	
C. Single liquid drop in immiscible liquid, drop formation, continuous phase coefficient	$\hat{k}_{c,f} = 4.6 \left(\frac{\rho_c}{M_c} \right)_{av} \sqrt{\frac{D_c}{\pi t_f}}$	<p>[T] Use arithmetic mole fraction difference. Based on rate of bubble growth away from fixed orifice. Approximately three times too high compared to experiments.</p>	[141] p. 402																																																	
D. Same as 5-21-C	$k_{L,c} = 0.386$ $\times \left(\frac{\rho_c}{M_c} \right)_{av} \left(\frac{D_c}{t_f} \right)^{0.5} \left(\frac{\rho_c \sigma g_c}{\Delta \rho g t_f \mu_c} \right)^{0.407} \left(\frac{g t_f^2}{d_p} \right)^{0.148}$	<p>[E] Average absolute deviation 11% for 20 data points for 3 systems.</p>	[141] p. 402 [144] p. 434																																																	
E. Single liquid drop in immiscible liquid, free rise or fall, discontinuous phase coefficient, stagnant drops	$k_{L,d,m} = \frac{-d_p}{6t} \left(\frac{\rho_d}{M_d} \right)_{av} \ln \left[\frac{6}{\pi^2} \sum_{j=1}^{\infty} \frac{1}{j^2} \exp \left[\left(\frac{-D_d j^2 \pi^2 t}{(d_p/2)^2} \right) \right] \right]$	<p>[T] Use with log mean mole fraction differences based on ends of column. t = rise time. No continuous phase resistance. Stagnant drops are likely if drop is very viscous, quite small, or is coated with surface active agent. $k_{L,d,m}$ = mean dispersed liquid M.T. coefficient.</p>	[141] p. 404 [144] p. 435																																																	
F. Same as 5-21-E	$\hat{k}_{L,d,m} = \frac{-d_p}{6t} \left(\frac{\rho_d}{M_d} \right)_{av} \ln \left[1 - \frac{\pi D_d^{1/2} t^{1/2}}{d_p/2} \right]$	<p>[S] See 5-21-E. Approximation for fractional extractions less than 50%.</p>	[141] p. 404 [144] p. 435																																																	
G. Same as 5-21-E, continuous phase coefficient, stagnant drops, spherical	$N_{Sh} = \frac{k_{L,c,m} d_c}{D_c} = 0.74 \left(\frac{\rho_c}{M_c} \right)_{av} N_{Re}^{1/2} (N_{Sc,c})^{1/3}$	<p>[E] $N_{Re} = \frac{v_s d_p \rho_c}{\mu_c}$, v_s = slip velocity between drop and continuous phase.</p>	[141] p. 407 [142][144] p. 436																																																	
H. Single bubble or drop with surfactant. Stokes flow.	$N_{Sh} = 2.0 + \alpha N_{Pe,s}^{\beta}, N_{Sh} = 2r\kappa/D$ $\alpha = \frac{5.49}{A + 6.10} + \frac{A}{A + 28.64}$ $\beta = \frac{0.35A + 17.21}{A + 34.14}$ <p>$2r = 2$ to $50 \mu\text{m}$, $A = 2.8\text{E}4$ to $7.0\text{E}5$ $0.0026 < N_{Pe,s} < 340$, $2.1 < N_{Ma} < 1.3\text{E}6$ $N_{Pe} = 1.0$ to 2.5×10^4, $N_{Re} = 2.2 \times 10^{-6}$ to 0.034</p>	<p>[T] A = surface retardation parameter $A = B\Gamma_o r / \mu D_s = N_{Ma} N_{Pe,s}$ $N_{Ma} = B\Gamma_o / \mu u$ = Marangoni no. Γ = surfactant surface conc. $N_{Pe,s}$ = surface Peclet number = ur/D_s, D_s = surface diffusivity N_{Pe} = bulk Peclet number For $A \gg 1$ acts like rigid sphere: $\beta \rightarrow 0.35$, $\alpha \rightarrow 1/2864 = 0.035$</p>	[120]																																																	
I. 5-21-E, oblate spheroid	$N_{Sh} = \frac{k_{L,c,m} d_3}{D_c} = 0.74 \left(\frac{\rho_c}{M_c} \right)_{av} (N_{Re,3})^{1/2} (N_{Sc,c})^{1/3}$ $N_{Re,3} = \frac{v_s d_3 \rho_c}{\mu_c}$	<p>[E] Used with log mean mole fraction. Differences based on ends of extraction column; 100 measured values $\pm 2\%$ deviation. Based on area oblate spheroid. v_s = slip velocity, $d_3 = \frac{\text{total drop surface area}}{\text{perimeter normal to flow}}$</p>	[141] p. 285, 406, 407																																																	
J. Single liquid drop in immiscible liquid, Free rise or fall, discontinuous phase coefficient, circulating drops	$k_{d,circ} = -\frac{d_p}{6\theta} \ln \left[\frac{3}{8} \sum_{j=1}^{\infty} B_j^2 \exp \left(-\frac{\lambda_j 64 D_d \theta}{d_p^2} \right) \right]$ <p style="text-align: center;">Eigenvalues for Circulating Drop</p> <table border="1" style="width: 100%; border-collapse: collapse;"> <thead> <tr> <th>$k_d d_p / D_d$</th> <th>λ_1</th> <th>λ_2</th> <th>λ_3</th> <th>B_1</th> <th>B_2</th> <th>B_3</th> </tr> </thead> <tbody> <tr> <td>3.20</td> <td>0.262</td> <td>0.424</td> <td></td> <td>1.49</td> <td>0.107</td> <td></td> </tr> <tr> <td>10.7</td> <td>0.680</td> <td>4.92</td> <td></td> <td>1.49</td> <td>0.300</td> <td></td> </tr> <tr> <td>26.7</td> <td>1.082</td> <td>5.90</td> <td>15.7</td> <td>1.49</td> <td>0.495</td> <td>0.205</td> </tr> <tr> <td>107</td> <td>1.484</td> <td>7.88</td> <td>19.5</td> <td>1.39</td> <td>0.603</td> <td>0.384</td> </tr> <tr> <td>320</td> <td>1.60</td> <td>8.62</td> <td>21.3</td> <td>1.31</td> <td>0.583</td> <td>0.391</td> </tr> <tr> <td>∞</td> <td>1.656</td> <td>9.08</td> <td>22.2</td> <td>1.29</td> <td>0.596</td> <td>0.386</td> </tr> </tbody> </table>	$k_d d_p / D_d$	λ_1	λ_2	λ_3	B_1	B_2	B_3	3.20	0.262	0.424		1.49	0.107		10.7	0.680	4.92		1.49	0.300		26.7	1.082	5.90	15.7	1.49	0.495	0.205	107	1.484	7.88	19.5	1.39	0.603	0.384	320	1.60	8.62	21.3	1.31	0.583	0.391	∞	1.656	9.08	22.2	1.29	0.596	0.386	<p>[T] Use with arithmetic concentration difference.</p> <p>θ = drop residence time. A more complete listing of eigenvalues is given by Refs. 62 and 76.</p> <p>$k_{L,d,circ}$ is m/s.</p>	[62][76][141] p. 405 [152] p. 523
$k_d d_p / D_d$	λ_1	λ_2	λ_3	B_1	B_2	B_3																																														
3.20	0.262	0.424		1.49	0.107																																															
10.7	0.680	4.92		1.49	0.300																																															
26.7	1.082	5.90	15.7	1.49	0.495	0.205																																														
107	1.484	7.88	19.5	1.39	0.603	0.384																																														
320	1.60	8.62	21.3	1.31	0.583	0.391																																														
∞	1.656	9.08	22.2	1.29	0.596	0.386																																														

5-72 HEAT AND MASS TRANSFER

TABLE 5-21 Mass-Transfer Correlations for Drops, Bubbles, and Bubble Columns (Continued)

Conditions	Correlations	Comments E = Empirical, S = Semiempirical, T = Theoretical	References°
K. Same as 5-21-J	$\hat{k}_{L,d,circ} = -\frac{d_p}{6\theta} \left(\frac{\rho_d}{M_d}\right)_{av} \ln \left[1 - \frac{R^{1/2} \pi D_d^2 \theta^{1/2}}{d_p/2} \right]$	[E] Used with mole fractions for extraction less than 50%, $R \approx 2.25$.	[141] p. 405
L. Same as 5-21-J	$N_{Sh} = \frac{\hat{k}_{L,d,circ} d_p}{D_d}$ $= 31.4 \left(\frac{\rho_d}{M_d}\right)_{av} \left(\frac{4D_d t}{d_p^2}\right)^{-0.34} N_{Sc,d}^{-0.125} \left(\frac{d_p v_s^2 \rho_c}{\sigma g_c}\right)^{-0.37}$	[E] Used with log mean mole fraction difference. d_p = diameter of sphere with same volume as drop. $856 \leq N_{Sc} \leq 79,800$, $2.34 \leq \sigma \leq 4.8$ dynes/cm.	[144] p. 435 [145]
M. Liquid drop in immiscible liquid, free rise or fall, continuous phase coefficient, circulating single drops	$N_{Sh,c} = \frac{k'_{L,c} d_p}{D_c}$ $= \left[2 + 0.463 N_{Re,drop}^{0.484} N_{Sc,c}^{0.330} \left(\frac{d_p g^{1/3}}{D_c^2}\right)^{0.072} \right] F$ $F = 0.281 + 1.615K + 3.73K^2 - 1.874K$ $K = N_{Re,drop}^{1/8} \left(\frac{\mu_c}{\mu_d}\right)^{1/4} \left(\frac{\mu_c v_s}{\sigma g_c}\right)^{1/6}$	[E] Used as an arithmetic concentration difference. $N_{Re,drop} = \frac{d_p v_s \rho_c}{\mu_c}$ Solid sphere form with correction factor F .	[82]
N. Same as 5-21-M, circulating, single drop	$N_{Sh} = \frac{k_{L,c} d_p}{D_c} = 0.6 \left(\frac{\rho_c}{M_c}\right)_{av} N_{Re,drop}^{1/2} N_{Sc,c}^{1/2}$	[E] Used as an arithmetic concentration difference. Low σ .	[141] p. 407
O. Same as 5-21-M, circulating swarm of drops	$k_{L,c} = 0.725 \left(\frac{\rho_c}{M_c}\right)_{av} N_{Re,drop}^{-0.43} N_{Sc,c}^{-0.58} v_s (1 - \phi_d)$	[E] Used as an arithmetic concentration difference. Low σ , disperse-phase holdup of drop swarm. ϕ_d = volume fraction dispersed phase.	[141] p. 407 [144] p. 436
P. Liquid drops in immiscible liquid, free rise or fall, discontinuous phase coefficient, oscillating drops	$N_{Sh} = \frac{k_{L,d,osc} d_p}{D_d}$ $= 0.32 \left(\frac{\rho_d}{M_d}\right)_{av} \left(\frac{4D_d t}{d_p^2}\right)^{-0.14} N_{Re,drop}^{0.68} \left(\frac{\sigma^3 g_c^2 \rho_c^2}{g \mu_c^4 \Delta \rho}\right)^{0.10}$	[E] Used with a log mean mole fraction difference. Based on ends of extraction column. $N_{Re,drop} = \frac{d_p v_s \rho_c}{\mu_c}$, $411 \leq N_{Re} \leq 3114$ d_p = diameter of sphere with volume of drop. Average absolute deviation from data, 10.5%. Low interfacial tension (3.5–5.8 dyn), $\mu_c < 1.35$ centipoise.	[141] p. 406 [144] p. 435 [145]
Q. Same as 5-21-P	$k_{L,d,osc} = \frac{0.00375 v_s}{1 + \mu_d / \mu_c}$	[T] Use with log mean concentration difference. Based on end of extraction column. No continuous phase resistance. $k_{L,d,osc}$ in cm/s, v_s = drop velocity relative to continuous phase.	[138] p. 228 [141] p. 405
R. Single liquid drop in immiscible liquid, range rigid to fully circulating	$N_{Sh,c,rigid} = \frac{k_c d_p}{D_c} = 2.43 + 0.774 N_{Re}^{0.5} N_{Sc}^{0.33} + 0.0103 N_{Re} N_{Sc}^{0.33}$ $N_{Sh,c,fully\ circular} = \left[\frac{2}{\pi^{0.5}} \right] N_{Pe,c}^{0.5}$ Drops in intermediate range: $\frac{N_{Sh,c} - N_{Sh,c,rigid}}{N_{Sh,c,fully\ circular} - N_{Sh,c,rigid}} = 1 - \exp [-(4.18 \times 10^{-3}) N_{Pe,c}^{0.42}]$	[E] Allows for slight effect of wake. Rigid drops: $10^4 < N_{Pe,c} < 10^6$ Circulating drops: $10 < N_{Re} < 1200$, $190 < N_{Sc} < 241,000$, $10^3 < N_{Pe,c} < 10^6$	[146] p. 58
S. Coalescing drops in immiscible liquid, discontinuous phase coefficient	$\hat{k}_{d,coal} = 0.173 \frac{d_p}{t_f} \left(\frac{\rho_d}{M_d}\right)_{av} \left(\frac{\mu_d}{\rho_d D_d}\right)^{-1.115} \times \left(\frac{\Delta \rho g d_p^2}{\sigma g_c}\right)^{1.302} \left(\frac{v_s^2 t_f}{D_d}\right)^{0.146}$	[E] Used with log mean mole fraction difference. 23 data points. Average absolute deviation 25%. t_f = formation time.	[141] p. 408
T. Same as 5-21-S, continuous phase coefficient	$\hat{k}_{c,coal} = 5.959 \times 10^{-4} \left(\frac{\rho}{M}\right)_{av} \times \left(\frac{D_c}{t_f}\right)^{0.5} \left(\frac{\rho_d u_s^3}{g \mu_c}\right)^{0.332} \left(\frac{d_p^2 \rho_c \rho_d v_s^3}{\mu_d \sigma g_c}\right)^{0.525}$	[E] Used with log mean mole fraction difference. 20 data points. Average absolute deviation 22%.	[141] p. 409

TABLE 5-21 Mass-Transfer Correlations for Drops, Bubbles, and Bubble Columns (Continued)

Conditions	Correlations	Comments E = Empirical, S = Semiempirical, T = Theoretical	References°
U. Single liquid drops in gas, gas side coefficient	$\frac{\hat{k}_g M_g d_p P}{D_{gs} \rho_g} = 2 + AN_{Re,g}^{1/2} N_{Sc,g}^{1/3}$ $A = 0.552$ or 0.60 . $N_{Re,g} = \frac{d_p \rho_g v_s}{\mu_g}$	[E] Used for spray drying (arithmetic partial pressure difference). v_s = slip velocity between drop and gas stream. Sometimes written with $M_g P / \rho_g = RT$.	[90] p. 388 [121]
V. Single water drop in air, liquid side coefficient	$k_L = 2 \left(\frac{D_L}{\pi t} \right)^{1/2}$, short contact times $k_L = 10 \frac{D_L}{d_p}$, long contact times	[T] Use arithmetic concentration difference. Penetration theory. t = contact time of drop. Gives plot for $k_C a$ also. Air-water system.	[90] p. 389
W. Single bubbles of gas in liquid, continuous phase coefficient, very small bubbles	$N_{Sh} = \frac{k'_c d_b}{D_c} = 1.0(N_{Re} N_{Sc})^{1/3}$	[T] Solid-sphere Eq. (see Table 5-20-B). $d_b < 0.1$ cm, k'_c is average over entire surface of bubble.	[105] [138] p. 214
X. Same as 5-21-W, medium to large bubbles	$N_{Sh} = \frac{k'_c d_b}{D_c} = 1.13(N_{Re} N_{Sc})^{1/2}$	[T] Use arithmetic concentration difference. Droplet equation: $d_b > 0.5$ cm.	[138] p. 231
Y. Same as 5-21-X	$N_{Sh} = \frac{k'_c d_b}{D_c} = 1.13(N_{Re} N_{Sc})^{1/2} \left[\frac{d_b}{0.45 + 0.2d_b} \right]$ $500 \leq N_{Re} \leq 8000$	[S] Use arithmetic concentration difference. Modification of above (X), $d_b > 0.5$ cm. No effect SAA for $d_p > 0.6$ cm.	[83][138] p. 231
Z. Taylor bubbles in single capillaries (square or circular)	$k_L a = 4.5 \left(\frac{Du_C}{L_{uc}} \right)^{1/2} \frac{1}{d_c}$ Applicable $\left(\frac{u_C + u_L}{L_{slug}} \right)^{0.5} > 3s^{-0.5}$	[E] Air-water L_{uc} = unit cell length, L_{slug} = slug length, d_c = capillary i.d. For most data $k_L a \pm 20\%$.	[153]
AA. Gas-liquid mass transfer in monoliths	$k_L a \approx 0.1 \left(\frac{P}{V} \right)^{1/4}$ P/V = power/volume (kW/m ³), range = 100 to 10,000	[E] Each channel in monolith is a capillary. Results are in expected order of magnitude for capillaries based on 5-21-Z. k_L is larger than in stirred tanks.	[93]
AB. Rising small bubbles of gas in liquid, continuous phase. Calderbank and Moo-Young correlation	$N_{Sh} = \frac{k'_c d_b}{D_c} = 2 + 0.31(N_{Gr})^{1/3} N_{Sc}^{1/3}$, $d_b < 0.25$ cm $N_{Re} = \frac{d_b^3 \rho_C - \rho_L g}{\mu_L D_L} = \text{Raleigh number}$	[E] Use with arithmetic concentration difference. Valid for single bubbles or swarms. Independent of agitation as long as bubble size is constant. Recommended by [136]. Note that $N_{Re} = N_{Gr} N_{Sc}$.	[47][66] p. 451 [88] p. 119 [152] p. 156 [136]
AC. Same as 5-21-AB, large bubbles	$N_{Sh} = \frac{k'_c d_b}{D_c} = 0.42(N_{Gr})^{1/3} N_{Sc}^{1/2}$, $d_b > 0.25$ cm $\frac{\text{Interfacial area}}{\text{volume}} = a = \frac{6 H_g}{d_b}$	[E] Use with arithmetic concentration difference. For large bubbles, k'_c is independent of bubble size and independent of agitation or liquid velocity. Resistance is entirely in liquid phase for most gas-liquid mass transfer. H_g = fractional gas holdup, volume gas/total volume.	[47][66] p. 452 [88] p. 119 [97] p. 249 [136]
AD. Bubbles in bubble columns. Hughmark correlation	$N_{Sh} = \frac{k_L d}{D} = 2 + b N_{Sc}^{0.546} N_{Re}^{0.779} \left(\frac{d_g^{1/3}}{D^{2/3}} \right)^{0.116}$ $b = 0.061$ single gas bubbles; $b = 0.0187$ swarms of bubbles, $V_s = \frac{V_g}{\phi_C} - \frac{V_L}{1 - \phi_C}$	[E] d = bubble diameter Air-liquid. Recommended by [136, 152]. For swarms, calculate N_{Re} with slip velocity V_s . ϕ_C = gas holdup V_G = superficial gas velocity Col. diameter = 0.025 to 1.1 m ρ_L = 776 to 1696 kg/m ³ μ_L = 0.0009 to 0.152 Pa·s	[55] [82] [152] p. 144
AE. Bubbles in bubble column	$k_L a = 0.00315 a_C^{0.59} \mu_{\text{eff}}^{-0.84}$	[E] Recommended by [136].	[57]

TABLE 5-21 Mass-Transfer Correlations for Drops, Bubbles, and Bubble Columns (Concluded)

Conditions	Correlations	Comments E = Empirical, S = Semiempirical, T = Theoretical	References*
AF. Bubbles in bubble column	$k_L = \frac{0.15D}{d_{Vs}} \left(\frac{v}{D} \right)^{1/2} N_{Re}^{3/4}$	[E] d_{Vs} = Sauter mean bubble diameter, $N_{Re} = d_{Vs} u_G \rho_L / \mu_L$. Recommended by [49] based on experiments in industrial system.	[49] [133]
AG. High-pressure bubble column	$k_L a = 1.77 \sigma^{-0.22} \exp(1.65 u_\epsilon - 65.3 \mu_\epsilon) \epsilon_g^{1.2}$ $790 < \rho_L < 1580 \text{ kg/m}^3$ $0.00036 < \mu_\epsilon < 0.0383 \text{ Pa}\cdot\text{s}$ $0.0232 < \sigma_\epsilon < 0.0726 \text{ N/m}$ $0.028 < u_\epsilon < 0.678 \text{ m/s}$ $0 < \mu_\epsilon < 0.00089 \text{ m/s}$	[E] Pressure up to 4.24 MPa. T up to 92°C. ϵ_g = gas holdup. Correlation to estimate ϵ_g is given. $0.045 < d_{col} < 0.45 \text{ m}$, $d_{col}/H_{col} > 5$ $0.97 < \rho_g < 33.4 \text{ kg/m}^3$	[96]
AH. Three phase (gas-liquid-solid) bubble column to solid spheres	$N_{sh} = \frac{k_L d_p}{D} = 2.0 + 0.545 N_{Sc}^{1/3} \left(\frac{e d_p^4}{\nu^3} \right)^{0.264}$ $N_{Sc} = 137$ to 50,000 (very wide range) d_p = particle diameter (solids)	[E] e = local energy dissipation rate/unit mass, $e = u_{gg}$ $N_{Sc} = \mu_L / (\rho_L D)$ Recommended by [136].	[129] [136]

See Table 5-22 for agitated systems.

*See the beginning of the "Mass Transfer" subsection for references.

practical purposes \hat{k}_C is independent of temperature and pressure in the normal ranges of these variables.

For modest changes in temperature the influence of temperature upon the interfacial area a may be neglected. For example, in experiments on the absorption of SO₂ in water, Whitney and Vivian [*Chem. Eng. Prog.*, **45**, 323 (1949)] found no appreciable effect of temperature upon $k'_C a$ over the range from 10 to 50°C.

With regard to the liquid-phase mass-transfer coefficient, Whitney and Vivian found that the effect of temperature upon $k_L a$ could be explained entirely by variations in the liquid-phase viscosity and diffusion coefficient with temperature. Similarly, the oxygen-desorption data of Sherwood and Holloway [*Trans. Am. Inst. Chem. Eng.*, **36**, 39 (1940)] show that the influence of temperature upon H_L can be explained by the effects of temperature upon the liquid-phase viscosity and diffusion coefficients (see Table 5-24-A).

It is important to recognize that the effects of temperature on the liquid-phase diffusion coefficients and viscosities can be very large and therefore must be carefully accounted for when using k_L or H_L data. For liquids the mass-transfer coefficient k_L is correlated as either the Sherwood number or the Stanton number as a function of the Reynolds and Schmidt numbers (see Table 5-24). Typically, the general form of the correlation for H_L is (Table 5-24)

$$H_L = b N_{Re}^a N_{Sc}^{1/2} \quad (5-306)$$

where b is a proportionality constant and the exponent a may range from about 0.2 to 0.5 for different packings and systems. The liquid-phase diffusion coefficients may be corrected from a base temperature T_1 to another temperature T_2 by using the Einstein relation as recommended by Wilke [*Chem. Eng. Prog.*, **45**, 218 (1949)]:

$$D_2 = D_1 (T_2/T_1) (\mu_1/\mu_2) \quad (5-307)$$

The Einstein relation can be rearranged to the following equation for relating Schmidt numbers at two temperatures:

$$N_{Sc2} = N_{Sc1} (T_1/T_2) (\rho_1/\rho_2) (\mu_2/\mu_1)^2 \quad (5-308)$$

Substitution of this relation into Eq. (5-306) shows that for a given geometry the effect of temperature on H_L can be estimated as

$$H_{L2} = H_{L1} (T_1/T_2)^{1/2} (\rho_1/\rho_2)^{1/2} (\mu_2/\mu_1)^{1-a} \quad (5-309)$$

In using these relations it should be noted that for equal liquid flow rates

$$H_{L2}/H_{L1} = (\hat{k}_{L1} a)_1 / (\hat{k}_{L1} a)_2 \quad (5-310)$$

Effects of System Physical Properties on \hat{k}_C and \hat{k}_L . When designing packed towers for nonreacting gas-absorption systems for which no experimental data are available, it is necessary to make corrections for differences in composition between the existing test data and the system in question. The ammonia-water test data (see Table 5-24-B) can be used to estimate H_C , and the oxygen desorption data (see Table 5-24-A) can be used to estimate H_L . The method for doing this is illustrated in Table 5-24-E. There is some conflict on whether the value of the exponent for the Schmidt number is 0.5 or 2/3 [Yadav and Sharma, *Chem. Eng. Sci.* **34**, 1423 (1979)]. Despite this disagreement, this method is extremely useful, especially for absorption and stripping systems.

It should be noted that the influence of substituting solvents of widely differing viscosities upon the interfacial area a can be very large. One therefore should be cautious about extrapolating $k_L a$ data to account for viscosity effects between different solvent systems.

Effects of High Solute Concentrations on k_C and k_L . As discussed previously, the stagnant-film model indicates that k_C should be independent of y_{BM} and k_C should be inversely proportional to y_{BM} . The data of Vivian and Behrman [*Am. Inst. Chem. Eng. J.*, **11**, 656 (1965)] for the absorption of ammonia from an inert gas strongly suggest that the film model's predicted trend is correct. This is another indication that the most appropriate rate coefficient to use in concentrated systems is k_C and the proper driving-force term is of the form $(y - y_i)/y_{BM}$.

The use of the rate coefficient \hat{k}_L and the driving force $(x_i - x)/x_{BM}$ is believed to be appropriate. For many practical situations the liquid-phase solute concentrations are low, thus making this assumption unimportant.

Influence of Chemical Reactions on k_C and k_L . When a chemical reaction occurs, the transfer rate may be influenced by the chemical reaction as well as by the purely physical processes of diffusion and convection within the two phases. Since this situation is common in gas absorption, gas absorption will be the focus of this discussion. One must consider the impacts of chemical equilibrium and reaction kinetics on the absorption rate in addition to accounting for the effects of gas solubility, diffusivity, and system hydrodynamics.

There is no sharp dividing line between pure physical absorption and absorption controlled by the rate of a chemical reaction. Most cases fall in an intermediate range in which the rate of absorption is limited both by the resistance to diffusion and by the finite velocity of the reaction. Even in these intermediate cases the equilibria between the various diffusing species involved in the reaction may affect the rate of absorption.

TABLE 5-22 Mass-Transfer Correlations for Particles, Drops, and Bubbles in Agitated Systems

Situation	Correlation	Comments E = Empirical, S = Semiempirical, T = Theoretical	References*														
<p>A. Solid particles suspended in agitated vessel containing vertical baffles, continuous phase coefficient</p>	$\frac{k'_{LT} d_p}{D} = 2 + 0.6 N_{Re,T}^{1/2} N_{Sc}^{1/3}$ <p>Replace v_{slip} with v_T = terminal velocity. Calculate Stokes' law terminal velocity</p> $v_{Ts} = \frac{d_p^2 \rho_p - \rho_c g}{18 \mu_c}$ <p>and correct:</p> <table border="1" data-bbox="400 447 808 495"> <tr> <td>$\frac{N_{Re,T}}{v_T/v_{Ts}}$</td> <td>1</td> <td>10</td> <td>100</td> <td>1,000</td> <td>10,000</td> <td>100,000</td> </tr> <tr> <td></td> <td>0.9</td> <td>0.65</td> <td>0.37</td> <td>0.17</td> <td>0.07</td> <td>0.023</td> </tr> </table> <p>Approximate: $k'_{LT} = 2k'_{LT}$</p>	$\frac{N_{Re,T}}{v_T/v_{Ts}}$	1	10	100	1,000	10,000	100,000		0.9	0.65	0.37	0.17	0.07	0.023	<p>[S] Use log mean concentration difference.</p> <p>Modified Frossling equation: $N_{Re,T} = \frac{v_{Ts} d_p \rho_c}{\mu_c}$</p> <p>(Reynolds number based on Stokes' law.)</p> $N_{Re,T} = \frac{v_T d_p \rho_c}{\mu_c}$ <p>(terminal velocity Reynolds number.)</p> <p>k'_{LT} almost independent of d_p.</p> <p>Harriott suggests different correction procedures. Range k'_{LT}/k'_{LT} is 1.5 to 8.0.</p>	<p>[74][138] p. 220-222 [110]</p> <p>[74]</p>
$\frac{N_{Re,T}}{v_T/v_{Ts}}$	1	10	100	1,000	10,000	100,000											
	0.9	0.65	0.37	0.17	0.07	0.023											
<p>B. Solid, neutrally buoyant particles, continuous phase coefficient</p>	$N_{Sh} = \frac{k'_L d_p}{D} = 2 + 0.47 N_{Re,p}^{0.62} N_{Sc}^{0.36} \left(\frac{d_{imp}}{d_{tank}} \right)^{0.17}$ <p>Graphical comparisons are in Ref. 88, p. 116.</p>	<p>[E] Use log mean concentration difference. Density unimportant if particles are close to neutrally buoyant. Also used for drops. Geometric effect (d_{imp}/d_{tank}) is usually unimportant. Ref. 102 gives a variety of references on correlations.</p> <p>[E] E = energy dissipation rate per unit mass fluid</p> $= \frac{Pg_c}{V_{tank} \rho_c}, P = \text{power}, N_{Re,p} = \frac{E^{1/3} d_p^{4/3}}{v}$	<p>[88] p. 115 [102] p. 132 [152] p. 523</p>														
<p>C. Same as 22-B, small particles</p>	$N_{Sh} = 2 + 0.52 N_{Re,p}^{0.52} N_{Sc}^{1/3}, N_{Re,p} < 1.0$	<p>[E] Terms same as above.</p>	<p>[88] p. 116</p>														
<p>D. Solid particles with significant density difference</p>	$N_{Sh} = \frac{k'_L d_p}{D} = 2 + 0.44 \left(\frac{d_p v_{slip}}{v} \right)^{1/2} N_{Sc}^{0.38}$	<p>[E] Use log mean concentration difference. N_{Sh} standard deviation 11.1%. v_{slip} calculated by methods given in reference.</p>	<p>[102] [110]</p>														
<p>E. Small solid particles, gas bubbles or liquid drops, $d_p < 2.5$ mm. Aerated mixing vessels</p>	$N_{Sh} = \frac{k'_L d_p}{D} = 2 + 0.31 \left[\frac{d_p^3 \rho_p - \rho_c }{\mu_c D} \right]^{1/3}$	<p>[E] Use log mean concentration difference. $g = 9.80665 \text{ m/s}^2$. Second term RHS is free-fall or rise term. For large bubbles, see Table 5-21-AC.</p>	<p>[46][67] p. 487 [97] p. 249</p>														
<p>F. Highly agitated systems; solid particles, drops, and bubbles; continuous phase coefficient</p>	$k'_L N_{Sc}^{2/3} = 0.13 \left[\frac{(PN_{tank}) \mu_c g_c}{\rho_c^2} \right]^{1/4}$	<p>[E] Use arithmetic concentration difference. Use when gravitational forces overcome by agitation. Up to 60% deviation. Correlation prediction is low (Ref. 102). (PN_{tank}) = power dissipated by agitator per unit volume liquid.</p>	<p>[47] [66] p. 489 [110]</p>														
<p>G. Liquid drops in baffled tank with flat six-blade turbine</p>	$k'_L a = 2.621 \times 10^{-3} \frac{(ND)^{1/2}}{d_{imp}}$ $\times \phi^{0.304} \left(\frac{d_{imp}}{d_{tank}} \right)^{1.582} N_{Re}^{1.929} N_{Oh}^{1.025}$	<p>[E] Use arithmetic concentration difference. Studied for five systems.</p> $N_{Re} = d_{imp}^2 N_{\rho_c} / \mu_c, N_{Oh} = \mu_c / (\rho_c d_{imp} \sigma)^{1/2}$ <p>ϕ = volume fraction dispersed phase. N = impeller speed (revolutions/time). For $d_{tank} = h_{tank}$, average absolute deviation 23.8%.</p>	<p>[144] p. 437</p>														
<p>H. Liquid drops in baffled tank, low volume fraction dispersed phase</p>	$N_{Sh} = \frac{k'_L d_p}{D} = 1.237 \times 10^{-5} N_{Sc}^{1/3} N^{2/3}$ $\times N_{Fr}^{5/12} \left(\frac{d_{imp}}{d_p} \right) \left(\frac{d_p}{D_{tank}} \right)^{1/2} \left(\frac{\rho_a d_p^2}{\sigma} \right)^{5/4} \phi^{-1/2}$ <p>Stainless steel flat six-blade turbine. Tank had four baffles. Correlation recommended for $\phi \leq 0.06$ [Ref. 146] $a = 6\phi/d_{32}$, where d_{32} is Sauter mean diameter when 33% mass transfer has occurred.</p>	<p>[E] 180 runs, 9 systems, $\phi = 0.01$. k_c is time-averaged. Use arithmetic concentration difference.</p> $N_{Re} = \left(\frac{d_{imp}^2 N_{Sc}}{\mu_c} \right), N_{Fr} = \left(\frac{d_{imp} N^2}{g} \right)$ <p>d_p = particle or drop diameter; σ = interfacial tension, N/m; ϕ = volume fraction dispersed phase; a = interfacial volume, 1/m; and $k_c \alpha D^{2/3}$ implies rigid drops.</p> <p>Negligible drop coalescence. Average absolute deviation—19.71%. Graphical comparison given by Ref. 143.</p>	<p>[143] [146] p. 78</p>														

5-76 HEAT AND MASS TRANSFER

TABLE 5-22 Mass-Transfer Correlations for Particles, Drops, and Bubbles in Agitated Systems (Concluded)

Situation	Correlation	Comments E = Empirical, S = Semiempirical, T = Theoretical	References*
I. Gas bubble swarms in sparged tank reactors	$k_L a \left(\frac{v}{g^2} \right)^{1/3} = C \left[\frac{P/V_L}{\rho(vg^4)^{1/3}} \right]^a \left[\frac{q_G}{V_L} \left(\frac{v}{g^2} \right)^{1/3} \right]^b$ <p>Rushton turbines: $C = 7.94 \times 10^{-4}$, $a = 0.62$, $b = 0.23$. Intermig impellers: $C = 5.89 \times 10^{-4}$, $a = 0.62$, $b = 0.19$.</p>	[E] Use arithmetic concentration difference. Done for biological system. O ₂ transfer. $h_{\text{tank}}/D_{\text{tank}} = 2.1$; P = power, kW. V_L = liquid volume, m ³ . q_G = gassing rate, m ³ /s. $k_L a$ = s ⁻¹ . Since $a = \text{m}^2/\text{m}^3$, v = kinematic viscosity, m ² /s. Low viscosity system. Better fit claimed with q_G/V_L than with u_G (see 5-22-J to N).	[131]
J. Same as 5-22-I	$k_L a = 2.6 \times 10^{-2} \left(\frac{P}{V_L} \right)^{0.4} u_G^{0.5}$	[E] Use arithmetic concentration difference. Ion free water $V_L < 2.6$, u_G = superficial gas velocity in m/s. $500 < P/V_L < 10,000$. P/V_L = watts/m ³ , V_L = liquid volume, m ³ .	[98] [123]
K. Same as 5-22-J	$k_L a = 2.0 \times 10^{-3} \left(\frac{P}{V_L} \right)^{0.7} u_G^{0.2}$	[E] Use arithmetic concentration difference. Water with ions. $0.002 < V_L < 4.4$, $500 < P/V_L < 10,000$. Same definitions as 5-22-I.	[98] [101]
L. Same as 5-22-I, baffled tank with standard blade Rushton impeller	$k_L a = 93.37 \left(\frac{P}{V_L} \right)^{0.76} u_G^{0.45}$	[E] Air-water. Same definitions as 5-22-I. $0.005 < u_G < 0.025$, $3.83 < N < 8.33$, $400 < P/V_L < 7000$. $h = D_{\text{tank}} = 0.305$ or 0.610 m. V_G = gas volume, m ³ , N = stirrer speed, rpm. Method assumes perfect liquid mixing.	[67] [98]
M. Same as 5-22-L	$k_L a \frac{d_{\text{imp}}^2}{D} = 7.57 \left[\frac{\mu_{\text{eff}}}{\rho D} \right]^{0.57} \left[\frac{\mu_C}{\mu_{\text{eff}}} \right]^{0.694} \times \left[\frac{d_{\text{imp}}^2 N \rho_L}{\mu_{\text{eff}}} \right]^{1.11} \left(\frac{u_G d}{\sigma} \right)^{0.447}$ <p>d_{imp} = impeller diameter, m; D = diffusivity, m²/s</p>	[E] Use arithmetic concentration difference. CO ₂ into aqueous carboxyl polymethylene. Same definitions as 5-22-L. μ_{eff} = effective viscosity from power law model, Pa·s. σ = surface tension liquid, N/m.	[98] [115]
N. Same as 5-22-L, bubbles	$\frac{k_L a d_{\text{imp}}^2}{D} = 0.060 \left(\frac{d_{\text{imp}}^2 N \rho}{\mu_{\text{eff}}} \right) \left(\frac{d_{\text{imp}}^2 N^2}{g} \right)^{0.19} \left(\frac{\mu_{\text{eff}} u_G}{\sigma} \right)^{0.6}$	[E] Use arithmetic concentration difference. O ₂ into aqueous glycerol solutions. O ₂ into aqueous millet jelly solutions. Same definitions as 5-22-L.	[98] [160]
O. Gas bubble swarm in sparged stirred tank reactor with solids present	$\frac{k_L a}{(k_L a)_0} = 1 - 3.54(\epsilon_s - 0.03)$ <p>$300 \leq P/V_{rx} < 10,000$ W/m³, $0.03 \leq \epsilon_s \leq 0.12$ $0.34 \leq u_G \leq 4.2$ cm/s, $5 < \mu_L < 75$ Pa·s</p>	[E] Use arithmetic concentration difference. Solids are glass beads, $d_p = 320$ μm. ϵ_s = solids holdup m ³ /m ³ liquid. $(k_L a)_0$ = mass transfer in absence of solids. Ionic salt solution—noncoalescing.	[38] [132]
P. Surface aerators for air-water contact	$\frac{k_L a}{N} = b N_p^{0.71} N_{Fr}^{0.48} N_{Re}^{0.82} \left(\frac{H}{d} \right)^{-0.54} \left(\frac{V}{d^3} \right)^{-1.08}$ <p>$b = 7 \times 10^{-6}$, $N_p = P/(\rho N^3 d^5)$ $N_{Re} = Nd^2 \rho_{\text{liq}}/\mu_{\text{liq}}$ $N_{Fr} = N^2 d/g$, $P/V = 90$ to 400 W/m³</p>	[E] Three impellers: Pitched blade downflow turbine, pitched blade upflow turbine, standard disk turbine. Baffled cylindrical tanks 1.0- and 1.5-m ID and 8.2 × 8.2-m square tank. Submergence optimized all cases. Good agreement with data. N = impeller speed, s ⁻¹ ; d = impeller diameter, m; H = liquid height, m; V = liquid volume, m ³ ; $k_L a$ = s ⁻¹ , g = acceleration gravity = 9.81 m/s ²	[113]
Q. Gas-inducing impeller for air-water contact	$k_L a V (v/g^2)^{1/3} d^3 = AN_{Fr}^B \left(\frac{V_A}{V} \right)^C$ <p>Single impeller: $A = 0.00497$, $B = 0.56$, $C = 0.32$ Multiple impeller: $A = 0.00746$, $B = 0.54$, $C = 0.38$</p>	[E] Same tanks and same definitions as in 5-22-P. V_A = active volume = $p/(\pi \rho g N d)$.	[113]
R. Gas-inducing impeller with dense solids	$Sh_{GL} = \frac{k_L a d_{st}^2}{D} = (1.26 \times 10^{-5}) N_{Re}^{1.8} N_{Sc}^{0.9} N_{We}^{-0.1}$ <p>$N_{Re} = \rho N d_{st}^2 \mu$, $N_{Sc} = \mu/(\rho D)$, $N_{We} = \rho N^2 d_{st}^3 / \sigma$</p>	[E] Hydrogenation with Raney-type nickel catalyst in stirred autoclave. Used varying T , p , solvents. d_{st} = stirrer diameter.	[78]

See also Table 5-21.

*See the beginning of the "Mass Transfer" subsection for references.

TABLE 5-23 Mass-Transfer Correlations for Fixed and Fluidized Beds

Transfer is to or from particles

Situation	Correlation	Comments E = Empirical, S = Semiempirical, T = Theoretical	References ^o												
A. For gases, fixed and fluidized beds, Gupta and Thodos correlation	$j_H = j_D = \frac{2.06}{\epsilon N_{Re}^{0.575}}, 90 \leq N_{Re} \leq A$ <p>Equivalent:</p> $N_{Sh} = \frac{2.06}{\epsilon} N_{Re}^{0.425} N_{Sc}^{1/3}$ <p>For other shapes:</p> $\frac{\epsilon j_D}{(\epsilon j_D)_{\text{sphere}}} = 0.79 \text{ (cylinder) or } 0.71 \text{ (cube)}$	<p>[E] For spheres. $N_{Re} = \frac{v_{\text{super}} d_p \rho}{\mu}$</p> <p>A = 2453 [Ref. 141], A = 4000 [Ref. 77]. For $N_{Re} > 1900$, $j_H = 1.05 j_D$. Heat transfer result is in absence of radiation.</p> $N_{Sh} = \frac{k' d_s}{D}$ <p>Graphical results are available for N_{Re} from 1900 to 10,300.</p> $a = \frac{\text{surface area}}{\text{volume}} = 6(1 - \epsilon)/d_p$ <p>For spheres, $d_p = \text{diameter}$. For nonspherical: $d_p = 0.567 \sqrt{\text{Part. Surf. Area}}$</p>	<p>[72][73]</p> <p>[77] p. 195 [141]</p>												
B. For gases, for fixed beds, Petrovic and Thodos correlation	$N_{Sh} = \frac{0.357}{\epsilon} N_{Re}^{0.641} N_{Sc}^{1/3}$ <p>$3 < N_{Re} < 900$ can be extrapolated to $N_{Re} < 2000$.</p>	<p>[E] Packed spheres, deep beds. Corrected for axial dispersion with axial Peclet number = 2.0. Prediction is low at low N_{Re}. N_{Re} defined as in 5-23-A.</p>	<p>[116][128] p. 214 [155]</p>												
C. For gases and liquids, fixed and fluidized beds	$j_D = \frac{0.4548}{\epsilon N_{Re}^{0.4069}}, 10 \leq N_{Re} \leq 2000$ $j_D = \frac{N_{Sh}}{N_{Re} N_{Sc}^{1/3}}, N_{Sh} = \frac{k' d_s}{D}$	<p>[E] Packed spheres, deep bed. Average deviation $\pm 20\%$. $N_{Re} = d_p v_{\text{super}} \rho / \mu$. Can use for fluidized beds. $10 \leq N_{Re} \leq 4000$.</p>	<p>[60][66] p. 484</p>												
D. For gases, fixed beds	$j_D = \frac{0.499}{\epsilon N_{Re}^{0.382}}$	<p>[E] Data on sublimation of naphthalene spheres dispersed in inert beds. $0.1 < N_{Re} < 100$, $N_{Sc} = 2.57$. Correlation coefficient = 0.978.</p>	<p>[80]</p>												
E. For liquids, fixed bed, Wilson and Geankoplis correlation	$j_D = \frac{1.09}{\epsilon N_{Re}^{2/3}}, 0.0016 < N_{Re} < 55$ <p>$165 \leq N_{Sc} \leq 70,600$, $0.35 < \epsilon < 0.75$</p> <p>Equivalent:</p> $N_{Sh} = \frac{1.09}{\epsilon} N_{Re}^{1/3} N_{Sc}^{1/3}$ $j_D = \frac{0.25}{\epsilon N_{Re}^{0.31}}, 55 < N_{Re} < 1500, 165 \leq N_{Sc} \leq 10,690$ <p>Equivalent: $N_{Sh} = \frac{0.25}{\epsilon} N_{Re}^{0.60} N_{Sc}^{1/3}$</p>	<p>[E] Beds of spheres,</p> $N_{Re} = \frac{d_p v_{\text{super}} \rho}{\mu}$ <p>Deep beds.</p> $N_{Sh} = \frac{k' d_s}{D}$	<p>[66] p. 484</p> <p>[77] p. 195</p> <p>[141] p. 287 [158]</p>												
F. For liquids, fixed beds, Ohashi et al. correlation	$N_{Sh} = \frac{k' d_s}{D} = 2 + 0.51 \left(\frac{E^{1/3} d_p^{4/3} \rho}{\mu} \right)^{0.60} N_{Sc}^{1/3}$ <p>E = Energy dissipation rate per unit mass of fluid</p> $= 50(1 - \epsilon) \epsilon^2 C_{D0} \left(\frac{v_r^3}{d_p} \right), \text{ m}^2/\text{s}^3$ $= \left[\frac{50(1 - \epsilon) C_D}{\epsilon} \right] \left(\frac{v_{\text{super}}^3}{d_p} \right)$ <p>General form:</p> $N_{Sh} = 2 + K \left(\frac{E^{1/3} D_p^{4/3} \rho}{\mu} \right)^\alpha N_{Sc}^\beta$ <p>applies to single particles, packed beds, two-phase tube flow, suspended bubble columns, and stirred tanks with different definitions of E.</p>	<p>[S] Correlates large amount of published data. Compares number of correlations, $v_r = \text{relative velocity, m/s}$. In packed bed, $v_r = v_{\text{super}}/\epsilon$.</p> <p>$C_{D0} = \text{single particle drag coefficient at } v_{\text{super}}$ calculated from $C_{D0} = AN_{Re}^{-m}$.</p> <table border="1" data-bbox="870 1429 1202 1515"> <thead> <tr> <th>N_{Re}</th> <th>A</th> <th>m</th> </tr> </thead> <tbody> <tr> <td>0 to 5.8</td> <td>24</td> <td>1.0</td> </tr> <tr> <td>5.8 to 500</td> <td>10</td> <td>0.5</td> </tr> <tr> <td>>500</td> <td>0.44</td> <td>0</td> </tr> </tbody> </table> <p>Ranges for packed bed:</p> <p>$0.001 < N_{Re} < 1000$, $505 < N_{Sc} < 70,600$,</p> $0.2 < \frac{E^{1/3} d_p^{4/3} \rho}{\mu} < 4600$ <p>Compares different situations versus general correlation. See also 5-20-F.</p>	N_{Re}	A	m	0 to 5.8	24	1.0	5.8 to 500	10	0.5	>500	0.44	0	<p>[108]</p>
N_{Re}	A	m													
0 to 5.8	24	1.0													
5.8 to 500	10	0.5													
>500	0.44	0													

5-78 HEAT AND MASS TRANSFER

TABLE 5-23 Mass Transfer Correlations for Fixed and Fluidized Beds (Continued)

Situation	Correlation	Comments E = Empirical, S = Semiempirical, T = Theoretical	References°
G. Electrolytic system. Pall rings. Transfer from fluid to rings.	Full liquid upflow: $N_{sh} = k_L d_p / D = 4.1 N_{Re}^{0.39} N_{Sc}^{1/3}$ $N_{Re} d_p u / \nu = 80$ to 550 Irrigated liquid downflow (no gas flow): $N_{Sh} = 5.1 N_{Re}^{0.44} N_{Sc}^{1/3}$	[E] d_c = diameter of sphere with same surface area as Pall ring. Full liquid upflow agreed with literature values. Schmidt number dependence was assumed from literature values. In downflow, N_{Re} used superficial fluid velocity.	[69]
H. For liquids, fixed and fluidized beds	$\epsilon j_D = \frac{1.1068}{N_{Re}^{0.72}}, 1.0 < N_{Re} \leq 10$ $\epsilon j_D = \frac{N_{Sh}}{N_{Re} N_{Sc}^{1/3}}, N_{Sh} = \frac{k' d_s}{D}$	[E] Spheres: $N_{Re} = \frac{d_p v_{super} \rho}{\mu}$	[59][66] p. 484
I. For gases and liquids, fixed and fluidized beds, Dwivedi and Upadhyay correlation	$\epsilon j_D = \frac{0.765}{N_{Re}^{0.82}} + \frac{0.365}{N_{Re}^{0.386}}$ Gases: $10 \leq N_{Re} \leq 15,000$. Liquids: $0.01 \leq N_{Re} \leq 15,000$. $N_{Re} = \frac{d_p v_{super} \rho}{\mu}, N_{Sh} = \frac{k' d_s}{D}$	[E] Deep beds of spheres, $j_D = \frac{N_{Sh}}{N_{Re} N_{Sc}^{1/3}}$ Best fit correlation at low conc. [52] Based on 20 gas studies and 17 liquid studies. Recommended instead of 5-23-C or E.	[59] [77] p. 196 [52]
J. For gases and liquids, fixed bed	$j_D = 1.17 N_{Re}^{-0.415}, 10 \leq N_{Re} \leq 2500$ $j_D = \frac{k'}{v_{av}} \frac{p_{BM}}{P} N_{Sc}^{2/3}$	[E] Spheres: Variation in packing that changes ϵ not allowed for. Extensive data referenced. $0.5 < N_{Sc} < 15,000$. Comparison with other results are shown. $N_{Re} = \frac{d_p v_{super} \rho}{\mu}$	[138] p. 241
K. For liquids, fixed and fluidized beds, Rahman and Streat correlation	$N_{Sh} = \frac{0.86}{\epsilon} N_{Re}^{1/3} N_{Sc}^{1/3}, 2 \leq N_{Re} \leq 25$	[E] Can be extrapolated to $N_{Re} = 2000$. $N_{Re} = d_p v_{super} \rho / \mu$. Done for neutralization of ion exchange resin.	[119]
L. Size exclusion chromatography of proteins	$N_{Sh} = \frac{k_L d}{D} = \frac{1.903}{\epsilon} N_{Re}^{1/3} N_{Sc}^{1/3}$	[E] Slow mass transfer with large molecules. Aqueous solutions. Modest increase in N_{Sh} with increasing velocity.	[79]
M. Liquid-free convection with fixed bed Raschig rings. Electrochemical.	$N_{Sh} = kd/D = 0.15 (N_{Sc} N_{Gr})^{0.32}$ $N_{Gr} = \text{Grashof no.} = gd^3 \Delta \rho / (\nu^2 \rho)$ If forced convection superimposed, $N_{Sh, overall} = (N_{Sh, forced}^3 + N_{Sh, free}^3)^{1/3}$	[E] d = Raschig ring diameter, h = bed height $1810 < N_{Sc} < 2532, 0.17 < d/h < 1.0$ $10.6 \times 10^6 < N_{Sc} N_{Gr} < 21 \times 10^7$	[135]
N. Oscillating bed packed with Raschig rings. Dissolution of copper rings.	Batch (no net solution flow): $N_{Sh} = 0.76 N_{Sc}^{0.33} N_{Re, v}^{0.7} (d_c/h)^{0.35}$ $503 < N_{Re, v} < 2892$ $960 < N_{Sc} < 1364, 2.3 < d_c/h < 7.6$	[E] $N_{Sh} = kd_c/D, N_{Re, v} = \text{vibrational } Re = \rho v_c d_c / \mu$ $v_c = \text{vibrational velocity (intensity)}$ $d_c = \text{col. diameter, } h = \text{column height}$ Average deviation is $\pm 12\%$.	[61]
O. For liquids and gases, Ranz and Marshall correlation	$N_{Sh} = \frac{k' d}{D} = 2.0 + 0.6 N_{Sc}^{1/3} N_{Re}^{1/2}$ $N_{Re} = \frac{d_p v_{super} \rho}{\mu}$	[E] Based on freely falling, evaporating spheres (see 5-20-C). Has been applied to packed beds, prediction is low compared to experimental data. Limit of 2.0 at low N_{Re} is too high. Not corrected for axial dispersion.	[121][128] p. 214 [155] [110]
P. For liquids and gases, Wakao and Funazkri correlation	$N_{Sh} = 2.0 + 1.1 N_{Sc}^{1/3} N_{Re}^{0.6}, 3 < N_{Re} < 10,000$ $N_{Sh} = \frac{k'_{lim} d_p}{D}, N_{Re} = \frac{\rho r v_{super} \rho}{\mu}$ $\frac{\epsilon D_{axial}}{D} = 10 + 0.5 N_{Sc} N_{Re}$	[E] Correlate 20 gas studies and 16 liquid studies. Corrected for axial dispersion with: Graphical comparison with data shown [128], p. 215, and [155]. D_{axial} is axial dispersion coefficient.	[128] p. 214 [155]
Q. Acid dissolution of limestone in fixed bed	$N_{Sh} = 1.77 N_{Re}^{0.56} N_{Sc}^{1/3} (1 - \epsilon)^{0.44}$ $20 < N_{Re} < 6000$	[E] Best fit was to correlation of Chu et al., <i>Chem. Eng. Prog.</i> , 49 (3), 141(1953), even though no reaction in original.	[94]
R. Semifluidized or expanded bed. Liquid-solid transfer.	$N_{Sh} = \frac{k'_{lim} d_p}{D} = 2 + 1.5 (1 - \epsilon_L) N_{Re}^{1/3} N_{Sc}^{1/3}$ $N_{Re} = \rho_p d_p u / \mu \epsilon_L, N_{Sc} = \mu / \rho D$	[E] ϵ_L = liquid-phase void fraction, ρ_p = particle density, ρ = fluid density, d_p = particle diameter. Fits expanded bed chromatography in viscous liquids.	[64] [159]

TABLE 5-23 Mass Transfer Correlations for Fixed and Fluidized Beds (Concluded)

Situation	Correlation	Comments E = Empirical, S = Semiempirical, T = Theoretical	References*
S. Mass-transfer structured packing and static mixers. Liquid with or without fluidized particles. Electrochemical	Fixed bed: $j' = 0.927N_{Re}^{0.572}$, $N'_{Re} < 219$ $j' = 0.443N_{Re}^{0.435}$, $219 < N'_{Re} < 1360$ Fluidized bed with particles: $j = 6.02N_{Re}^{0.885}$, or $j' = 16.40N_{Re}^{-0.950}$ Natural convection: $N_{Sh} = 0.252(N_{Sc}N_{Gr})^{0.299}$ Bubble columns: Structured packing: $N_{St} = 0.105(N_{Re}N_{Fr}N_{Sc}^2)^{-0.268}$ Static mixer: $N_{St} = 0.157(N_{Re}N_{Fr}N_{Sc}^2)^{-0.298}$	[E] Sulzer packings, $j' = \frac{k \cos \beta}{v} N_{Sc}^{2/3}$, β = corrugation incline angle. $N_{Re} = v' d_h \rho / \mu$, $v' = v_{super} / (\epsilon \cos \beta)$, d_h = channel side width. Particles enhance mass transfer in laminar flow for natural convection. Good fit with correlation of Ray et al., <i>Intl. J. Heat Mass Transfer</i> , 41 , 1693 (1998). $N_{Gr} = g \Delta \rho Z' / \rho \mu^2$, Z = corrugated plate length. Bubble column results fit correlation of Neme et al., <i>Chem. Eng. Technol.</i> , 20 , 297 (1997) for structured packing. N_{St} = Stanton number = kZ/D N_{Fr} = Froude number = v_{super}^2 / gz	[48]
T. Liquid fluidized beds	$N_{Sh} = \frac{2\xi/\epsilon^m + \left[\frac{(2\xi/\epsilon^m)(1-\epsilon)^{1/2}}{1-(1-\epsilon)^{1/3}} - 2 \right] \tan h(\xi/\epsilon^m)}{\frac{\xi/\epsilon^m}{1-(1-\epsilon)^{1/2}} - \tan h(\xi/\epsilon^m)}$ where $\xi = \left[\frac{1}{(1-\epsilon)^{1/3}} - 1 \right] \frac{\alpha}{2} N_{Sc}^{1/3} N_{Re}^{1/2}$ This simplifies to: $N_{Sh} = \frac{\epsilon^{1-2m}}{(1-\epsilon)^{1/3}} \left[\frac{1}{(1-\epsilon)^{1/3}} - 1 \right] \frac{\alpha^2}{2} N_{Re} N_{Sc}^{2/3} \quad (N_{Re} < 0.1)$	[S] Modification of theory to fit experimental data. For spheres, $m = 1$, $N_{Re} > 2$. $N_{Sh} = \frac{k_L d_p}{D}, \quad N_{Re} = \frac{V_{super} d_p \xi}{\mu}$ $m = 1$ for $N_{Re} > 2$; $m = 0.5$ for $N_{Re} < 1.0$; ϵ = voidage; α = const. Best fit data is $\alpha = 0.7$. Comparison of theory and experimental ion exchange results in Ref. 92.	[92] [106] [125]
U. Liquid fluidized beds	$N_{Sh} = 0.250 N_{Re}^{0.023} N_{Ga}^{0.306} \left(\frac{\rho_s - \rho}{\rho} \right)^{0.282} N_{Sc}^{0.410} \quad (\epsilon < 0.85)$ $N_{Sh} = 0.304 N_{Re}^{-0.057} N_{Ga}^{0.332} \left(\frac{\rho_s - \rho}{\rho} \right)^{0.297} N_{Sc}^{0.404} \quad (\epsilon > 0.85)$ This can be simplified (with slight loss in accuracy at high ϵ) to $N_{Sh} = 0.245 N_{Ga}^{0.323} \left(\frac{\rho_s - \rho}{\rho} \right)^{0.300} N_{Sc}^{0.400}$	[E] Correlate amount of data from literature. Predicts very little dependence of N_{Sh} on velocity. Compare large number of published correlations. $N_{Sh} = \frac{k_L d_p}{D}, \quad N_{Re} = \frac{d_p \rho v_{super}}{\mu}, \quad N_{Ga} = \frac{d_p^3 \rho^2 g}{\mu^2}$ $N_{Sc} = \frac{\mu}{\rho D}$ $1.6 < N_{Re} < 1320, 2470 < N_{Ga} < 4.42 \times 10^6$ $0.27 < \frac{\rho_s - \rho}{\rho} < 1.114, 305 < N_{Sc} < 1595$	[151]
V. Liquid film flowing over solid particles with air present, trickle bed reactors, fixed bed	$N_{Sh} = \frac{k_L}{aD} = 1.8 N_{Re}^{1/2} N_{Sc}^{1/3}, 0.013 < N_{Re} < 12.6$ two-phases, liquid trickle, no forced flow of gas. $N_{Sh} = 0.8 N_{Re}^{1/2} N_{Sc}^{1/3}$, one-phase, liquid only.	[E] $N_{Re} = \frac{L}{a\mu}$, irregular granules of benzoic acid, $0.29 \leq d_p \leq 1.45$ cm. L = superficial liquid flow rate, kg/m ² s. a = surface area/col. volume, m ² /m ³ .	[130]
W. Supercritical fluids in packed bed	$\frac{N_{Sh}}{(N_{Sc} N_{Gr})^{1/4}} = 0.5265 \left(\frac{N_{Re}^{1/2} N_{Sc}^{1/3}}{(N_{Sc} N_{Gr})^{1/4}} \right)^{1.6808} + 2.48 \left \left(\frac{N_{Re}^2 N_{Sc}^{1/3}}{N_{Gr}} \right)^{0.6439} - 0.8768 \right ^{1.553}$	[E] Natural and forced convection. $0.3 < N_{Re} < 135$.	[99]
X. Cocurrent gas-liquid flow in fixed beds	Downflow in trickle bed and upflow in bubble columns.	Literature review and meta-analysis. Analyzed both downflow and upflow. Recommendations for best mass- and heat-transfer correlations (see reference).	[95]
Y. Liquid-solid transfer. Electrochemical reaction. Lessing rings. Transfer from liquid to solid	Liquid only: $N_{Sh} = kd/D = 1.57 N_{Sc}^{1/3} N_{Re}^{0.46}$ $1390 < N_{Sc} < 4760, 166 < N_{Re} < 722$ Cocurrent two-phase (liquid and gas) in packed bubble column: $N_{Sh} = 1.93 N_{Sc}^{1/3} N_{Re}^{0.34} N_{Re, gas}^{0.11}$ $60 < N_{Re, gas} < 818, 144 < N_{Re} < 748$	[E] Electrochemical reactors only. d = Lessing ring diameter, $1 < d < 1.4$ cm, $N_{Re} = \rho v_{super} d / \mu$, Deviation $\pm 7\%$ for both cases. $N_{Re, gas} = \rho_{gas} V_{super, gas} d / \mu_{gas}$ Presence of gas enhances mass transfer.	[75]

NOTE: For $N_{Re} < 3$ convective contributions which are not included may become important. Use with logarithmic concentration difference (integrated form) or with arithmetic concentration difference (differential form).

*See the beginning of the "Mass Transfer" subsection for references.

TABLE 5-24 Mass-Transfer Correlations for Packed Two-Phase Contactors—Absorption, Distillation, Cooling Towers, and Extractors (Packing Is Inert)

Situation	Correlations	Comments E = Empirical, S = Semiempirical, T = Theoretical	References*																																																																																								
A. Absorption, counter-current, liquid-phase coefficient H_L , Sherwood and Holloway correlation for random packings	$H_L = a_L \left(\frac{L}{\mu_L} \right)^n N_{Sc,L}^{0.5}, L = \text{lb/hr ft}^2$ <hr/> <p style="text-align: center;">Ranges for 5-24-B (G and L)</p> <table border="1" style="width: 100%; border-collapse: collapse;"> <thead> <tr> <th>Packing</th> <th>a_C</th> <th>b</th> <th>c</th> <th>G</th> <th>L</th> <th>a_L</th> <th>n</th> </tr> </thead> <tbody> <tr> <td colspan="8" style="text-align: center;">Raschig rings</td> </tr> <tr> <td>3/8 inch</td> <td>2.32</td> <td>0.45</td> <td>0.47</td> <td>200–500</td> <td>500–1500</td> <td>0.00182</td> <td>0.46</td> </tr> <tr> <td>1</td> <td>7.00</td> <td>0.39</td> <td>0.58</td> <td>200–800</td> <td>400–500</td> <td>0.010</td> <td>0.22</td> </tr> <tr> <td>1</td> <td>6.41</td> <td>0.32</td> <td>0.51</td> <td>200–600</td> <td>500–4500</td> <td>—</td> <td>—</td> </tr> <tr> <td>2</td> <td>3.82</td> <td>0.41</td> <td>0.45</td> <td>200–800</td> <td>500–4500</td> <td>0.0125</td> <td>0.22</td> </tr> <tr> <td colspan="8" style="text-align: center;">Bert saddles</td> </tr> <tr> <td>1/2 inch</td> <td>32.4</td> <td>0.30</td> <td>0.74</td> <td>200–700</td> <td>500–1500</td> <td>0.0067</td> <td>0.28</td> </tr> <tr> <td>1/2</td> <td>0.811</td> <td>0.30</td> <td>0.24</td> <td>200–800</td> <td>400–4500</td> <td>—</td> <td>—</td> </tr> <tr> <td>1</td> <td>1.97</td> <td>0.36</td> <td>0.40</td> <td>200–800</td> <td>400–4500</td> <td>0.0059</td> <td>0.28</td> </tr> <tr> <td>1.5</td> <td>5.05</td> <td>0.32</td> <td>0.45</td> <td>200–1000</td> <td>400–4500</td> <td>0.0062</td> <td>0.28</td> </tr> </tbody> </table>	Packing	a_C	b	c	G	L	a_L	n	Raschig rings								3/8 inch	2.32	0.45	0.47	200–500	500–1500	0.00182	0.46	1	7.00	0.39	0.58	200–800	400–500	0.010	0.22	1	6.41	0.32	0.51	200–600	500–4500	—	—	2	3.82	0.41	0.45	200–800	500–4500	0.0125	0.22	Bert saddles								1/2 inch	32.4	0.30	0.74	200–700	500–1500	0.0067	0.28	1/2	0.811	0.30	0.24	200–800	400–4500	—	—	1	1.97	0.36	0.40	200–800	400–4500	0.0059	0.28	1.5	5.05	0.32	0.45	200–1000	400–4500	0.0062	0.28	<p>[E] From experiments on desorption of sparingly soluble gases from water. Graphs [Ref. 138], p. 606. Equation is dimensional. A typical value of n is 0.3 [Ref. 66] has constants in kg, m, and s units for use in 5-24-A and B with \hat{k}_G in kgmole/s m^2 and \hat{k}_L in kgmole/s m^2 (kgmol/m³). Constants for other packings are given by Refs. 104, p. 187 and 152, p. 239.</p> $H_L = \frac{L_M}{\hat{k}_L a}$ <p>$L_M = \text{lbmol/hr ft}^2, \hat{k}_L = \text{lbmol/hr ft}^2, a = \text{ft}^2/\text{ft}^3, \mu_L$ in lb/(hr ft). Range for 5-24-A is $400 < L < 15,000 \text{ lb/hr ft}^2$</p>	<p>[104] p. 187 [105] [138] p. 606 [157] [156]</p>
Packing	a_C	b	c	G	L	a_L	n																																																																																				
Raschig rings																																																																																											
3/8 inch	2.32	0.45	0.47	200–500	500–1500	0.00182	0.46																																																																																				
1	7.00	0.39	0.58	200–800	400–500	0.010	0.22																																																																																				
1	6.41	0.32	0.51	200–600	500–4500	—	—																																																																																				
2	3.82	0.41	0.45	200–800	500–4500	0.0125	0.22																																																																																				
Bert saddles																																																																																											
1/2 inch	32.4	0.30	0.74	200–700	500–1500	0.0067	0.28																																																																																				
1/2	0.811	0.30	0.24	200–800	400–4500	—	—																																																																																				
1	1.97	0.36	0.40	200–800	400–4500	0.0059	0.28																																																																																				
1.5	5.05	0.32	0.45	200–1000	400–4500	0.0062	0.28																																																																																				
B. Absorption counter-current, gas-phase coefficient H_G , for random packing	$H_G = \frac{G_M}{\hat{k}_G a} = \frac{a_G(G)^b N_{Sc,G}^{0.5}}{(L)^c}$	<p>[E] Based on ammonia-water-air data in Fellingner's 1941 MIT thesis. Curves: Refs. 104, p. 186 and 138, p. 607. Constants given in 5-24-A. The equation is dimensional. $G = \text{lb/hr ft}^2, G_M = \text{lbmol/hr ft}^2, \hat{k}_G = \text{lbmol/hr ft}^2$.</p>	<p>[104] p. 189 [138] p. 607 [157]</p>																																																																																								
C. Absorption and distillation, counter-current, gas and liquid individual coefficients and wetted surface area, Onda et al. correlation for random packings	$\frac{k'_G RT}{a_p D_G} = A \left(\frac{G}{a_p \mu_G} \right)^{0.7} N_{Sc,G}^{1/3} (a_p d_p')^{-2.0}$ $k'_L \left(\frac{\rho_L}{\mu_L} \right)^{1/3} = 0.0051 \left(\frac{L}{a_w \mu_L} \right)^{2/3} N_{Sc,L}^{-1/2} (a_p d_p')^{0.4}$ <p>$k'_L = \text{lbmol/hr ft}^2 \text{ (lbmol/ft}^3 \text{) [kgmol/s m}^2 \text{ (kgmol/m}^3 \text{)]}$</p> $\frac{a_w}{a_p} = 1 - \exp \left\{ \begin{array}{l} -1.45 \left(\frac{\sigma_c}{\sigma} \right)^{0.75} \left(\frac{L}{a_p \mu_L} \right)^{0.1} \\ \times \left(\frac{L^2 a_p}{\rho_L^2 g} \right)^{-0.05} \left(\frac{L}{\rho_L \sigma a_p} \right)^{0.2} \end{array} \right\}$	<p>[E] Gas absorption and desorption from water and organics plus vaporization of pure liquids for Raschig rings, saddles, spheres, and rods. d_p' = nominal packing size, a_p = dry packing surface area/volume, a_w = wetted packing surface area/volume. Equations are dimensionally consistent, so any set of consistent units can be used. σ = surface tension, dynes/cm. $A = 5.23$ for packing $\geq 1/2$ inch (0.012 m) $A = 2.0$ for packing $< 1/2$ inch (0.012 m) $k'_G = \text{lbmol/hr ft}^2 \text{ atm [kg mol/s m}^2 \text{ (N/m}^2 \text{)]}$</p> <p>Critical surface tensions, $\sigma_c = 61$ (ceramic), 75 (steel), 33 (polyethylene), 40 (PVC), 56 (carbon) dynes/cm.</p> $4 < \frac{L}{a_w \mu_L} < 400$ $5 < \frac{G}{a_p \mu_G} < 1000$ <p>Most data $\pm 20\%$ of correlation, some $\pm 50\%$. Graphical comparison with data in Ref. 109.</p>	<p>[44] [90] p. 380 [109][149] p. 355 [156]</p>																																																																																								
D. Distillation and absorption, counter-current, random packings, modification of Onda correlation, Bravo and Fair correlation to determine interfacial area	<p>Use Onda's correlations (5-24-C) for k'_G and k'_L. Calculate:</p> $H_G = \frac{G}{k'_G a_p P M_G}, H_L = \frac{L}{k'_L a_p \rho_L}, H_{OG} = H_G + \lambda H_L$ $\lambda = \frac{m}{L_M / G_M}$ $a_e = 0.498 a_p \left(\frac{\sigma^{0.5}}{Z^{0.4}} \right) (N_{Ca,L} N_{Re,G})^{0.392}$ $N_{Re,G} = \frac{6G}{a_p \mu_G}, N_{Ca,L} = \frac{L \mu_L}{\rho_L \sigma g_c} \text{ (dimensionless)}$	<p>[E] Use Bolles & Fair (Ref. 43) database to determine new effective area a_e to use with Onda et al. (Ref. 109) correlation. Same definitions as 5-24-C. P = total pressure, atm; M_G = gas, molecular weight; m = local slope of equilibrium curve; L_M/G_M = slope operating line; Z = height of packing in feet. Equation for a_e is dimensional. Fit to data for effective area quite good for distillation. Good for absorption at low values of $(N_{Ca,L} \times N_{Re,G})$, but correlation is too high at higher values of $(N_{Ca,L} \times N_{Re,G})$.</p>	<p>[44]</p>																																																																																								

TABLE 5-24 Mass-Transfer Correlations for Packed Two-Phase Contactors—Absorption, Distillation, Cooling Towers, and Extractors (Packing Is Inert) (Continued)

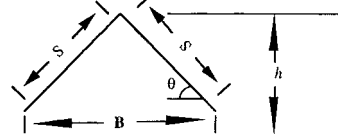
Situation	Correlations	Comments E = Empirical, S = Semiempirical, T = Theoretical	References ^o																														
<p>E. Absorption and distillation, countercurrent gas-liquid flow, random and structured packing. Determine H_L and H_C</p>	$H_C = \left(\frac{0.226}{f_p} \right) \left(\frac{N_{Sc}}{0.660} \right)^b \left(\frac{G_x}{6.782} \right)^{-0.5} \left(\frac{G_y}{0.678} \right)^{0.35}$ $H_L = \left(\frac{0.357}{f_p} \right) \left(\frac{N_{Sc}}{372} \right)^{0.5} \left(\frac{G_x/\mu}{6.782/0.0008937} \right)^{0.3}$ <p>Relative transfer coefficients [91], f_p values are in table:</p> <table border="1" data-bbox="414 428 808 571"> <thead> <tr> <th>Size, in.</th> <th>Ceramic Raschig rings</th> <th>Ceramic Berl saddles</th> <th>Metal Pall rings</th> <th>Metal Intalox</th> <th>Metal Hypac</th> </tr> </thead> <tbody> <tr> <td>0.5</td> <td>1.52</td> <td>1.58</td> <td>—</td> <td>—</td> <td>—</td> </tr> <tr> <td>1.0</td> <td>1.20</td> <td>1.36</td> <td>1.61</td> <td>1.78</td> <td>1.51</td> </tr> <tr> <td>1.5</td> <td>1.00</td> <td>—</td> <td>1.34</td> <td>—</td> <td>—</td> </tr> <tr> <td>2.0</td> <td>0.85</td> <td>—</td> <td>1.14</td> <td>1.27</td> <td>1.07</td> </tr> </tbody> </table> <p>Norton Intalox structured: 2T, $f_p = 1.98$; 3T, $f_p = 1.94$.</p>	Size, in.	Ceramic Raschig rings	Ceramic Berl saddles	Metal Pall rings	Metal Intalox	Metal Hypac	0.5	1.52	1.58	—	—	—	1.0	1.20	1.36	1.61	1.78	1.51	1.5	1.00	—	1.34	—	—	2.0	0.85	—	1.14	1.27	1.07	<p>[S] H_C based on NH_3 absorption data (5-28B) for which $H_{C, \text{base}} = 0.226$ m with $N_{Sc, \text{base}} = 0.660$ at $G_{x, \text{base}} = 6.782$ kg/(sm²) and $G_{y, \text{base}} = 0.678$ kg/(sm²) with 1/2 in. ceramic Raschig rings. The exponent b on N_{Sc} is reported as either 0.5 or as 2/3.</p> $f_p = \frac{H_C \text{ for } \text{NH}_3 \text{ with } 1/2 \text{ Raschig rings}}{H_C \text{ for } \text{NH}_3 \text{ with desired packing}}$ <p>H_L based on O_2 desorption data (5-24-A). Base viscosity, $\mu_{\text{base}} = 0.0008937$ kg/(ms). H_L in m. $G_y < 0.949$ kg/(sm²), $0.678 < G_x < 6.782$ kg/(sm²). Best use is for absorption and stripping. Limited use for organic distillation [156].</p>	<p>[66] p. 686, 659 [138] [156]</p>
Size, in.	Ceramic Raschig rings	Ceramic Berl saddles	Metal Pall rings	Metal Intalox	Metal Hypac																												
0.5	1.52	1.58	—	—	—																												
1.0	1.20	1.36	1.61	1.78	1.51																												
1.5	1.00	—	1.34	—	—																												
2.0	0.85	—	1.14	1.27	1.07																												
<p>F. Absorption, cocurrent downward flow, random packings, Reiss correlation</p>	<p>Air-oxygen-water results correlated by $k'_L a = 0.12E_L^{0.5}$. Extended to other systems.</p> $k'_L a = 0.12E_L^{0.5} \left(\frac{D_L}{2.4 \times 10^5} \right)^{0.5}$ $E_L = \left(\frac{\Delta p}{\Delta L} \right)_{2\text{-phase}} v_L$ <p>$\frac{\Delta p}{\Delta L}$ = pressure loss in two-phase flow = lbf/ft² ft</p> $k'_C a = 2.0 + 0.91E_C^{2/3} \text{ for } \text{NH}_3$ $E_g = \left(\frac{\Delta p}{\Delta L} \right)_{2\text{-phase}} v_g$ <p>v_g = superficial gas velocity, ft/s</p>	<p>[E] Based on oxygen transfer from water to air 77°F. Liquid film resistance controls. ($D_{\text{water}} @ 77^\circ\text{F} = 2.4 \times 10^{-5}$). Equation is dimensional. Data was for thin-walled polyethylene Raschig rings. Correlation also fit data for spheres. Fit $\pm 25\%$. See [122] for graph.</p> $k'_L a = s^{-1}$ $D_L = \text{cm/s}$ $E_L = \text{ft, lbf/s ft}^3$ $v_L = \text{superficial liquid velocity, ft/s}$ <p>[E] Ammonia absorption into water from air at 70°F. Gas-film resistance controls. Thin-walled polyethylene Raschig rings and 1-inch Intalox saddles. Fit $\pm 25\%$. See [122] for fit. Terms defined as above.</p>	<p>[122] [130] p. 217</p> <p>[122]</p>																														
<p>G. Absorption, stripping, distillation, counter-current, H_L and H_C, random packings, Bolles and Fair correlation</p>	<p>For Raschig rings, Berl saddles, and spiral tile:</p> $H_L = \frac{\phi C_{\text{flood}}}{3.28} N_{Sc,L}^{0.5} \left(\frac{Z}{3.05} \right)^{0.15}$ <p>$C_{\text{flood}} = 1.0$ if below 40% flood—otherwise, use figure in [54] and [157].</p> $H_C = \frac{A\psi(d'_{\text{col}})^{mZ^{0.33}N_{Sc,G}^{0.5}}}{\left[L \left(\frac{\mu_L}{\mu_{\text{water}}} \right)^{0.16} \left(\frac{\rho_{\text{water}}}{\rho_L} \right)^{1.25} \left(\frac{\sigma_{\text{water}}}{\sigma_L} \right)^{0.8} \right]^n}$ <p>Figures for ϕ and ψ in [42 and 43] Ranges: $0.02 < \phi > 0.300$; $25 < \psi < 190$ m.</p>	<p>[E] Z = packed height, m of each section with its own liquid distribution. The original work is reported in English units. Cornell et al. (Ref. 54) review early literature. Improved fit of Cornell's ϕ values given by Bolles and Fair (Refs. [42], [43]) and [157].</p> <p>$A = 0.017$ (rings) or 0.029 (saddles) d'_{col} = column diameter in m (if diameter > 0.6 m, use $d'_{\text{col}} = 0.6$) $m = 1.24$ (rings) or 1.11 (saddles) $n = 0.6$ (rings) or 0.5 (saddles)</p> <p>L = liquid rate, kg/(sm²), $\mu_{\text{water}} = 1.0$ Pa·s, $\rho_{\text{water}} = 1000$ kg/m³, $\sigma_{\text{water}} = 72.8$ mN/m (72.8 dyn/cm). H_C and H_L will vary from location to location. Design each section of packing separately.</p>	<p>[42, 43, 54] [77] p. 428 [90] p. 381 [141] p. 353 [157] [156]</p>																														
<p>H. Distillation and absorption. Counter-current flow. Structured packings. Gauze-type with triangular flow channels, Bravo, Rocha, and Fair correlation</p>	<p>Equivalent channel:</p>  <p>Use modified correlation for wetted wall column (See 5-18-F)</p> $N_{Sh,v} = \frac{k'_L d_{\text{eq}}}{D_v} = 0.0338 N_{Re,v}^{0.8} N_{Sc,v}^{0.333}$ $N_{Re,v} = \frac{d_{\text{eq}} \rho_v (U_{v,\text{eff}} + U_{L,\text{eff}})}{\mu_v}$ <p>Calculate k'_L from penetration model (use time for liquid to flow distance s). $k'_L = 2(D_L U_{L,\text{eff}}/\pi s)^{1/2}$.</p>	<p>[T] Check of 132 data points showed average deviation 14.6% from theory. Johnstone and Figford [Ref. 84] correlation (5-18-F) has exponent on N_{Re} rounded to 0.8. Assume gauze packing is completely wet. Thus, $a_{\text{eff}} = a_p$ to calculate H_C and H_L. Same approach may be used generally applicable to sheet-metal packings, but they will not be completely wet and need to estimate transfer area.</p> <p>L = liquid flux, kg/s m², G = vapor flux, kg/s m². Fit to data shown in Ref. [45].</p> $H_C = \frac{G}{k'_L a_p \rho_v}, H_L = \frac{L}{k'_L a_p \rho_L}$ <p>effective velocities</p> $U_{v,\text{eff}} = \frac{U_{L,\text{super}}}{\epsilon \sin \theta}, U_{L,\text{eff}} = \frac{3\Gamma}{2\rho_L} \left(\frac{\rho_L g}{3\mu_L \Gamma} \right)^{0.333}, \Gamma = \frac{L}{\text{Per}}$ $\text{Per} = \frac{\text{Perimeter}}{\text{Area}} = \frac{4S + 2B}{Bh}$	<p>[45] [63] p. 310, 326 [149] p. 356, 362 [156]</p>																														

TABLE 5-24 Mass-Transfer Correlations for Packed Two-Phase Contactors—Absorption, Distillation, Cooling Towers, and Extractors (Packing Is Inert) (Concluded)

Situation	Correlations	Comments E = Empirical, S = Semiempirical, T = Theoretical	References°																									
I. Distillation and absorption, counter-current flow. Structured packing with corrugations. Rocha, Bravo, and Fair correlation.	$N_{Sh,G} = \frac{k_g S}{D_g} = 0.054 N_{Re}^{0.8} N_{Sc}^{0.33}$ $u_{e,eff} = \frac{u_{g,super}}{\epsilon(1-h_L)\sin\theta}, \quad u_{L,eff} = \frac{u_{liq,super}}{\epsilon h_L \sin\theta}$ $k_L = 2 \left(\frac{D_L C_E u_{L,eff}}{\pi S} \right)$ $H_{OC} = H_G + \lambda H_L = \frac{u_{g,super}}{k_g a_e} + \frac{\lambda u_{L,super}}{k_L a_e}$ <p>Interfacial area:</p> $\frac{a_e}{a_p} = F_{SE} \frac{29.12 (N_{We} N_{Fr})^{0.15} S^{0.359}}{N_{Re,L}^{0.2} \epsilon^{0.6} (1 - 0.93 \cos \gamma) (\sin \theta)^{0.3}}$ <p>Packing factors:</p> <table border="1" data-bbox="410 614 809 719"> <thead> <tr> <th></th> <th>a_p</th> <th>ϵ</th> <th>F_{SE}</th> <th>θ</th> </tr> </thead> <tbody> <tr> <td>Flexi-pac 2</td> <td>233</td> <td>0.95</td> <td>0.350</td> <td>45°</td> </tr> <tr> <td>Gempak 2A</td> <td>233</td> <td>0.95</td> <td>0.344</td> <td>45°</td> </tr> <tr> <td>Intalox 2T</td> <td>213</td> <td>0.95</td> <td>0.415</td> <td>45°</td> </tr> <tr> <td>Mellapak 350Y</td> <td>350</td> <td>0.93</td> <td>0.350</td> <td>45°</td> </tr> </tbody> </table>		a_p	ϵ	F_{SE}	θ	Flexi-pac 2	233	0.95	0.350	45°	Gempak 2A	233	0.95	0.344	45°	Intalox 2T	213	0.95	0.415	45°	Mellapak 350Y	350	0.93	0.350	45°	<p>[E, T] Modification of Bravo, Rocha, and Fair (5-24-H). Same definitions as in (5-24-H) unless defined differently here. Recommended [156].</p> <p>h_L = fractional hold-up of liquid</p> <p>C_E = factor for slow surface renewal</p> <p>$C_E \sim 0.9$</p> <p>a_e = effective area/volume (1/m)</p> <p>a_p = packing surface area/volume (1/m)</p> <p>F_{SE} = surface enhancement factor</p> <p>γ = contact angle; for sheet metal, $\cos \gamma = 0.9$ for $\sigma < 0.055$ N/m</p> <p>$\cos \gamma = 5.211 \times 10^{-16.8336}$, $\sigma > 0.055$ N/m</p> <p>$\lambda = \frac{m}{L/V}$, $m = \frac{dy}{dx}$ from equilibrium</p>	[124], [156]
	a_p	ϵ	F_{SE}	θ																								
Flexi-pac 2	233	0.95	0.350	45°																								
Gempak 2A	233	0.95	0.344	45°																								
Intalox 2T	213	0.95	0.415	45°																								
Mellapak 350Y	350	0.93	0.350	45°																								
J. Rotating packed bed (Higee)	$\frac{k_L a d_p}{D a_p} \left(1 - 0.93 \frac{V_o}{V_i} - 1.13 \frac{V_t}{V_i} \right) = 0.65 N_{Sc}^{0.5}$ $\times \left(\frac{L}{a_p \mu} \right)^{0.17} \left(\frac{d_p^3 \rho^2 a_c}{\mu^2} \right)^{0.3} \left(\frac{L^2}{\rho a_p \sigma} \right)^{0.3}$ <p>500 ≤ N_{Sc} ≤ 1.2 E5; 0.0023 ≤ $L/(a_p \mu)$ ≤ 8.7</p> <p>120 ≤ $(d_p^3 \rho^2 a_c)/\mu^2$ ≤ 7.0 E7; 3.7 E - 6 ≤ $L^2/(\rho a_p \sigma)$ ≤ 9.4 E - 4</p> <p>9.12 ≤ $\frac{k_L a d_p}{D a_p}$ ≤ 2540</p>	<p>[E] Studied oxygen desorption from water into N_2. Packing 0.22-mm-diameter stainless-steel mesh.</p> <p>$\epsilon = 0.954$, $a_p = 829$ (1/m), $h_{bed} = 2$ cm.</p> <p>a = gas-liquid area/vol (1/m)</p> <p>L = liquid mass flux, kg/(m²S)</p> <p>a_c = centrifugal accel, m²/S</p> <p>V_o, V_t, V_i = volumes inside inner radius, between outer radius and housing, and total, respectively, m³. Coefficient (0.3) on centrifugal acceleration agrees with literature values (0.3–0.38).</p>	[50]																									
K. High-voidage packings, cooling towers, splash-grid packings	$\frac{(Ka)_H V_{tower}}{L} = 0.07 + A' N'^{n'}$ <p>A' and n' depend on deck type (Ref. 86), 0.060 ≤ $A' \leq 0.135$, 0.46 ≤ $n' \leq 0.62$.</p> <p>General form fits the graphical comparisons (Ref. 138).</p>	<p>[E] General form. $G_a = \text{lb dry air/hr ft}^2$.</p> <p>$L = \text{lb/h ft}^2$, N' = number of deck levels.</p> <p>$(Ka)_H$ = overall enthalpy transfer coefficient = $\frac{\text{lb water}}{\text{lb dry air}}$</p> <p>$V_{tower}$ = tower volume, ft³/ft².</p> <p>If normal packings are used, use absorption mass-transfer correlations.</p>	[86][104] p. 220 [138] p. 286																									
L. Liquid-liquid extraction, packed towers	Use k values for drops (Table 5-21). Enhancement due to packing is at most 20%.	[E] Packing decreases drop size and increases interfacial area.	[146] p. 79																									
M. Liquid-liquid extraction in rotating-disc contactor (RDC)	$\frac{k_{e,RDC}}{k_c} = 1.0 + 2.44 \left(\frac{N}{N_{Cr}} \right)^{2.5}$ $N_{Cr} = 7.6 \times 10^{-4} \left(\frac{\sigma}{d_{drop} \mu_c} \right) \left(\frac{H}{D_{tank}} \right)$ $\frac{k_{d,RDC}}{k_d} = 1.0 + 1.825 \left(\frac{N}{N_{Cr}} \right) \frac{H}{D_{tank}}$	<p>k_c, k_d are for drops (Table 5-21) Breakage occurs when $N > N_{Cr}$. Maximum enhancement before breakage was factor of 2.0.</p> <p>N = impeller speed</p> <p>H = compartment height, D_{tank} = tank diameter,</p> <p>σ = interfacial tension, N/m.</p> <p>Done in 0.152 and 0.600 m RDC.</p>	[36][146] p. 79																									
N. Liquid-liquid extraction, stirred tanks	See Table 5-22-E, F, G, and H.	[E]																										

See also Sec. 14.

°See the beginning of the “Mass Transfer” subsection for references.

The gas-phase rate coefficient \hat{k}_C is not affected by the fact that a chemical reaction is taking place in the liquid phase. If the liquid-phase chemical reaction is extremely fast and irreversible, the rate of absorption may be governed completely by the resistance to diffusion in the gas phase. In this case the absorption rate may be estimated by

knowing only the gas-phase rate coefficient \hat{k}_C or else the height of one gas-phase transfer unit $H_G = G_M/(\hat{k}_C a)$.

It should be noted that the highest possible absorption rates will occur under conditions in which the liquid-phase resistance is negligible and the equilibrium back pressure of the gas over the solvent is zero.

Such situations would exist, for instance, for NH_3 absorption into an acid solution, for SO_2 absorption into an alkali solution, for vaporization of water into air, and for H_2S absorption from a dilute-gas stream into a strong alkali solution, provided there is a large excess of reagent in solution to consume all the dissolved gas. This is known as the gas-phase mass-transfer limited condition, when both the liquid-phase resistance and the back pressure of the gas equal zero. Even when the reaction is sufficiently reversible to allow a small back pressure, the absorption may be gas-phase-controlled, and the values of \hat{k}_G and H_G that would apply to a physical-absorption process will govern the rate.

The liquid-phase rate coefficient k_L is strongly affected by fast chemical reactions and generally increases with increasing reaction rate. Indeed, the condition for zero liquid-phase resistance ($m\hat{k}_L$) implies that either the equilibrium back pressure is negligible, or that \hat{k}_L is very large, or both. Frequently, even though reaction consumes the solute as it is dissolving, thereby enhancing both the mass-transfer coefficient and the driving force for absorption, the reaction rate is slow enough that the liquid-phase resistance must be taken into account. This may be due either to an insufficient supply of a second reagent or to an inherently slow chemical reaction.

In any event the value of \hat{k}_L in the presence of a chemical reaction normally is larger than the value found when only physical absorption occurs, \hat{k}_L^0 . This has led to the presentation of data on the effects of chemical reaction in terms of the "reaction factor" or "enhancement factor" defined as

$$\phi = \hat{k}_L / \hat{k}_L^0 \geq 1 \quad (5-311)$$

where \hat{k}_L = mass-transfer coefficient with reaction and \hat{k}_L^0 = mass-transfer coefficient for pure physical absorption.

It is important to understand that when chemical reactions are involved, this definition of \hat{k}_L is based on the driving force defined as the difference between the concentration of *unreacted* solute gas at the interface and in the bulk of the liquid. A coefficient based on the total of both unreacted and reacted gas could have values *smaller* than the physical-absorption mass-transfer coefficient \hat{k}_L^0 .

When liquid-phase resistance is important, particular care should be taken in employing any given set of experimental data to ensure that the equilibrium data used conform with those employed by the original author in calculating values of \hat{k}_L or H_L . Extrapolation to widely different concentration ranges or operating conditions should be made with caution, since the mass-transfer coefficient \hat{k}_L may vary in an unexpected fashion, owing to changes in the apparent chemical-reaction mechanism.

Generalized prediction methods for \hat{k}_L and H_L do not apply when chemical reaction occurs in the liquid phase, and therefore one must use actual operating data for the particular system in question. A discussion of the various factors to consider in designing gas absorbers and strippers when chemical reactions are involved is presented by Astarita, Savage, and Bisio, *Gas Treating with Chemical Solvents*, Wiley (1983) and by Kohl and Nielsen, *Gas Purification*, 5th ed., Gulf (1997).

Effective Interfacial Mass-Transfer Area a In a packed tower of constant cross-sectional area S the differential change in solute flow per unit time is given by

$$-d(G_M S y) = N_A a dV = N_A a S dh \quad (5-312)$$

where a = interfacial area effective for mass transfer per unit of packed volume and V = packed volume. Owing to incomplete wetting of the packing surfaces and to the formation of areas of stagnation in the liquid film, the effective area normally is significantly less than the total external area of the packing pieces.

The effective interfacial area depends on a number of factors, as discussed in a review by Charpentier [*Chem. Eng. J.*, **11**, 161 (1976)]. Among these factors are (1) the shape and size of packing, (2) the packing material (for example, plastic generally gives smaller interfacial areas than either metal or ceramic), (3) the liquid mass velocity, and (4), for small-diameter towers, the column diameter.

Whereas the interfacial area generally increases with increasing liquid rate, it apparently is relatively independent of the superficial gas mass velocity below the flooding point. According to Charpentier's review, it appears valid to assume that the interfacial area is independent of the column height when specified in terms of unit packed volume (i.e., as a). Also, the existing data for chemically reacting gas-liquid systems (mostly aqueous electrolyte solutions) indicate that

the interfacial area is independent of the chemical system. However, this situation may not hold true for systems involving large heats of reaction.

Rizzuti et al. [*Chem. Eng. Sci.*, **36**, 973 (1981)] examined the influence of solvent viscosity upon the effective interfacial area in packed columns and concluded that for the systems studied the effective interfacial area a was proportional to the kinematic viscosity raised to the 0.7 power. Thus, the hydrodynamic behavior of a packed absorber is strongly affected by viscosity effects. Surface-tension effects also are important, as expressed in the work of Onda et al. (see Table 5-24-C).

In developing correlations for the mass-transfer coefficients \hat{k}_G and \hat{k}_L , the various authors have assumed different but internally compatible correlations for the effective interfacial area a . It therefore would be inappropriate to mix the correlations of different authors unless it has been demonstrated that there is a valid area of overlap between them.

Volumetric Mass-Transfer Coefficients $\hat{K}_G a$ and $\hat{K}_L a$ Experimental determinations of the individual mass-transfer coefficients \hat{k}_G and \hat{k}_L and of the effective interfacial area a involve the use of extremely difficult techniques, and therefore such data are not plentiful. More often, column experimental data are reported in terms of overall volumetric coefficients, which normally are defined as follows:

$$K'_{G a} = n_A / (h_T S p_T \Delta y_{1m}^0) \quad (5-313)$$

$$\text{and} \quad K_{L a} = n_A / (h_T S \Delta x_{1m}^0) \quad (5-314)$$

where $K'_{G a}$ = overall volumetric gas-phase mass-transfer coefficient, $K_{L a}$ = overall volumetric liquid-phase mass-transfer coefficient, n_A = overall rate of transfer of solute A , h_T = total packed depth in tower, S = tower cross-sectional area, p_T = total system pressure employed during the experiment, and Δx_{1m}^0 and Δy_{1m}^0 are defined as

$$\Delta y_{1m}^0 = \frac{(y - y^0)_1 - (y - y^0)_2}{\ln [(y - y^0)_1 / (y - y^0)_2]} \quad (5-315)$$

$$\text{and} \quad \Delta x_{1m}^0 = \frac{(x^0 - x)_2 - (x^0 - x)_1}{\ln [(x^0 - x)_2 / (x^0 - x)_1]} \quad (5-316)$$

where subscripts 1 and 2 refer to the bottom and top of the tower respectively.

Experimental $K'_{G a}$ and $K_{L a}$ data are available for most absorption and stripping operations of commercial interest (see Sec. 14). The solute concentrations employed in these experiments normally are very low, so that $K_{L a} \approx \hat{K}_{L a}$ and $K'_{G a} p_T \approx \hat{K}'_{G a}$, where p_T is the total pressure employed in the actual experimental-test system. Unlike the individual gas-film coefficient $\hat{k}_G a$, the overall coefficient $\hat{K}'_{G a}$ will vary with the total system pressure except when the liquid-phase resistance is negligible (i.e., when either $m = 0$, or $\hat{k}_L a$ is very large, or both).

Extrapolation of $K'_{G a}$ data for absorption and stripping to conditions other than those for which the original measurements were made can be extremely risky, especially in systems involving chemical reactions in the liquid phase. One therefore would be wise to restrict the use of overall volumetric mass-transfer-coefficient data to conditions not too far removed from those employed in the actual tests. The most reliable data for this purpose would be those obtained from an operating commercial unit of similar design.

Experimental values of H_{OG} and H_{OL} for a number of distillation systems of commercial interest are also readily available. Extrapolation of the data or the correlations to conditions that differ significantly from those used for the original experiments is risky. For example, pressure has a major effect on vapor density and thus can affect the hydrodynamics significantly. Changes in flow patterns affect both mass-transfer coefficients and interfacial area.

Chilton-Colburn Analogy On occasion one will find that heat-transfer-rate data are available for a system in which mass-transfer-rate data are not readily available. The Chilton-Colburn analogy [90, 53] (see Tables 5-17-G and 5-19-T) provides a procedure for developing estimates of the mass-transfer rates based on heat-transfer data. Extrapolation of experimental j_M or j_H data obtained with gases to predict liquid systems (and vice versa) should be approached with caution, however. When pressure-drop or friction-factor data are available, one may be able to place an upper bound on the rates of heat and mass transfer of $f/2$. The Chilton-Colburn analogy can be used for simultaneous heat and mass transfer as long as the concentration and temperature fields are independent [Venkatesan and Fogler, *AIChE J.*, **50**, 1623 (2004)].

This page intentionally left blank